FIRES AND VEGETATION IN NAMIBIAN ECOSYSTEMS – A MODELLING STUDY BASED ON REMOTE SENSING

DISSERTATION

zur Erlangung des akademischen Grades eines
Doktors der Naturwissenschaften (Dr. rer. nat.)
an der Fakultät für Biologie, Chemie und Geowissenschaften
der Universität Bayreuth

vorgelegt von

Manuel Mayr

aus *Steyr, Österreich*

Bayreuth, Januar 2019

Die vorliegende Arbeit wurde in der Zeit von Mai 2013 bis März 2018 in Bayreuth am Lehrstuhl Klimatologie unter Betreuung von Herrn Professor Dr. Cyrus Samimi angefertigt.

Vollständiger Abdruck der von der Fakultät für Biologie, Chemie und Geowissenschaften der Universität Bayreuth genehmigten Dissertation zur Erlangung des akademischen Grades eines Doktors der Naturwissenschaften (Dr. rer. nat.).

Dissertation eingereicht am: 23.01.2019

Zulassung durch die Promotionskommission: 13.02.2019

Wissenschaftliches Kolloquium: 31.05.2019

Amtierender Dekan: Prof. Dr. Stefan Peiffer

Prüfungsausschuss:

Prof. Dr. Cyrus Samimi	(Gutachter)
Prof. Dr. Carl Beierkuhnlein	(Gutachter)
Prof. Dr. Thomas Köllner	(Vorsitz)
Prof. Dr. Steven Higgins	

"It is the one who lies by a fire who feels the heat."

- Namibian proverb

ABSTRACT

Fires are a regular feature of savanna ecosystems worldwide. Although Namibia is the most arid country across Sub-Saharan Africa, the seasonal occurrence of fires is widespread. Humans and biophysical controls are known to govern the spatio-temporal patterns of fire. Yet, the interplay among the controlling factors and their individual contribution to the generation of fires lack generality. An overall impact of fire on vegetation and its structure is controversial – especially in drier regions. Remote sensing provides a unique means for the assessment and modelling of fire regimes and vegetation. Earth observation missions such as the Moderate-Resolution Imaging Spectroradiometer (MODIS) offer consistent records of fire and quantitative vegetation parameters. The scale of observation in space and time impose an inherent source of uncertainty with any remotely-sensed dataset. As such, background contamination and phenology usually complicate the discrimination of sparse green vegetation. Unmanned Aerial Vehicles (UAV) introduce new 3D opportunities for optical remote sensing, however their full potential remains to be explored.

In the present study, remote sensing and spatial modelling are the primary tools for a quantitative investigation of fire and vegetation parameters across Namibia. Several spatial datasets are applied to achieve this task. These range from readily-available thematic products from Earth observation over higher-resolution RapidEye and UAV imagery to vector datasets. Fire regimes are analysed and modelled using a set of common statistical and machine learning techniques. Field measurements and upscaling techniques are combined in order to comparatively explore the estimates of Leaf Area Index (LAI). Imagery generated from an UAV mission facilitates the reconstruction of vegetation structure in 3D by means of a photogrammetric approach known as Structure-from-Motion – Multi-View Stereopsis (SfM-MVS). Woody individuals are then delineated in order to yield approximate stand structures.

The results show that productivity is the major control of fire activity in Namibia. A distinct increase in both Burned Area (BA) and Fire Occurrence (FO) with a mean annual precipitation above 400 mm is observed and located in the northern parts of the country. Although humans are known to account for the majority of ignitions, their activities also consume the fuels that are required for burning. Hence, increasing densities of population and livestock reduce fire activity across the country.

A case study from Owamboland in northern Namibia confirms the uncertainties that are associated with the spectral remote sensing of low-productivity ecosystems. As such, a mean underestimation of 0.34 ($\pm$0.2) is found with the estimates of LAI from MODIS (MOD15A2), which are compared to an empirically-calibrated model of LAI. In contrast to the general underestimation by MOD15A2, overestimations of LAI are apparent in the case of a recent fire in the region.

Image-Based Point Clouds (IBPC) and the autonomous use of an UAV are found to be suitable for the assessment of woody vegetation and stand-scale heights in the northern Otjozondjupa region. The height parameters derived from this approach outline a promising agreement with field measurements, with an R^2 of approximately 0.7 and RMSE generally $<$1.9 m. However, no significant height reductions are found with the long-term presence of fire. Instead persistent grazing reduces the stands' heights which may be indicative of woody encroachment.

This thesis contributes to the causal understanding of fire and the patterns fire creates in dry savannas, which is an important prerequisite for national policy decisions and the anticipation of

future fire activity. It is concluded that fire has limited capabilities for a sustainable alteration of vegetation structure as woody communities are often adapted to fire. Future research should therefore explicitly consider the role of individual species in woody communities in order to quantify the structural impact of different fire regimes. UAVs and active remote sensing techniques could assist such studies. Finally, it is suggested that the human dimension of fire is inadequately captured by moderate-resolution fire records as controlled burnings, which are usually smaller, are likely to be underrepresented. Regional studies that explicitly aim at addressing the human dimension of fire should thus apply fire records of higher resolution.

ZUSAMMENFASSUNG

Feuer ist ein Bestandteil global auftretender Savannenökosysteme. Auch in Namibia, dem aridesten Land im Subsaharischen Afrika, sind saisonal auftretende Brände weit verbreitet. Neben biophysikalischen Einflussgrößen steuert vor allem der Mensch die raum-zeitlichen Muster dieser Brände. Das Zusammenspiel und die Wichtigkeit einzelner Einflussgrößen entziehen sich jedoch einer generellen Regelmäßigkeit. Des Weiteren werden die Auswirkungen solcher Brände auf die Vegetation und deren Struktur, speziell in trockeneren Regionen, kontrovers diskutiert. Die Fernerkundung bietet einzigartige Mittel zur Erfassung und Modellierung von Feuerregimen und der Vegetation. Erdbeobachtungsmissionen, wie der Moderate-Resolution Imaging Spectroradiometer (MODIS), liefern konsistente Datenreihen von Bränden und quantitativen Vegetationsparametern. Jedoch haftet Fernerkundungsdaten, schon aufgrund der räumlichen und zeitlichen Charakteristika des erfassenden Sensors, immer eine gewisse Unschärfe an. So erschweren die Einflüsse der darunterliegenden Oberfläche und der Phänologie eine fernerkundliche Ableitung grüner Vegetation und geringer Bedeckungsgrade. Unbemannte Flugobjekte (UAV) verleihen der optischen Fernerkundung bisher nicht vorhandene Möglichkeiten der dreidimensionalen Oberflächenerfassung. Gleichzeitig ist deren Anwendung Gegenstand aktueller Forschung.

Die vorliegende Studie nutzt vorwiegend Fernerkundung und Methoden der räumlichen Modellierung, um Feuer und Vegetationsparameter in Namibia quantitativ zu untersuchen. Dabei findet eine Vielzahl räumlicher Datensätze Anwendung, die von vollständig vorverarbeiteten Fernerkundungsprodukten globalen Ausmaßes, über höheraufgelöste RapidEye- und UAV-Bilddaten, bis hin zu Vektordatensätzen reichen. Auf Basis gängiger statistischer Verfahren und Machine Learning werden Feuerregime analysiert und modelliert. Um fernerkundliche Ableitungen des Blattflächenindex (LAI) im Vergleich zu betrachten, werden Geländemessungen und Methoden zur Überbrückung von Skalensprüngen (upscaling) angewandt. Eigens mit einem UAV beflogene Bilddaten dienen der dreidimensionalen Rekonstruktion von Gehölzbeständen. Dabei kommt ein neueres photogrammetrisches Verfahren, die sogenannte Structure-from-Motion – Multi-View Stereopsis (SfM-MVS), zum Einsatz. Es wird versucht, die Gehölze auf Ebene von Individuen abzuleiten, um eine möglichst repräsentative Bestandsstruktur zu erlangen.

Die Ergebnisse zeigen, dass der Produktivität eine Hauptrolle bei der Begrenzung von Bränden zukommt. Sowohl das räumliche Ausmaß (BA) als auch die Häufigkeit (FO) der Brände steigen bei einem mittleren Jahresniederschlag von >400 mm an. Derartige Niederschlagsmengen sind vor allem im Norden Namibias vorhanden. Obwohl der Mensch wohl die Hauptentzündungsquelle in Namibia darstellt, beschränken seine Aktivitäten ebenso die Verfügbarkeit von brennbarer Biomasse. Auf nationaler Ebene wirken gesteigerte Bevölkerungs- und Viehdichten daher Feuer reduzierend.

Bekannte Unsicherheiten der rein spektralen Ableitung von grüner Vegetation und geringen Bedeckungsgraden bestätigen sich in einer Fallstudie im Owamboland (Nordnamibia). Ausdruck dessen ist eine im Vergleich mittlere Unterschätzung des LAI von 0,34 ($\pm$0,2) durch das MODIS-Produkt (MOD15A2) gegenüber dem empirisch kalibrierten Modell. Jedoch kehrt sich diese Beziehung im Bereich einer kurz zuvor von Feuer erfassten Fläche um. Es wird daher empfohlen, Fernerkundungsdaten in Regionen geringer Produktivität systematisch auf die Auswirkungen des Bildhintergrunds und räumlicher Skalen(-sprünge) zu untersuchen.

Eine autonome Nutzung von UAVs und die 3D-Rekonstruktion auf Basis von bildbasierten Punktwolken erlauben hier eine angemessene Erfassung der Höhen in Gehölzbeständen. Der verwendete Ansatz erzielt eine vielversprechende Übereinstimmung mit den Geländemessungen in der nördlichen Otjozondjupa Region (R^2 um 0,7 bzw. RMSE <1,9 m). Jedoch zieht das längerfristige Vorhandensein von Bränden keine signifikante Änderung der Gehölzhöhen nach sich. Im Gegensatz dazu führt eine stetige Beweidung zur Verringerung der betrachteten Höhenparameter, was als Indiz für eine voranschreitende Verbuschung gewertet werden kann.

Die vorliegende Studie versteht sich als Beitrag um Feuer in Trockensavannen – sowohl in Bezug auf ihre Ursache als auch auf die daraus entstehenden Landschaftsmuster – besser zu verstehen. Damit einher geht eine besondere Relevanz der Studie für Handlungsentscheidungen auf nationaler Ebene sowie für mögliche Veränderungen des Feuerregimes in Zukunft. Auf Basis der Ergebnisse kann geschlossen werden, dass Brände in Trockensavannen lediglich eine geringe Beeinflussung der Vegetationsstruktur nach sich ziehen, da die Gehölzgemeinschaften wohl weitestgehend daran angepasst sind. Hierbei sollte die Rolle einzelner Arten innerhalb einer Gehölzgemeinschaft Gegenstand weiterer Forschung sein, um Veränderungen der Bestandsstruktur in Abhängigkeit von unterschiedlichen Brandcharakteristika besser quantifizieren zu können. UAVs und aktive Fernerkundungssensoren können dazu wertvolle Beiträge leisten. Des Weiteren wird vermutet, dass der menschliche Einfluss in der vorgestellten Analyse insgesamt unterschätzt wird. Dem liegt zu Grunde, dass die verwendeten Fernerkundungsdaten von mittlerer Auflösung kontrollierte und damit kleinere Feuer nicht ausreichend erfassen. Regionale Studien, die sich auf höher auflösende Fernerkundungsdaten stützen, sollten den gesamten Wirkungskomplex des Menschen auf Feuer detaillierter erfassen können.

ACKNOWLEDGEMENTS

I would like to initially express my sincere gratitude to my supervisor, Cyrus Samimi, for giving me the opportunity to follow up on my interests in remote sensing and Namibia. I appreciate the constant trust in my work, the guidance and the encouragement for my scientific ideas. A special thanks goes to Kim Vanselow, who supported the progress of this thesis at many stages. Thank you for the expertise on statistical modelling in R as well as for the insights into academic realities and publishing. The Graduate School of the University of Bayreuth deserve my gratitude for bridging some tough months during this thesis and facilitated my participation in several scientific events. Many thanks to the German Academic Exchange Service (DAAD) for the travel scholarship I received. Michael Überbacher from Soleon shall be thanked for the hands-on technical support with UAV issues.

All former and current members of the Working Group of Climatology at the University of Bayreuth deserve to be acknowledged here for their individual contributions to a productive, yet friendly atmosphere – also outside the office. I want to especially mention Lisi Ofner who has been a great friend and colleague throughout the years. Thank you for your company on numerous trips to Southern Africa, your insights into biology and ecology and your constantly positive mood. All of this would not have been possible without you! Many thanks also to Sophia Malß who joined us in the field for her M.Sc. thesis.

Conducting research in foreign countries is exceptionally linked to local people that contribute to the success of such work in different ways. Thank you, Lameck Mwewa, for your support with logistics and bureaucracy in Namibia. Johan Le Roux's knowledge on fire from an academic and practitioner's perspective has been invaluable. I wish to thank Paula and Uwe (†) Gressmann for their warm support and hospitality, as well as their insights into rangeland realities. The same shall be expressed to the family Vermaag – Mr. Vermaag's coffee is undisputedly the best in the region! Furthermore, I thank the family Van der Merwe, Joseph Kawimbi from M'Kata Community Forest, and the staff at Kanovlei Forestry Station – especially Wilson Muyenga – for their cooperation and for their support during our field work. The Roof of Africa in Windhoek has always been a base when we came to Namibia – thank you Thorsten, Terry and Axi (also for the astronomical experience)!

Daniela Kretz has, on several occasions, been confronted with the raw versions of my written words and has not yet refused to read and correct them. Thank you for your patience and the great work! There are many more people inside and outside the university that remain unnamed here. Yet these people have made Bayreuth a remarkable experience over the years, and I deeply thank each of them for being the way they are.

CONTENTS

LIST OF FIGURES

LIST OF TABLES

ABBREVIATIONS AND ACRONYMS

AON ..... Atlas Of Namibia
BA ..... Burned Area
CHM ..... Canopy Height Model
CV ..... Cross-Validation
DEM ..... Digital Elevation Model
DLR ..... German Aerospace Centre (Deutsches Zentrum für Luft- und Raumfahrt)
dNBR ..... differenced Normalized Burn Ratio
DSM ..... Digital Surface Model
EIS ..... Environmental Information System of Namibia
EVI ..... Enhanced Vegetation Index
FPAR ..... Fraction of absorbed Photosynthetically Active Radiation
GCP ..... Ground Control Point
GIS ..... Geographic Information System
GLM ..... Generalized Linear Models
GNSS ..... Global Navigation Satellite System
IBPC ..... Image-Based Point Cloud
INS ..... Inertial Navigation System
LAI ..... Leaf Area Index
LiDAR ..... Light Detection And Ranging
LIS ..... Lightning Imaging Sensor
LUT ..... Look-Up Table
MAP ..... Mean Annual Precipitation
MARS ..... Multivariate Adaptive Regression Splines
MAUP ..... Modifiable Areal Unit Problem
METEOSAT ..... METEOrological SATellite mission
MODIS ..... MODerate-resolution Imaging Spectroradiometer
MVC ..... Maximum Value Composite
MVS ..... Multi-View Stereopsis
MWIR ..... Mid-Wave InfraRed
NDVI ..... Normalized Difference Vegetation Index
NIR ..... Near InfraRed
OSM ..... OpenStreetMap
QA ..... Quality Assurance
R^2 ..... Coefficient of determination
RaDAR ..... Radio Detection And Ranging
RESA ..... RapidEye Science Archive
RF ..... Random Forest
RMSE ..... Root Mean Square Error
RPART ..... Regression Trees from Recursive Partitioning
RTM ..... Radiative Transfer Model
SAC ..... Spatial AutoCorrelation

SAR ..... Synthetic Aperture RaDAR
SfM ..... Structure-from-Motion
SVI ..... Spectral Vegetation Index
SVR ..... Support Vector Machines for Regression
SWIR ..... Short-Wave InfraRed
TAMSAT..... Tropical Applications of Meteorology using SATellite data and ground-based observations
TIR ..... Thermal InfraRed
TMPA ..... TRMM Multisatellite Precipitation Analysis
TRMM ..... Tropical Rainfall Measuring Mission
UAV ..... Unmanned Aerial Vehicle
VALERI ..... Validation of Land European Remote sensing Instruments
VHRMC ..... Very High Resolution gridded lightning Monthly Climatology

PART I
RESEARCH CONCEPT

1. MOTIVATION AND RESEARCH QUESTIONS

Fire is a phenomenon of global occurrence and relevance. Across Southern African savannas, vast areas burn during the dry season. In Namibia, climate and human land use are two major controls of fire and vegetation. Yet fire and the spatio-temporal patterns it forms are not fully understood in its complexity. Furthermore, fire's impact on woody vegetation is perceived to be controversial. Remote sensing is a valuable source of information for the observation and understanding of land surface processes and phenomena at different scales. Consequently, the datasets obtained from a suite of available remote sensing systems – from satellite missions of differing scopes to airborne systems such as the emerging Unmanned Aerial Vehicles (UAV) – are frequently applied in quantitative modelling of vegetation and fire. This thesis intends to contribute to the understanding of fire and its impact on vegetation in the dry savannas of Namibia. Moreover, it highlights the potentials and limitations of optical remote sensing for the quantitative estimation of vegetation in such regions.

The present thesis is structured as follows: PART I is dedicated to framing the research by initially imparting the reader with current knowledge on the nexus of vegetation, humans, and fire in the context of Southern Africa savannas and relevant remote sensing research. Gaps in knowledge are identified thereof, which are then considered in the guiding questions and the hypotheses to be addressed. Chapter 2 introduces the study areas and highlights datasets and key methods that were applied. Three peer-reviewed manuscripts (Chapters 4, 5, and 6) that together embody the central research activity of this thesis are presented in PART II. Based on the manuscripts, results and implications are discussed and reflected upon with regards to additional research needs (PART III). Finally, the Appendix (PART IV) lists the author's further contributions to the topic and contains the declaration of honour.

1.1. Savannas, humans, and the role of fire

Savannas are flammable ecosystems (Bond and Keeley, 2005; Simpson et al., 2016) that account for almost two thirds of the global extent of fire (Randerson et al., 2012). Unlike other fire-prone ecosystems, such as boreal forests or Mediterranean shrublands, grass fuels the propagation of fires in savannas. Evidence and simulations suggest that their historic expansion, as well as the simultaneous retreat of tropical forest in the Late Miocene was substantially linked to C4 grasses[1] and the occurrence of fire (Cerling et al., 1997; Scheiter et al., 2012). These fires were, of course, ignited by lightning. An intentional use of fire by human ancestors is documented as early as 400,000 years ago (Roebroeks and Villa, 2011).

In their current distribution, tropical grassy biomes, i.e. savannas and grasslands, occupy approximately 20-25% of the terrestrial surface, where they are characterised by the simultaneous presence of C4 grasses and a discontinuous woody layer (Bond, 2008; Scholes and Archer, 1997). These characteristics may be found in regions with a Mean Annual Precipitation (MAP) of up to 2500 mm in South America (Lehmann et al., 2011), but with C4 grasslands occurring in extremely dry regions such as the Namib desert as well. Among African savannas, woody vegetation cover varies from virtually zero to >80% (Sankaran et al., 2005) and as Bond (2008) states, climate alone

[1] The C4 photosynthetic pathway, as opposed to the "older" C3, is considered an evolutionary adaption to warm and dry climate as it reduces water losses from transpiration (Ehleringer and Monson, 1993).

fails to explain their vegetation. In this regard, Scholes (2003) emphasizes the heterogeneous appearance that covers arid shrublands to dry forests indicating that any attempt to set limits within the savanna continuum would be "unavoidably arbitrary" (Scholes, 2003, p. 258). This diversity in vegetation structure and the mechanisms behind coexistence in general have challenged ecologists ever since. Some early and still intensively debated reflections on this issue were based on observations from Namibia by Walter (1939, in Ward et al., 2013). Since then, a variety of explanations and models have been proposed for coexistence and the controls of woody vegetation in savannas (for reviews see Scholes and Archer (1997), Sankaran et al. (2004), and Bond (2008)). Following the latter author, these separate into bottom-up, i.e. water and soil nutrients, and top-down, i.e. demographic bottlenecks created by fire and herbivory, controls. Yet their relative importance and the interactions across environmental gradients remain a debated issue (e.g. Higgins et al., 2010; Midgley et al., 2010; Sankaran et al., 2008) and seem to vary on the inter-continental scale (e.g. Lehmann et al., 2014). By means of maximum woody cover across African savannas, Sankaran et al. (2005) identified stable, resource-limited (<650 mm MAP) and instable, disturbance-driven savannas. As a consequence, fire and herbivory would alter community structure and dynamics only within the climatic framework in dry savannas.

Fire impacts have been studied through the use of dynamic vegetation models (e.g. Lehsten et al., 2016), but also from plot-based replicated fire manipulation and exclusion experiments that were often carried out in protected areas across Southern Africa (see van Wilgen et al. (2007) and Furley et al. (2008) for overviews). However, abundant herbivory is likely a bias in these empirical studies. Many experiments point to the legacies in vegetation structure as a result of fire history that are, for instance, expressed by an altered size distributions of the woody community (e.g. Higgins et al., 2007; Kennedy and Potgieter, 2003; Levick et al., 2015). Fire frequency and intensity are often regarded as important determinants of shifted woody height distributions (e.g. Govender et al., 2006; Smit et al., 2010). Yet, as Higgins et al. (2007) conclude, woody demographics are resilient to fire. This suggests that certain species are adapted to fire and have evolved traits that allow them to persist, e.g. through resprouting, and to resist, e.g. through a thick bark (see Allen, 2008). Hence, the community composition would be largely irresponsive to the fire regime, but fire exclusion may be accompanied by species responses especially from the herbaceous stratum (van Wilgen et al., 2007). There appears to be a general tendency towards stronger fire impacts as a function of productivity (Furley et al., 2008; van Wilgen et al., 2007), but variations may arise with the species affected. For instance, hardly any fire impacts on the size distribution of a woodland community were found in a study from Namibia's Kavango region (Geldenhuys, 1977). Despite comparable MAP, fire-induced mortalities of the fire-sensitive species *Acacia erioloba* were high, particularly among taller individuals (Seymour and Huyser, 2008). Studies that explicitly addressed a gradient in MAP find a relatively higher reduction of woody cover at drier sites (e.g. Devine et al., 2015; Smit et al., 2010). The above illustrates some of the controversy associated with the role of fire in shaping savannas, but implies its function as a tool in order to manage landscapes and to achieve certain desirable goals.

Relatively little is known about the extent of early human land use in Southern Africa. The largest but probably most sustained impact on vegetation was of an indirect nature: the arrival of European colonists marked the beginning of a rigorous depletion of (mega-)herbivores and the simultaneous introduction of livestock (Hoffman, 2003). The extent of deforestation in Namibia is not comparable to more humid tropical regions, extensive clearings for cultivation are, however, reported in Northern Namibia (e.g. Mendelsohn et al., 2000; Siiskonen, 1996; Strohbach, 2013). Commercial and subsistence livestock ranching on private and communal land is widespread across Namibia and stocking rates are generally high (Mendelsohn et al., 2002). Pasture degradation, such as the shift from palatable perennial to less palatable annual grass communities or the massive spread of highly

persistent woody species known as “encroachers”, is an issue in Namibia (de Klerk, 2004; Mendelsohn et al., 2002) as well as across semi-arid rangelands worldwide (e.g. Maestre et al., 2009; O'Connor et al., 2014; van Auken, 2009). A general causal explanation of woody encroachment is not available but land use alone may be an insufficient explanation (see D‘Odorico et al. (2012) for a recent synthesis). In fact, studies also point to the importance of climatic anomalies (e.g. Higgins et al., 2000) and, more recently, to global drivers (e.g. Bond and Midgley, 2012; Stevens et al., 2016; Wigley et al., 2010). Long-term management practices have contributed to the development of woody encroachment in Namibia, where fire has been applied as a traditional tool in order to clear and clean land, replenish pastures, control pests or hunt game. This perception was, however, largely replaced during the first half of the last century by a view that aimed at the exclusion and suppression of fire – at least from a state authority’s perspective. Prescribed burning in protected areas such as the Etosha National Park was a “necessary evil” in order to prevent massive fuel accumulation. Only recently fire is being more and more rehabilitated in Namibia for the management of protected areas and rangelands – also with regards to woody encroachment (see Beatty, 2011; MAWF, 2012; MET, 2016).

The above suggests that the human dimension of fire is likely the product of the interrelations among socio-economy, culture and policy. Humans possess tremendous leverage to directly and intentionally manipulate fire activity by impacting the timing and number of ignitions as well as through their efforts to actively supress fire (e.g. Archibald, 2016; Bowman et al., 2011). Livestock grazing, croplands, and human infrastructure reduce fuel loads, i.e. the biomass available for burning, and, by fragmenting the landscape, the connectivity of fuels. Indeed, the majority of fires in Southern Africa are lit by humans[2] (e.g. Archibald et al., 2009; 2010b; Roy et al., 2008), and studies highlight the importance of land use and its intensity (e.g. Archibald et al., 2009; Hudak et al., 2004; Le Roux, 2011; Mishra et al., 2016; Stellmes et al., 2013), as well as policy (e.g. Pricope and Binford, 2012) in addressing fire activity. There is global (e.g. Andela et al., 2017; Knorr et al., 2014) and regional (e.g. Archibald et al., 2009; Swetnam et al., 2016) evidence that the net effect of human activity on fire may be dominated by the indirect leverage of altering fuels. Likewise fire is strongly embedded in a framework of climate and its variability (e.g. Krawchuk and Moritz, 2011; Pausas and Ribeiro, 2013). For instance, moist areas of high productivity such as South-East Asia burn excessively during dry spells that are imposed by El Nino conditions there (e.g. Page et al., 2002). At the arid end of fire-prone ecosystems, the atmospheric conditions would facilitate fire on a seasonal basis, but such regions are limited in productivity. Productivity peaks from one or several consecutive years with above-average precipitation are necessary in order to accumulate enough grass biomass to fuel a fire (e.g. Archibald et al., 2010a; Heinl et al., 2007). However, some semi-arid regions such as North-Eastern Namibia burn on a quasi-annual basis (Siljander, 2009; Verlinden and Laamanen, 2006). The resultant spatio-temporal patterns of fire, i.e. the fire regime, are thus the product of complex and regionally specific interactions of climate, vegetation, and humans. Their empirical examination is usually facilitated by records obtained from remote sensing (Krawchuk and Moritz, 2014; see Chapter 1.2), but poses some general methodological difficulties. For instance, most of the controlling variables of fire can only be measured indirectly (see Figure 1), while their selection can never be complete and is always arbitrary to some degree (e.g. Krebs et al., 2010). Empirical studies from regions with strong contrasts in climate and land management, such as Namibia, could contribute to our general understanding of fire on Earth. The controls of fire as well as its impact on vegetation structure in such “extreme” regions are also relevant to the parameterization of process-based models and to the response of fire regimes in the face of a changing climate (e.g. Hantson et al., 2016).

[2] Human-caused fires, albeit intentionally or unintentionally, make up approximately 90% of the total fire numbers worldwide (Costafreda-Aumedes et al., 2017).

1.2. Remote sensing of vegetation and fire

Remotely-sensed data of the land surface is a primary source of information for the analysis and monitoring of ecological processes and phenomena. In many cases, the spectral information detected from remote sensing provides the only means to sample large areas in its spatial variability and ideally in a systematic, repeated, and objective manner (Eisfelder et al., 2012; Roy et al., 2011). The variables derived from remote sensing are critical to many research domains, including greenhouse gas emissions from biomass burning (e.g. Alleaume et al., 2005; Lehsten et al., 2009; Randerson et al., 2012; Scholes et al., 2011; Stroppiana et al., 2010), as well as fire regimes. Likewise, the quantification of biosphere-atmosphere interactions at different scales often relies on biophysical parameters such as the Leaf Area Index (LAI) in order to estimate carbon and water fluxes (e.g. Sellers et al., 1997; Turner et al., 2006; Yan et al., 2012). The "primary data" behind such applications and models, which are in many cases operationally produced satellite remote sensing products of global scope, need to be evaluated for their accuracy and limitations. For vegetation products, such as the estimates of LAI from the Moderate-resolution Imaging Spectroradiometer (MODIS), evaluations based on field measurements that are carried out across different biomes and gradients of productivity are essential (Garrigues et al., 2008). However, the scaling of point-based field measurements to the areal measurements delivered from remote sensing data is a pervasive problem with such evaluation efforts (Tian et al., 2002; Wu and Li, 2009). In order to reliably overcome the large gap in scale between the two data sources, the aforementioned authors recommend an intermediate step whereby field measurements are first related to high-resolution remote sensing data. The resultant high-resolution estimates are then upscaled to the coarser-scale estimates such as from MODIS.

Studies that evaluate MODIS LAI in low-productivity ecosystems are generally sparse, and savannas depict a challenge due their heterogeneous appearance in terms of structure and phenology (e.g. Garrigues et al., 2008; Fang et al., 2013a; 2013b). Contradicting results are reported for the accuracy of MODIS LAI in (semi-)arid regions. The results range from occasionally severe underestimation (e.g. Scholes et al., 2004; Sprintsin et al., 2009; Tian et al., 2002; Zhang et al., 2007) to overestimations (e.g. Fensholt et al., 2004; Privette et al., 2002; Sea et al., 2011).

Optical satellite remote sensing faces some general uncertainties in the derivation of vegetation properties in (semi-)arid regions. Vegetation cover is often sparse and organized in patches. Hence, the underlying soil strongly contributes to the spectral signature of vegetation. Background contaminations are likely to increase as a function of decreasing spatial resolution (Tian et al., 2002), whereas certain Spectral Vegetation Indices (SVIs) were designed to theoretically minimize contaminations (see Bannari et al., 1995). Nevertheless, classic SVIs that incorporate the red and Near Infrared (NIR) spectra remain to be applied throughout semi-arid regions (Eisfelder et al., 2012). Distinct seasonality is a typical feature of semi-arid lands: during the dry season, dry grass, litter, and the woody components of vegetation constitute major proportions of the reflective properties in vegetation stands, which complicates the derivation of green vegetation (Asner, 1998; van Leeuwen and Huete, 1996). Several approaches that apply a variety of sensors have evolved to address these (see Li and Guo (2016) for a recent review). Given that pure pixels of soil, photosynthetic and non-photosynthetic vegetation are available, spectral mixture analysis on hyperspectral data can be used in order to derive the respective proportions of the contributing surfaces (e.g. Asner and Heidebrecht, 2002; Guerschman et al., 2009), but was also shown to be limited (e.g. Okin et al., 2001). Some studies used the Short-Wave Infrared (SWIR) spectrum to quantify dry vegetation (e.g. Jacques et al., 2014), whereas others aimed at the varying phenology of grass and woody species apparent from time series decomposition in order to distinguish them from

one another (e.g. Brandt et al., 2016; Kahiu and Hanan, 2018; Verbesselt et al., 2006; Wagenseil and Samimi, 2006).

The traditional techniques of optical remote sensing are largely restricted to the horizontal domain, although the vertical dimension of vegetation structure may to some degree be expressed through indirect relationships with spectral information. The typical spatial resolutions of satellite missions range from several metres to several kilometres and can be thought of as an additional constraint for deriving meaningful vertical information in heterogeneous canopies. For instance, texture analysis applied to (very) high-resolution imagery could approximately derive vegetation heights (e.g. Kayitakire et al., 2006; Petrou et al., 2015). The standard approach to estimate three-dimensional (3D) structures of vegetation, however, involves active sensors (Bergen et al., 2009; Dandois and Ellis, 2010). Laser altimetry, i.e. Light Detection And Ranging (LiDAR), and Radio Detection And Ranging (RaDAR), which comprises certain microwave spectra, have proven their suitability in measuring canopy objects by intercepting the sensor's emitted radiation in their 3D distribution (Bergen et al., 2009; Lefsky et al., 2002). Especially LiDAR is attractive for the study of canopies as it potentially allows for the derivation of complete 3D profiles of objects through full-waveform returns (Wagner et al., 2008). As a spaceborne LiDAR mission is temporarily no longer available (e.g. Simard et al., 2011), airborne systems are usually applied. For instance, airborne LiDAR data have been used to study fire (e.g. Levick et al., 2015; Smit et al., 2010) and herbivore impacts (e.g. Asner et al., 2009) on 3D vegetation structure in the savannas of Kruger National Park, South Africa. In addition, Wessels et al. (2011) focus on the land-use related differences in savanna structure using LiDAR. Spaceborne Synthetic Aperture RaDAR (SAR) data are increasingly applied in these ecosystems as well (e.g. Mathieu et al., 2013; Naidoo et al., 2015; 2016).

Recently, UAVs have gained much attention in the remote sensing community. Their obvious benefit is a flexible and application-oriented data acquisition at potentially ultra-high spatial resolution. Although the potential of UAVs for environmental applications has already been noted in the early 1980s, developments in micro-electronics and computer vision have enabled UAVs to become an active part of research since the mid-2000s (Hardin and Jensen, 2011). All kinds of sophisticated sensors (e.g. LiDAR, multispectral, hyperspectral, or Thermal Infrared (TIR)) can now be mounted on lightweight UAVs, however consumer-grade cameras remain to be an inexpensive, yet powerful sensor alternative – at least for applications that do not require quantitative analyses of spectral information. Dandois & Ellis (2010) were perhaps the first to demonstrate the potential of UAV-acquired Image-Based Point Clouds (IBPC) for deriving canopy information in 3D. Since then, a number of studies have derived top-of-the-canopy heights in forests and artificial vegetation stands based on Canopy Height Models (CHM) generated from IBPC (e.g. Lisein et al., 2013; Torres-Sánchez et al., 2015; Zarco-Tejada et al., 2014). UAVs are increasingly used in order to assess disturbance impacts on vegetation and its recovery thereof. For instance, quantifications of insect tree damage (Klein Hentz and Strager, 2018; Näsi et al., 2015), the investigation of forest recovery from anthropogenic disturbances (Chen et al., 2017; Hird et al., 2017), and the identification of small-scale spectral variations in a post-fire environment (Fernández-Guisuraga et al., 2018) have been fulfilled from UAV-derived datasets. However, as UAVs are an emerging technology, the workflows for data processing remain to some degree experimental and a general knowledge on the performance of such datasets across different environments and observational settings is scarce (Dandois et al., 2015).

The remote sensing of fire is essentially a multi-temporal problem and covers two main foci: (i) the detection of fire and (ii) the study of its effects, whereas overlaps between the two exist. The obvious immediate effect of fire is a removal of biomass that is largely driven by the direct physical controls of fire and culminates in an individual fire's behaviour (Figure 1). The associated spectral

changes with an area burned may be tracked by an SVI or the differenced Normalized Burn Ratio (dNBR) from pre- and post-fire imagery (Lentile et al., 2006). Such indices are used as proxies for the determination of the ecological impact or the severity of fire (e.g. Lutz et al., 2011; van Wagtendonk et al., 2004). The severity essentially depends on the criteria considered. For instance, the fire severity of a grass fire may be high, i.e. the biomass removed is extensive, but the burn severity in this case is relatively low, as the grass community is likely to regenerate within the next rainy season. Furthermore, the long-term effects of fire such as the suppression of certain species or demographic legacies in the woody community, both of which are of interest for management purposes, require the study of the fire regime. Global remote sensing products provide a reasonable means to detect these spatio-temporal patterns of fire (Krawchuk and Moritz, 2014; Mouillot et al., 2014). With many remote sensing missions, the observational records are nowadays long enough to derive "fire normals" (*sensu* Lutz et al., 2011) that are characterized by the main parameters of a fire regime such as their spatial extent and temporal occurrence (Figure 1).

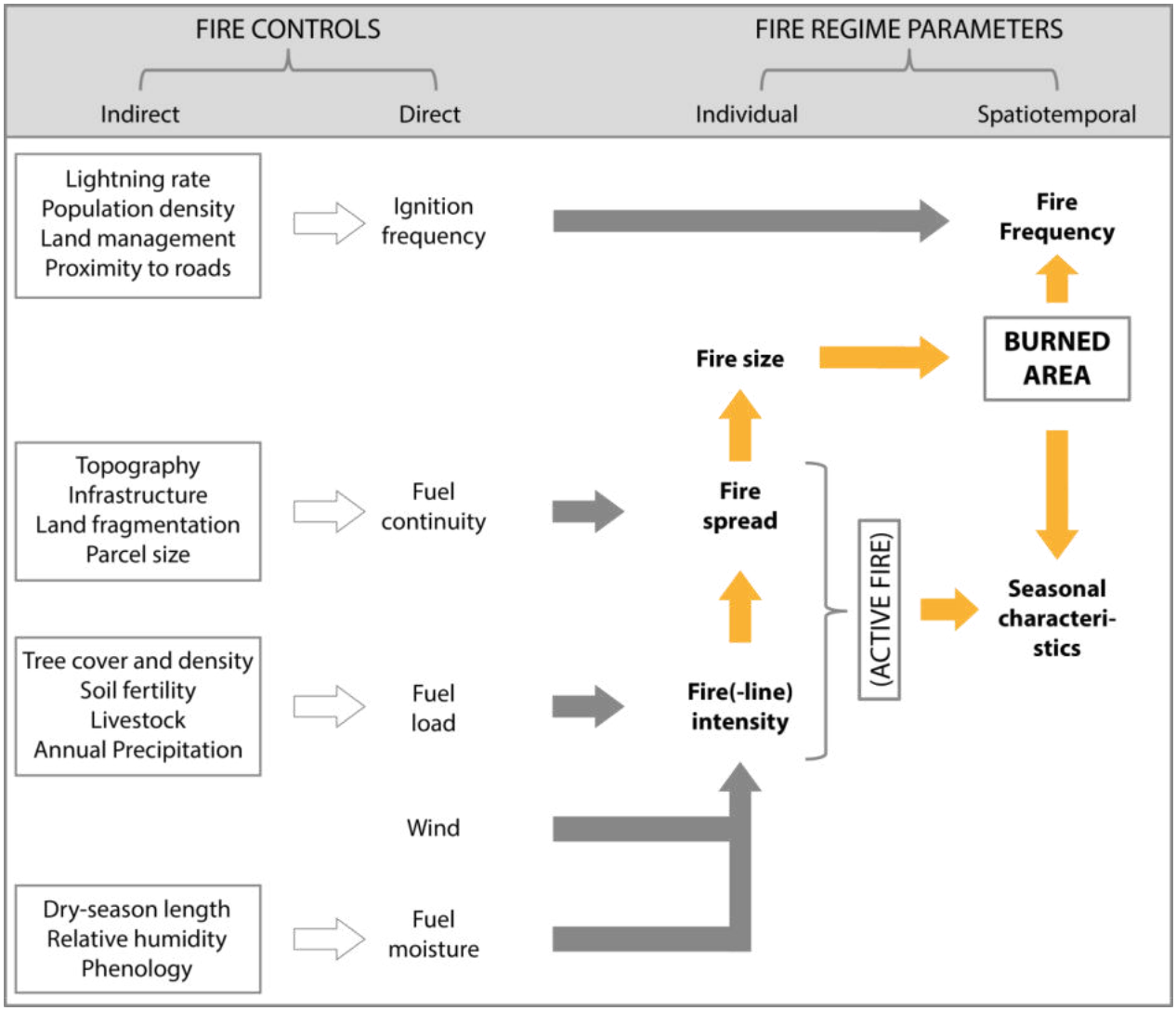

Figure 1: A conceptual model of fire controls and regime parameters (in bold) in the context of geospatial analysis. The model illustrates principal links between the direct physical controls of fire and the outcome fire (regime) parameters. Direct measurements of these controls are often difficult or even impossible (e.g. ignition) especially in post-hoc analyses. Therefore, measurable indirect controls work as a substitute. Fire regime parameters can be assessed from two types of globally available satellite products (in capital letters; the MODIS nomenclature is used). All geospatial datasets are given in boxes. Based on Archibald et al. (2009).

Two principal techniques are available for the detection of fire from remote sensing (Justice et al., 2002; Roy et al., 2011): (i) active fire detection from hotspots and (ii) post-fire Burned Area (BA) mapping. The energy released during combustion is detectable in certain spectra of the Mid-Wave Infrared (MWIR; 3,000-5,000 nm) and TIR (10,500-12,500 nm). Therefore, active fires can be detected by anomalies in these spectra, also in relation to their surroundings (Giglio et al., 2003). While this approach is accurate in terms of location and timing of a fire, its detective capabilities are limited by satellite overpass frequency and cloud obscuration, which typically results in an underestimation of the spatial extent of burning (e.g. Eva and Lambin, 1998; Roy et al., 2008). In contrary to hotspot detection, the removal of biomass and the residue combustion products, such as charcoal and ash, cause a variation in the spectral signal that is persistent on the short-term (Pereira, 2003; Trigg and Flasse, 2000). As a consequence, BA can be discriminated from multi-temporal approaches (e.g. Roy et al., 2005). While BA is regarded as being more reliable than active fire products, some general biases in global BA products are apparent and especially relevant to savannas (see Laris (2005)). Given the spatial resolution of 500 m of the MODIS BA product, an omission of low-intensity and small-sized fires is likely. Varying accuracies were retrieved in studies that evaluated MODIS BA using fire records based on high-resolution imagery. Laris (2005) reports underestimations of 90% in a West African savanna, whereas Roy and Boschetti (2009) find correct detections of up to 75% in Southern Africa. The most recent version of MODIS BA includes the active fire approach for an initial selection of BA candidates, which aims at higher detections of small fires (Giglio et al., 2016). Due to the global release in spring 2017, this version could not be applied for this thesis.

1.3. Research questions and hypotheses

The vegetation of dry savannas is affected by a number of factors, one of which is potentially fire. Fires are the result of a complex interplay of the biophysical framework and human actions in a region. Remote sensing provides unique means for the quantification of vegetation and an assessment of fire on a spatio-temporal basis. Optical remote sensing is prone to uncertainties in dry environments and UAV accuracy benchmarks and applications are evolving steadily. The present thesis is designed to contribute to current research from a thematic and a methodological perspective. It aims at the quantitative spatial modelling of vegetation and fire regimes in Namibia thereby using remote sensing as both a primary data input to statistical models and a technique that is a subject of investigation itself. As such, a number of remotely-sensed and other spatial datasets of varying scale are applied. This thesis focuses on some pending questions regarding the human component of fire and the ecology of fire in dry savannas.

Three main research questions are addressed within this thesis:

i. Which controls determine the fire activity across Namibia?

ii. How is dry-season vegetation captured in different approaches of optical remote sensing, and what is the role of scale?

iii. What is the impact of fire on the quantitative attributes of woody vegetation?

Taking into account prior research and current knowledge, three hypotheses are accordingly proposed:

Hypothesis 1: Namibia's fire activity generally follows a productivity gradient. Human activities have the potential to alter this relationship on smaller spatial scales.

Fire activity in dry savannas is fuel-limited. MAP depicts a primary control of productivity, and its importance for the resultant fire regimes has been confirmed in studies from Southern Africa (Archibald et al., 2009; 2010a) and specifically Namibia (Le Roux, 2011). Humans are the sole source capable to directly and deliberately manipulate fires and manage these. It is unclear if they eventually limit or facilitate fire at lower population densities. Humans may increase the occurrence but simultaneously limit the spatial extent of fire. Previous studies in the region largely determined the controls of fire from bivariate correlations and single predictive models. Fire regimes are, however, a highly multidimensional problem. A complete assessment of the governing controls behind Namibia's fire regimes and their relative importance are not available. Such fire regime modelling ideally includes a comparison of different predictive techniques in order to increase the robustness of results (Bar Massada et al., 2012).

Hypothesis 2: Regionally-calibrated, spectral estimates of green vegetation during the dry season deviate from those obtained with a global satellite product. Due to a coarser base resolution, the latter yields higher generalization and lower estimates of green vegetation.

Green vegetation in Namibia's Owamboland is largely restricted to riparian areas and certain woody species during the dry season. Highly heterogeneous patterns and generally low covers of green vegetation are thus present at this time of the year. Small-scale heterogeneity could obviously be more accurately captured by smaller entities of observation, i.e. at a higher spatial resolution. With sparse covers the contribution of surfaces and materials other than green vegetation to the spectral signals detected from remote sensing increases. In contrast to green vegetation, the spectral signals of non-photosynthetic vegetation and bare soil across the optical spectrum are both characterized by a roughly linear increase of reflectance with increasing wavelength. Background surfaces such as sandy soils could excessively contaminate the signals of green vegetation as a function of brightness. With the discrimination of green vegetation, such contaminations usually result in an underestimation, which may also be an issue of spatial resolution (Tian et al., 2002). Whereas mixed pixels are generally acknowledged as a problem apparent with spectral remote sensing, only little is known about the translation of background contaminations across spatial scales. Given the large extent of (seasonally-) dry regions and the frequent use of global remotely-sensed vegetation datasets such as MODIS LAI, their accuracy under dry-season conditions requires further investigation. Accordingly, previous studies from semi-arid regions have often found MODIS LAI to underestimate local or regional estimates of LAI (e.g. Scholes et al., 2004; Sprintsin et al., 2009; Tian et al., 2002; Zhang et al., 2007).

Hypothesis 3: The long-term fire regime is reflected by the vertical stand structure. Thus, the presence of fire leads to stand-scale height reductions of woody vegetation, which can be assessed using optical UAV data.

Fires in dry savannas are mostly of a low intensity, where their impact is often restricted to the surface stratum. Canopy scorching is, however, reported from Namibia's Kavango and Zambezi regions (Verlinden and Laamanen, 2006), and fire damage and mortality may essentially vary according to the species affected (e.g. Seymour and Huyser, 2008). The long-term presence of fire, as

opposed to its absence, should be expressed in a reduction of the average woody heights on stand scale. This effect is not necessarily the result of fewer adult individuals, but rather a larger proportion of small individuals that are inhibited in reaching adult heights. It is hypothesized that IBPCs, which can be derived from ultra-high resolution UAV imagery, provide sufficient accuracies to detect such disturbance legacies in the 3D stand structure. The discontinuity of savanna canopies could be beneficial to the autonomy of UAV systems, as ground points are not obscured and the base heights of woody vegetation may be extracted from the IBPC (e.g. Jensen and Mathews, 2016). Dry-season phenology, which includes partly leaf-off conditions, could be beneficial in this regard but may complicate the retrieval of height information from woody individuals.

2. MATERIALS AND METHODS

2.1.Study areas

Namibia is a dry country. Climate is hyper-arid along the coast but sub-humid conditions with up to approximately 700 mm Mean Annual Precipitation (MAP) characterize the Zambezi region of North-Eastern Namibia (Mendelsohn et al., 2002). Although inter-annual rainfall variability is generally high, a significant increase in precipitation has been observed across Southern Africa in recent decades, which has been attributed to a strengthening of the Walker cell (Maidment et al., 2015). Indeed, parts of North-Western Namibia have received higher precipitation amounts since 2000, and a greening trend has been observed in the North-East (Hoscilo et al., 2015). This greening may, however, also be indicative of woody encroachment. Vegetation structure largely follows the climatic gradient from south-west to north-east (Mendelsohn et al., 2002). Only sparse grass cover is found along the coast. Shrublands of the Karoo are located in the south but reach far north along the highlands of the Great Escarpment. Savannas that range from feather-leaved shrublands to broad-leaved woodlands characterize Central and Northern Namibia, respectively. Soil depth and minimum temperatures generally increase towards the Kalahari Basin in the east, and depict further determinants of vegetation across Northern Namibia (Mendelsohn et al., 2002). Azonal formations, such as with the Cuvelai drainage in Owamboland or along (ephemeral) rivers, reflect the edaphic situation.

Livestock ranging is a widely spread practice throughout Namibia. The "veterinary fence"[3] marks a segregating line – not only for historical reasons. It largely separates communally-administered lands in the north from privately-held, commercial rangelands in the south that are important for meat production and export (Figure 2). Where the population density of Namibia is generally among the lowest worldwide, a considerable proportion of the country's rural population live in the northern regions, especially in Owamboland. Overall, 14% of the country is owned by the government, with protected areas covering large portions thereof (Mendelsohn et al., 2002).

The research conducted within this thesis considered three different study areas which are depicted in Figure 2. The fire regime was investigated at the national scale and involved all areas that experienced fire within the period of 2000–2016. In addition, two (case) study areas were located in Owamboland and the northern Otjozondjupa region. Both of these were selected with regards to distinct environmental heterogeneity and human-related gradients. For instance, the study area in Owamboland covers a strong decrease in population density from north to south. Natural vegetation in Owamboland is diverse: broad-leaved shrub- and woodlands are interspersed by ephemeral water bodies and saline grasslands in the lowlands (Mendelsohn et al., 2000). The study area in northern Ojtozondjupa emphasized the variations in land use and tenure that are accompanied by differences in grazing intensity and fire regime (Le Roux, 2011; see also Figure 3). Further information on the study areas is given in the respective sections of the manuscripts (Chapters 4, 5, 6).

[3] Veterinary fences were built across Southern Africa in order to prevent livestock from animal diseases. In Namibia, initial veterinary fencing occurred around 1900, but its present-day extent results from the exhaustive efforts to control recurring outbreaks of foot-and-mouth disease during the 1960s.

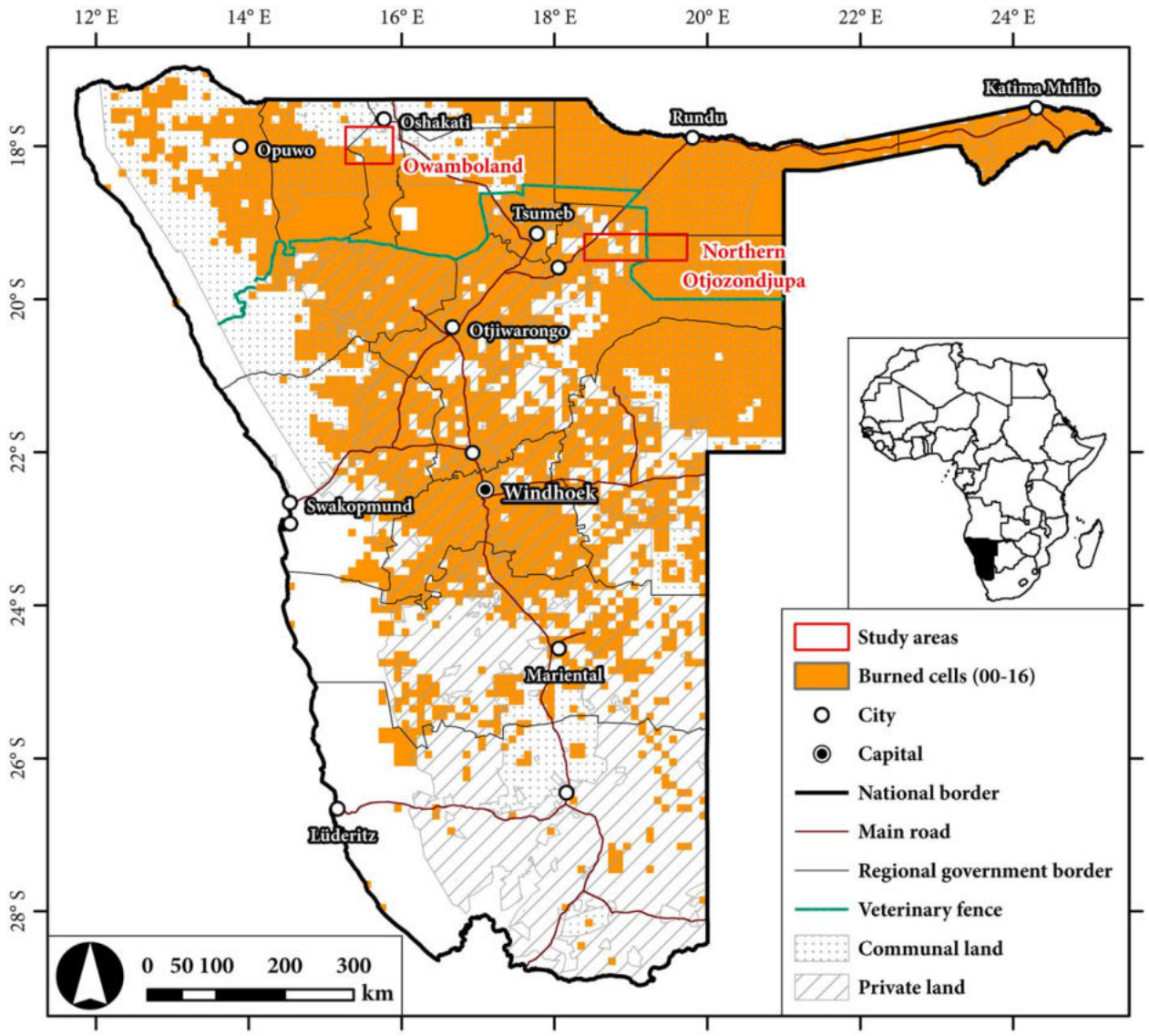

Figure 2: The study areas in Namibia. The map shows the extent of fire at 0.1°-resolution from 2000 to 2016 (burned cells in orange) as well as the two (case) study areas (in red) in Owamboland and northern Otjozondjupa. All burned cells were included in order to model the fire regime of Namibia. The Leaf Area Index (LAI) was modelled in Owamboland, and stand-scale heights of woody vegetation were assessed in the northern Otjozondjupa region.

2.2. Field data

Field measurements in remote areas are usually conducted with a limited amount of time available. Hence, efficient sampling strategies that explicitly target the study objectives are needed. A prior consideration of the extent and heterogeneity of the area, scale and accuracy requirements, validity in terms of representativeness and sample size, as well as the purpose of the survey are thus vital (McCoy, 2005). The specific purposes of the field data applied within this thesis were to calibrate spectral data for a biophysical parameter of vegetation, namely LAI, on the regional scale (Chapter 2.2.1) and to verify a remotely-sensed model of canopy height on stand-scale (Chapter 2.2.2). Both

purposes consider field measurements as the reference data[4] of the current vegetation condition for remotely-sensed datasets. As a consequence, these time-critical measurements and ancillary data ought to be collected close to the timing of the remote sensing observations in order to reflect their spectral and spatial properties (Jones and Vaughan, 2010; Lillesand et al., 2008). All sampling plots were also geo-located using a hand-held Global Navigation Satellite System (GNSS)-receiver with Geographic Information System (GIS)-capability.

As Curran and Williamson (1985) conclude, capturing the variability at all spatial scales is of outmost priority when collecting reference data for remote sensing. Although this view appears futile in a strict sense, the importance of capturing scale-dependent variability efficiently is also recognized in vegetation ecology (e.g. Roleček et al., 2007). A two-step scheme consisting of a plot selection and the actual measurements conducted on sub-plots was applied to address these needs:

i) Stratification, i.e. the categorization of a landscape by some comprehensible criterion such as vegetation structure or disturbance regime, was an important initial consideration in the field. Also with regards to accessibility and logistics, plot selection aimed at representative entities of the stratification and a maximum of intra-plot homogeneity. Admittedly, the latter is generally difficult to achieve in savannas. A preferential plot selection is prone to bias and generally violates statistical randomness in the first place. Likewise it is highly efficient in capturing gross ecological heterogeneity from representative units (Roleček et al., 2007).

ii) Sampling on sub-plots was conducted using systematic approaches. Although true statistical randomness was once again lacking, these intended to adequately resolve intra-plot heterogeneity of vegetation structure in a consistent and objective manner.

2.2.1. Leaf Area Index

The Leaf Area Index (LAI), i.e. the one-sided (projected[5]) leaf area per area horizontal ground, is one of the most widely used canopy descriptors (Ollinger, 2011). A field-based estimation of LAI is either destructive, i.e. leaves are harvested, or indirectly estimated from canopy light interception measurements that often use the gap fraction approach (Bréda, 2003; Jonckheere et al., 2004). As all canopy elements contribute to light interception, indirect methods measure a Plant Area Index (PAI) in a strict sense. Phenology and spatial clumping of foliage and individuals further complicate the estimates of real LAI in savanna ecosystems (Ryu et al., 2010).

A dataset of indirect LAI estimates from 109 plots and ancillary data[6], which originated from the author's diploma thesis (Mayr, 2012), was applied here. As canopy structure and productivity in the region largely follow edaphic conditions and human activities (Mendelsohn et al., 2000), sampling plot selection took into account the compositional and structural properties of the vegetation and topographic elevation. Plot size was chosen with regards to the spatial properties of the RapidEye imagery (Chapter 2.3.7). Following the Validation of Land European Remote sensing Instruments (VALERI) project (Garrigues et al., 2002), a systematic sampling approach, using regular intervals

[4] Classical remote sensing terminology refers to "ground truth", which is somehow misleading as it implies an absolute accuracy of the field measurements (Jones and Vaughan, 2010).
[5] Definitions vary with application. Projected leaf area includes leaf angular distributions as seen from above and is related to the remotely-sensed estimation of LAI. One-sided leaf area emphasizes on biosphere-atmosphere interaction, and is most common with field measured LAI.
[6] E.g. dominant species, relative terrain position, and total plant cover.

along two perpendicular intersecting transects was adapted and applied for the creation of this dataset.

2.2.2. Woody heights

Gradients of fire frequency and grazing impacts were the main criteria of stratification and preceded the selection of plots used for height measurements. These prevailing disturbance regimes, which were retrieved from expert interviews, field recognition, and satellite observations, were assumed to be indicative of the long-term situation. Further conditions for plot selection were related to the requirements of the UAV mission (Chapter 2.3.8), and included even terrain and moderate canopy cover. Along a regular grid of points, upward facing hemispherical photographs were taken as part of a related M.Sc. thesis (Malß, 2017). Rather than applying a fixed radius around the grid points, all individuals of woody vegetation >1.5m that were contained within the photographs were instantly sampled. Height was derived from trigonometric measurements using a laser device with angular capabilities and a magnifying scope. The trigonometric method[7] is prominent in forestry as it is fast and provides realistic accuracies of 0.1-0.5 m (West, 2015). As the scope was oriented towards plot heights rather than individuals, per-plot averages and maxima were calculated to represent the stands' vertical structure.

2.3. Spatial data and products

A large set of spatial datasets (raster and vector) from different sources were applied within this thesis (Table 1). This section lists their main properties. Aerial surveys were conducted by means of an Unmanned Aerial Vehicle (UAV). Spatial referencing of the UAV datasets was obtained *post hoc* using photogrammetric methods (Chapter 2.4.3). Nevertheless, the UAV data are listed here as well.

2.3.1. Lightning rate

Until April 2015, the Lightning Imaging Sensor (LIS) aboard the Tropical Rainfall Measuring Mission (TRMM; Kummerow et al., 1998) recorded instant brightness variations from lightning along a latitudinal belt of ±38° around the equator. Where night-time optical discrimination of lightning appears straightforward, the day-time detection rates from LIS are approximately 70% (Albrecht, 2016). With the Very High Resolution gridded lightning Monthly Climatology (VHRMC) dataset (Albrecht et al., 2016), LIS observations from 1998 to 2013 are processed to yield monthly flash rate densities at 0.1°-resolution. As lightning is a potential source of ignition, the LIS-VHRMC of the respective dry-season months was included here in order to study Namibia's fire regimes.

[7] Trigonometric height estimation combines one distance measurement and two angular measurements at ground- and top level, respectively.

2.3.2. Precipitation

Monthly and 10-day precipitation estimates for the African continent are available from the Tropical Applications of Meteorology using Satellite data and ground-based observations (TAMSAT) dataset (Tarnavsky et al., 2014). Building on several METEOSAT observations per day, TAMSAT covers a continuous record from 1983 to present at a resolution of 0.0735°, which corresponds to approximately 4 km. Based on the simple premise that cloud height is proportional to the amount of precipitation, cloud-top temperatures as detected from Thermal Infrared (TIR) imagery allow for the estimation of precipitation – at least in convective systems. However, as Kidd and Huffman (2011) note, this relationship is indirect and affected by regional and temporal variations. As a consequence, TAMSAT combines TIR observations with a regional calibration based on historical gauge records (Tarnavsky et al., 2014). Gauge records are sparse and generally decreasing in numbers across Southern Africa (Hughes, 2006; Layberry et al., 2006). In addition, their spatial representativeness is limited in convective precipitation regimes. TAMSAT was preferred over gauge-only and more sophisticated satellite products, such as the TRMM Multisatellite Precipitation Analysis (TMPA) product (Huffman et al., 2007), within this thesis due to its long-term reliability as well as spatial resolution and consistency.

Dataset	Temporal coverage	Spatial resolution	Temporal resolution	Usage
MCD45A1 v5.1	2000-2016	500 m	monthly	fire regime
MOD13A1 v6	2000-2016	500 m	16-day	NDVI phenology
LIS-VHRMC	1998-2013	0.1°	monthly	dry-season lightning
TAMSAT v2	1998-2016 (1983-2016)	0.0375°	monthly (10-day)	precipitation
SRTM v4.1	2000	3-arc sec.	static	terrain
OSM	Dec 2016	-	static	road network
AON/EIS	various	-	static	various biophysical and human-related variables
RapidEye L3A	Nov 2010	6.5 m	static	5 bands
MOD15A2 v5	Nov 2010	1 km	static (8-day)	LAI
UAV	Sept 2015	<2 cm	static	CHM

Table 1: Overview of the spatial datasets used in this thesis. Horizontal lines between the datasets distinguish the datasets according to their main application in the manuscripts of this thesis. Note that the spatial coverage and temporal resolution are only given as applied here and may differ from the general availability of the dataset.

2.3.3. Terrain

A Digital Elevation Model (DEM) of global coverage at three-arc seconds[8] is provided by the Shuttle Radar Topography Mission (SRTM). Where vertical errors of the DEM are generally <16 m, missing data in regions with low textures, such as deserts, were largely filled with the newest release of the dataset (i.e. version 4.1; Jarvis et al., 2008). Surface roughness, i.e. the elevation range covered by the cells surrounding a central pixel in a DEM (Wilson et al., 2007), was calculated from the SRTM DEM as a surrogate of terrain properties that potentially influence the spread of fire.

2.3.4. MODIS products

The Moderate-resolution Imaging Spectroradiometer (MODIS) aboard the Aqua and Terra satellites is one of the most prominent Earth observation missions. It provides global coverage within two days and covers 36 spectral bands (visible to TIR) with spatial resolutions from 250 m to 1 km thereby facilitating a large suite of land, ocean, and atmospheric applications and the monitoring thereof (Lillesand et al., 2008). Numerous readily-processed products are derived from spectral MODIS data. Three MODIS land products (Justice et al., 1998) were used in this thesis and are listed in the subchapters below.

2.3.4.1. Burned Area

The MODIS Burned Area (BA) product (MCD45A1 version 5.1) is delivered monthly and at a resolution of 500 m. It maps the recent burning of pixels and assigns the approximate date of first occurrence with a detection precision of $\pm$ eight days (Roy et al., 2008). Daily Terra and Aqua MODIS surface reflectances of the previous and following months are partly included in the derivation of BA of a respective month. The algorithm is a bi-directional reflectance model-based change detection approach described by Roy et al. (2005): spectral variations due to sensor-viewing and illumination conditions are predicted across time[9] and compared to the respective observed reflectances in order to discriminate consistent and significant changes in the NIR and two SWIR bands, which are sensitive to burned surfaces. A MCD45A1-record that covered the period from April 2000 to March 2016 was applied in order to derive the fire regime parameters for Namibia and to investigate their controls.

2.3.4.2. Vegetation Index

Similar to the considerations described in Chapter 2.4.1, two proxies of vegetation greenness are contained in the MODIS Vegetation Index product (MOD13A1; Huete et al., 2002). First, the Normalized Difference Vegetation Index (NDVI), which is probably the most widely used remotely-sensed vegetation proxy, and second the Enhanced Vegetation Index (EVI). These are both delivered at a 500 m-resolution. Version 6 of MOD13A1 constitutes a 16-day Maximum Value Composite (MVC) where the compositing value of a pixel is determined by a consideration of the two highest observations of NDVI (if available) and their viewing angles[10], respectively (Didan et al., 2015). As saturation problems that are typically related to NDVI in regions of high biomass (Huete et al., 2002)

[8] Three-arc seconds correspond to a spatial resolution of approximately 90m at the equator.
[9] A minimum of 16 days is considered, which is extended (e.g. due to the presence of clouds) until at least seven observations are reached (Boschetti et al., 2013).
[10] Observations closer to nadir view are preferred in this procedure.

were not expected to occur in Namibia, NDVI was preferred over EVI in order to derive phenological metrics (see Chapter 2.4.2).

2.3.4.3. Leaf Area Index/Fraction of absorbed Photosynthetically Active Radiation

The MODIS LAI/Fraction of absorbed Photosynthetically Active Radiation (FPAR) product (MOD15A2; Myneni et al., 2002) applies a physical approach to produce the per-pixel output LAI/FPAR at a resolution of 1 km. The algorithm, which is described by Knyazikhin et al. (1998), is based on the inversion of a 3D Radiative Transfer Model (RTM)[11]. However, different inversion solutions may lead to the same simulated reflectance – known as the ill-posed inverse problem (Combal et al., 2003). In order to constrain the set of possible solutions, the MOD15A2 algorithm applies biome-specific parameterizations for the typical spectral reflectance and their respective uncertainties in so-called Look-Up Tables (LUT). If several solutions are available, their average is used to compute the daily LAI retrieval. Otherwise, an empirical back-up algorithm is applied and is based on the NDVI (Knyazikhin et al., 1998). In compositing, daily LAI retrievals are then selected using the maximum FPAR value across an eight-day period (Yang et al., 2006). Only a single eight-day composite of MOD15A2 that had the highest temporal agreement with the RapidEye imagery (Chapter 2.3.7) was selected for this thesis.

2.3.5. Environmental Information System of Namibia

The Environmental Information System of Namibia (EIS; www.the-eis.com) hosts a bulk of publications and (spatial) datasets from different contributors. Among these are spatial datasets from the Atlas Of Namibia (AON; Mendelsohn et al., 2002), which is probably the most comprehensive, complete and accurate source of socioeconomic and environmental data for Namibia. For instance, gridded population density from this source includes the national census as well as regional population surveys from different government directorates. Overall, the estimated total population of Namibia was 3% higher as compared to census-only estimates (Mendelsohn et al., 2002). Given the regional abundance of informal settlements in Namibia, the population dataset as provided by the AON is intended to be superior to global spatial datasets, such as Gridded Population of the World (Doxsey-Whitfield et al., 2015), and to reflect the spatial distribution of the rural population with higher accuracy.

2.3.6. OpenStreetMap

OpenStreetMap (OSM) is a mainly volunteer-based global mapping project that is distributed under the CreativeCommons BY-SA 2.0 license[12]. OSM is a serious source of vector map data, also in developing countries, and its dynamics have gained attention in the field of rapid response and disaster mapping (e.g. Zook et al., 2010). In order to derive a complete road network of Namibia, a full extract of the OSM database (Geofabrik and OpenStreetMap contributors, 2016) was used in this thesis. Roads can impact fire in different ways. For instance, roads separate the landscape and may

[11] A RTM generally describes the relationship between a set of canopy characteristics (e.g. LAI, canopy cover, and background soil contribution), i.e. the input, and spectral reflectance, i.e. the output. Given a proper RTM, the more inputs are known, the more accurate the outputs will be.
[12] See https://creativecommons.org/licenses/by-sa/2.0/ for further information.

inhibit the spread of fire. Road density may be a proxy for ignitions due to negligence, but at the same time enhances the accessibility for fire fighting activities.

2.3.7. RapidEye

RapidEye is a five-satellite constellation offering five spectral bands (from blue to NIR) at a spatial resolution of 5 m, which is resampled from a nominal resolution of 6.5 m (RapidEye AG, 2011). Further technical details on the mission are given by Tyc et al. (2005). At present, RapidEye is part of the commercial brand Planet Labs Germany, but imagery was formerly available at no cost for scientific applications through the RapidEye Science Archive (RESA) hosted by the German Aerospace Centre (DLR). This thesis applied a single scene of orthorectified and sensor-calibrated RapidEye imagery (Level 3A). RapidEye's high resolution was intended to adequately capture vegetation in its spatial heterogeneity. A notable feature of the sensor's multispectral configuration is a red-edge band (690-730 nm) as it may improve the derivation of canopy parameters from RapidEye imagery in low-productivity regions (e.g. Li et al., 2012; Ramoelo et al., 2012; Schumacher et al., 2016). However, other studies that applied Rapid Eye's red-edge band in arid environments report no improvements thereof (e.g. Ehammer et al., 2010; Zandler et al., 2015).

2.3.8. Unmanned Aerial Vehicle surveys

UAVs have matured to serious remote sensing systems that allow autonomous and flexible data acquisition at potentially high resolutions (Colomina and Molina, 2014; Nex and Remondino, 2014). However, aerial surveys with such systems require considerable pre-survey preparation and post-processing to yield meaningful spatial data (see Chapter 2.4.3).

In accordance with the field measurements described in Chapter 2.2.2, 19 flights were carried out using a Soleon Coanda x12 multi-rotor UAV. Compared to fixed-wing UAVs, multi-rotor UAVs provide only a limited spatial range, where the area sampled within a single flight is typically small, but benefit from increased stability during the flight and vertical take-off/landing near or within the sampling plots. With regards to the aims of this aerial survey, a sufficient spatial resolution and overlap of the imagery were two major prerequisites in order to allow for a posterior 3D reconstruction of canopy elements (Dandois et al., 2015; Salamí et al., 2014). The imaging sensors aboard the UAV were two consumer-grade cameras, Nikon 1 V3, both with a sensor size of 13.2 × 8.8 mm and a respective resolution of 18.4 megapixels. Focal lengths were fixed to 10 mm in order to cover a large field-of-view. Taking into account the optical properties of the sensors, the routes for autonomous sampling by means of an autopilot were planned using waypoints in a "lawnmower mode" (Anderson et al., 2014). These routes were programmed with a flight altitude of 60-70 m and waypoint densities facilitating an image acquisition with nominal sideward and forward image overlaps of 50%. This setup generally yielded a spatial resolution of <2 cm and with each object along the inner flight lines being contained by approximately four images taken from different angles. In order to ensure consistent overlaps across the entire plots of field sampling, the aerial coverage was larger and planned with a spatial buffer around the field plots.

The UAV mission yielded a total of 29 gigabytes of raw imagery. Flight telemetry from the UAV's integrated Inertial Navigation System (INS)/GNSS unit contained – among numerous other

parameters – the position, orientation, and altitude of the UAV during image acquisition. The mentioned telemetry parameters were essential for the *post hoc* derivation of spatial information from the imagery (see Chapter 2.4.3). All flights were carried out under clear skies and at high solar angles in order to largely avoid radiometric variations as a result of illumination conditions and shadows, both of which would complicate the post-processing of imagery (Carrivick et al., 2016; Dandois et al., 2015). Quantitative spectral analyses, such as the derivation of SVI (Chapter 2.4.1), were not achievable as the cameras lacked the necessary radiometric calibration (Candiago et al., 2015). Unfortunately, a LiDAR system, which is often argued to be the most accurate system for aerial 3D applications (Dandois and Ellis, 2010; Leberl et al., 2010; Ota et al., 2015), was not available for this thesis.

2.4. Data processing

2.4.1. Spectral vegetation indices

Mathematical combinations of spectral bands represent a classic tool in the field of optical remote sensing. Owing to the characteristic spectral response of the materials contained, adequate band combinations facilitate the discrimination of different target surfaces and ideally reduce the signal variations caused by atmospheric properties, sensor viewing geometry, terrain or surface background signals (Baret and Guyot, 1991; Jones and Vaughan, 2010). With regards to green foliage, strong absorptions by chlorophyll across the visible spectrum and by cell water content in certain spectra of the SWIR, respectively, contrast with the high reflectance of vital cell tissue in the NIR. As such, the combination of spectra results in potentially useful information for the study of vegetation. For instance, combinations incorporating the red and NIR are frequently applied, as their contrast is sensitive to the amount and vitality of vegetation present. A vast list of SVIs of varying complexity and (sensor-specific) spectra have been proposed (see Bannari et al. (1995) for an overview) in order to quantitatively derive and monitor vegetation and its condition.

Considerable uncertainties are associated with the application of satellite-based SVI and real-world canopies. Firstly, as a function of spatial resolution of the sensor, the spectral signal detected is a spatial average across the entity of observation, i.e. the pixel. Secondly, radiative transfer at vegetated surfaces is complex (Jones and Vaughan, 2010; Ollinger, 2011; Sellers, 1985): foliage arrangement (e.g. leaf angles) and chemical properties, non-photosynthetic canopy components (e.g. litter, stems, fruits, and flowers), but also shadows and background conditions (e.g. soil, understorey vegetation) all contribute to the spectral signal detected. When considering the low to moderate plant covers of dry savannas, their distinct spatial clumping of individuals, and the offset phenology (e.g. green canopy vs. senescent herbaceous understorey), the spectral signals of green vegetation are likely to be complicated. Although SVI are accepted proxies for biophysical (e.g. aboveground biomass, LAI, and fractional cover), and biochemical (e.g. nitrogen, chlorophyll) properties of vegetation, they often only yield moderate correlations with field-measured quantities (Glenn et al., 2008; Sellers, 1985). Furthermore, no single SVI has been identified as “the best” across different species, canopy architectures, and leaf structures (Huete, 2014; Viña et al., 2011). In order to relate field-measured properties of vegetation to their representation in satellite imagery, a large set of sensor-specific candidate SVI had to be considered (see Chapter 5 for a full overview).

2.4.2. Time series analysis

A distinct feature of operationally-produced remote sensing data is the potential to monitor ecological processes and phenomena based on the temporal integration of systematic discrete time steps. Each individual raster in the temporal domain covers the same spatial extent and resolution, i.e. the spatial domain. Resultantly, per-pixel analyses may be performed similar to non-spatial time series. Given a sufficient temporal record (e.g. 2000-2016 in case of the MODIS products), the typical behaviour[13] in terms of time and magnitude of an observed variable can be characterized according to its temporal aggregation and descriptive statistics. For instance, per-pixel TAMSAT monthly precipitation sums were aggregated to annual sums[14] and subsequently averaged across the full period of observation to yield MAP.

The calculation of metrics from satellite time series suffers from data gaps and quality issues. Temporary instrument failure, limited observations due to prolonged cloud cover (in the case of land surface products), as well as atmospheric, and sensor-viewing properties may contribute to time series gaps and observations of varying quality (Eklundh and Jönsson, 2017; Goward et al., 1991). As a consequence, satellite time series are often delivered in aggregated time steps, which also holds benefits for their processing performance. MODIS products are made available with a Quality Assurance (QA) layer that indicates the quality of retrieval for each pixel. Accordingly, the MODIS time series used within this thesis (MCD45A1 and MOD13A1; see Chapter 2.3.4) were filtered to include only retrievals of highest quality. This constrained the MCD45A1 BA record (see Figure 3), while intending to increase its reliability.

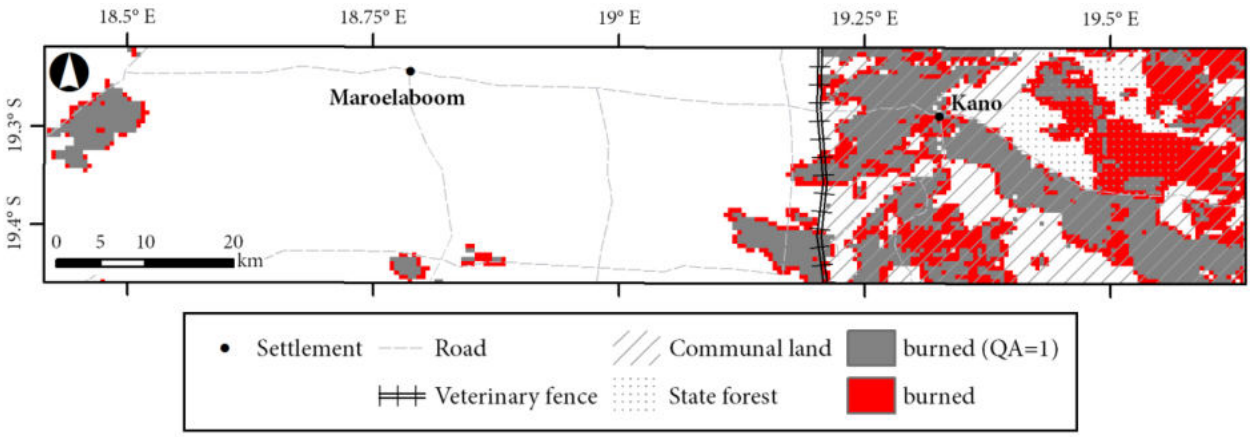

Figure 3: Exemplary illustration of the MCD45A1 Quality Assurance (QA) layer for the study area in northern Otjozondjupa, Namibia. Burned area sums from April 2012 to March 2013 (in red) were filtered to highest-quality retrievals only (QA=1; in grey).

As NDVI time series, such as the MOD13A1 product, are sensitive to changes in green vegetation, they facilitate the derivation of phenological metrics. In order to close the gaps arising from quality filtering and to deal with noise in the data, smoothing functions, which are fitted per-pixel, are usually applied. Noisy observations frequently introduce a negative bias. Hence, smoothing functions intend to fit to the upper envelope of the data (Eklundh and Jönsson, 2017). The present thesis fitted

[13] Different terminologies are used within scientific disciplines to describe the typical behaviour of a variable: e.g. climatologies in atmospheric sciences, or fire regime (parameters) in fire ecology, respectively.
[14] Annual sums of precipitation were calculated from September to August of the next year with regards to the initialization of the rainy season across large parts of Namibia.

the MOD13A1 NDVI record using a double logistic function (Beck et al., 2006). The suitability of the double logistic function for unimodal growing seasons has been confirmed across various canopy architectures (e.g. Atkinson et al., 2012; Butt et al., 2011; Fischer, 1994; Hird and McDermid, 2009). Seasonally-decomposed phenological metrics were then averaged per pixel and across the NDVI record. However, a trend analysis, as has been performed on comparable datasets (e.g. Andela et al., 2017; Brandt et al., 2016; Fensholt et al., 2009; Maidment et al., 2015), was beyond the scope of this work.

2.4.3. Unmanned Aerial Vehicle photogrammetry

Photogrammetry generally aims at making measurements from imagery. Established photogrammetric methods for aerial triangulation[15] were not designed for surveys using an UAV (Colomina and Molina, 2014). Their inefficiency with the use of UAV imagery arises from uncalibrated cameras in terms of lens geometry and distortion, and the irregularities in image acquisition such as variations in overlap and camera attitude, i.e. the 3D position and orientation. Thus the determination of interior and exterior image orientations and the 3D scene reconstruction thereof are nowadays frequently accomplished by computer vision techniques (Carrivick et al., 2016; Colomina and Molina, 2014). The Structure-from-Motion (SfM) - Multi-View Stereopsis (MVS) approach provides a flexible, yet to some degree arbitrary, framework to process UAV imagery (see Westoby et al. (2012), or Carrivick et al. (2016) for detailed overviews). In brief, so-called tie points, which are based on the recognition of common scale-invariant features among the imagery (e.g. Lowe, 2004) are initially identified with SfM-MVS photogrammetry. From the tie points, camera position and orientation are estimated, and planar image points are re-projected into 3D coordinates. The product of this bundle (block) adjustment is a sparse Image-Based Point Cloud (IBPC). At this stage, spatial reference data, such as high-accuracy Ground Control Points (GCP), are introduced in order to optimize the absolute positioning of the sparse IBPC. As absolute spatial accuracy was not a priority here, only the flight telemetry data from the on-board INS/GNSS (see Chapter 2.3.8) were used for spatial referencing. Subsequently, computationally intensive MVS algorithms that iteratively optimize the 3D reconstruction using textural image information and filtering procedures were applied. The resultant dense IBPC was then spatially interpolated in order to yield a Digital Surface Model (DSM) and to derive an orthomosaic (see Figure 4).

2.4.4. Derivation of canopy height

The estimates of canopy height from 3D remote sensing data, i.e. a Canopy Height Model (CHM), may provide spatially consistent insights into stand structure. In a first step, a CHM was derived from the difference in height between the canopy and ground level (Chen et al., 2006). In order to adequately reflect the stand structure, a delineation of individuals and their maximum height from the CHM was necessary. However, this is admittedly a difficult task when it comes to connected crowns with similar heights of individuals, or irregularly shaped crowns. Hence, open and uneven canopies in savannas should be fairly well suited for an automated delineation as compared to closed forest canopies. Several methods are reported in the literature, which are reviewed by Ke and Quackenbush (2011) and, with a focus on LiDAR, by Zhen et al. (2016). Rather than a survey-grade, high-resolution DEM of the solid ground which was not available for northern Otjozondjupa, a

[15] Aerial triangulation describes the process of solving orientations and positions for a set of overlapping imagery with the aim of producing a single aligned image.

separate DEM was derived from a classification of the ground points contained in the dense IBPC (Chapter 2.4.3.). Watershed segmentation was then performed on the CHM, whereby crowns were "filled" around local maxima points.

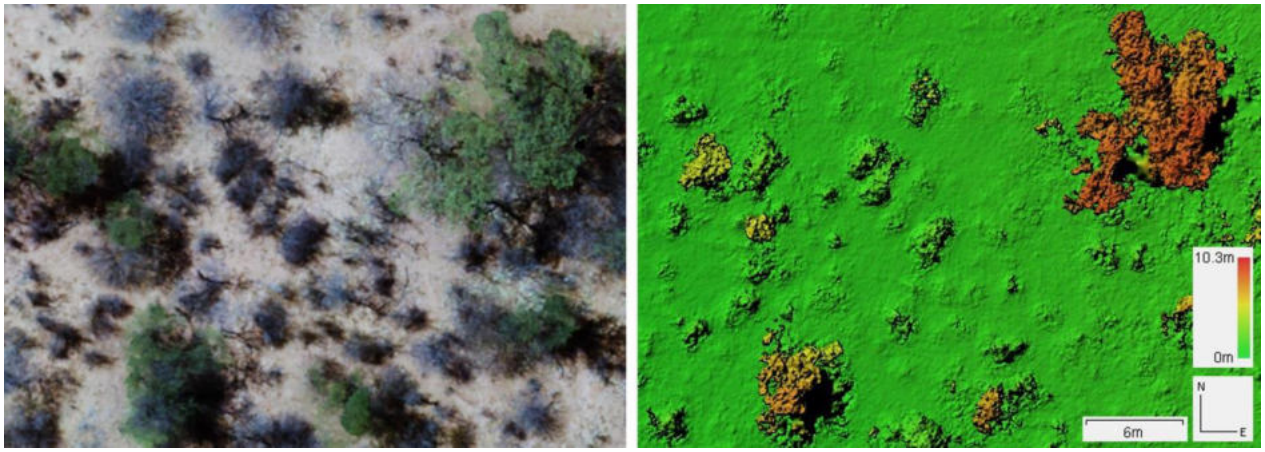

Figure 4: Exemplary orthomosaic (left) and hill-shaded Digital Surface Model (DSM; right) near Farm Rooidag, Namibia, that were created using Unmanned Aerial Vehicle (UAV) photogrammetry.

2.4.5. Spatial aggregation and upscaling

Several datasets of different resolution and type (e.g. raster vs. vector) were included in this thesis. In order to facilitate their combined analyses, each dataset had to be aggregated to the resolution of the coarsest respective dataset. The preservation of a maximum of information across scale is a central question in these regards (Hay et al., 1997). One should be aware that different scales of observation may result in different implications drawn thereof – an issue more generally known as the Modifiable Areal Unit Problem (MAUP; Dark and Bram, 2007).

Also data conversions, such as from vector- to raster data format, are likely to introduce errors in shape as a function of the raster's resolution. Spatial aggregation, as was achieved with resampling techniques and descriptive functions, is usually accompanied by a reduction in variance (Hay et al., 1997). Variance reduction may also be desirable for smoothing noisy data and to enhance processing performance, as was done with the output UAV CHM. A special case of spatial aggregation was the upscaling from discrete point measurements of vegetation attributes to satellite imagery where a statistical model determined the required transfer function (see Chapter 2.5.1).

2.5. Predictive Modelling

Predictive models aim at revealing the relationships within a set of data with the intention to forecast, i.e. to predict, a certain outcome variable (Kuhn and Johnson, 2013). An initial understanding of the problem context is therefore essential to yield meaningful models. By selecting relevant data and processing it in an adequate modelling framework forecasting can be envisaged. Adequacy of the prediction is determined by the stated modelling problem in combination with the data's characteristics, such as dimensions, variable type(s), and expected relationships among the

variables. Two different predictive modelling problems of varying complexity[16] were addressed in this thesis. These are briefly outlined below.

2.5.1. Upscaling using linear regression

Field measurements are probably the closest approach to reality in terms of accuracy and scale. However they are mostly of a discrete spatial nature. Remote sensing measurements are usually consistent in space and certain spectral bands are sensitive to green vegetation (Chapter 2.4.1). Spectral information, as synthetized by a SVI, can be indirectly related to field-measured canopy parameters using a statistical model. Thus, remote sensing is used as a scaling tool with the intention to extrapolate information in space. Empirical-statistical modelling, or upscaling, is a standard tool in the evaluation and validation of global-scale satellite products on a regional basis (Justice et al., 2000; Liang et al., 2002; Morisette et al., 2006). Upscaling is usually performed on high-resolution imagery as an intermediate step. Simple linear regression models that relate plot-averaged LAI samples, i.e. the response, with the averaged SVIs of the corresponding RapidEye pixels were conducted here. The final model was selected based on the highest agreement as outlined by the coefficient of determination (R^2). Non-linear models were not considered due to the low range of LAI in Owamboland. The application of non-linear transfer functions in heterogeneous environments also introduces a scaling bias, which would have necessitated further corrections (see Garrigues et al., 2006; Jiang et al., 2018).

2.5.2. Fire regime modelling

Conceptually, the complexity behind a fire regime arises from the interaction of multiple environmental and human-related processes (Figure 1). This complexity of processes is translated to statistics as predictor variables. Predictors indirectly measure one or more processes at different scales, include different data types (e.g. continuous vs. categorical) and distributions, and may show various relationships (e.g. (non-) linear or additive) with the fire regime or other predictors. An ideal modelling framework should be able to sufficiently address all of these properties, however, such a framework and setting is not available. Rather, each modelling framework has its specific assumptions, strengths, and weaknesses (Kuhn and Johnson, 2013). A broad range of different modelling approaches from traditional statistics and machine learning were considered in this thesis in order to analyse Namibia's fire regimes. These included Generalized Linear Models (GLM; Nelder and Wedderburn, 1972), Multivariate Adaptive Regression Splines (MARS; Friedman, 1991), Regression Trees from Recursive Partitioning (RPART; Breiman et al., 1984), Random Forest (RF; Breiman, 2001), and Support Vector Machines for Regression (SVR; Vapnik, 1995).

An ensemble interpretation of model outputs is beneficial in the thorough identification of the fire regime's major controls, and thus the most important predictors. For this specific task, ordination methods, such as Multidimensional Non-Metric Scaling (NMDS) technique, as frequently applied in plant community ecology, could have been an alternative. Although ordination has been applied with fire regimes (e.g. Moreno and Chuvieco, 2016), it is rather an exploratory tool dedicated to vivid graphical representations of complex data settings, than a modelling framework (Wildi, 2013). As the focus of fire regime modelling was on predictive power rather than on transferability in space or time, the principle of parsimony (see Crawley (2007)) was neglected here.

[16] Complexity refers to the properties of data structure here.

Instead, a large set of predictors that were selected with regards to their relevance for the fire regime, and based on a redundancy-removal procedure, were included in the models.

2.6. Model evaluation

Evaluation generally describes a crucial procedure to assess the performance, i.e. the accuracy and precision of a model based on a specified reference (Willmott et al., 1985). The reference denotes some independent observations or another model that is regarded as the "truth". These observations can be field measurements or, in the case of a model comparison, simply another model. From a statistical perspective, independence of the reference is achieved either by splitting a set of observations into separate partitions for model building and evaluation, or resampling techniques such as cross-validation (CV; Kuhn and Johnson, 2013). With *k*-fold CV, a set of observations is separated into *k* subsets of approximately equal size. In an iterative procedure, a model is trained from *k*–1 subsets, where the remaining fold subset is resampled, i.e. its values are randomly permuted, and used for evaluation of the trained model (Kuhn and Johnson, 2013). As the presence of spatial autocorrelation (SAC) potentially underestimates true model errors (Dormann et al., 2007; Dorner et al., 2002), spatial CV setups, where the evaluation partition is spatially clustered, were additionally investigated following Brenning and Ruß (2010). An assessment of the individual predictor's importance in the models was achieved by means of a permutation-based approach (Altmann et al., 2010; Strobl et al., 2007).

Different measures to quantify a model's performance or to outline its errors have been proposed. For qualitative outputs, such as the delineation of woody individuals (Chapter 2.4.4), an error matrix of correct vs. incorrect delineations was applied here. For quantitative outputs, three groups of performance measures could be distinguished (Legates and McCabe, 1999; Moriasi et al., 2007): "goodness-of-fit" from standard regression, dimensionless relative measures, and those outlining an error in terms of the output's unit. The Root Mean Square Error (RMSE) is a prominent example of the latter. As certain performance measures are inappropriate or of limited reliability under certain circumstances[17], Legates and McCabe (1999) recommend the consideration of at least one measure from two of the three groups outlined above. This recommendation was largely followed in the quantitative models of this thesis. Visual inspection was an additional valuable, yet subjective evaluation strategy for the mapped model outputs.

2.7. Software

A suite of commercial and open software was applied in the fulfilment of this thesis. These include (in alphabetical order): Agisoft PhotoScan, ESRI ArcGIS and ArcPad, GPXViewer2, LI-COR FV2200, Microimages TNTmips, Mikrokopter GPXTool and MKTool, MODIS Re-projection Tool, QGIS, R and distributed packages, SAGA-GIS, and TIMESAT.

[17] For instance, correlation-based measures such as R^2 are tied to the assumptions of the linear model, whereas RMSE suffers from sensitivity to outliers.

PART II
PUBLICATIONS

3. LIST OF MANUSCRIPTS AND PERSONAL CONTRIBUTIONS

Manuscript 1 (Chapter 4)

Authors: Manuel J. Mayr, Kim A. Vanselow, Cyrus Samimi

Title: Fire regimes at the arid fringe: a 16-year remote sensing perspective (2000-2016) on the controls of fire activity in Namibia from spatial predictive models

Journal: Ecological Indicators (2018), 91, 324–337. DOI: 10.1016/j.ecolind.2018.04.022

Personal contribution: Study design (75%), dataset compilation (100%), data processing and analysis (80%), manuscript writing and artwork (90%), corresponding author

Manuscript 2 (Chapter 5)

Authors: Manuel J. Mayr, Cyrus Samimi

Title: Comparing the Dry Season *In-Situ* Leaf Area Index (LAI) Derived from High-Resolution RapidEye Imagery with MODIS LAI in a Namibian Savanna

Journal: Remote Sensing (2015), 7 (4), 4834–4857. DOI: 10.3390/rs70404834

Personal contribution: Study design (40%), *in situ* data acquisition (100%), data processing and analysis (100%), manuscript writing and artwork (90%), corresponding author

Manuscript 3 (Chapter 6)

Authors: Manuel J. Mayr, Sophia Malß, Elisabeth Ofner, Cyrus Samimi

Title: Disturbance feedbacks on the height of woody vegetation in a savannah: a multi-plot assessment using an unmanned aerial vehicle (UAV)

Journal: International Journal of Remote Sensing (2017), 39 (14), 4761–4785. DOI: 10.1080/01431161.2017.1362132

Personal contribution: Study design (90%), *in situ* and UAV data acquisition (80%), data processing and analysis (100%), manuscript writing and artwork (100%), corresponding author

4. MANUSCRIPT 1: FIRE REGIMES AT THE ARID FRINGE: A 16-YEAR REMOTE SENSING PERSPECTIVE (2000-2016) ON THE CONTROLS OF FIRE ACTIVITY IN NAMIBIA FROM SPATIAL PREDICTIVE MODELS

Manuel J. Mayr, Kim A. Vanselow, Cyrus Samimi

Ecological Indicators (2018), 91, 324–337.
DOI: 10.1016/j.ecolind.2018.04.022

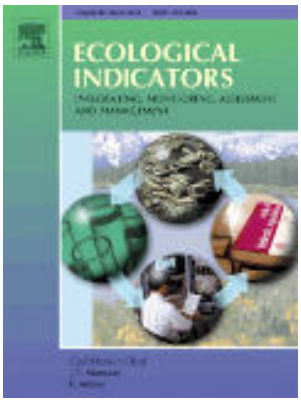

Ecological Indicators 91 (2018) 324–337

Contents lists available at ScienceDirect

Ecological Indicators

journal homepage: www.elsevier.com/locate/ecolind

Original Articles

Fire regimes at the arid fringe: A 16-year remote sensing perspective (2000–2016) on the controls of fire activity in Namibia from spatial predictive models

M.J. Mayr[a,*], K.A. Vanselow[b], C. Samimi[a,c,d]

[a] Department of Geography, University of Bayreuth, Universitätsstr. 30, 95447 Bayreuth, Germany
[b] Department of Geography, University of Erlangen-Nuremberg, Wetterkreuz 15, 91058 Erlangen, Germany
[c] Bayreuth Center of Ecology and Environmental Research, University of Bayreuth, Dr. Hans-Frisch-Straße 1-3, 95448 Bayreuth, Germany
[d] Institute of African Studies, University of Bayreuth, Wölfelstr. 2, 95444 Bayreuth, Germany

ARTICLE INFO

Keywords:
Fire ecology
Fuel limitation
Machine-learning
Dry savanna
Spatial autocorrelation
Model comparison

ABSTRACT

Dry-season fires affect the grassland and savanna ecosystems in Namibia and other regions around the globe. Whereas climate, especially precipitation, has been found to constrain fire activity in (semi-)arid regions through productivity, the feedbacks with human systems lack generalization. Here, we assess the biophysical and human-related controls of fire activity in Namibia based on a 16-year record (2000–2016) of the MODIS Burned Area product (MCD45A1). The two derived parameters of fire activity include burned area (positive continuous) and the number of fire occurrences (zero-inflated counts), and are individually investigated at a 0.1°-resolution by means of five common statistical and machine-learning techniques. We evaluate performance and consistency among the models using the adjusted coefficient of determination and the root mean square error, which is obtained from 5-repeated 10-fold cross-validation. A comparable measure of predictor importance among the models is assessed by means of a permutation-based approach. As spatial autocorrelation is present for both parameters of fire activity, we consider this with a spatial cross-validation setup, where *k*-Means clusters of geographic coordinates are used to derive the test partitions. We find complex machine-learning techniques generally improve the predictions of both parameters of fire activity. Our results confirm the exceptional importance of mean annual precipitation for fire activity across Namibia and highlight human impacts as an additional control of fuel availability. Apart from an increase of burned area and fire occurrences at a mean annual precipitation of approximately 400 mm, population and livestock densities strongly limit fire activity in the best-performing Random Forest models. The largest burned areas are found with moderate green-up rates of vegetation, which we attribute to the presence of open landscapes. The consideration of spatial autocorrelation generally decreases model performances but the relative decreases are higher for the models of burned area, which we attribute to the increased spatial autocorrelation present with this response variable. Resultantly, we recommend accounting for spatial autocorrelation in the evaluation of spatial ecological models and the assessment of predictor importance. Although Namibia's land use practices denote a special case, our model may be of relevance to other regions located at the arid fringe of fire-affected ecosystems and those with projected future aridification.

1. Introduction

Southern Africa is a hotspot of global fire activity (Andela et al., 2017; Giglio et al., 2013). The evolution and maintenance of these savanna and grassland ecosystems have been causally linked to recurring fire occurrence (Bond, 2008; Bond and Keeley, 2005; Cerling et al., 1997). Fires impact greenhouse gases and aerosol emissions (Bond et al., 2013; Giglio et al., 2013; Lehsten et al., 2009), vegetation succession (Heinl et al., 2007; Keeley et al., 2005), nutrient cycling (Coetsee et al., 2010; Pivello et al., 2010) and species composition/diversity (Pausas and Verdú, 2008; Uys et al., 2004). Thus, their spatio-temporal patterns are critical inputs for global climate and dynamic vegetation models (Mouillot et al., 2014; Thonicke et al., 2010). Global climate change is likely to alter these patterns (Bowman et al., 2009; Krawchuk et al., 2009), yet large uncertainties about the direction and regional influence remain (Settele et al., 2014). Hence, the assessment

* Corresponding author.
E-mail address: manuel.mayr@uni-bayreuth.de (M.J. Mayr).

https://doi.org/10.1016/j.ecolind.2018.04.022
Received 12 December 2017; Received in revised form 8 April 2018; Accepted 9 April 2018

of the typical fire occurrence in a region, i.e. the fire regime, and a detailed understanding of its controls build a vital framework to address these uncertainties and to potentially adapt policies.

Operationally produced fire records from Earth observation systems, such as the National Aeronautics and Space Administration's (NASA) Moderate-resolution Imaging Spectroradiometer (MODIS) Burned Area (BA) product (Roy et al., 2005), are currently widely used in the fire research domain as they are globally available and of unique spatial and temporal consistency. With almost 20 years in orbit, the MODIS BA record also allows for the capturing of variability of lower-frequency fire recurrence, such as those found at the arid fringe of fire-affected ecosystems.

Within the (semi-)arid spectrum of fire-affected ecosystems, such as Namibia, fire activity is generally constrained by productivity (Krawchuk and Moritz, 2011; Pausas and Ribeiro, 2013). Thus, the availability of (surface) fuels, which is a function of preceding precipitation and its variability, limit the initiation and spread of fires, although atmospheric conditions during dry season would promote these. The importance of climate-fuel interactions for fire regimes has been confirmed at various scales and for different savanna regions – e.g. Northern Australia (Spessa et al., 2005), Eastern (Nelson et al., 2012) and Southern Africa (Archibald et al., 2009, 2010a; Heinl et al., 2006; O'Connor et al., 2011; van Wilgen et al., 2004). Fire activity in Namibia follows a distinct climatic gradient from the arid South and West to the more humid North-East, where approximately 30–50% of the land area burns on an annual basis (Verlinden and Laamanen, 2006).

Biophysical determination accounts for the framework of fire occurrence. However, humans strongly impact fire regimes as they accidently and deliberately ignite fires, while simultaneously directly and indirectly suppressing them (Archibald et al., 2012; Guyette et al., 2002). Indirect human suppression pathways act on fuel load via reduction as well as fragmentation, e.g. from land conversion or livestock grazing. All over Southern Africa the majority of fires are intentionally lit by humans (Archibald et al., 2010b), who use fire as a tool for land management (e.g. hunting, pest control, land clearance, nutrient recycling, green shoot initiation, among others). Accordingly, Archibald et al. (2010a) conclude that the climatic controls on fire are stronger in protected areas, which are hypothesized to be less affected by humans as compared to the whole subcontinent. However, generalizations of human impacts on the fire regime appear difficult, even at a regional scale. Increasing human densities were found to reduce BA (Archibald et al., 2009), and shift fire size distributions towards smaller, more frequent fires (Archibald et al., 2010b). Le Roux (2011) finds Namibian fire regimes to differ among land tenures which he attributed to the corresponding fire management strategies and capabilities. The importance of management is supported by a study of the Kavango-Zambezi Transfrontier Conservation Area (Pricope and Binford, 2012), that documents the marked differences in BA and fire recurrence as a function of the fire policies in the five countries involved (including Namibia).

A large set of facilitating and limiting variables of biophysical and human origin and their complex interactions may, thus, be responsible for the observed patterns of fire activity in a region. State-of-the-art predictive modeling techniques help us to quantitatively understand such patterns and to unveil the dependencies behind these. So-called machine-learning algorithms are often shown to improve complex pattern identification as compared to conventional statistical methods in the fire research domain (e.g. Amatulli et al., 2006; Bar Massada et al., 2012; Bedia et al., 2014; Cortez and Morais, 2007; Faivre et al., 2016; Rodrigues and de la Riva, 2014; de Vasconcelos et al., 2001), as well as other disciplines (e.g. Goetz et al., 2015; Singal et al., 2013 – among many others). However, no single method has been identified as the best method, rather each has different strengths and weaknesses (e.g. with the handling of factor predictors and extreme values, the treatment of interactions, and interpretability).

With regards to predictive modeling, a major limitation of the approach arises from the fact that the ignitions can only be inferred from indirect variables (Krawchuk and Moritz, 2014). The exact occurrence of an ignition, especially of unintentional origin or from lightning, carries an indeterminable uncertain degree of stochasticity. As fires originate from an ignition source and propagate under facilitating conditions, their observations are likely to be autocorrelated, i.e. their patterns show distinct spatial, but also temporal dependencies. Where the presence of Spatial Autocorrelation (SAC) violates the assumption of independence with parametric techniques, its negligence may generally result in biased models (Dormann et al., 2007; Dorner et al., 2002). Best-practice spatial modeling accounts for SAC, either by including SAC as a separate (weighing) variable in the model or removing SAC from the observations, e.g. by selection of a non-correlated subset (see Dormann et al. (2007) for an overview). Another approach is to correct for the underestimation of model errors as a result of SAC by spatially clustering the evaluation partitions in a cross-validation procedure (Ruß and Brenning, 2010). Hence, the full set of observations may be used to fit the model and the effects of SAC on model performance. In addition, predictor importance can easily be assessed by comparing 'non-spatial' vs. 'spatial' evaluations across various predictive techniques.

Here, we apply a predictive modeling approach to investigate the controls of two main fire regime parameters derived from a 16-year Earth-observation record, namely Burned Area (BA) and Fire Occurrence (FO), in Namibia. We use five common statistical and machine-learning techniques to predict BA, which is positive-continuous, and FO, which comprises zero-inflated counts. We assess the models' performance and consistency, and consider spatial dependency structures as indicated by SAC. Precipitation is hypothesized to be the primary control of overall fire activity in Namibia as it determines fuel availability. Human activities (e.g. land fragmentation or tenure) could alter and even override the climate-fire relationship. We expect that human activities may lead to diverse feedbacks on fire activity, i.e. they negatively affect the spatial extent of fires (BA) but could cause more frequent fires (FO). Both fire regime parameters should show distinct spatial structures, which would justify the consideration of SAC in the model evaluation. Furthermore, we expect complex interactions with biophysical and human-related predictors, favoring the usage of machine-learning over conventional statistical techniques.

The expected insights of our work contribute to the highly-needed quantitative understanding of the linkage between biophysical and human systems (Beringer et al., 2015). As fire management plans and policy decisions are often determined nationwide, our investigation on the national scale could deduce important implications for the management of fire and ecosystems in Namibia, as well as for countries with comparable environmental conditions and land use practices. Ultimately, our case study may prove as a reference for the understanding of fire regime responses to future aridification as proposed for many savanna regions (Kirtman et al., 2013).

2. Materials and methods

2.1. Study area

In Namibia, the most arid country of Sub-Saharan Africa, precipitation is largely restricted to the Austral summer, where the dependence on convective complexes introduces a pronounced spatial variability in intra-seasonal water availability (Blamey and Reason, 2013). Inter-annual variability of precipitation is a function of aridity due to the increasing dependence on single events for Mean Annual Precipitation (MAP). Relative variability is most pronounced in the West and South of Namibia and the North and North-East reach the highest MAP of up to approximately 600 mm (Mendelsohn et al., 2002). The gradient of MAP largely determines natural vegetation, but edaphic properties may alter this pattern of productivity. For instance, high salinity in the proximity of ephemeral water bodies facilitates the

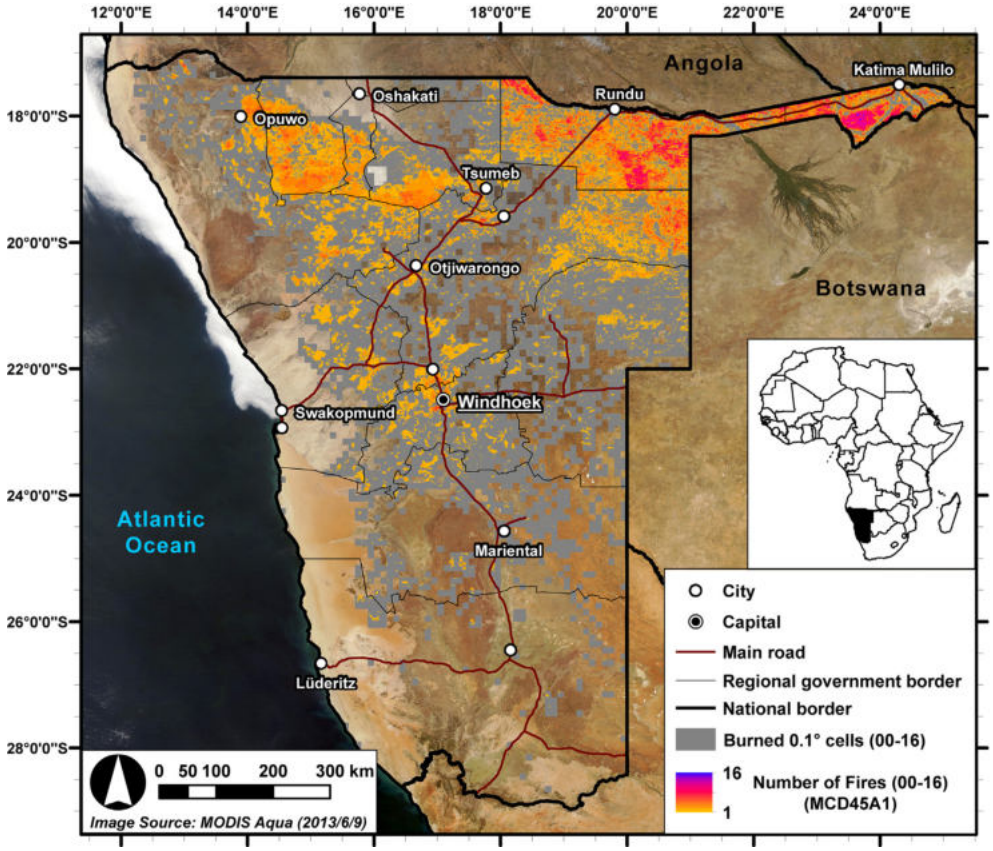

Fig. 1. Map showing Namibia and the extent of fire within the period April 2000–March 2016. The burned cells (in grey; n = 3700), which are the scope of this study, contain at least one fire within the period of observation. These were derived from a spatial aggregation to 0.1°-resolution based on NASA's MODIS Burned Area product (MCD45A1 at 500 m-resolution; in color). (For interpretation of the references to color in this figure legend, the reader is referred to the web version of this article.)

formation of azonal grasslands in Northern-Central Namibia (Mayr and Samimi, 2015). Wetter regions of the country are characterized by feather-leaved (mainly *Acacia* spp.) and broad-leaved savannas, which also form woodlands (e.g. *Colophospermum mopane, Baikiaea plurijuga*) in the North-East.

Approximately 17% of Namibia is covered by protected areas (MET, 2016), but vast areas that are privately-held, especially in Central Namibia, or communally-administered are used for livestock farming. High stocking rates are often associated with the expansion of woody vegetation, i.e. bush encroachment (de Klerk, 2004; Mayr et al., 2017; Wagenseil and Samimi, 2007). Fire suppression and exclusion are regarded as contributing factors to bush encroachment among others (but see O'Connor et al., 2014).

National fire policy has targeted the strict avoidance of fires since colonial times. However, recent considerations in fire management give increased consideration to prescribed and controlled burning in some communal areas (Beatty, 2011) as well as in protected areas and their surroundings (MET, 2016). Approximately half of the country experienced fire within the period 2000–2016 (Fig. 1). These burned areas are under investigation in this study.

2.2. Data

2.2.1. Response variables

2.2.1.1. MODIS monthly burned area (MCD45A1). The MODIS burned area product (MCD45A1) is the most frequently applied satellite-based fire estimate (Mouillot et al., 2014). It uses daily MODIS Aqua and Terra reflectance with a bi-directional change detection approach to discriminate burned areas and assign an approximate date of burning (Roy et al., 2008). Evaluation studies from Southern Africa, partly including Namibia, revealed low errors of omission but high errors of commission, especially for smaller fires (de Klerk et al., 2012; Tsela et al., 2014), making it a conservative estimate of burned areas. Yet true detections were reported as high as 75% for the region (Roy and Boschetti, 2009).

A 16-year time series (April 2000–March 2016) of three MCD45A1 v5.1 tiles (h19v10, h19v11, h20v10) covering Namibia were downloaded from the NASA's Land Processes Distributed Active Archive Center (LPDAAC) via the United States Geological Survey (USGS) Earth Resources Observation and Science (EROS) Center (https://e4ftl01.cr.usgs.gov/MOTA/MCD45A1.051/). The tiles of the monthly time series were mosaicked and re-projected to geographic coordinates (World Geodetic System 1984; WGS84) using the MODIS Re-projection Tool (MRT). We filtered the monthly mosaics for the Days-Of-Year (DOY) of the corresponding month and limited the burned pixels to highest-quality retrievals only (i.e. *Quality Assessment* = 1). Annual burned area sums from April to March were calculated, which is in accordance with Boschetti and Roy (2008) for Southern African savannas. It should be noted that June 2001 was missing in the time series due to technical problems related to the MODIS instrument (Boschetti et al., 2013). No filling was applied for this month. Two response variables of per-pixel fire activity could be derived: the total number of Fire Occurrences within the 16 years (FO) and, by correcting for latitude, the approximate mean Burned Area in km^2 (BA).

2.2.2. Predictor variables of the biophysical environment

2.2.2.1. Terra MODIS 16-day composite NDVI (MOD13A1). The Normalized Difference Vegetation Index (NDVI) is a reflectance based proxy for photosynthetically active vegetation. The MOD13A1 product (Huete et al., 2002), which is derived from daily Terra MODIS surface reflectance observations, provides 16-day Maximum Value Composites (MVC) of NDVI. Due to the MVC being prone to noise introduced from viewing geometry, atmospheric composition and cloud contamination, such datasets need to be corrected by the application of a smoothing function (Chen et al., 2004).

In analogy to the MCD45A1 dataset, a time series (6 April 2000–21

Table 1
Overview of the variables used in this study including the names and descriptions of the individual response and predictor variables that were spatially aggregated to the variable of coarsest resolution (i.e. 0.1°), the corresponding units (where applicable), the original resolution (for rasters), and the data source. Predictor variables shown in italic letters ($n = 11$) were excluded from further analysis after predictor pre-selection and thus are not part of the models. For further explanation, please see text.

Name	Description	Unit	Original Res.	Data source
Response variables				
Burned Area (BA)	Mean annual sums (2000–2016)	km^2	500 m	MCD45A1 (v5.1)
Fire Occurrences (FO)	Majority number of occurrences (2000–2016)	n		
Predictor variables of the biophysical environment				
Lightning Rate (LR)	Mean of Apr-Nov sums (1998–2013)	$n\ km^{-2}\ day^{-2}$	0.1°	LIS-VHRMC
Mean Annual Precipitation (MAP)	Mean of annual sums (1998–2016)	mm	0.0375°	TAMSAT (v2)
Early Season Precipitation (PSON)	*Mean of Sept-Oct-Nov sums (1998–2016)*			
Main Season Precipitation (PDJF)	*Mean of Dec-Jan-Feb sums (1998–2016)*			
Late Season Precipitation (PMAM)	*Mean of Mar-Apr-May sums (1998–2016)*			
Surface Roughness (SR)	Mean surface roughness	–	0.00083°	SRTM 3-arc (v4.1)
NDVI Start-of-Season (VSOS)	Mean start-of-season (2000–2016)	DOY	500 m	MOD13A1 (v6)
NDVI End-of-Season (VEOS)	*Mean end-of-season (2000–2016)*	DOY		
NDVI Length-of-Season (VLOS)	Mean length-of-season (2000–2016)	DOY		
NDVI Middle-of-Season (VMOS)	*Mean middle-of-season (2000–2016)*	DOY		
NDVI Amplitude (VAMP)	*Mean seasonal amplitude (2000–2016)*	–		
NDVI Base Value (VBV)	Mean seasonal base value (2000–2016)	–		
NDVI Maximum (VMAX)	*Mean seasonal maximum (2000–2016)*	–		
NDVI Left Derivative (VLD)	Mean seasonal left derivative (green-up) (2000–2016)	–		
NDVI Right Derivative (VRD)	*Mean seasonal right derivative (brown-off) (2000–2016)*	–		
NDVI Small Integral (VSINT)	*Mean seasonal small integral (2000–2016)*	–		
Sub-biomes (SBIOM)	*Levels of sub-biomes (n = 4)*	–	–	AON/EIS
Herbivore Diversity (HDIV)	Ranks of natural herbivore diversity (n = 3)	–	–	
Predictor variables of human activity				
Roads and Railways (RR)	Summed length of roads and railways	km	–	OSM/Geofabrik, AON/EIS
Bush Encroachment (BENC)	Binary of bush encroachment	–	–	AON/EIS
Land Tenure (LTEN)	Levels of land tenure (n = 3)	–	–	
Land Use (LU)	*Levels of land use (n = 4)*	–	–	
Livestock Density (LSD)	Mean total biomass of livestock	$kg\ ha^{-2}$	10 km	
Population Density (POPD)	Mean population density (around year 2000)	$n\ km^{-2}$	1 km	
Power Lines (PWL)	Summed length of power lines (June 2009)	km	–	NamPower/EIS

March 2016) of the three MOD13A1 v6 tiles were downloaded from the NASA's LPDAAC/EROS (https://e4ftl01.cr.usgs.gov/MOLT/MOD13A1.006/) and pre-processed in MRT. Following (Fensholt et al., 2009), we included only binary numbers ≤8 from the NDVI quality assessment layer, but additionally filtered the pixels for their land mask and cloud shadow attributes.

Further processing of the NDVI time series was completed via TIMESAT v3.3 (Jönsson and Eklundh, 2004). Based on visual inspection of per-pixel time series all over Namibia, we chose a double-logistic filter in order to fill the gaps resulting from the quality-based selection, and to smooth the seasonal NDVI signals. The output NDVI metrics per season were averaged using the mean, whereby temporal metrics containing DOY (e.g. start of the growing season (VSOS)) were rounded to integers. Table 1 provides an overview of the derived NDVI metrics.

2.2.2.2. TAMSAT monthly precipitation. The Tropical Applications of Meteorology using SATellite data and ground-based observations (TAMSAT) dataset (Tarnavsky et al., 2014) combines a Thermal Infrared (TIR) cold cloud detection approach with regional gauge calibration. As the TIR data originate from Meteosat, TAMSAT covers the period 1983-present with an approximate spatial resolution of 4 km. The TAMSAT approach has performed well in different African regions (Asadullah et al., 2008; Dinku et al., 2007), but also underestimates amounts of precipitation (Maidment et al., 2014; Thorne et al., 2001; Young et al., 2014). As Maidment et al. (2014) point out, accurate representations of low precipitation amount and inter-annual variability is a priority of the TAMSAT approach. This suggests that this is a dataset that is suitable for Namibia.

We downloaded the complete TAMSAT v2.0 monthly and dekadal (i.e. a 10-day period) datasets from https://www.tamsat.org.uk/data/archive. Available fine fuels, such as grass, are often considerably determined by the two preceding rainy seasons (Siegfried, 1981; van Wilgen et al., 2004). Therefore we used a monthly time series from September 1998 to August 2016 for the calculation of Mean Annual Precipitation (September–August; MAP), and mean seasonal precipitation amounts for the early season (September–October–November; PSON), the main season (December–January–February; PDJF), and the late season (March–April–May, PMAM). Two months of the monthly time series in use were missing (January 1999, September 2006). These gaps were filled by summing the two dekades of the corresponding month, which were available from the dekadal TAMSAT dataset, and the mean (1983–2016) of the missing dekade.

2.2.2.3. SRTM 3-Arc-second elevation. Ten 5 × 5 degree (°) tiles of NASA's Shuttle Radar Topology Mission (SRTM) 3-Arc-second v4.1 elevation product were retrieved from the CGIAR Consortium for Spatial Information database (CGIAR-CSI; http://srtm.csi.cgiar.org/) (Jarvis et al., 2008). Compared to earlier versions, missing data for deserts were largely filled in this dataset. We calculated the Surface Roughness (SR) as a measure of terrain heterogeneity from the mosaicked tiles.

2.2.2.4. LIS-VHRMC lightning. Daily lightning flash rates covering the period 1998–2013 were available at 0.1°-resolution from the Lightning Imaging Sensor – Very High Resolution gridded lightning Monthly Climatology (LIS-VHRMC) product (Albrecht et al., 2016) which is provided by NASA's Earthdata portal (https://urs.earthdata.nasa.gov/). The mean of annually summed Lightning flash Rates (LR) was calculated, restricting to the months of potential lightning-caused fire ignition (April–November).

2.2.2.5. Sub-biomes. A categorical vector dataset of the (Sub-) Biomes of Namibia (SBIOM) was available from the Atlas Of Namibia (AON; Mendelsohn et al., 2002) and retrieved from the Environmental

Information System Namibia (EIS; http://www.the-eis.com/). In order to achieve a balanced distribution of the levels, biomes of the 'Succulent Karoo' and the 'Nama Karoo', were merged to a class 'Karoo'. Similarly, pans and desert levels were combined to yield the class 'Desert, Pans'. The biome 'Tree-and-Shrub-Savanna' was split along a line feature provided by the dataset to yield separate levels of feather-leaved- and broad-leaved savanna.

2.2.2.6. Herbivore diversity. The number of large mammalian natural herbivores was available as a vector dataset from the AON/EIS. Although Herbivore Diversity (HDIV), which largely coincides with their overall abundance in Namibia (Mendelsohn et al., 2002), may reflect human activities (e.g. hunting vs. conservation), these were attributed to the biophysical environment. We reclassified the number of herbivore species to ranked levels corresponding to low (≤ 2 species), moderate (3–6 species) and high diversity (≥ 7 species).

2.2.3. Predictor variables of human activity

Raster and vector data from the Atlas Of Namibia (AON; Mendelsohn et al., 2002), which were available from EIS, were regarded as the best-available source at the national scale in terms of resolution, completeness and reliability. The AON/EIS was the main source for the predictors of human activity. If not otherwise mentioned below, the data originated from this source and the references given in Mendelsohn et al. (2002).

2.2.3.1. Bush encroachment. Based on a vector dataset containing the approximate contiguous areas of bush encroachment and the corresponding species of encroachment, we created a binary dataset of non-encroached and encroached areas (BENC). According to the dataset, approximately 52% of the study area were subject of encroaching woody species.

2.2.3.2. Land use and tenure. In order to reduce levels and to increase their balance, the vector datasets of land use and tenure were reclassified. This resulted in the following levels for Land Use (LU): 'large-scale agriculture' (8.8% of the study area), 'small-scale agriculture' (80.5%), 'protected' (i.e. areas for conservation and mining; 9.5%), and 'other' (i.e. urban areas and resettlements; 1.2%). For Land Tenure (LTEN), we separated between 'communal', 'governmental', and 'private' controls of land, where the latter also includes private-held land in communal and urban areas. The largest proportion of the study area was 'private' land (52%), whereas 36% and 12% were under communal and government controls, respectively.

2.2.3.3. Livestock density. Livestock Densities (LSD), which is the total biomass of cattle, goats, sheep, and donkeys, were available in kg ha^{-1} and at a 10-km-resolution. As national parks were masked in the original dataset, these areas were set to null. Still, mean LSD across the study area was 14.58 kg ha^{-1} with maxima of approximately 220 kg ha^{-1}.

2.2.3.4. Population density. Population Densities (POPD) around the year 2000 in n km^{-2} were available at a 1-km-resolution. Although spatial population estimates in developing countries may be inaccurate due to the lack of census availability and informal housing, we believe the AON/EIS dataset utilized here, which combines several sources (see Mendelsohn et al. (2002) for further details), was the most suitable for Namibia. The generally low population numbers across Namibia are outlined by a mean POPD of 2.22 people km^{-2} in the study area.

2.2.3.5. Power lines. Power Lines (PWL), which are a potential source of ignition but are often accompanied cut lines that fragment fuels, were provided by the Namibia Power Corporation Ltd. (NamPower) and available from EIS for June 2009. We filtered the dataset for existing and overhead power lines only.

2.2.3.6. Roads and railways. Roads and Railways (RR) were merged from two sources in order to form a predictor of land fragmentation. Where the railway network was available from AON/EIS, roads were retrieved from a database extract of OpenStreetMap (OSM) on 12 December, 2016, which was provided by Geofabrik GmbH (http://download.geofabrik.de/africa/namibia.html). All roads equal to or higher than tertiary (i.e. Namibian D-roads) were merged with the railroad dataset.

2.2.4. Spatial aggregation

Our analysis was carried out at a 0.1°-resolution to match the spatial resolution of the coarsest scaled variable in the dataset, which was the LIS-VHRMC lightning record. The 0.1°-resolution yielded a sample of 3700 grid cells that contained at least one burned MCD45A1-pixel within the period of observation (April 2000–March 2016; Fig. 1).

The response variables were aggregated using the mean BA and the majority FO of all MCD45A1-pixels contained within the 0.1° grid cell. Positive continuous and integer (count) data types could be derived for BA and FO, respectively. The quantitative predictors of precipitation (MAP, PSON, PDJF, and PMAM), topography (SL and SR), vegetation/phenology (VSOS, VEOS, VLOS, VMOS, VAMP, VBV, VMAX, VLD, VRD, and VSINT), livestock density (LSD), and population density (POPD) were aggregated using the mean. Instead line-based predictors (RR, PWL) were aggregated and rasterized using the sum, whereas for polygon-based predictors (SBIOM, BENC, HDIV, LTEN, and LU) the level corresponding to the maximum area within the 0.1° grid cell was used. Table 1 provides a full overview of all response and predictor variables derived here as well as their properties.

2.3. Methods

2.3.1. Pre-selection of predictor variables

In order to decrease model complexity, we pre-selected the initial predictors and their groups by means of multicollinearity and redundancy removal. The seasonal precipitation measures (PSON, PDJF; and PMAM) were all highly correlated ($R^2 > 0.89$; not shown) with Mean Annual Precipitation (MAP). Therefore, only MAP was included for further analysis. From ten initial NDVI-based predictors of vegetation and phenology, only four predictors (VSOS, VLOS, VBV, and VLD) were included based on a backward-stepwise Variance Inflation Factor (VIF) procedure using a threshold ≤ 5. The association among categorical predictors was assessed from pairwise Cramer's *V*. Strong associations (Cramer's $V > 0.5$) were found for LTEN vs. LU and SBIOM vs. BENC. LU and SBIOM were eliminated from the dataset due to higher imbalance of the levels of LU and an assumed strong dependency of SBIOM by MAP. In total, 11 of the 25 initial predictors were excluded through the process of pre-selection (cf. Table 1).

2.3.2. Spatial autocorrelation

We tested the response variables (BA and FO) for spatial autocorrelation (SAC), as it would have implications for the estimation of model performance and predictor importance (see Sections 2.3.4-5). Based on spatial dependencies outlined by the global Moran's *I* (Moran, 1950), we graphically assessed SAC from correlograms using R package 'ncf' (Bjornstad, 2016). Uniform distance classes of 110 km were assumed, which corresponds to approximately ten cells in the 0.1° resolution dataset.

2.3.3. Predictive modeling

We tested the ability of, and the agreement among, different modeling techniques to predict the response variables BA and FO in a mixed-data type setting consisting of continuous and factor predictors. Both responses covered a sample of 3700 observations and had a right-skew distribution. BA was positive continuous, whereas FO covered zero-inflated counts with excess discrete zeros ($n = 854$) as a result of the spatial aggregation using the majority. BA and FO were also

considerably correlated (Spearman correlation coefficient of 0.68; not shown).

Five common statistical and machine-learning techniques were compared in this study, including: (i) Generalized Linear Models (GLM; Nelder and Wedderburn, 1972), (ii) Multivariate Adaptive Regression Splines (MARS; Friedman, 1991), (iii) Regression Trees from Recursive Partitioning (RPART; Breiman et al., 1984), (iv) Random Forest (RF; Breiman, 2001), and (v) Support Vector Machines for Regression (SVR; Vapnik, 1995). These were selected with regards to the broad range of techniques and complexity covered (e.g. parametric vs. non-parametric, regression-based vs. tree-based (ensemble) techniques). Each of the techniques offered multiple configuration settings for model building. If not otherwise mentioned below, we used the default settings.

GLMs extend multiple regression for the exponential family of distributions through the application of a canonical link function (Crawley, 2007; Dobson, 2002). We estimated the optimal distribution for fitting the GLM of BA by estimating the power parameter of the variance-mean function with the R package 'tweedie' (Dunn and Smyth, 2005). A power parameter of two was retrieved, which is a Gamma distribution. The GLM of BA was fitted using a Gamma distribution with logarithmic link function (log link). For FO, we applied a hurdle model (Mullahy, 1986) that separately treats zeros and positive counts. Initially, a binomial model (with logit link) was used for the determination of the zero vs. non-zero components. We subsequently fitted the non-zeros to a negative binomial distribution (with log link) in order to account for the left-truncated counts. For this, we used an implementation of the hurdle model provided with the R package 'pscl' (Zeileis et al., 2008).

The non-parametric MARS is an extension of multiple regression. In an adaptive procedure, MARS initially creates two separate hinge-functions for each predictor by searching for the optimal split positions (Kuhn and Johnson, 2013). This forward selection is likely to yield complex models and over-fit the data. Superfluous model terms are subsequently removed based on a generalized Cross-Validation (CV) procedure (Hastie et al., 2009). We used an implementation of the MARS algorithm in the R package 'earth' (Milborrow, 2017) and forced predictor inclusion in the model.

Regression trees apply 'if-then' conditions to seek for homogenous groups within the data in order to optimally predict a response variable (Kuhn and Johnson, 2013). With the Classification and Regression Tree (CART) algorithm (Breiman et al., 1984), the nodes of the binary tree are created from the predictor and the split values that lead to the highest reduction in overall Sums of Squares Error (SSE). With RPART, this hierarchical procedure is repeated until there is no further reduction in SSE, i.e. no extra information is gained from a node. Thus, RPART may create highly complex trees that lack interpretability and are prone to over-fitting (Kuhn and Johnson, 2013; Loh, 2011).

In order to avoid over-fitting, the RF algorithm creates an ensemble of tree predictions, known as a forest, each generated with a different bootstrapping sample of the predictor dataset (Breiman, 2001). Additionally, each node split within a single RF tree is determined by the optimal subset of randomly selected predictors. The mean of the RF trees is then used for the final prediction. Here, we used the tuning function implemented in the R package 'randomForest' (Liaw and Wiener, 2002) to estimate the optimal number of random variables used for node splitting (*mtry*) as indicated by the minimum Out-of-Bag (OOB) error from a total of 1000 iterations (*ntree* = 1000).

SVR is an extension of the algorithm originally developed for classification problems (Cortes and Vapnik, 1995; Vapnik, 1999). SVR maps feature data at higher-dimensional space so that feature separation can be realized by linear functions, so-called 'hyperplanes'. The aim is to maximize the margins defined by boundary points, the eponymous 'support vectors', around the hyperplanes (Kuhn and Johnson, 2013). This projection is achieved by (non-linear) kernel functions. We applied a radial kernel function due to its suitability with non-linear problems (Kuhn and Johnson, 2013). Kernel parameters such as Cost (*C*), which moderates model complexity and accuracy, and Epsilon (ϵ), which defines the threshold margins around the Cost Function $[-\epsilon, \epsilon]$, essentially regularize the SVR solution (Karatzoglou et al., 2006; Smola and Schölkopf, 2004). We trained our models for the optimum *C*- and ϵ-parameters using the grid search function provided with R package 'e1071' (Meyer et al., 2017).

2.3.4. Model performance

We evaluated the performance of each of the five modeling techniques to predict BA and FO using two different goodness-of-fit measures:

i) the adjusted coefficient of determination (adj.-R^2) that allows for an assessment of the percentage of variance explained by the predicted model;
ii) the Root Mean Square Error (RMSE) as an absolute measure of performance.

As the RMSE was regarded more reliable here, our interpretation of the models focused on this measure. We calculated the RMSE using repeated *k*-fold Cross-Validation (CV) from the R package 'sperrorest' (Brenning, 2012). We chose a 5-repeated 10-fold CV (i.e. 50 iterations), which was regarded as a trade-off between acceptable levels of variance and bias as well as moderate computational times (Kuhn and Johnson, 2013). In order to account for potential SAC among the observations of BA and FO, separate CV runs using conventional and spatial setups were conducted. In contrast to the conventional setup, the test partition (i.e. approximately 10% of the observations in case of a 10-fold CV) within an individual iteration of the spatial CV is selected based on *k*-Means clustering of the observations' geographic coordinates (Ruß and Brenning, 2010). As a result, spatial autocorrelation between training and test partitions would be largely reduced and allow for an unbiased assessment of model performance.

2.3.5. Spatial predictor importance

We used a permutation-based approach that randomly generates the values of one predictor while the other predictors remain unaltered (Altmann et al., 2010; Strobl et al., 2007). Hence, the decrease (or increase, in case of 'disturbing' predictors) in prediction error is due to the permutation only and facilitates a comparison of the Spatial Predictor Importance (SPI) between different modeling techniques. We estimated the SPI as outlined by alterations of RMSE from 50 iterations within the spatial CV procedure described.

All data processing and modeling steps were carried out in R v3.3.2 (R Core Team, 2016) and QGIS 'Wien' v2.8 (QGIS Development Team, 2015).

3. Results

3.1. Model performance

Most predictive models were able to reproduce the general patterns of Burned Area (BA) in Namibia (Fig. 2). Only the GLM yielded a vast underestimation of BA which is also reflected by the highest Root Mean Square Errors (RMSE) and the lowest adjusted R^2 among all predictive modeling techniques under investigation here (Table 2). It is also interesting to note that the performance of the GLM increased (i.e. RMSE decreased) by approximately 14% when considering spatial structures in the model evaluation. With the MARS, RPART, RF, and SVR models of BA, RMSEs increased in the range of 26–58% from conventional (non-spatial) to spatial cross-validation (Table 2), which was expected due to the presence of Spatial Autocorrelation (SAC) among the observations (Fig. 3).

The MARS, RPART, RF, and SVR (Fig. 2c–f) tended to smooth BA in their predictions as compared to the observed reference (MCD45A1; Fig. 2a). Consequently, the maxima BA in North-Eastern Namibia could

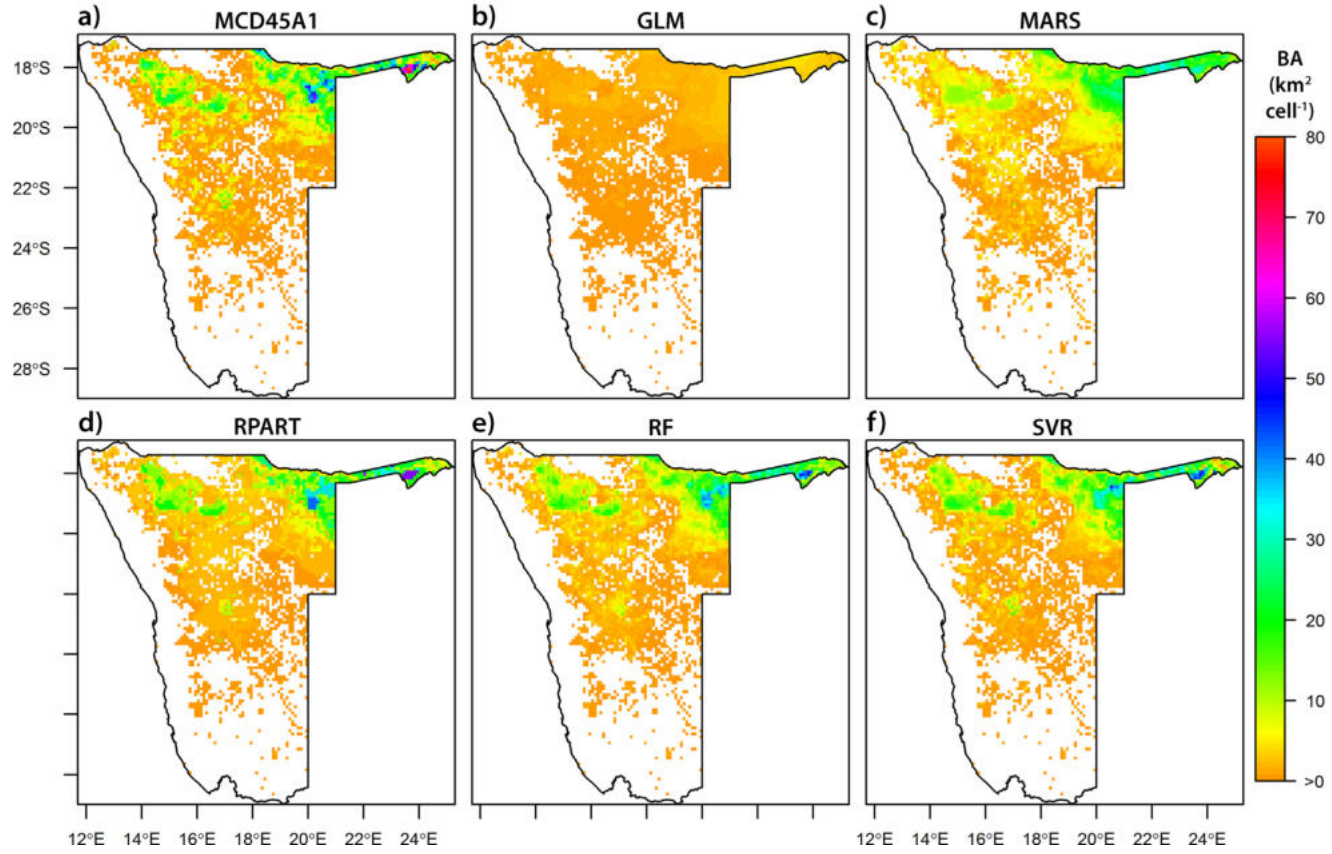

Fig. 2. Observed and predicted Burned Area (BA) of Namibia from April 2000–March 2016. Figures depict a) the observed BA based on the MODIS Burned Area product (MCD45A1) aggregated to 0.1°-resolution using the mean of annual sums (n = 3700); as well as the predicted BA from b) Generalized Linear Models (GLM); c) Multivariate Adaptive Regression Splines (MARS); d) Recursive Partitioning (RPART); e) Random Forest (RF); and f) Support Vector Regression (SVR).

only partly be reproduced by these models and the predictions were often unable to map the abrupt transitions of BA. This smoothing was most expressed in the MARS model, whereas RPART could often reproduce regions of higher BA. The RF and SVR models appeared to best reproduce patterns and extremes of BA. The RF yielded the highest model performances for BA by means of RMSE, whereas adj.-R^2 was slightly higher with RPART and SVR (Table 2).

The predictions of Fire Occurrence (FO) were visually more consistent among the models as compared to BA. However, as with BA, the distinct patchiness of FO (e.g. in the eastern Kavango Region) could only partly be reproduced (Fig. 4). Lower non-zero values of FO in Central Namibia were generally underestimated, but were most adequately captured with the MARS, RF, and SVR models. Underestimations of FO maxima were more expressed in the MARS and SVR models (Fig. 4c, f) but also the GLM, which was the only model that also overestimated FO in the western parts of the Zambezi Region (Fig. 4b). Furthermore, the GLM yielded the highest RMSE errors in both the non-spatial and spatial CV setups, whereas the increase of RMSE from spatial CV was also largest with the GLM (+119%; Table 2). SAC was present with the observations of FO but of a lower magnitude as compared to BA (Fig. 3). Resultantly, an evaluation using spatial CV increased the RMSEs (< +35%) for the MARS, RPART, RF, and SVR models (Table 2). The highest model performances by means of RMSE were retrieved with the RF, as was the case for BA. Yet adj.-R^2 was again slightly higher for RPART and SVR.

In essence, the highest model performances for both responses as outlined by the RMSE were retrieved with RF. However, the adj.-R^2 ranked the RPART and SVR models slightly higher for both responses. Apart from the GLM of BA, RMSEs generally increased with the consideration of SAC in the evaluation of the models. From a visual inspection of the prediction maps, all models tended to underestimate the maxima of the observed responses and to smooth proximal

Table 2
Performance of the five predictive models for Burned Area (BA) and Fire Occurrence (FO). The mean prediction errors are outlined by the Root Mean Square Error (RMSE), which was assessed using a 5-repeated, 10-fold Cross-Validation (CV). The table lists the RMSEs from conventional CV ('RMSE (non-spatial)') and spatial CV ('RMSE (spatial)'), where test partitions with the latter are created from k-Means clustering of the sample's geographic coordinates; the relative difference in RMSE between conventional and spatial CV ('ΔRMSE (%)'); and the adjusted coefficient of determination ('adj.-R2').

	BA (km² cell⁻¹)				FO (n cell⁻¹)			
	RMSE (non-spatial)	RMSE (spatial)	ΔRMSE (%)	adj.-R^2	RMSE (non-spatial)	RMSE (spatial)	ΔRMSE (%)	adj.-R^2
Generalized Linear Models (GLM)	8.59	7.35	−14.47	0.42	1.08	2.37	+119.25	0.25
Multivariate Adaptive Regression Splines (MARS)	5.54	7.00	+26.36	0.59	0.95	1.08	+14.54	0.40
Recursive Partitioning (RPART)	5.19	6.57	+26.71	0.81	0.91	0.98	+7.87	0.70
Random Forest (RF)	3.97	5.94	+49.69	0.78	0.76	0.94	+23.44	0.60
Support Vector Regression (SVR)	4.37	6.92	+58.19	0.83	0.84	1.13	+34.17	0.64

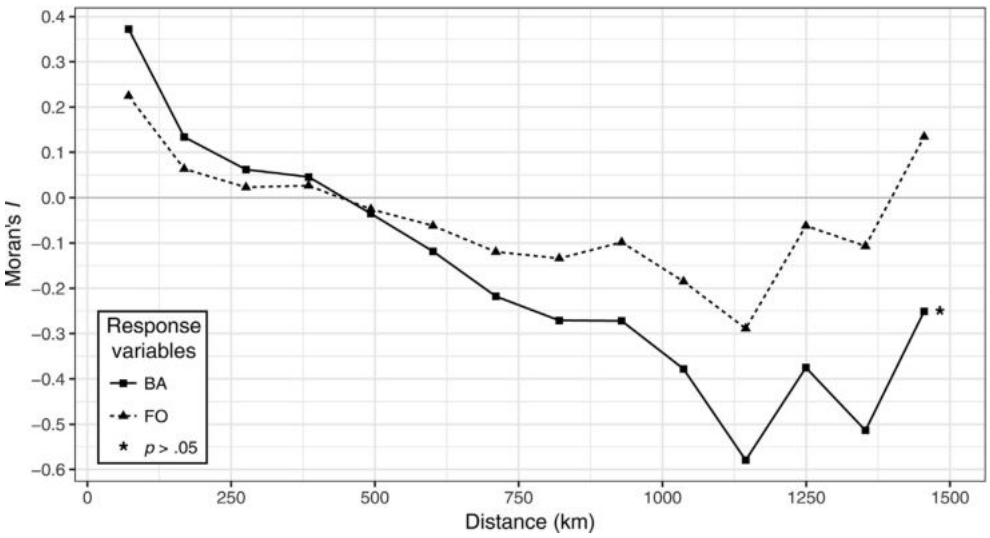

Fig. 3. Correlograms of the response variables (BA and FO). Fourteen equidistant classes of 110 km and their Spatial Autocorrelation (SAC) as indicated by the Moran's *I* are depicted. A typical pattern of spatial dependence with positive SAC at near distances, and *vice versa*, is encountered for both responses. Significance (at the 0.05-level; assessed from 99 permutations) is encountered for all but one discrete class (denoted by '*').

heterogeneities.

3.2. Spatial predictor importance

Due to the presence of SAC with both responses (Fig. 3), only the Spatial Predictor Importance (SPI), i.e. from permutations within the spatial CV, are reported here.

With all BA models, Mean Annual Precipitation (MAP) was consistently of exceptional importance (Fig. 5). MAP had the highest SPI in four models and its SPI in the RPART model was only slightly lower than Population Density (POPD). POPD was also among the top-three predictors in the RF and SVR models. Beyond the importance of MAP and POPD, there was less agreement among the models with regards to predictors of high SPI. In this regard, Lightning Rate (LR) was important in the GLM, MARS and SVR models. The phytophenological predictors green-up rate of NDVI (Left Derivative; VLD) and seasonal minimum of NDVI (Base Value; VBV) were both of notable SPI in two of the five models under investigation here. The predictors Surface Roughness (SR) and Bush Encroachment (BENC) were generally of little importance and SR even negatively affected model performance in the

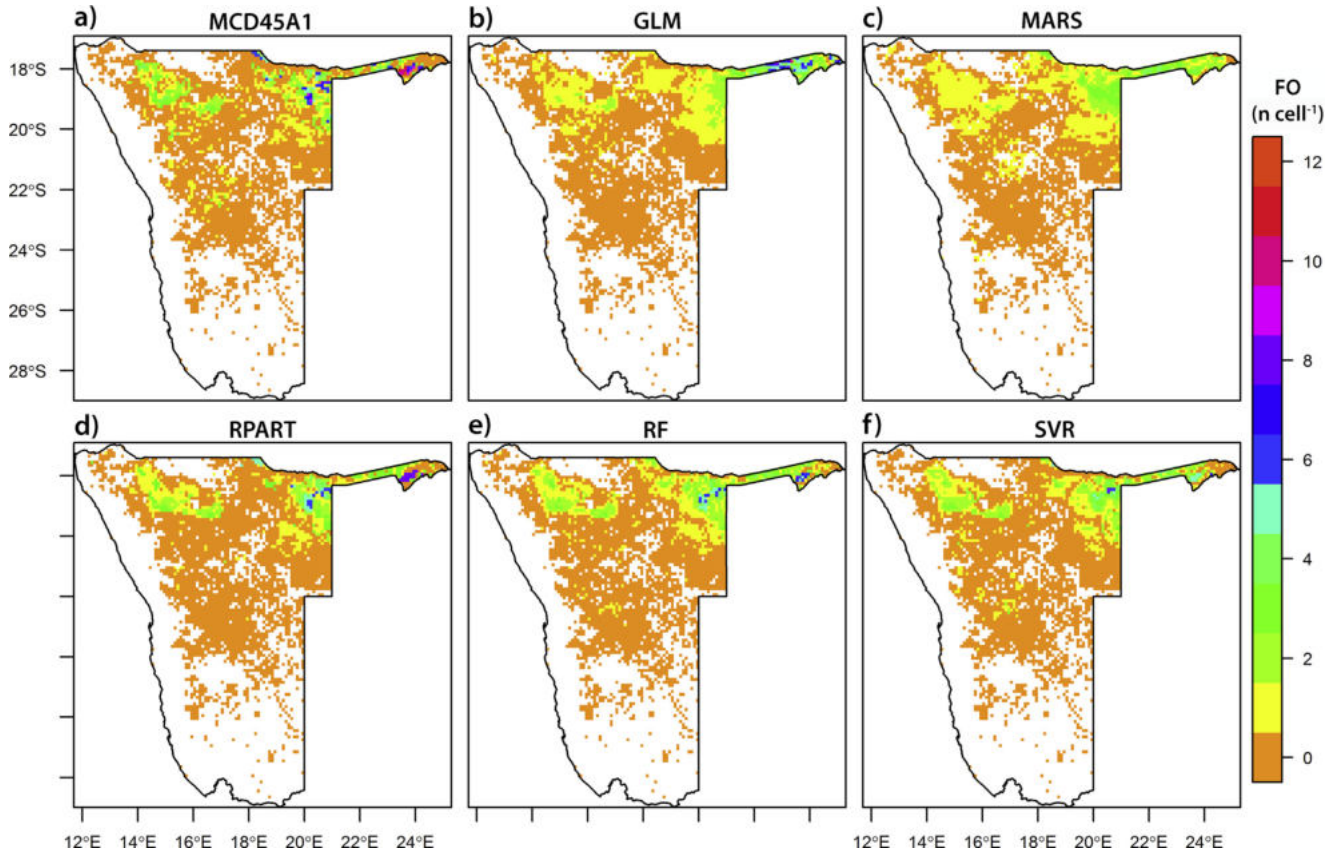

Fig. 4. Observed and predicted Fire Occurrence (FO) of Namibia April 2000–March 2016. Figures depict a) the observed FO based on the MODIS Burned Area product (MCD45A1) aggregated to 0.1° resolution using the majority (n = 3700; including 854 zeros); as well as the predicted FO from b) Generalized Linear Models (GLM); c) Multivariate Adaptive Regression Splines (MARS); d) Recursive Partitioning (RPART); e) Random Forest (RF); and f) Support Vector Regression (SVR).

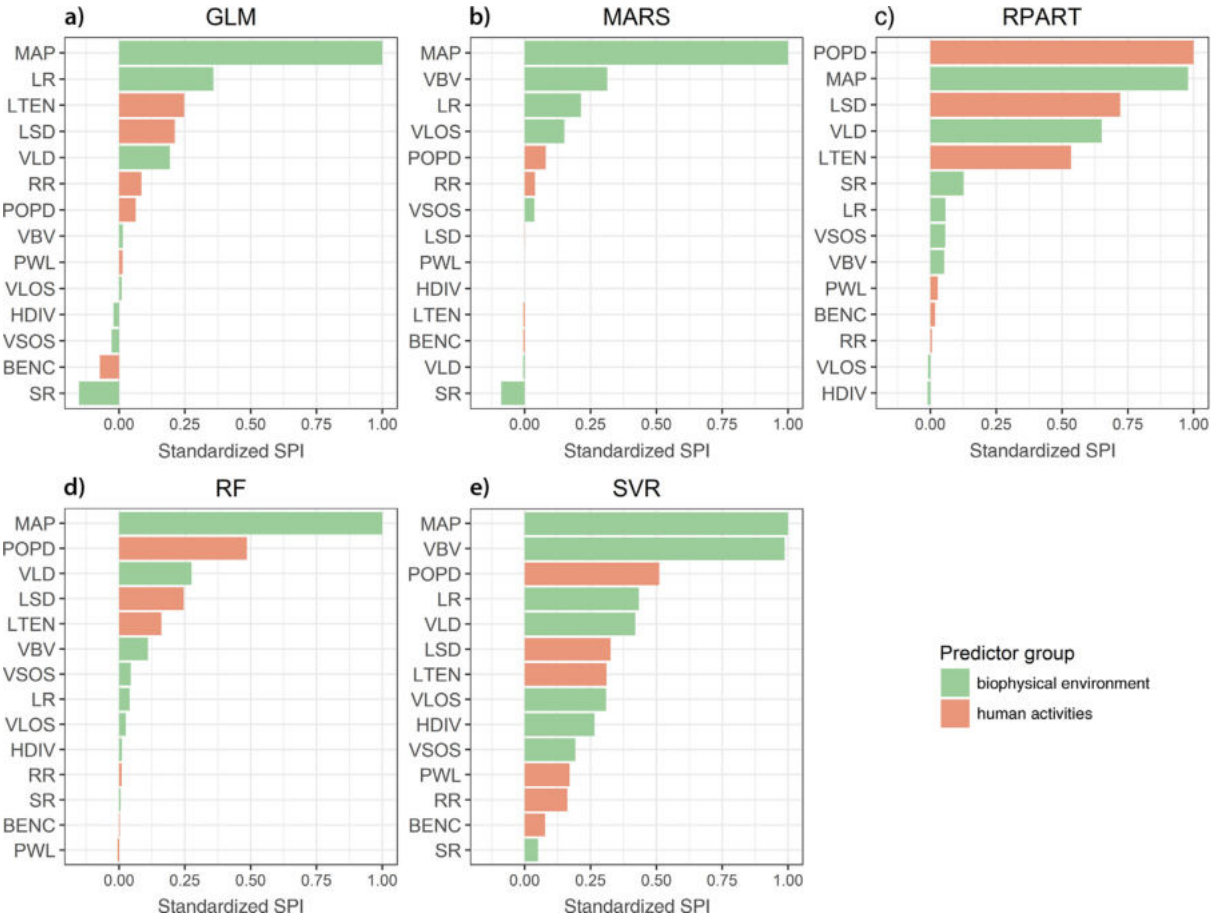

Fig. 5. Spatial Predictor Importance (SPI) of the Burned Area (BA) models: a) Generalized Linear Models (GLM); b) Multivariate Adaptive Regressions Splines (MARS); c) Recursive Partitioning (RPART); d) Random Forest (RF); and e) Support Vector Regression (SVR). SPI was calculated from alterations of the Root Mean Square Error (RMSE) within the spatial cross-validation setup by randomly permuting (n = 50) each of the 14 predictors individually. SPI was then standardized based on division by the predictor of highest importance in the corresponding model. The plots also show the predictors' correspondence to the biophysical environment (in green) or human activities (in orange). (For interpretation of the references to color in this figure legend, the reader is referred to the web version of this article.)

GLM and MARS models.

The primate importance of MAP obtained less agreement with the Fire Occurrence (FO) models as compared to the BA models. However, MAP had the highest and second-highest SPI in all models except for the GLM (Fig. 6). VLD and VBV yielded the highest SPI in the GLM and SVR models, whereas POPD had the highest SPI in the RPART model. Livestock Density (LSD) was of high SPI in four models, but was the least important in the MARS model, where its SPI was negative.

Across the set of BA and FO models under investigation, MAP was the single most important predictor. RPART models consistently outlined POPD as the most important predictor. The predictors related to human activities, POPD and LSD, but also the phytophenological predictors, VLD and VBV, yielded high SPI in many cases. Apart from MAP, no clear pattern regarding the differential importance of biophysical vs. human-related predictors appeared. In many cases, the models outlined a strong gradient in SPI from the (two) highest predictors to the remaining predictor. This pattern was more dominant among the BA models.

3.3. Response dependence

Based on the findings of the previous two sections, the response dependence on the three most important predictors was assessed in the best performing models by means of RMSE, namely the Random Forest (RF).

The highest BA was modeled for areas with high rainfall, low population, and moderate green-up rates. Predicted BA largely followed the gradient of Mean Annual Precipitation (MAP), which was by far the most important predictor of BA (Fig. 5d), with higher BA generally restricted to MAP $>$ 400 mm (Fig. 7a). Likewise, low green-up rates of NDVI (VLD) resulted in low BA, but the highest BA was predicted with moderate VLD. Large scatter of BA appeared with low values of population density (POPD), but high BA was limited to low POPD: e.g. only BA $<$ 30 km^2 $cell^{-1}$ was predicted with more than five inhabitants km^{-2} (POPD $>$ 5).

The dependencies on MAP and POPD retrieved for the predicted FO largely resemble those of BA (Fig. 7b). FO was even more strongly limited by POPD and its importance was almost equal to MAP (Fig. 6d). Additionally, Livestock Density (LSD) exhibited a limiting effect on the predictions of FO, with frequent fire recurrence, i.e. high FO, only predicted for low LSD.

4. Discussion

4.1. Cross-model findings

Seven of ten predictive models ranked Mean Annual Precipitation (MAP) as the most important predictor of fire activity across Namibia (Figs. 5 and 6). The response variables Burned Area (BA) and Fire Occurrence (FO) were considerably correlated. It appears that the five predictive modeling techniques applied here were in many cases able to determine similar relationships with the predictors for both the positive

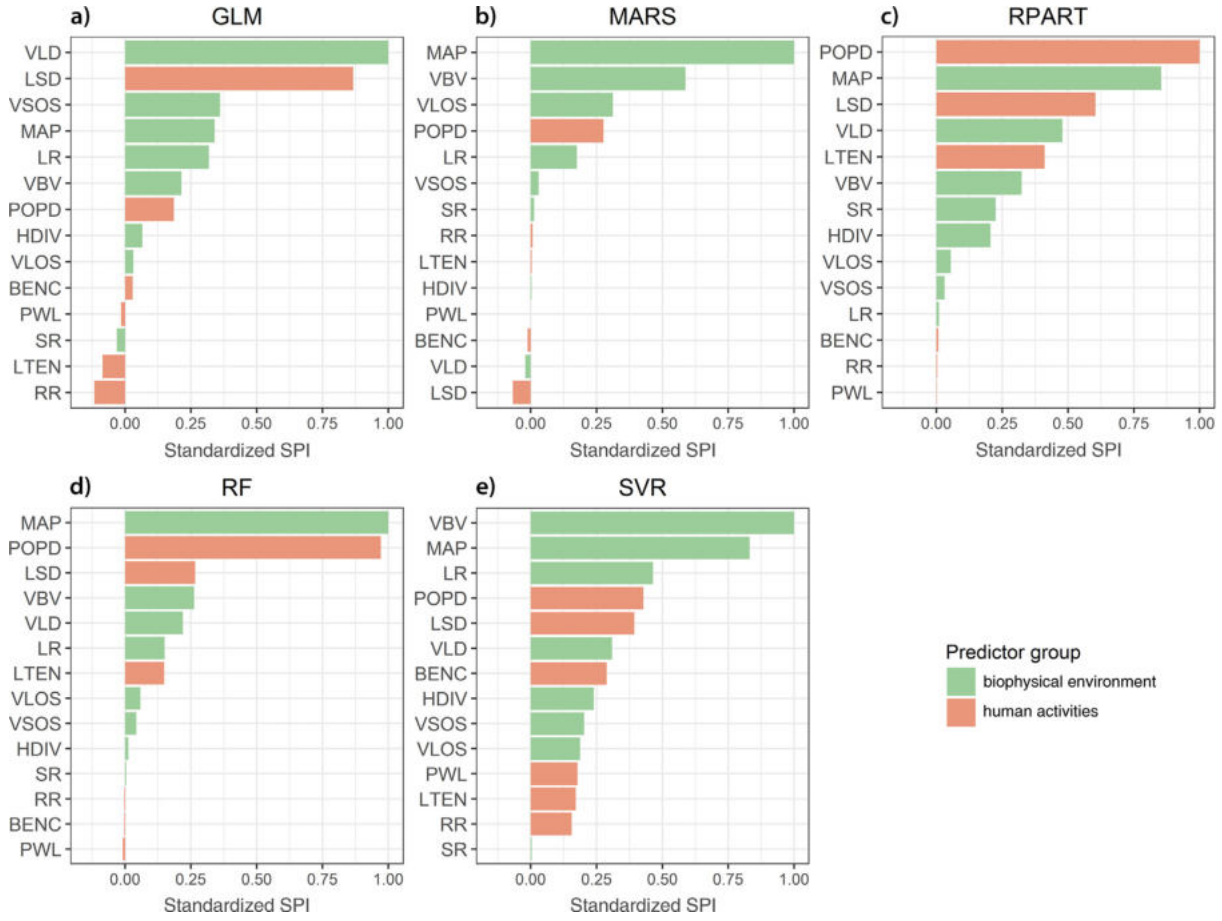

Fig. 6. Same as Fig. 5 but for the Fire Occurrence (FO) models.

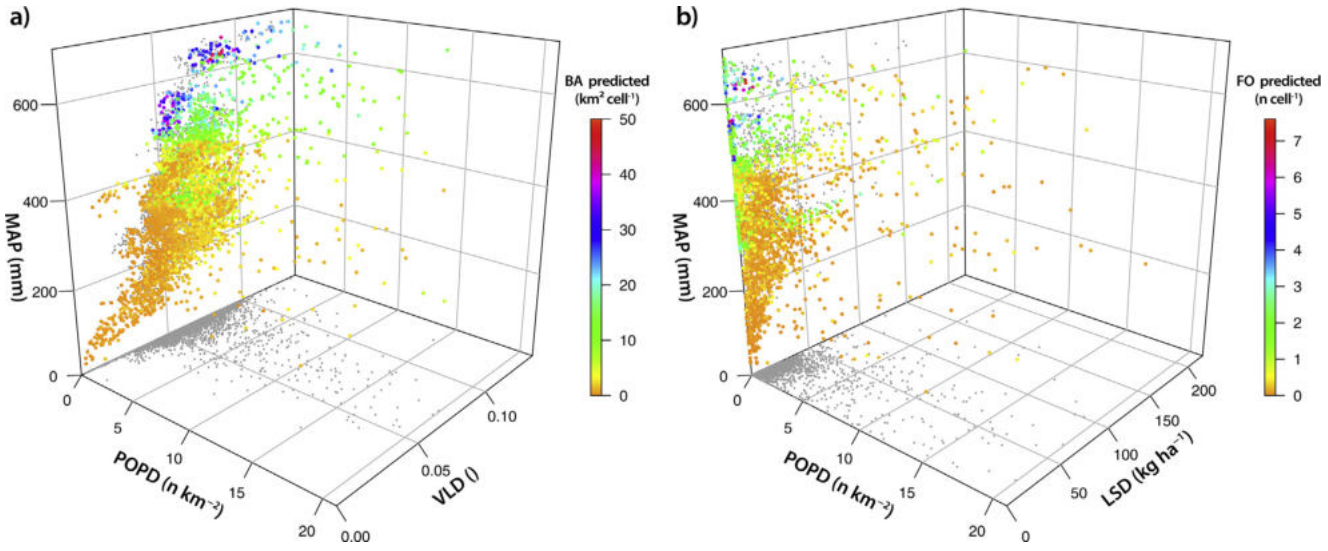

Fig. 7. Dependence of the predicted response in the Random Forest (RF) models: a) Burned Area (BA) vs. Mean Annual Precipitation (MAP), Population Density (POPD), and green-up rate of NDVI (Left Derivative; VLD); b) Fire Occurrence (FO) vs. MAP, POPD, and Livestock Density (LSD). The 3D-plots show the influence of the three predictors with the highest Spatial Predictor Importance (SPI; cf. Figs. 5d and 6d) on the response variable predicted by the RF (in color). Note that 60 of the total 3700 observations were omitted in the figures for reasons of graphical presentation here (i.e. urban areas with POPD > 20 omitted). (For interpretation of the references to color in this figure legend, the reader is referred to the web version of this article.)

continuous BA and the zero-inflated FO. Given that the distribution of both responses was strongly right-skewed, with frequent low BA and FO across Namibia, this might explain the underestimation of the maxima in the models. All models except for the BA Generalized Linear Model (GLM; Fig. 2b) were able to reproduce the general patterns of BA and FO. This is also reflected in the numerical evaluation of model performance, where the BA GLM yielded a substantially higher non-spatial Root Mean Square Error (RMSE) and lower adjusted coefficients of determination (adj.-R^2) as compared to the other models (Table 2). This model was also unique in the way that its RMSE decreased when

applying the spatial Cross-Validation (CV) setup. Although the RMSE of the 50 spatial CV iterations was lower, the variance and maxima among the individual CV iterations increased as compared to its non-spatial setup (not shown). This may be the result of the rather uniform prediction of BA and little indication of spatial structures with this model's predictions (Fig. 2b). The general underestimation by the BA GLM likely reflects the response's distribution, i.e. many low and few high BA values, being inadequately fit with the model's assumed Gamma distribution.

Spatial dependency patterns of fire activity, represented through Spatial Autocorrelation (SAC), were observed and confirmed to be significant for both BA and FO by the correlograms (Fig. 3). The lower, but more realistic model performances retrieved from spatial CV, met our expectations. Apart from the GLM, the relative increases of the RMSE were more apparent in the models of BA, which also had higher SAC as compared to those of the FO models. Lower performances in spatial CV were also found with models that are not violated in their basic assumptions from the presence of SAC, such as the Random Forest (RF; Cutler et al., 2007). As a consequence, we would argue that SAC should generally be considered in performance evaluations if not included as a separate predictor.

Through our graphical (Figs. 2 and 4) and numerical evaluation (Table 2) of the predictions, we conclude that the machine-learning techniques outperformed the GLM, which is in accordance with our initial hypothesis. This finding is likely the result of their ability to detect complex (non-linear) relationships and non-additive interactions, as well as their flexibility with skewed distributions of the response. The performance of statistical techniques, such as GLM, essentially reflects the degree to which the response variable follows its assumed distribution in the model.

Among the machine-learning techniques, the predictions were relatively consistent, but the RF yielded the highest performances in terms of RMSE for BA and FO using non-spatial and spatial CV. This finding is consistent with other studies comparing predictive modeling techniques in a fire-related context (e.g. Faivre et al., 2016; Rodrigues and de la Riva, 2014). Yet we admit that the adj.-R^2 was slightly higher for the predictions with RPART and SVR as compared to RF. We focused on RMSE our investigations of model performance as it allowed to evaluate spatial and non-spatial error setups and to assess individual predictor importance in each model.

4.2. Controls of fire activity in the Random Forest (RF) models

The RF models consistently outlined MAP and Population Density (POPD) as the two most important predictors, however for the FO models POPD was almost of equal importance to MAP.

It was unexpected that the most important predictors related to human activities, namely POPD and Livestock Density (LSD), were of a 'fuel-limiting' nature in the two best-performing models (Fig. 7a, b). This agrees well with the general negative feedback of POPD on FO found in a global study (Knorr et al., 2014), but contradicts the finding of more frequent fires with increasing population across Southern Africa (Archibald et al., 2010b).

The direct influence of livestock on fuel removal appears reasonable. Its fire-limiting effect may also reflect an uncertain amount of tenure and management practices as farmers make efforts to protect their livestock and pastures from fire (*sensu* Le Roux, 2011). The predictor Land Tenure (LTEN) yielded only moderate importance in the RF models.

The green-up rate of NDVI (Left Derivative; VLD) was ranked as the third-most important predictor of BA. Interestingly, the highest BA was predicted with moderate levels of VLD (Fig. 7b). As the green-up rate combines time and overall magnitude, areas of moderate VLD may correspond to open woodlands with sufficient grass biomass that rapidly evolves with the onset of the vegetation period.

4.3. (Non-)stationarity of controls

All models executed here assume the relationships of fire activity with the drivers to be of a stationary nature across the fire-affected area of Namibia and the period of observation (2000–2016). However, it can be hypothesized that these would vary as a function of the scale of investigation, i.e. the areal extent, and resolution. Some predictors that are of a clearly non-stationary nature over the period of observation (e.g. population, roads or power lines; cf. Table 1), were assumed to be constant in our study. Different controls of fire activity were reported in the case of Southern California and separate models were used to infer these (Faivre et al., 2016). In a study covering continental-scale Sub-Saharan Africa, (Sá et al., 2011) the non-stationarity of fire controls is modeled using Geographically Weighted Regression (GWR). GWR was not an option with our dataset due to the limitations of the assumptions associated with the linear model (Brunsdon et al., 1998).

We considered only cells that burned within the period 2000–2016 in this study. It would, however, be interesting to conduct binary models that investigate the controls behind burned and unburned classes. The issue was partly addressed with the FO models that included zeros as a result of a spatial aggregation using the majority values of the respective pixels. Yet the issue would need further investigation – especially on smaller spatial scales. Vast unburned areas along the coast and in the South of Namibia are simply too arid to burn. Instead in Central Owamboland, i.e. in proximity to the city of Oshakati (Fig. 1), the lack of fire is likely the result of high population densities, which would concur with our models. Low fire activity and its exclusion in parts of the Otjozondjupa Region, i.e. eastwards of the cities of Tsumeb and Otjiwarongo (Fig. 1), may eventually reflect people's attitude towards fire there. Fire is largely neglected as a land management tool and landowners aim at fire suppression on these privately-owned commercial farmlands (Le Roux, 2011). Where our study focused on the national scale and thus applied a scale of observation of 0.1°, regional studies may be carried out at higher spatio-temporal resolution and may be able to consider additional predictors. For instance, Verlinden and Laamanen (2006) investigated annual fire recurrence from Landsat imagery in Namibia's Kavango and Zambezi Regions. Their results suggest livestock density and preceding rainfalls to be of negligible importance for annual BA, but the implementation of fire management efforts, such as cut lines and awareness programs, led to significant declines in BA.

Although it was beyond the scope of our investigation, an analysis of the annual and time-lagged controls of fire activity, such as last fire and fuel accumulation, could shed light into the potential dynamics of the controls behind Namibia's fire regimes. Biennial precipitation sums were found to drive fire occurrence in Etosha National Park (Siegfried, 1981), but this relationship could be weakened where fuels are largely removed by natural and domestic herbivory. As Krawchuk and Moritz (2014) point out, a general agreement on whether averaged predictors or their extremes and inter-annual variation should be favored is lacking. In a study from boreal Canada that compared the annual vs. average controls of fire activity, the relationships varied little (Parisien et al., 2014). To the best of our knowledge this issue has not yet been addressed in detail for Southern African savannas but we acknowledge that it is of crucial relevance for the assessment of potential future fire activity based on stationary controls (e.g. Mann et al., 2016).

4.4. Data quality of MCD45A1

As a ground-based national fire inventory does not exist for Namibia, the MODIS Burned Area product (MCD45A1 v5.1) was the best choice to derive the records of the fire regime parameters at the time of conducting the analyses. A major drawback of such datasets from moderate-resolution sensors are the low detection rates of obscured understory fires, and – what is likely more crucial with semi (-arid) savanna ecosystems – the detection of small and low-intensity

fires (Krawchuk and Moritz, 2014).

In early 2017, the MCD64A1 v6 product was launched which is based on a hybrid algorithm described by Giglio et al. (2009). This version of MCD64A1 applies multi-temporal change detection known from MCD45A1 and additionally makes use of active fire hotspots, which aims at lower omission errors, increased detection of small fires, and improving detections under cloudy conditions (Giglio et al., 2016). Where the latter is probably negligible due to mostly clear conditions during Namibia's fire season, our records of BA and FO may benefit from an improved detection of small fires, which is a limitation of MCD45A1. The detection problems of low-intensity fires from croplands are reported to remain with the new MCD64A1 dataset (Zhu et al., 2017). An evaluation of our findings based on MCD64A1 is a declared follow-up task of this study.

5. Conclusion

The study presented here has confirmed the fuel limitation of (semi-)arid ecosystems. Based on a 16-year record (April 2000-March 2016) derived from the MODIS Burned Area product (MCD45A1) and a large set of environmental and human-related predictors, we assessed the controls of two main fire regime parameters in Namibia, namely Burned Area (BA) and Fire Occurrence (FO). We examined the predictive performance of five common statistical and machine-learning techniques and considered the effects of spatial autocorrelation in their evaluation. Machine-learning techniques improved the predictions of BA and FO, which we attribute to their ability to detect complex non-linear interactions. Where model performances generally decreased with the consideration of spatial effects and even showed indications of proportionality, we recommend accounting for potential spatial autocorrelation.

Our findings highlight the exceptional importance of average precipitation for fire activity across Namibia. Precipitation indirectly controls fire activity by productivity and, thus, by the availability of (surface) fuels. In the Random Forest models which performed best according to the Root Mean Square Error, both fire regime parameters were predicted to increase above an approximate threshold of 400 mm. A certain openness of the landscape, which was indicated by moderate levels of vegetation green-up, appeared to be beneficial to BA and, hence, the extent of fires. Human activities, such as the number of inhabitants and livestock amount, modify the biophysical determination of fire activity on smaller spatial scales as they additionally 'consume' fuels. Resultantly, consistent negative relationships were retrieved for both fire regime parameters.

Although smaller and lower-intensity fires are largely missed with the MCD45A1 record and non-stationarity of the relationships retrieved cannot be neglected, our findings may facilitate a framework for an effective and adaptive fire management in Namibia. The adaptation of our model to other regions, however, needs further testing as the land use practices and the low population in Namibia may limit transferability.

Conflicts of interest

None.

Funding

Manuel J. Mayr was supported by the University of Bayreuth's Graduate School and received travel funding from the German Academic Exchange Service (DAAD).

Acknowledgments

We gratefully acknowledge Johan Le Roux for several fruitful discussions and Daniela Kretz for her constructive remarks on the use of the English language.

References

Albrecht, R.I., Goodman, S.J., Buechler, D.E., Blakeslee, R.J., Christian, H.J., 2016. LIS 0.1 Degree Very High Resolution Gridded Lightning Monthly Climatology (VHRMC). NASA Global Hydrology Center DAAC, Huntsville, AL. https://ghrc.nsstc.nasa.gov/hydro/details/lisvhrmc (accessed 6 March 2017). DOI: 10.5067/LIS/LIS/DATA302.

Altmann, A., Tolosi, L., Sander, O., Lengauer, T., 2010. Permutation importance. A corrected feature importance measure. Bioinformatics 26 (10), 1340–1347. http://dx.doi.org/10.1093/bioinformatics/btq134.

Amatulli, G., Rodrigues, M.J., Trombetti, M., Lovreglio, R., 2006. Assessing long-term fire risk at local scale by means of decision tree technique. J. Geophys. Res. Biogeosci. 111, G04S05. http://dx.doi.org/10.1029/2005JG000133.

Andela, N., Morton, D.C., Giglio, L., Chen, Y., van der Werf, G.R., Kasibhatla, P.S., DeFries, R.S., Collatz, G.J., Hantson, S., Kloster, S., Bachelet, D., Forrest, M., Lasslop, G., Li, F., Mangeon, S., Melton, J.R., Yue, C., Randerson, J.T., 2017. A human-driven decline in global burned area. Science 356 (6345), 1356–1362. http://dx.doi.org/10.1126/science.aal4108.

Archibald, S., Nickless, A., Govender, N., Scholes, R.J., Lehsten, V., 2010a. Climate and the inter-annual variability of fire in southern Africa. A meta-analysis using long-term field data and satellite-derived burnt area data. Glob. Ecol. Biogeogr. 19 (6), 794–809. http://dx.doi.org/10.1111/j.1466-8238.2010.00568.x.

Archibald, S., Roy, D.P., van Wilgen, B.W., Scholes, R.J., 2009. What limits fire? An examination of drivers of burnt area in Southern Africa. Glob. Change Biol. 15 (3), 613–630. http://dx.doi.org/10.1111/j.1365-2486.2008.01754.x.

Archibald, S., Scholes, R.J., Roy, D.P., Roberts, G., Boschetti, L., 2010b. Southern African fire regimes as revealed by remote sensing. Int. J. Wildland Fire 19 (7), 861. http://dx.doi.org/10.1071/WF10008.

Archibald, S., Staver, A.C., Levin, S.A., 2012. Evolution of human-driven fire regimes in Africa. Proc. Natl. Acad. Sci. U.S.A. 109 (3), 847–852. http://dx.doi.org/10.1073/pnas.1118648109.

Asadullah, A., McIntyre, N., Kigobe, M., 2008. Evaluation of five satellite products for estimation of rainfall over Uganda/Evaluation de cinq produits satellitaires pour l'estimation des précipitations en Ouganda. Hydrol. Sci. J. 53 (6), 1137–1150. http://dx.doi.org/10.1623/hysj.53.6.1137.

Bar Massada, A., Syphard, A.D., Stewart, S.I., Radeloff, V.C., 2012. Wildfire ignition-distribution modelling. A comparative study in the Huron-Manistee National Forest, Michigan, USA. Int. J. Wildland Fire 22 (2), 174–183. http://dx.doi.org/10.1071/WF11178.

Beatty, R., 2011. Annexes – CBFiM case studies. Annex 1: CBFiM in Namibia: the Caprivi Integrated Fire Management programme. In: FAO (Food and Agriculture Organization of the United Nations), Community-based fire management. A Review. FAO, Rome, pp. 41–47. http://www.fao.org/docrep/015/i2495e/i2495e10.pdf (accessed 5 November 2016).

Bedia, J., Herrera, S., Gutiérrez, J.M., 2014. Assessing the predictability of fire occurrence and area burned across phytoclimatic regions in Spain. Nat. Hazards Earth Syst. Sci. 14 (1), 53–66. http://dx.doi.org/10.5194/nhess-14-53-2014.

Beringer, J., Hutley, L.B., Abramson, D., Arndt, S.K., Briggs, P., Bristow, M., Canadell, J.G., Cernusak, L.A., Eamus, D., Edwards, A.C., Evans, B.J., Fest, B., Goergen, K., Grover, S.P., Hacker, J., Haverd, V., Kanniah, K., Livesley, S.J., Lynch, A., Maier, S., Moore, C., Raupach, M., Russell-Smith, J., Scheiter, S., Tapper, N.J., Uotila, P., 2015. Fire in Australian savannas. From leaf to landscape. Glob. Change Biol. 21 (1), 62–81 DOI: 10.1111/gcb.12686.

Bjornstad, O.N., 2016. ncf: Spatial Nonparametric Covariance Functions. R Package Version 1.1-7. https://cran.r-project.org/package=ncf (accessed 9 January 2017).

Blamey, R.C., Reason, C.J.C., 2013. The role of mesoscale convective complexes in Southern Africa summer rainfall. J. Clim. 26 (5), 1654–1668. http://dx.doi.org/10.1175/JCLI-D-12-00239.1.

Bond, T.C., Doherty, S.J., Fahey, D.W., Forster, P.M., Berntsen, T., DeAngelo, B.J., Flanner, M.G., Ghan, S., Kärcher, B., Koch, D., Kinne, S., Kondo, Y., Quinn, P.K., Sarofim, M.C., Schultz, M.G., Schulz, M., Venkataraman, C., Zhang, H., Zhang, S., Bellouin, N., Guttikunda, S.K., Hopke, P.K., Jacobsen, M.Z., Kaiser, J.W., Klimont, Z., Lohmann, U., Schwarz, J.P., Shindell, D., Storelvmo, T., Warren, S.G., Zender, C.S., 2013. Bounding the role of black carbon in the climate system: a scientific assessment. J. Geophys. Res. Atmos. 118, 5380–5552. http://dx.doi.org/10.1002/jgrd.50171.

Bond, W.J., 2008. What limits trees in C 4 grasslands and savannas? Annu. Rev. Ecol. Evol. Syst. 39 (1), 641–659. http://dx.doi.org/10.1146/annurev.ecolsys.39.110707.173411.

Bond, W.J., Keeley, J.E., 2005. Fire as a global 'herbivore': the ecology and evolution of flammable ecosystems. Trends Ecol. Evol. 20 (7), 387–394. http://dx.doi.org/10.1016/j.tree.2005.04.025.

Boschetti, L., Roy, D., Hoffmann, A.A., Humber, M., 2013. MODIS Collection 5.1 Burned Area Product – MCD45. User's Guide Version 3.0.1. http://modis-fire.umd.edu/files/MODIS_Burned_Area_Collection51_User_Guide_3.0.pdf (accessed 10 December 2016).

Boschetti, L., Roy, D.P., 2008. Defining a fire year for reporting and analysis of global interannual fire variability. J. Geophys. Res. 113 (G3), 525. http://dx.doi.org/10.1029/2008JG000686.

Bowman, D.M.J.S., Balch, J.K., Artaxo, P., Bond, W.J., Carlson, J.M., Cochrane, M.A., D'Antonio, C.M., DeFries, R.S., Doyle, J.C., Harrison, S.P., Johnston, F.H., Keeley, J.E., Krawchuk, M.A., Kull, C.A., Marston, J.B., Moritz, M.A., Prentice, I.C., Roos, C.I., Scott, A.C., Swetnam, T.W., van der Werf, G.R., Pyne, S.J., 2009. Fire in the earth system. Science 324, 481–484. http://dx.doi.org/10.1126/science.1163886.

Breiman, L., 2001. Random forests. Mach. Learn. 45 (1), 5–32. http://dx.doi.org/10.

1023/A:1010933404324.
Breiman, L., Friedman, J.H., Stone, C.J., Olshen, R.A., 1984. Classification and Regression Trees. Wadsworth, Belmont, CA.
Brenning, A., 2012. Spatial cross-validation and bootstrap for the assessment of prediction rules in remote sensing: the R package sperrorest. In: IGARSS (IEEE International Geoscience and Remote Sensing Symposium) 2012. Munich, Germany, pp. 5372–5375. http://doi.org/10.1109/IGARSS.2012.6352393.
Brunsdon, C., Fotheringham, S., Charlton, M., 1998. Geographically weighted regression. modelling spatial non-stationarity. J. R. Stat. Soc. D 47 (3), 431–443. http://dx.doi.org/10.1111/1467-9884.00145.
Cerling, T.E., Harris, J.M., MacFadden, B.J., Leakey, M.G., Quade, J., Eisenmann, V., Ehleringer, J.R., 1997. Global vegetation change through the Miocene/Pliocene boundary. Nature 389, 153–158. http://dx.doi.org/10.1038/38229.
Chen, J., Jönsson, P., Tamura, M., Gu, Z., Matsushita, B., Eklundh, L., 2004. A simple method for reconstructing a high-quality NDVI time-series data set based on the Savitzky-Golay filter. Remote Sens. Environ. 91 (3–4), 332–344. http://dx.doi.org/10.1016/j.rse.2004.03.014.
Coetsee, C., Bond, W.J., February, E.C., 2010. Frequent fire affects soil nitrogen and carbon in an African savanna by changing woody cover. Oecologia 162 (4), 1027–1034. http://dx.doi.org/10.1007/s00442-009-1490-y.
Cortes, C., Vapnik, V., 1995. Support-vector networks. Mach. Learn. 20 (3), 273–297. http://dx.doi.org/10.1007/BF00994018.
Cortez, P., Morais, A., 2007. A data mining approach to predict forest fires using meteorological data. In: Neves, J., Santos, M.F., Machado, J. (Eds.), New Trends in Artificial Intelligence. Proceedings of the 13th EPIA 2007 – Portuguese Conference on Artificial Intelligence. Guimarães, Portugal, pp. 512–523.
Crawley, M.J., 2007. The R Book. John Wiley & Sons, Chichester, England, Hoboken, NJ.
Cutler, D.R., Edwards, T.C., Beard, K.H., Cutler, A., Hess, K.T., Gibson, J., Lawler, J.J., 2007. Random forests for classification in ecology. Ecology 88 (11), 2783–2792. http://dx.doi.org/10.1890/07-0539.1.
Dinku, T., Ceccato, P., Grover-Kopec, E., Lemma, M., Connor, S.J., Ropelewski, C.F., 2007. Validation of satellite rainfall products over East Africa's complex topography. Int. J. Remote Sens. 28 (7), 1503–1526. http://dx.doi.org/10.1080/01431160600954688.
Dobson, A.J., 2002. An Introduction to Generalized Linear Models, second ed. Chapman & Hall/CRC, Boca Raton, CA.
Dormann, C.F., McPherson, J.M., Araújo, M.B., Bivand, R., Bolliger, J., Carl, G., Davies, R.G., Hirzel, A., Jetz, W., Kissling, W.D., Kühn, I., Ohlemüller, R., Peres-Neto, P.R., Reineking, B., Schröder, B., Schurr, F.M., Wilson, R., 2007. Methods to account for spatial autocorrelation in the analysis of species distributional data. A review. Ecography 30 (5), 609–628. http://dx.doi.org/10.1111/j.2007.0906-7590.05171.x.
Dorner, B., Lertzman, K., Fall, J., 2002. Landscape pattern in topographically complex landscapes: issues and techniques for analysis. Landscape Ecol. 17 (8), 729–743. http://dx.doi.org/10.1023/A:1022944019665.
Dunn, P.K., Smyth, G.K., 2005. Series evaluation of Tweedie exponential dispersion model densities. Stat. Comput. 15 (4), 267–280. http://dx.doi.org/10.1007/s11222-005-4070-y.
Faivre, N.R., Jin, Y., Goulden, M.L., Randerson, J.T., 2016. Spatial patterns and controls on burned area for two contrasting fire regimes in Southern California. Ecosphere 7 (5), e01210. http://dx.doi.org/10.1002/ecs2.1210.
Fensholt, R., Rasmussen, K., Nielsen, T.T., Mbow, C., 2009. Evaluation of earth observation based long term vegetation trends – intercomparing NDVI time series trend analysis consistency of Sahel from AVHRR GIMMS, Terra MODIS and SPOT VGT data. Remote Sens. Environ. 113 (9), 1886–1898. http://dx.doi.org/10.1016/j.rse.2009.04.004.
Friedman, J.H., 1991. Multivariate adaptive regression splines. Ann. Stat. 19 (1), 1–67. http://dx.doi.org/10.1214/aos/1176347963.
Giglio, L., Boschetti, L., Roy, D., Hoffmann, A.A., Humber, M., 2016. Collection 6 MODIS Burned Area Product User's Guide. Version 1.0. http://modis-fire.umd.edu/files/MODIS_C6_BA_User_Guide_1.0.pdf (accessed 24 July 2017).
Giglio, L., Loboda, T., Roy, D.P., Quayle, B., Justice, C.O., 2009. An active-fire based burned area mapping algorithm for the MODIS sensor. Remote Sens. Environ. 113 (2), 408–420. http://dx.doi.org/10.1016/j.rse.2008.10.006.
Giglio, L., Randerson, J.T., van der Werf, G.R., 2013. Analysis of daily, monthly, and annual burned area using the fourth-generation global fire emissions database (GFED4). J. Geophys. Res. Biogeosci. 118 (1), 317–328. http://dx.doi.org/10.1002/jgrg.20042.
Goetz, J.N., Brenning, A., Petschko, H., Leopold, P., 2015. Evaluating machine learning and statistical prediction techniques for landslide susceptibility modeling. Comput. Geosci. 81, 1–11. http://dx.doi.org/10.1016/j.cageo.2015.04.007.
Guyette, R.P., Muzika, R.M., Dey, D.C., 2002. Dynamics of an anthropogenic fire regime. Ecosystems 5 (5), 472–486. http://dx.doi.org/10.1007/s10021-002-0115-7.
Hastie, T., Tibshirani, R., Friedman, J., 2009. The Elements of Statistical Learning, second ed. Springer, New York, NY.
Heinl, M., Neuenschwander, A., Sliva, J., Vanderpost, C., 2006. Interactions between fire and flooding in a southern African floodplain system (Okavango Delta, Botswana). Landscape Ecol. 21 (5), 699–709. http://dx.doi.org/10.1007/s10980-005-5243-y.
Heinl, M., Sliva, J., Murray-Hudson, M., Tacheba, B., 2007. Post-fire succession on savanna habitats in the Okavango Delta wetland, Botswana. J. Trop. Ecol. 23 (6), 705–713. http://dx.doi.org/10.1017/S0266467407004452.
Huete, A., Didan, K., Miura, T., Rodriguez, E.P., Gao, X., Ferreira, L.G., 2002. Overview of the radiometric and biophysical performance of the MODIS vegetation indices. Remote Sens. Environ. 83 (1–2), 195–213. http://dx.doi.org/10.1016/S0034-4257(02)00096-2.
Jarvis, A., Reuter, H.I., Nelson, A., Guevara, E., 2008. Hole-filled SRTM for the Globe Version 4. CGIAR-CSI SRTM 90m Database. http://srtm.csi.cgiar.org (accessed 14 June 2017).
Jönsson, P., Eklundh, L., 2004. TIMESAT – a program for analyzing time-series of satellite sensor data. Comput. Geosci. 30 (8), 833–845. http://dx.doi.org/10.1016/j.cageo.2004.05.006.
Karatzoglou, A., Meyer, D., Hornik, K., 2006. Support vector machines in R. J. Stat. Softw. 15 (9), 1–28. http://dx.doi.org/10.18637/jss.v015.i09.
Keeley, J.E., Fotheringham, C.J., Baer-Keeley, M., 2005. Determinants of post-fire recovery and succession in mediterranean-climate shrublands of California. Ecol. Appl. 15 (5), 1515–1534. http://dx.doi.org/10.1890/04-1005.
Kirtman, B., Power, S.B., Adedoyin, J.A., Boer, G.J., Bojariu, R., Camilloni, I., Doblas-Reyes, F.J., Fiore, A.M., Kimoto, M., Meehl, G.A., Prather, M., Sarr, A., Schär, C., Sutton, R., van Oldenborgh, G.J., Vecchi, G., Wang, H.J., 2013. Near-term climate change. projections and predictability. In: Stocker, T.F., Qin, D., Plattner, G.-K., Tignor, M., Allen, S.K., Boschung, J., Nauels, A., Xia, Y., Bex, V., Midgley, P.M. (Eds.), Climate Change 2013. The Physical Science Basis. Contribution of Working Group I to the Fifth Assessment Report of the Intergovernmental Panel on Climate Change. Cambridge University Press, Cambridge, UK, New York, NY, pp. 953–1028.
de Klerk, H.M., Wilson, A.M., Steenkamp, K., 2012. Evaluation of satellite-derived burned area products for the fynbos, a Mediterranean shrubland. Int. J. Wildland Fire 21 (1), 36–47. http://dx.doi.org/10.1071/WF11002.
de Klerk, J.N., 2004. Bush Encroachment in Namibia. Report on Phase 1 of the Bush Encroachment Research, Monitoring and Management Project. Ministry of Environment and Tourism, Windhoek, Namibia. http://www.the-eis.com/data/literature/Bush%20Encoachment%20in%20Namibia_deKlerk2004_1.pdf (accessed 24 October 2013).
Knorr, W., Kaminski, T., Arneth, A., Weber, U., 2014. Impact of human population density on fire frequency at the global scale. Biogeosciences 11 (4), 1085–1102. http://dx.doi.org/10.5194/bg-11-1085-2014.
Krawchuk, M.A., Moritz, M.A., 2011. Constraints on global fire activity vary across a resource gradient. Ecology 92 (1), 121–132. http://dx.doi.org/10.1890/09-1843.1.
Krawchuk, M.A., Moritz, M.A., 2014. Burning issues. Statistical analyses of global fire data to inform assessments of environmental change. Environmetrics 25 (6), 472–481. http://dx.doi.org/10.1002/env.2287.
Krawchuk, M.A., Moritz, M.A., Parisien, M.-A., van Dorn, J., Hayhoe, K., 2009. Global pyrogeography: the current and future distribution of wildfire. PLoS One 4 (4), e5102. http://dx.doi.org/10.1371/journal.pone.0005102.
Kuhn, M., Johnson, K., 2013. Applied Predictive Modeling. Springer, New York, NY.
Le Roux, J., 2011. The Effect of Land Use Practices on the Spatial and Temporal Characteristics of Savanna Fires in Namibia (Doctoral Dissertation). Friedrich-Alexander-University of Erlangen-Nuremberg, Germany.
Lehsten, V., Tansey, K., Balzter, H., Thonicke, K., Spessa, A., Weber, U., Smith, B., Arneth, A., 2009. Estimating carbon emissions from African wildfires. Biogeosciences 6, 349–360. http://dx.doi.org/10.5194/bg-6-349-2009.
Liaw, A., Wiener, M., 2002. Classification and regression by randomForest. R News 2 (3), 18–22.
Loh, W.-Y., 2011. Classification and regression trees. Wiley Interdisc. Rev. Data Min. Knowl. Discov. 1 (1), 14–23. http://dx.doi.org/10.1002/widm.8.
Mann, M.L., Batllori, E., Moritz, M.A., Waller, E.K., Berck, P., Flint, A.L., Flint, L.E., Dolfi, E., 2016. Incorporating anthropogenic influences into fire probability models. Effects of human activity and climate change on fire activity in California. PLoS One 11 (4), e0153589. http://dx.doi.org/10.1371/journal.pone.0153589.
Mayr, M.J., Malß, S., Ofner, E., Samimi, C., 2017. Disturbance feedbacks on the height of woody vegetation in a savannah. A multi-plot assessment using an unmanned aerial vehicle (UAV). Int. J. Remote Sens. 32 (3), 1–25. http://dx.doi.org/10.1080/01431161.2017.1362132.
Mayr, M.J., Samimi, C., 2015. Comparing the dry season *in-situ* leaf area index (LAI) derived from high-resolution RapidEye imagery with MODIS LAI in a Namibian Savanna. Remote Sens. 7, 4834–4857. http://dx.doi.org/10.3390/rs70404834.
Mendelsohn, J.M., Jarvis, A., Roberts, C., Robertson, T., 2002. Atlas of Namibia – A Portrait of the Land and Its People. David Philip Publishers, Cape Town, South Africa.
MET (Ministry of Environment and Tourism), 2016. Fire Management Strategy for Namibia's Protected Areas. MET – Directorate of Wildlife and National Parks, Windhoek, Namibia. http://www.met.gov.na/files/downloads/66c_Fire%20Management_Strategy%20Final%20Version.pdf (accessed 15 December 2016).
Meyer, D., Dimitriadou, E., Hornik, K., Weingessel, A., Leisch, F., 2017. e1071: Misc Functions of the Department of Statistics (e1071), TU Wien. R Package version 1.6-8. https://cran.r-project.org/package=e1071 (accessed 13 March 2017).
Milborrow, S., 2017. Earth: Multivariate Adaptive Regression Splines. Derived from mda:mars by T. Hastie and R. Tibshirani. R Package Version 4.5.1. https://cran.r-project.org/package=earth (accessed 14 August 2017).
Moran, P.A.P., 1950. Notes on continuous stochastic phenomena. Biometrika 37 (1/2), 17–23. http://dx.doi.org/10.2307/2332142.
Mouillot, F., Schultz, M.G., Yue, C., Cadule, P., Tansey, K., Ciais, P., Chuvieco, E., 2014. Ten years of global burned area products from spaceborne remote sensing – a review. Analysis of user needs and recommendations for future developments. Int. J. Appl. Earth Observ. 26, 64–79. http://dx.doi.org/10.1016/j.jag.2013.05.014.
Mullahy, J., 1986. Specification and testing of some modified count data models. J. Econometr. 33 (3), 341–365. http://dx.doi.org/10.1016/0304-4076(86)90002-3.
Nelder, J.A., Wedderburn, R.W.M., 1972. Generalized linear models. J. R. Stat. Soc. A 135 (3), 370–384.
Nelson, D.M., Verschuren, D., Urban, M.A., Hu, F.S., 2012. Long-term variability and rainfall control of savanna fire regimes in equatorial East Africa. Glob. Change Biol. 18 (10), 3160–3170. http://dx.doi.org/10.1111/j.1365-2486.2012.02766.x.
O'Connor, T.G., Mulqueeny, C.M., Goodman, P.S., 2011. Determinants of spatial variation in fire return period in a semiarid African savanna. Int. J. Wildland Fire 20 (4), 540–549. http://dx.doi.org/10.1071/WF08142.

O'Connor, T.G., Puttick, J.R., Hoffman, M.T., 2014. Bush encroachment in southern Africa. Changes and causes. Afr. J. Range For. Sci. 31 (2), 67–88. http://dx.doi.org/10.2989/10220119.2014.939996.

Parisien, M.-A., Parks, S.A., Krawchuk, M.A., Little, J.M., Flannigan, M.D., Gowman, L.M., Moritz, M.A., 2014. An analysis of controls on fire activity in boreal Canada. Comparing models built with different temporal resolutions. Ecol. Appl. 24 (6), 1341–1356. http://dx.doi.org/10.1890/13-1477.1.

Pausas, J.G., Ribeiro, E., 2013. The global fire-productivity relationship. Glob. Ecol. Biogeogr. 22 (6), 728–736. http://dx.doi.org/10.1111/geb.12043.

Pausas, J.G., Verdú, M., 2008. Fire reduces morphospace occupation in plant communities. Ecology 89 (8), 2181–2186. http://dx.doi.org/10.1890/07-1737.1.

Pivello, V.R., Oliveras, I., Miranda, H.S., Haridasan, M., Sato, M.N., Meirelles, S.T., 2010. Effect of fires on soil nutrient availability in an open savanna in Central Brazil. Plant Soil 337 (1–2), 111–123. http://dx.doi.org/10.1007/s11104-010-0508-x.

Pricope, N.G., Binford, M.W., 2012. A spatio-temporal analysis of fire recurrence and extent for semi-arid savanna ecosystems in southern Africa using moderate-resolution satellite imagery. J. Environ. Manage. 100, 72–85. http://dx.doi.org/10.1016/j.jenvman.2012.01.024.

QGIS Development Team, 2015. QGIS (Quantum Geographical Information System). Version 2.8.3 'Wien'. https://qgis.org (accessed on 11 December 2017).

R Core Team, 2016. R: A Language and Environment for Statistical Computing. Version 3.3.2. R Foundation for Statistical Computing, Vienna, Austria. https://www.r-project.org/ (accessed 11 December 2017).

Rodrigues, M., de la Riva, J., 2014. An insight into machine-learning algorithms to model human-caused wildfire occurrence. Environ. Modell. Softw. 57, 192–201. http://dx.doi.org/10.1016/j.envsoft.2014.03.003.

Roy, D.P., Boschetti, L., 2009. Southern Africa validation of the MODIS, L3JRC, and GlobCarbon burned-area products. IEEE Trans. Geosci. Remote Sens. 47 (4), 1032–1044. http://dx.doi.org/10.1109/TGRS.2008.2009000.

Roy, D.P., Boschetti, L., Justice, C.O., Ju, J., 2008. The collection 5 MODIS burned area product – global evaluation by comparison with the MODIS active fire product. Remote Sens. Environ. 112 (9), 3690–3707. http://dx.doi.org/10.1016/j.rse.2008.05.013.

Roy, D.P., Jin, Y., Lewis, P.E., Justice, C.O., 2005. Prototyping a global algorithm for systematic fire-affected area mapping using MODIS time series data. Remote Sens. Environ. 97 (2), 137–162. http://dx.doi.org/10.1016/j.rse.2005.04.007.

Ruß, G., Brenning, A., 2010. Data mining in precision agriculture. Management of spatial information. In: Hüllermeier, E., Kruse, R., Hoffmann, F. (Eds.), Computational Intelligence for Knowledge-Based Systems Design. Springer, Heidelberg, Berlin, Germany, pp. 350–359.

Sá, A.C.L., Pereira, J.M.C., Charlton, M.E., Mota, B., Barbosa, P.M., Fotheringham, A.S., 2011. The pyrogeography of sub-Saharan Africa: a study of the spatial non-stationarity of fire–environment relationships using GWR. J. Geogr. Syst. 13 (3), 227–248. http://dx.doi.org/10.1007/s10109-010-0123-7.

Settele, J., Scholes, R.J., Betts, R., Bunn, S., Leadley, P., Nepstad, D., Overpeck, J.T., Taboada, M.A., 2014. Terrestrial and inland water systems. In: Field, C.B., Barros, V.R., Dokken, D.J., Mach, K.J., Mastrandrea, M.D., Bilir, T.E., Chatterjee, M., Ebi, K.L., Estrada, Y.O., Genova, R.C., Girma, B., Kissel, E.S., Levy, A.N., MacCracken, S., Mastrandrea, P.R., White, L.L. (Eds.), Climate Change 2014. Impacts, Adaptions, Vulnerability. Part A: Global and Sectoral Aspects. Contribution of Working Group II to the Fifth Assessment Report of the Intergovernmental Panel on Climate Change. Cambridge University Press, Cambridge, UK, New York, NY, pp. 271–359.

Siegfried, W.R., 1981. The incidence of veld-fire in the Etosha National Park, 1970–1979. Madoqua 12 (4), 225–230.

Singal, A.G., Mukherjee, A., Elmunzer, B.J., Higgins, P.D.R., Lok, A.S., Zhu, J., Marrero, J.A., Waljee, A.K., 2013. Machine learning algorithms outperform conventional regression models in predicting development of hepatocellular carcinoma. Am. J. Gastroenterol. 108 (11), 1723–1730. http://dx.doi.org/10.1038/ajg.2013.332.

Smola, A.J., Schölkopf, B., 2004. A tutorial on support vector regression. Stat. Comput. 14, 199–222. http://dx.doi.org/10.1023/B:STCO.0000035301.49549.88.

Spessa, A., McBeth, B., Prentice, C., 2005. Relationships among fire frequency, rainfall and vegetation patterns in the wet-dry tropics of northern Australia: an analysis based on NOAA-AVHRR data. Glob. Ecol. Biogeogr. 14 (5), 439–454. http://dx.doi.org/10.1111/j.1466-822x.2005.00174.x.

Strobl, C., Boulesteix, A.-L., Zeileis, A., Hothorn, T., 2007. Bias in random forest variable importance measures: illustrations, sources and a solution. BMC Bioinformatics 8 (1), 25. http://dx.doi.org/10.1186/1471-2105-8-25.

Tarnavsky, E., Grimes, D., Maidment, R., Black, E., Allan, R.P., Stringer, M., Chadwick, R., Kayitakire, F., 2014. Extension of the TAMSAT satellite-based rainfall monitoring over Africa and from 1983 to present. J. Appl. Meteorol. Climatol. 53 (12), 2805–2822. http://dx.doi.org/10.1175/JAMC-D-14-0016.1.

Thonicke, K., Spessa, A., Prentice, I.C., Harrison, S.P., Dong, L., Carmona-Moreno, C., 2010. The influence of vegetation, fire spread and fire behaviour on biomass burning and trace gas emissions. Results from a process-based model. Biogeosciences 7 (6), 1991–2011. http://dx.doi.org/10.5194/bg-7-1991-2010.

Thorne, V., Coakeley, P., Grimes, D., Dugdale, G., 2001. Comparison of TAMSAT and CPC rainfall estimates with raingauges, for southern Africa. Int. J. Remote Sens. 22, 1951–1974.

Tsela, P., Wessels, K., Botai, J., Archibald, S., Swanepoel, D., Steenkamp, K., Frost, P., 2014. Validation of the two standard MODIS satellite burned-area products and an empirically-derived merged product in South Africa. Remote Sens. 6 (2), 1275–1293. http://dx.doi.org/10.3390/rs6021275.

Uys, R.G., Bond, W.J., Everson, T.M., 2004. The effect of different fire regimes on plant diversity in southern African grasslands. Biol. Conserv. 118 (4), 489–499. http://dx.doi.org/10.1016/j.biocon.2003.09.024.

van Wilgen, B.W., Govender, N., Biggs, H.C., Ntsala, D., Funda, X.N., 2004. Response of savanna fire regimes to changing fire-management policies in a large African National Park. Conserv. Biol. 18 (6), 1533–1540. http://dx.doi.org/10.1111/j.1523-1739.2004.00362.x.

Vapnik, V.N., 1995. The Nature of Statistical Learning Theory. Springer, New York, NY.

Vapnik, V.N., 1999. An overview of statistical learning theory. IEEE Trans. Neural Netw. 10 (5), 988–999. http://dx.doi.org/10.1109/72.788640.

de Vasconcelos, M.J.P., Silva, S., Tomé, M., Alvim, M., Pereira, J., 2001. Spatial prediction of fire ignition probabilities: comparing logistic regression and neural networks. Photogramm. Eng. Remote Sens. 67 (1), 73–81.

Verlinden, A., Laamanen, R., 2006. Long term fire scar monitoring with remote sensing in Northern Namibia: relations between fire frequency, rainfall, land cover, fire management and trees. Environ. Monit. Assess. 112 (1–3), 231–253. http://dx.doi.org/10.1007/s10661-006-1705-1.

Wagenseil, H., Samimi, C., 2007. Woody vegetation cover in Namibian savannahs. A modelling approach based on remote sensing. Erdkunde 61 (4), 325–334. http://dx.doi.org/10.3112/erdkunde.2007.04.03.

Young, M.P., Williams, C.J.R., Chiu, J.C., Maidment, R.I., Chen, S.-H., 2014. Investigation of discrepancies in satellite rainfall estimates over Ethiopia. J. Hydrometeor. 15 (6), 2347–2369. http://dx.doi.org/10.1175/JHM-D-13-0111.1.

Zeileis, A., Kleiber, C., Jackman, S., 2008. Regression models for count data in R. J. Stat. Softw. 27 (8). http://dx.doi.org/10.18637/jss.v027.i08.

Zhu, C., Kobayashi, H., Kanaya, Y., Saito, M., 2017. Size-dependent validation of MODIS MCD64A1 burned area over six vegetation types in boreal Eurasia. Large underestimation in croplands. Sci. Rep. 7 (1), 4181. http://dx.doi.org/10.1038/s41598-017-03739-0.

5. MANUSCRIPT 2: COMPARING THE DRY SEASON *IN-SITU* LEAF AREA INDEX (LAI) DERIVED FROM HIGH-RESOLUTION RAPIDEYE IMAGERY WITH MODIS LAI IN A NAMIBIAN SAVANNA

Manuel J. Mayr, Cyrus Samimi

Remote Sensing (2015), 7 (4), 4834–4857.
DOI: 10.3390/rs70404834

Remote Sens. **2015**, *7*, 4834-4857; doi:10.3390/rs70404834

OPEN ACCESS

remote sensing

ISSN 2072-4292

www.mdpi.com/journal/remotesensing

Article

Comparing the Dry Season *In-Situ* Leaf Area Index (LAI) Derived from High-Resolution RapidEye Imagery with MODIS LAI in a Namibian Savanna

Manuel J. Mayr [1,*] and Cyrus Samimi [1,2]

[1] Department of Geography, University of Bayreuth, Universitätsstr. 30, 95447 Bayreuth, Germany; E-Mail: cyrus.samimi@uni-bayreuth.de

[2] Bayreuth Center of Ecology and Environmental Research (BAYCEER), University of Bayreuth, Dr. Hans-Frisch-Str. 1-3, 95448 Bayreuth, Germany

* Author to whom correspondence should be addressed; E-Mail: manuel.mayr@uni-bayreuth.de; Tel.: +49-921-554-656; Fax: +49-921-552-314.

Academic Editors: Xin Li, Yuei-An Liou, Qinhuo Liu, Heiko Balzter and Prasad S. Thenkabail

Received: 28 January 2015 / Accepted: 15 April 2015 / Published: 20 April 2015

Abstract: The Leaf Area Index (LAI) is one of the most frequently applied measures to characterize vegetation and its dynamics and functions with remote sensing. Satellite missions, such as NASA's Moderate Resolution Imaging Spectroradiometer (MODIS) operationally produce global datasets of LAI. Due to their role as an input to large-scale modeling activities, evaluation and verification of such datasets are of high importance. In this context, savannas appear to be underrepresented with regards to their heterogeneous appearance (e.g., tree/grass-ratio, seasonality). Here, we aim to examine the LAI in a heterogeneous savanna ecosystem located in Namibia's Owamboland during the dry season. Ground measurements of LAI are used to derive a high-resolution LAI model with RapidEye satellite data. This model is related to the corresponding MODIS LAI/FPAR (Fraction of Absorbed Photosynthetically Active Radiation) scene (MOD15A2) in order to evaluate its performance at the intended annual minimum during the dry season. Based on a field survey we first assessed vegetation patterns from species composition and elevation for 109 sites. Secondly, we measured *in situ* LAI to quantitatively estimate the available vegetation (mean = 0.28). Green LAI samples were then empirically modeled (LAI_{model}) with high resolution RapidEye imagery derived Difference Vegetation Index (DVI) using a linear regression ($R^2 = 0.71$). As indicated by several measures of model performance, the comparison with MOD15A2 revealed moderate consistency mostly due to overestimation by the aggregated LAI_{model}.

Model constraints aside, this study may point to important issues for MOD15A2 in savannas concerning the underlying MODIS Land Cover product (MCD12Q1) and a potential adjustment by means of the MODIS Burned Area product (MCD45A1).

Keywords: dry season; savanna; Leaf Area Index; vegetation pattern; RapidEye; MOD15A2; empirical modeling; Namibia

1. Introduction

Savannas are characterized as ecosystems where the co-existence of woody and grass species is moderated by resources and disturbances. One hypothesis in this context is that different phenological cycles of woody and herbaceous species are one reason for their co-existence [1,2]. Deep-root water uptake allows woody species to initiate early leaf expansion and to prolong the leaves into the dry season. Contrarily, grass growth is stimulated by the first precipitation events yet they wither as soon as near-surface water vanishes. Thus, the general term "growing season" appears imprecise for such regions [3].

The Leaf Area Index (LAI) is a quantitative measure of the green vegetation available per surface area. Hence, it is a proxy for the above-mentioned phenological cycles. Several definitions exist (*cf.* [4]), they typically vary according to the field of application of LAI (e.g., vegetation growth and phenology, potential physiological activity, light attenuation under plant canopies). Of these, a widely acknowledged definition of LAI is the one-sided, or hemi-surface, leaf area per unit of the horizontal land below. Besides being a proxy for plant growth the LAI is an important biophysical parameter for the interaction between plants and the atmosphere because processes like photosynthesis and evapotranspiration are linked to LAI [5,6]. Thus, the LAI is often used to model and monitor evapotranspiration, Net Primary Production (NPP) and Net Ecosystem Exchange (NEE) at different scales (e.g., [7–10]).

Such applications require LAI in a sufficient medium to high resolution [8,9], which could be derived with ground-based methods and through remote sensing, only the latter allowing LAI estimates for larger regions in a cost effective way. For monitoring purposes, a high temporal resolution as provided by MODIS is critical. Hence, often a combination of different spatial and temporal resolutions is needed, which requires validation and up-scaling [11].

In this context, ground-based methods for assessing LAI are essential. They include (semi-)direct, such as harvesting of leaves or allometric relationships, and indirect approaches [12]. The predominant benefits of indirect methods arise from their non-destructive nature and an increased spatial sampling rate, whereas direct methods are considered the most reliable measurements [13]. With indirect methods, the spatial heterogeneity of canopy elements is inferred using photosensitive instruments, which either record the transmitted radiation at multiple points (multi-sensor array) or from a single sensor with angular capacity [13]. Sensors with angular capacity most frequently apply the concept of gap fraction, *i.e.*, the fraction of sky visible from below a canopy in any specific direction, in order to determine canopy gaps [14]. The actual derivation of LAI is subsequently achieved by inversion and the application of a light extinction model [13]. Such models relate the recorded transmission of radiation through a canopy to idealized, randomly arranged canopy architecture [14,15]. In real canopies, however, leaf inclination angles are species-specific and often reflect phenology, whereas clumping of foliage is

initially caused by plant morphology. Van Gardingen *et al.* [16] report that clumping alone may reduce indirect estimates of LAI by up to 50%. Consequently, Chen & Black [17] introduced the term "effective LAI" (LAI_{eff}) for optically derived LAI. Furthermore, most optical devices fail to discriminate green tissue from other canopy elements (Stem or Woody Area Index (SAI, WAI, respectively)), which actually leads to a plant area index (PAI) [12,18].

LAI can also be estimated using remote sensing techniques with the advantage of increased spatial sampling. Here, LAI is mapped based on the relationship between *in situ* samples and spectral information sensitive to vegetation. However, such empirical-statistical models lack transferability to other regions due to varying atmospheric and surface conditions as well as the sensor-view sun conditions [19]. Nevertheless, their application on a regional scale is justified through their simplicity and subsequent short computational times [20].

Earth-observation systems, such as NASA's Moderate Resolution Imaging Spectroradiometer (MODIS) mission, operationally produce global LAI datasets (MOD15A2). These datasets are generated using the physical approach, *i.e.*, Radiative Transfer Models (RTM) that link surface reflectance (output) with the structural parameters of a canopy (input) through a set of approximations for canopy architecture, leaf properties, and the sensor-view sun conditions [6,20]. The actual derivation of a biophysical variable is achieved through RTM model inversion. Several uncertainties are associated with the physical approach, and summarized by Garrigues *et al.* [6]. The accuracy of datasets such as MOD15A2 is critical for the applications that use these. Hence, many efforts have been put into the evaluation and validation of MOD15A2 for different biomes (e.g., [21–26]). A direct validation of MODIS with ground measurements is not possible because of scale differences. Hence, validation studies often use high to medium resolution datasets to scale up *in situ* LAI. The derived datasets are then again scaled up to allow for a comparison with MOD15A2 [23,26].

Independent of the method applied, the determination of LAI in savannas is a complex task, yet relatively few studies have focused on the inaccuracies that arise from high heterogeneity and small-scale patchiness in such ecosystems [27]. Furthermore, phenological aspects are often neglected in studies assessing LAI [18]. Remote sensing applications traditionally focus on green vegetation for practical reasons. Phenology and senescent vegetation as structural and functional components of ecosystem dynamics seem to be gaining more attention recently [28]. Furthermore, dry-season grass and litter availability are especially important in savanna ecosystems, as they serve as the fine fuels that promote seasonally occurring fires [29].

Thus, the objectives of this paper are to:

(1). Assess ground-based dry-season LAI in a Namibian savanna ecosystem;
(2). upscale LAI field measurements to high-resolution RapidEye imagery;
(3). and compare an *in situ*-calibrated model of LAI with the MODIS LAI product (MOD15A2) in order to evaluate its performance.

2. Study Area

The region of interest covers an area of about 2915 km^2 in the Ovamboland, situated in Northern-Central Namibia (*cf.* Figure 1). According to Mendelsohn *et al.* [30], the region's climate is classified as semi-arid with precipitation being restricted to the austral summer months due to a seasonal

shift of the Congo Air Boundary and the establishment of a stable high-pressure cell over Southern Africa during the austral winter. Mean annual precipitation (MAP) in the region varies between 400 and 500 mm [30]. Aside from distinct inter-annual variability of local precipitation, the region's hydrological regime is predominantly controlled by the rivers of the Cuvelai-Iishana system, which originate in the Encoco Highlands of Angola (MAP ~800 mm) [30]. As a consequence of the topography, the seasonal waters of the Cuvelai spread and meander southwards from the Angolan-Namibian border in channels (known as Iishana) forming a delta-like network that repeatedly experiences devastating floods towards the end of the rainy season [31]. The interplay of alternating drought and flood, together with the highest solar irradiance rates throughout Namibia, explain why salinity is a major issue in the region [32]. Aside from the environmental conditions, human activities, and especially high livestock densities, have a considerable role in the formation of patterns in, as well as the composition of the edaphic grasslands and shrub lands around the Iishana.

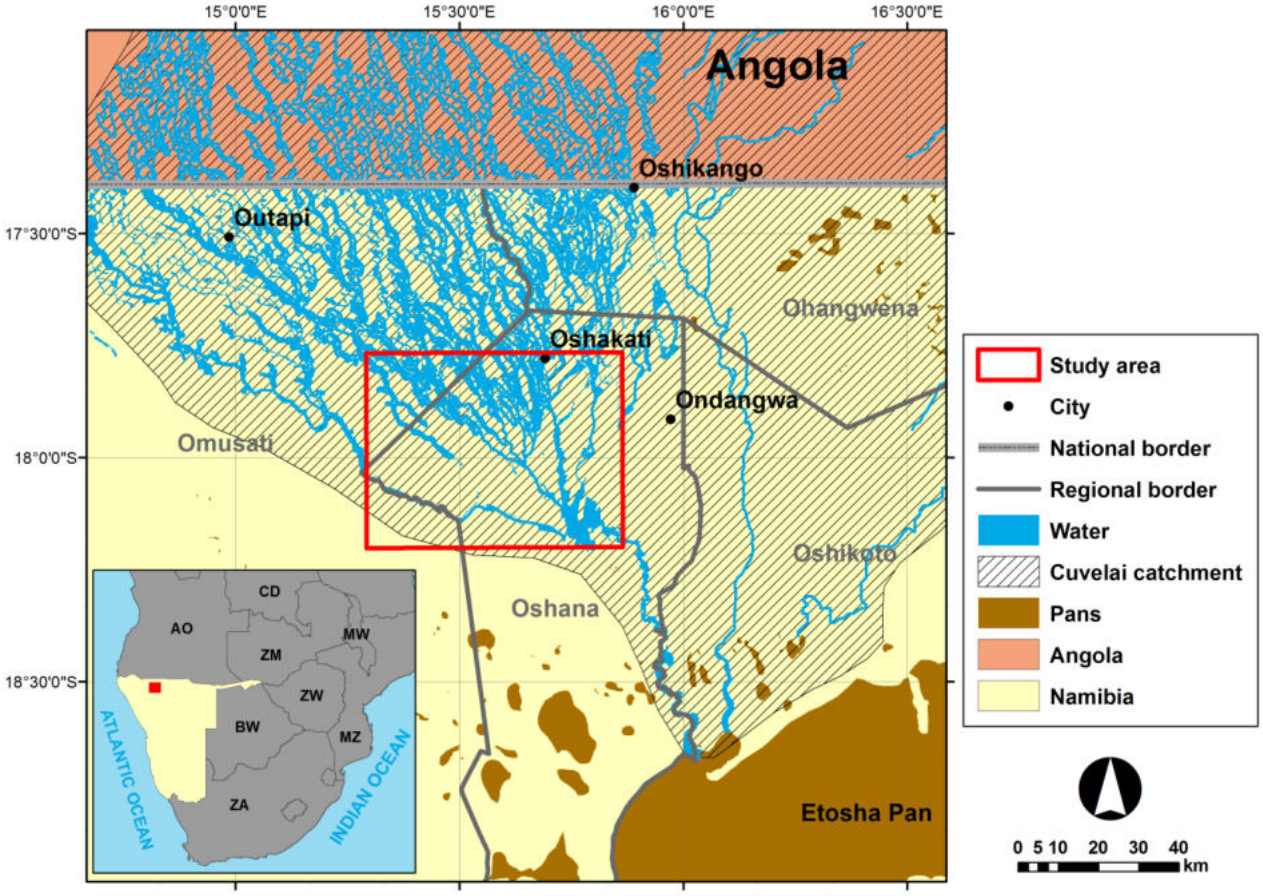

Figure 1. Map of Northern-Central Namibia illustrating the study area and the Cuvelai catchment.

3. Materials and Methods

3.1. Remote Sensing Data

3.1.1. RapidEye

The RapidEye mission consists of five satellites, which provide a 5 m-spatial resolution and cover the three visible bands (blue: 440–510 nm, green: 520–590 nm, red: 630–685 nm), a red-edge (RE) band

(690–730 nm), and a near-infrared (NIR) band (760–850 nm) [33]. A set of "RapidEye Ortho-Level 3A" scenes, acquired on 10 November 2010, was used in this study. These data are delivered with radiometric, sensor, and geometric corrections already applied and assigned to UTM projection (Zone 33S) with WGS 84 datum. No *post hoc* atmospheric correction was performed, because it is not improving results for single date images [34]. Digital numbers (DN) were converted to values of top-of-atmosphere radiance following the RapidEye Product Specifications [33] and, subsequently, to at-ground reflectances by applying the equations given in Mather & Koch [35].

3.1.2. MODIS

Since 2007, the most recent version, "Collection 5" of the MODIS LAI/FPAR product (MOD15A2) has been available. Compared to the preceding "Collection 4", the land cover map (an aggregated scheme of the MODIS Land Cover product (MCD12Q1)) used for parameterization of the look-up-tables (LUT) has been modified. Thus, the biome-specific estimation of LAI is now expanded from six to eight [36]. Furthermore, the LUTs were recalculated using a new stochastic RTM [37]. This refinement of the main algorithm is expected to enhance "high quality" LAI retrievals. "Collection 5" is also the first to provide quality indication measures such as the standard deviation of LAI per pixel, *i.e.*, the accuracy of solutions as retrieved by the main algorithm [38], and a quality control (QC) layer providing information about the emergence of a pixel value (e.g., main or empirical back-up retrieval algorithm, cloud contamination, *etc.*).

A MOD15A2-scene covering an 8-day period from 9 to 16 November 2010, was the best temporal match to the RapidEye image. This scene was obtained from the "USGS MODIS Reprojection Tool Web Interface" (accessible via: mrtweb.cr.usgs.gov) in order to ensure the data were available in the same coordinate system as the RapidEye images. Further processing steps included clipping to the extent of the study area and applying the scale factor (DN × 0.1) for the derivation of LAI values. The information contained by the supplied MOD15A2-QC layer revealed mainly high quality retrievals.

3.2. Field Data

3.2.1. Site Selection

During a field survey at the end of the dry season in October and November 2010 the transitional period of the vegetation prior to the first rains was assessed. In order to determine typical vegetation attributes and phenological status Functional Landscape Units (FLU) of vegetation and landscape parameters were sampled. Functional entities are generally dependent on scale and thus subject to complication by the fuzzy nature of ecological boundaries and gradients [39]. As the field data was also intended to serve as the ground-truth for the remote sensing data, scale had to be considered in relation to the spatial resolution of the RapidEye images, especially with regards to areas of relative homogeneity. Such sampling is referred to as "nested", as the scale of observation determines the perception of an entity [40]. Representative plots of at least 30 × 30 m (6 × 6 pixels) within a FLU and a minimum buffer of 10 m to the adjacent FLU were chosen and geo-located using a GPS. Based on experience in the field, these plots (termed Elementary Sampling Units (ESU)), were preferentially selected via a stratified approach.

3.2.2. Recorded Parameters

In total, data from 109 vegetation covered ESUs were collected. These were mainly located around two sites: (i) IIpopo, and (ii) Omulunga, situated in the central regions of the study area. The vegetation parameters surveyed included: (i) estimated plant cover (in %), (ii) the corresponding relative contribution of the main species for each stratum (if available), (iii) terrain position, and finally (iv) LAI.

3.2.3. Leaf Area Index

Indirect measurements of LAI (hereinafter termed: LAI_{2200}) were conducted for each of the vegetated ESUs using a Li-Cor LAI-2200 Plant Canopy Analyzer device. The sensors record the canopy transmittances of diffuse radiation from above and below canopy records at five concentric zenith angle ranges (centered at 7°, 22°, 38°, 52°, and 68°) in order to derive canopy interception by inversion [41]. For the internal computation of LAI_{2200}, Li-Cor's "horizontal canopy model" (also known as "Poisson model") was used. Here, the radiative transfer through a canopy is described by an extension of the Beer-Lambert law [12]. For a hypothesized canopy with an infinite (and hence infinitely thin) number of statistically independent, horizontal layers the probability of incident light to experience a particular number of contacts with these canopy layers is expressed by a Poisson distribution [42]. Following Weiss *et al.* [5], the probability of no contact (P), or the gap fraction (F), for incident irradiance at any zenith (θ) and azimuth angle (ϑ) is:

$$P(\theta,\vartheta) = F(\theta,\vartheta) = exp\left[\frac{-G(\theta,\vartheta)LAI}{\cos\theta}\right] = exp[-k(\theta,\vartheta)LAI] \quad (1)$$

where $G(\theta,\vartheta)$ is the so-called G-function, which denotes the mean projected area of a unit leaf area in the direction (θ,ϑ). The term $\cos\theta$ accounts for an increased cross-section of canopy to be passed at larger zenith angles [43]. Together the two parameters $G(\theta,\vartheta)$ and $\cos\theta$ form the canopy extinction coefficient ($k(\theta,\vartheta)$).

LAI_{2200} is calculated using the mean contact number ($\overline{K_i}$) and the weighing factors (W_i) for each of the five concentric zenith angles as follows [41]:

$$LAI_{2200} = \int_0^{\pi/2} -\frac{\overline{\ln P(\theta)}}{S(\theta)}\Delta\theta \sin\theta = 2\sum_{i=1}^{5}\overline{K_i}\,W_i \quad (2)$$

where $S(\theta)$ denotes the path length at the incident angle θ.

Although the "horizontal canopy model" assumes that foliage elements are randomly distributed, the device computes an approximate parameter of the spatial distribution of foliage from its view angles known as the Apparent Clumping Factor (ACF), which, thus, accounts for foliage clumping.

All samples were conducted according to the "Li-Cor LAI-2200 Plant Canopy Analyzer Instruction Manual" [41]. As overcast sky conditions are not existent during the dry season, the sampling predominantly took place at low solar elevation angles as recommended by Kobayashi *et al.* [44]. Additionally, the sensor was always shaded from direct illumination by the operator. A 45° view cap was used to reduce the underestimating influence of canopy gaps [45]. Each LAI_{2200} measurement consisted of at least one reference measurement (above-canopy) and several below-canopy measurements, taken just above the ground. In the sampling scheme, measurements were made at 5 m

intervals along two perpendicularly intersecting transects (*cf.* Figure 2), following a modified systematic approach given in Garrigues *et al.* [46].

The device-internal calculation of LAI_{2200} solely applied the standard settings with the exception of transmittances >1.0. In this case, transmittance values were "clipped" to 1.0 (above-canopy irradiance = below-canopy irradiance), as, especially when using narrow view caps, the possibility of having no vegetation within the sensor's view is present [41].

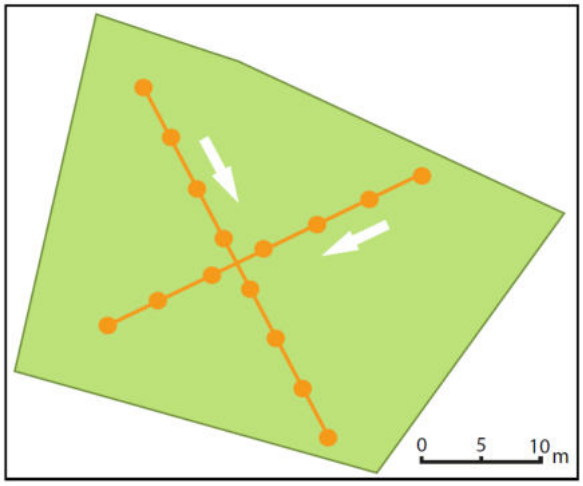

Figure 2. Schematic illustration of spatial sampling for ESU I66: measurements were made at 5 m intervals along two perpendicularly intersecting transects. Points (orange) indicate the 15 measurements below the canopy in ESU I66 (green). Directions of the sampling process are indicated by the white arrows.

3.3. Empirical-Statistical Modeling of LAI

In order to map LAI on a fine scale, it is necessary to establish a statistical relationship between *in situ* measured LAI (LAI_{2200}) and the reflectances contained in the RapidEye pixels. Thus, variation in spectral information is assumed to result from variation in LAI only [25]. In reality, this assumption is hampered by a number of uncertainties (e.g., optical and structural species-specific leaf properties, background illumination, topography, and interference of radiation with the atmosphere or sensor viewing geometry) [43]. Numerous Spectral Vegetation Indices (SVI) have been proposed (*cf.* [47] for an overview) in order to minimize external noise and to accentuate the spectral signal of (green) vegetation from non-vegetated surfaces [48].

In a first step, SVIs including RapidEye's RE band and several established SVIs were computed from the band reflectances (Table 1). For each ESU, the mean of the respective SVI was compiled from all pixels where the centroid was contained within the respective ESU. Due to RapidEye's band configuration, only classes of green vegetation ("*open woodland*" and "*Colophospermum mopane shrub land*"; *cf.* Figure 3) could be used in this process. Other ESUs were excluded due to mainly senescent vegetation, or spectral interference from surface heterogeneity (e.g., "*wetlands*"). In order to determine the most accurate relationship between the two parameters, a correlation analysis was performed for the paired observations of LAI_{2200} and respective SVIs. The agreement of the variables was identified using the Coefficient of Determination (R^2). Although the relationship between LAI and SVIs has often been

reported to appear non-linear, as a saturation of the SVI is likely to occur with more dense canopies [15,49], only linear models were tested. This can be justified because sparse vegetation is dominant, and therefore only a small range of LAI_{2200} is represented by the ESUs.

Table 1. Spectral Vegetation Indices (SVI) used in this study. The last four SVIs include the red-edge band of RapidEye.

Spectral Vegetation Index	Equation	Reference
Simple Ratio (SR)	NIR/R	[50]
Difference Vegetation Index (DVI)	$NIR - R$	[51]
Normalized Difference Vegetation Index (NDVI)	$(NIR - R)/(NIR + R)$	[52]
Transformed Vegetation Index (TVI)	$\sqrt{((NIR - R)/(NIR + R) + 0.5)}$	[53]
Soil-adjusted Vegetation Index (SAVI)	$(NIR - R)/(NIR + R + SL)\ (1 + SL)$	[49]
Enhanced Vegetation Index (EVI)	$2\ (NIR - R)/(L + (C_1\ NIR) + (C_2\ R))$	[49]
Simple Ratio ($SR_{NIR/RE}$)	NIR/RE	[54]
Simple Ratio ($SR_{RE/R}$)	RE/R	[54]
Normalized Difference Vegetation Index ($NDVI_{NIR/RE}$)	$(NIR - RE)/(NIR + RE)$	[54]
Normalized Difference Vegetation Index ($NDVI_{RE/R}$)	$(RE - R)/(RE + R)$	-
NOTE: SL = 0.1, L = 1.0, C_1 = 6.0, and C_2 = 7.5	-	-

Figure 3. Exemplary sites of green vegetation in the study area: (**left**) *Colophospermum mopane* shrub lands. (**right**) Open woodlands, mainly containing Makalani palms (*Hyphaene petersiana*).

As the estimation of LAI from remote sensing gives "real" LAI values, an absolute value of 0.35 was subtracted *post hoc* from the empirically calibrated LAI_{model}. This aimed to account for the contribution of WAI to the LAI_{2200} samples and was adopted from Privette *et al.* [21], who corrected *in situ* estimates of LAI in a validation study of MOD15A2 in the Kalahari in a similar manner. Furthermore, negative values of LAI_{model} were set to zero (no vegetation).

3.4. Comparing the Empirical Model with MODIS LAI (MOD15A2)

In order to allow for a comparison between high-resolution modeled LAI (LAI_{model}) from RapidEye and MOD15A2, the LAI_{model} was co-registered (to minimize geometric errors) and spatially aggregated (to match the 1 × 1 km spatial resolution of MOD15A2) [55]. The median was used for the aggregation of the LAI_{model}, due to its robustness in dealing with extreme values, which are more pronounced at high

resolution. Nevertheless, as a pixel-by-pixel comparison is hampered by locational errors and the fact that the MODIS retrieval algorithm offers a mean value of possible solutions, Yang *et al.* [56] recommend a comparison only be carried out at a multi-pixel scale.

The aggregated LAI_{model} only distinguishes between vegetated and non-vegetated pixels. The pixels classified as "urban" in the MOD15A2 scene were used as a mask in the aggregated LAI_{model} to exclude potentially mixed pixels, which may result from a mosaic of gardens and sealed surfaces in urban areas. The remaining non-vegetated pixels in the MOD15A2 scene were all assigned to "LAI = 0".

The consistency between the aggregated LAI_{model} and MOD15A2 was tested by several metrics of model performance after Kanniah *et al.* [57]. These include:

(1). the Coefficient of determination (R^2) to specify the proportion of variance between two models explained by the predictor variable;

(2). the Root-Mean-Square-Error (RMSE), which is calculated using:

$$RMSE = \sqrt{\frac{\sum_{i=1}^{n}(x_i - y_i)^2}{n}} \quad (3)$$

where x_i is the predictor variable (*i.e.*, the aggregated LAI_{model}), y_i is the estimated variable (*i.e.*, MOD15A2), and n is the sample size (*i.e.*, the number of pixels);

(3). the Relative Predictive Error (RPE), which provides a directional measure from mean difference between x_i and y_i in percent and is defined as:

$$RPE = \frac{(\bar{y}-\bar{x})}{\bar{x}}\ 100 \quad (4)$$

with: $\bar{y}$, the mean of $\sum_{i=1}^{n} y_i$, and $\bar{x}$, the mean of $\sum_{i=1}^{n} x_i$;

(4). the Modified Index of Agreement (mIOA) [58]:

$$mIOA = 1 - \frac{\sum_{i=1}^{n}|x_i - y_i|}{\sum_{i=1}^{n}(|x_i - \bar{y}_i| + |y_i - \bar{y}_i|)} \quad (5)$$

The last measure provides a dimensionless index value, where 0 would indicate no fit and 1 would indicate a perfect fit between the models. In comparison to the original IOA (as used in [57]), mIOA has been shown to be more robust concerning errors introduced by outliers [59].

4. Results

4.1. Field Data

A total of 13 different vegetated FLUs were identified in the field following Mueller-Dombois & Ellenberg [39]. Several main FLUs were extended in terms of species composition (e.g., dominance of a certain species) and terrain position (*cf.* Table 2). Terrain position clearly affects species composition, as it reflects edaphic properties, such as soil salinity. Thus, low land grasslands ("*grassland tufts*", "*seasonally flooded grassland*", and "*Rennera limnophila forbs*") are often characterized by salt-tolerant species, such as *Sporobolus iocladus*, *Leptochloa fusca*, *Rennera limnophila*, or *Willkommia sarmentosa* (Table 2). In general, lower elevation FLUs show a tendency towards lower total plant cover, which may partly be attributed to recurring seasonal flooding. However, selective grazing likely alters this situation significantly and, thus, explains the wide range of plant cover in these FLUs. A potential influence of

selective grazing in grasslands at higher elevation could be indicated by the dominance of non-palatable species, such as *Aristida stipoides* and *Odyssea paucinervis*. In contrast, increasing plant cover as a function of elevation could also result from the contribution of shrub and tree strata, which are almost exclusively related to middle and top terrain position in the data.

Table 2. Overview of the *in situ* FLUs, their characteristics, and sample size ("No. of ESUs").

FLU	Description	Characteristic Species	Total Plant Cover (%)	Predominant Terrain Position	No. of ESUs
open woodland	tree cover (>5 m) >30% or trees are dominant	*H. petersiana*	30–90	middle-top	9
wooded shrub land	shrub cover >30%	*Acacia arenaria, Acacia hebeclada tr.*	50–60	top	8
P.-L. leubnitziae shrub land	shrub cover >30%	*Pechuel-Loschea leubnitziae*	40–70	top	8
C. mopane shrub land	shrub cover >30%	*C. mopane*	40–70	middle-top	8
grassland tufts	grassland at low elevation, tuft forming species	*S. iocladus, Eragrostis lehmanniana*	10–40	bottom-middle	7
grassland medium	grassland at medium elevation	*A. stipoides, W. sarmentosa*	5–30	middle	11
grassland high	grassland at high elevation	*A. stipoides, O. paucinervis*	40–70	top	8
shrub-wooded grassland	grassland with shrub cover <30%	*A. stipoides, O. paucinervis, A arenaria, A. hebeclada tr.*	20–80	middle-top	11
P.-L. leubnitziae grassland	grassland with shrub cover <30%	*A. stipoides, O. paucinervis, P-L. leubnitziae*	20–50	top	7
seasonally flooded grassland	grassland in minor depressions, tall-growing species *vs.* intense grazing	*L. fusca, S. iocladus, Elytrophorus globularis*	10–90	bottom-middle	16
R. limnophila forbs	*R. limnophila* dominant	*R. limnophila*	10–20	bottom-middle	8
agricultural land	remains of *Pennisetum glaucum*	-	10	top	4
wetland	co-existence of vegetation, water surface and bare soil	-	40–60	bottom-middle	4

4.2. In Situ LAI (LAI_{2200})

Due to the sparse vegetation present at the time of the sampling, the overall mean LAI_{2200} was 0.28, with a standard error of LAI_{2200} (SEL) of ±0.05 (n = 109). A median of 0.21 indicates a skewness of distribution towards lower values of LAI_{2200} (*cf.* Table 3). For the two classes of green vegetation (n = 17), mean LAI_{2200} was 0.47, with SEL ±0.1, which appears to be noticeably higher than the overall average, though the smaller sample size might be responsible for the increase. At the same time, Apparent Clumping Factors (ACF) for the green vegetation samples are lower as compared to the overall sample.

Accordingly, the difference between LAI_{2200} and effective LAI (LAI_{eff}) increases. Lower ACFs appear to be reasonable for these classes, as the overall sample largely consists of grassland sites (68 out of 109 sites). Hereby, the spatial distribution of foliage elements in grassland sites can be assumed to be more regular on site scale as compared to shrub lands.

Table 3. Descriptive statistics of *in situ* LAI (LAI_{2200}) and associated parameters (SEL, ACF, number of samples per site and LAI_{eff}) for all sites (n = 109) and the sites of green vegetation only (n = 17). Note that LAI_{eff} was calculated by multiplying LAI_{2200} with the respective ACF.

		LAI_{2200}	SEL	ACF	No. of Samples	LAI_{eff}
Overall (n = 109)	*Mean*	0.28	0.05	0.90	19	0.24
	Min.	0.01	0.00	0.63	14	0.01
	Max.	2.09	0.26	0.99	33	1.65
	Median	0.21	0.04	0.93	19	0.20
Green vegetation only (n = 17)	*Mean*	0.47	0.10	0.83	18	0.37
	Min.	0.22	0.04	0.66	15	0.20
	Max.	1.14	0.26	0.94	25	0.75
	Median	0.44	0.09	0.87	18	0.33

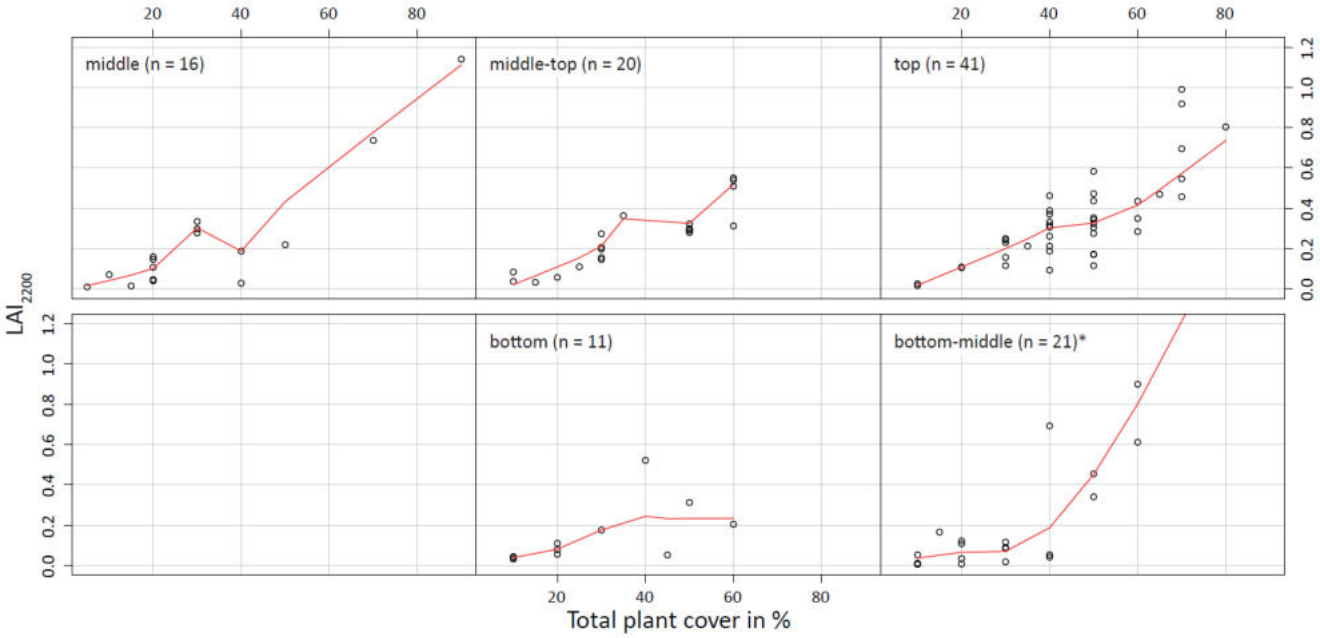

Figure 4. Conditional plots for LAI_{2200} and estimated total plant cover in %, per terrain position class. The black circles denote the samples from an ESU, the red lines show the respective LOESS smoothing lines (NOTE: the "bottom-middle"-plot only shows 20 from 21 samples due to presentation purposes).

The dependence of vegetation in the region on elevation and livestock grazing, as hypothesized in Section 4.1, is also found in the LAI_{2200} values, which generally correlate quite well with the total plant cover estimation ($R^2 = 0.61$; not depicted). Changes in these patterns determined by elevation may arise from grazing (e.g., the maximum LAI_{2200} (= 2.09) was measured at a fenced grassland site at a lower elevation). The conditional plots shown in Figure 4 mainly confirm that increasing terrain position (*i.e.*,

an increase in elevation) seems to result in higher total plant cover and LAI_{2200}. As is illustrated by the LOESS (Locally Weighted Scatterplot Smoothing) line, a near-linear trend between LAI_{2200} and total plant cover is found for higher elevated FLUs. However, this relationship is partly perturbed by fencing and species of little grazing value in FLUs of bottom to middle elevation.

4.3. Empirical-Statistical Modeling

The relationships found for the *in situ* green vegetation samples and SVIs revealed mostly moderate correlations (Table 4). This was also true for the experimental SVIs – meaning that, for this study, no advancements were achieved with the use of the RapidEye RE band. The NDVI and similar indices also provided unsatisfactory results as shown in other regions with spares vegetation (e.g., [60]). However, a sophisticated relationship between the green vegetation LAI_{2200} samples and the DVI was found ($R^2 = 0.71$). The use of a linear model seemed to be best practice as the green vegetation LAI_{2200} samples generally had low values that only covered a range of about 0.92 (*cf.* Table 3). Thus, with the LAI_{2200} serving as the explaining variable for the DVI, a linear model could be established (*cf.* Figure 5) with the transfer function:

$$LAI_{model} = \frac{DVI}{0.09} - 0.102. \quad (6)$$

Table 4. Correlations between LAI_{2200} and SVIs from linear regression.

SVI	SR	$SR_{NIR/RE}$	$SR_{RE/R}$	DVI	NDVI	$NDVI_{NIR/RE}$	$NDVI_{RE/R}$	TVI	EVI	SAVI
R^2	0.48 *	0.55 *	0.37 *	0.71 *	0.49 *	0.56 *	0.36 **	0.49 *	0.32 **	0.57 *

NOTE: * Significance (2-tailed) $p < 0.01$; ** Significance (2-tailed) $p < 0.05$

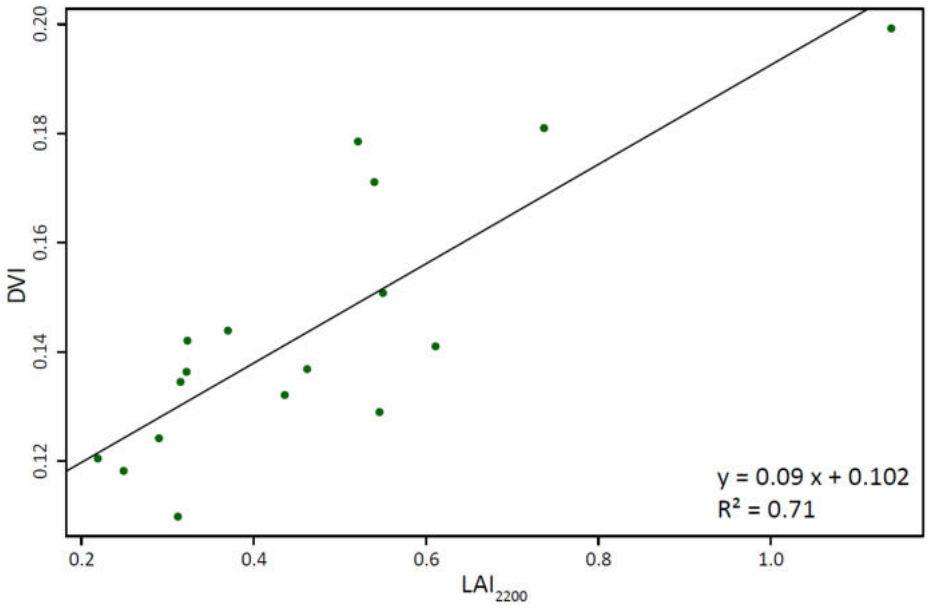

Figure 5. Bivariate plots of *in situ* LAI_{2200} and DVI derived from RapidEye imagery. The linear regression model ($R^2 = 0.71$) is indicated by the solid line, whereas green points represent samples of the classes "C. mopane shrub land"and "open woodland" (n = 17). Note the different origins of axes in the figure.

The mean of LAI_{model} was 0.57 (±0.37). As can be seen from Figure 6a, larger areas of high LAI, *i.e.*, dense vegetation, were found at the western and north-eastern edges of the study area, whereas the highest LAI (11.85) was located within an irrigated park like area in the urban area of Oshakati. The central regions, where the test sites and the 17 sites used for the model were located, mainly consist of grasslands. Thus, they are characterized by lower LAIs. Extensive non-vegetated areas were found in southern and south-eastern parts of the region. As already observed for the field data, the vegetation density is related to the topographic position.

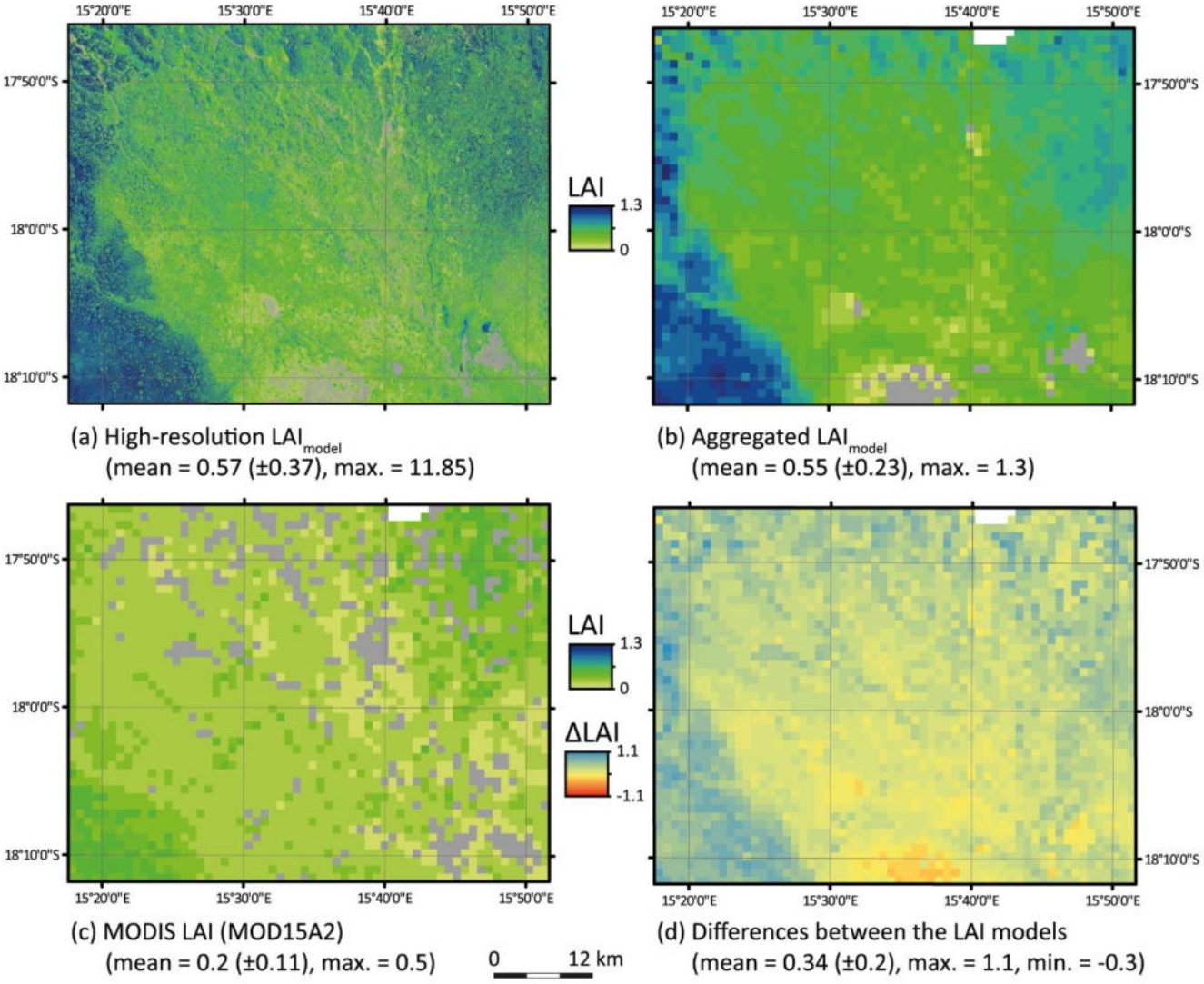

Figure 6. LAI maps of the study region: (**a**) High-resolution map of LAI_{model} (5 × 5 m) based on the transfer function given in Equation (6). For cartographic reasons, no differentiation for pixels with a LAI_{model} > 1.3 was made. (**b**) Aggregated map of the LAI_{model}. (**c**) 8-day mean MODIS LAI (MOD15A2) map (spatial resolution: 1 × 1 km). (**d**) Absolute difference between (**b**) and (**c**), where positive values indicate the aggregated LAI_{model} to exceed MOD15A2, and vice versa. (NOTE: For (**b**) and (**d**), urban areas, as classified by (**c**), were a priori excluded from processing).

4.4. Comparison of the High-Resolution LAI_{model} with MOD15A2

The aggregation of the high-resolution LAI_{model} to the resolution of MOD15A2 (1 km) reduced the effects of spatial heterogeneity and the influence of extreme values; the maximum LAI_{model} pixel value decreased from 11.85 in the high-resolution model to 1.3 at moderate resolution (aggregated LAI_{model}). However, as illustrated by Figure 6b, the spatial patterns of LAI are preserved, which is further expressed by a similar mean with a moderate variance, which decreased by 0.02 to 0.55.

The MOD15A2 scene used here, generally points to a more uniformly distributed LAI in regions, which can be attributed to the more coarse initial spatial resolution of MOD15A2. Though the spatial patterns of LAI coincidence at a multi-pixel scale, only moderate consistency was found regarding the magnitude of LAI between the two models. This is especially true for areas with a higher LAI (e.g., western margin of the study area), where the variation between the aggregated LAI_{model} and MOD15A2 often exceeds 0.5 LAI units (max. = 1) (*cf.* Figure 6d). For the central and southern parts of the study area, the offset is lower (often around 0.1–0.3 units LAI). Though the mean of the aggregated LAI_{model} is higher than MOD15A2, certain areas in the central south also show an underestimation up to 0.3 units LAI.

One major source of inconsistency between the aggregated LAI_{model} and MOD15A2 is related to the differing spatial distribution of non-vegetated pixels, which can already be recognized through visual interpretation (grey in Figure 6b,c). Further confirmation comes from the calculated measures of model performance (*cf.* Table 5): whereas RMSE and RPE only show minor improvements, the R^2 from linear regression and the mIOA reveal a distinct increase in model fit if all non-vegetated pixels from the MOD15A2 scene are excluded.

Table 5. Comparing the aggregated LAI_{model} and MODIS LAI. Measures of model performance for all pixels (upper row; n = 2811) and vegetated pixels only in the MOD15A2 scene (lower row; n = 2448): the linear model equation and the corresponding Coefficient of Determination (R^2), Root-Mean-Square Error (RMSE), Relative Predictive Error (RPE) and the Modified Index of Agreement (mIOA).

x	Pixels Valid (n)	Linear Model	R^2	RMSE	RPE	mIOA
MODIS LAI	2811	y = 0.8463x + 0.371	0.182	0.40	−62.97%	0.13
MODIS LAI > 0	2448	y = 1.3396x + 0.2521	0.293	0.39	−59.18%	0.42

5. Discussion

5.1. Sampling

A critical issue for retrieving *in situ* environmental parameters is the determination of a suitable sampling strategy [61,62]. The preferential-stratified approach, as applied here, risks the inclusion of circular reasoning. The data retrieved might merely reflect the environmental criteria used for stratification [63]. On the other hand, this strategy is highly effective for the sampling of the maximum diversity of FLUs with a relatively small number of samples. In contrast, purely random approaches have the potential to show limited representativeness (oversampling of frequently occurring FLUs, undersampling of rare or spatially restricted FLUs). Furthermore, their common perception as being statistically independent is initially impaired by a general spatial auto-correlation of vegetation [63].

5.2. In Situ LAI

Compared to other biomes, savannas are underrepresented in studies focusing on the indirect sampling of LAI [64], where even fewer deal with dry season LAI. For example, Boulain *et al.* [10] investigated a shrub land fallow in Western Niger (MAP = 479 mm) with the annual minima of LAI ranging between 0.1 and 0.2. From Southern Africa, Privette *et al.* [21] report a mean dry season LAI of 0.8 in Zambia (MAP = 950 mm), whereas a mean dry season LAI of 0.79 (±0.13) was found in several Miombo woodland sites in Northern Mozambique (MAP = 900 mm) [65]. Within the Kalahari Transect [64], two shrub land sites located in Tsane (MAP = 350 mm) and Okwa (MAP = 424 mm) in Botswana were sampled during a drought period within the growing season. Here, LAI ranged between 0.51 and 0.83 in Tsane and between 0.19 and 1.75 in Okwa. In a study from Australia [66], dry season LAI means ranged from 0.1 to 2.1 along an precipitation gradient from below 400 mm/yr to above 1200 mm/yr. Therefore, a mean LAI_{2200} of 0.28 (±0.05) in our study region in Northern-Central Namibia with a MAP between 400 and 500 mm is well in the range of the other studies carried out in dry-season savanna environments.

Ryu *et al.* [27] attribute the great challenge of accurately deriving LAI from indirect methods in savannas to the quantification of a spatially representative element clumping index (Ω). The ACF, as provided with the estimates from the Li-Cor LAI-2200 instrument, gives an approximate measure of clumping. Instruments measuring gap-size distribution, such as the "Tracing Radiation and Canopy Architecture (TRAC)"-device or Digital Hemispherical Photography (DHP), would provide a more correct derivation of Ω [27]. Another possibility to account for the non-random distribution of vegetation elements is the *post hoc* incorporation of an external, satellite-derived Ω (e.g., from [67]). However, the ACF values, as calculated with the instrument used here, seem to produce reasonable results. Specifically, "Open woodland" appears to occupy the lowest ACF, while grasslands mostly account for the highest ACFs, *i.e.*, relatively little clumping is observed (not shown). The same is confirmed by Ryu *et al.* [68], who conclude that the ACF gives a good approximation of clumping at site level, whereas the additional usage of an external Ω would possibly result in an "overcorrection" of foliage clumping with this device.

The contribution of non-photosynthetic canopy elements, woody area index (WAI), to estimates of LAI is the subject of an on-going controversy [16]. Owing to the fact that woody components are inherently spatially auto-correlated with the photosynthetic features of a canopy, the contribution of WAI to LAI_{2200} is likely to decrease as the growing season proceeds. For grasses and non-deciduous species, variations in foliage shape (e.g., leaf roll up) and inclination may introduce biases, not only for the contribution of WAI, but also for LAI determination itself. Phenology may further affect optically-derived LAI estimates, as with senescent leaves the transmittance of radiation increases and, hence, LAI is underestimated [6].

5.3. Empirical-Statistical Modeling

High-resolution satellite images, such as the RapidEye scene used in this study, enable the proper mapping of landscape heterogeneity and spatially distinct phenomena. In accordance with Ehammer *et al.* [54], who report no improvement of LAI and FPAR modeling from SVIs incorporating RapidEye's RE band in a Central-Asian agro-ecosystem, the correlations of SVIs using the RE band with LAI_{2200} were only

moderate in this study (*cf.* Table 4). The insignificance of the RE band for the detection of LAI found here may be attributed to the broad range covered by this band (40 nm). Another reason could be the poorly distinctive inflexion point of the RE band and, thus, a nearly linear slope for vegetation reflectance between R and NIR bands.

For the creation of the high-resolution map of LAI (LAI_{model}), a linear transfer function was established as the highest agreement for all SVIs tested was found between LAI_{2200} and the DVI (*cf.* Table 4). The DVI has often been found to be linearly related with LAI [43,69]. As mentioned earlier, an *in situ* quantification of WAI could not be performed. The adopted value of 0.35 for WAI was subtracted from LAI_{model} with the aim of approximately transferring the empirically calibrated LAI to estimates of "real" LAI. As the latter measure is given by MOD15A2, this processing step was the best practice possible to carry out a comparison, being aware that such approaches simplify the diverse nature of WAI.

Qi *et al.* [20] point out that also the general relationship between a given SVI and LAI may differ substantially with the vegetation types considered. A major limitation of the applied transfer function is that only 17 of all 109 sample sites contained mainly green vegetation at this time of the year. Grasslands, which cover large parts of the study area, could not be included in the model calibration. Nevertheless, the full range of LAI was covered by the 17 samples, which are representative for the region. The excluded samples had mostly very low LAIs. Including them would have caused a concentration of low values in the regression model shown in Figure 5.

As the signal detected by a given SVI refers to the amount of green vegetation [49], senescent vegetation would only have been indirectly detected by the SVI as a function of reduced soil background reflectance. In general, the noise introduced by the underlying soil and litter is regarded as a major challenge associated with SVIs [69–71]. Litter and standing senescent vegetation together with bright and dry sandy soils in the study area may serve as a severe source of error for the detected spectral signals. Accordingly, in sparsely vegetated ecosystems, soil background reflectance leads to an overestimation of the SVI and, hence, of the derived biophysical variables as well [70]. To date, several approaches have been developed to account for soil background reflectance. A simple example is the SAVI. However, the SAVI achieved only moderate performance in this study (*cf.* Table 4). Other approaches to discriminate senescent vegetation and litter make use of the Short-Wave and Mid-Wave Infrared spectra (SWIR, MWIR). Marsett *et al.* [72] introduced the Soil Adjusted Total Vegetation Index (SATVI), while other approaches used a combination of NDVI and the Cellulose Absorption Index (CAI) to discriminate green and senescent vegetation from bare soil [73]. However, SWIR and MWIR spectra are not covered by the RapidEye bands.

5.4. Comparison with MOD15A2

In general, the conclusions drawn from a comparison between *in situ* LAI and satellite-derived LAI products often lack spatial coverage due to the discrete nature of *in situ* measurements. Scholes *et al.* [64] compared *in situ* LAI estimates with a respective MOD15A2 scene concluding that MOD15A2 tended towards underestimation with increasing aridity as compared to AccuPAR ceptometer estimates. Privette *et al.* [21] found that MOD15A2 tended towards overestimation for dry sites and the contrary for wet sites. Fensholt *et al.* [23] report that MOD15A2 overestimated LAI, especially during the dry

season in Senegal. Tian *et al.* [22] again, find underestimations of LAI using MOD15A2 in savanna ecosystems, which they generally attribute to increased soil background contamination with lower spatial image resolution as well as the heterogeneity of these ecosystems.

The approach followed in this study was to model *in situ* LAI_{2200} with a low level of generalization, *i.e.*, using high resolution data. The spatial aggregation of this LAI_{model} enabled a comparison with MOD15A2 for the entire study area. However, only a moderate agreement between these two models was found (*cf.* Table 5). For large parts of the study area, overestimation was found, which often exceeded the range of the standard deviation of MOD15A2 (*cf.* Figure 7a). This overestimation is in accordance with some of the above-mentioned studies. However, certain areas in the south of our study area show an opposite trend (*cf.* Figure 6d). The results presented here and the conclusions drawn from the above-mentioned studies highlight the inconsistencies associated with LAI estimations in savanna ecosystems.

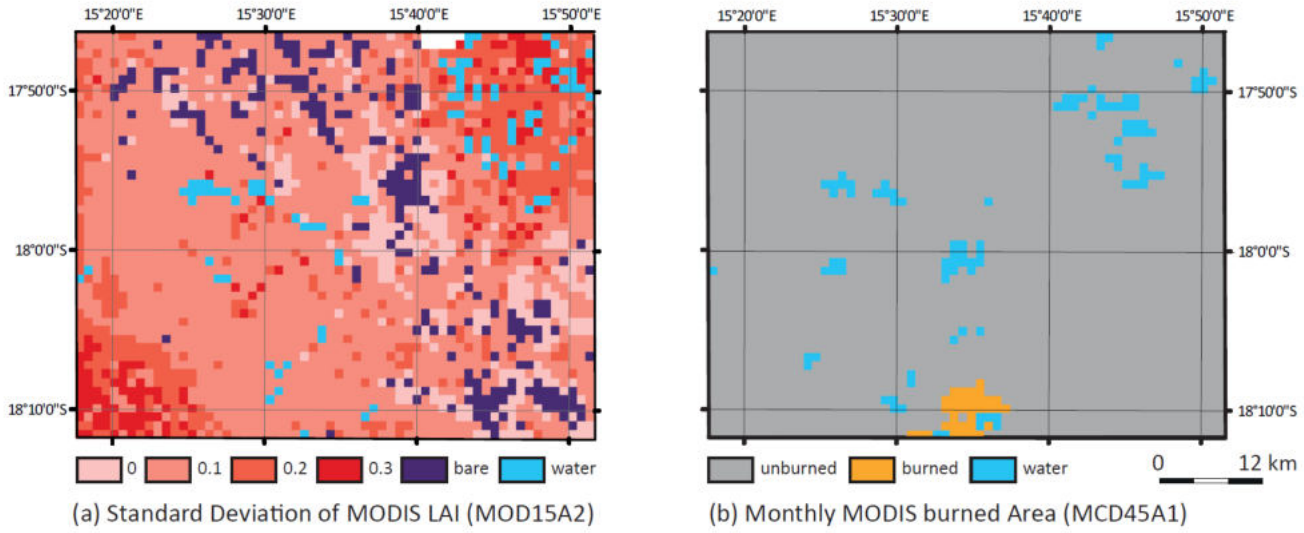

Figure 7. (**a**) Standard deviation of MODIS LAI (MOD15A2) and non-vegetated pixels (grey in Figure 6c) separated into desert (black) and water (blue). **(b)** Monthly MODIS Burned Area (MCD45A1) product from September 2010.

As the main MOD15A2 algorithm relies on a land cover map (*i.e.*, the MCD12Q1 product) for the structural canopy attributes, one critical issue for the performance of MOD15A2 is the correct biome allocation [24]. Fang *et al.* [74] compared global datasets of the MOD15A2 and MCD12Q1 for the time span from 2003 to 2009, concluding that biome misclassification and, thus, LAI overestimation would be highest for savannas, again in accordance with our results. For our study region, biomes were correctly assigned in MCD12Q1 ("annual broadleaf vegetation" and "annual grass vegetation"; not depicted). However, the classification of non-vegetated pixels in MOD15A2 apparently affected the model performance negatively (*cf.* Table 5). Differing initial spatial, temporal, and spectral resolutions as well as the aggregation process can be hypothesized to ultimately result in an inconsistent distribution of non-vegetated pixels between high-resolution models and the MOD15A2 product. Non-vegetated pixels, as assigned by MCD12Q1, are *a priori* excluded from computation of MOD15A2 [75]. For the study area, the temporal resolution of MCD12Q1, which represents the annual average of the preceding

year, could lead to errors due to sparse vegetation cover as well as intra-annually changing land cover resulting from seasonal flooding, drought or fire. These effects are illustrated through the varying distribution of water bodies from MCD12Q1 (*cf.* Figure 7a) and the MODIS Burned Area Product (MCD45A1; *cf.* Figure 7b). For the monthly MCD45A1, water bodies are derived from daily MODIS surface spectral reflectances (MOD09) by applying thresholds for NDVI (<0.1), band 7 (<0.04) and/or the quality assessment (QA) table [76].

Furthermore, our LAI model appears to show sensitivity to ecological disturbance from fire. The MCD45A1 product identifies the burning of a region, located in the central-southern part of the study area (*cf.* Figure 7b), to have occurred on Sep 23 and 24, 2010. Although no quantitative estimate of the intensity of these fires can be drawn, its spatial extent (34 pixels or km^2) is not negligible. However, this vegetation anomaly is not detected in the MOD15A2 scene. Though the causality of this issue needs a further examination, it may point to a potential for optimization of MOD15A2 by the incorporation of vegetation anomalies derived from MCD45A1.

6. Conclusions

The study presented here used field and remote sensing data to assess dry-season vegetation patterns, thereby focusing on LAI in a savanna ecosystem located in Northern-Central Namibia. In order to expand pattern identification from a point to a regional scale, we used an empirical-statistical approach to model LAI. Due to senescent vegetation, a constrained number of LAI_{2200} samples were used in this process. Nevertheless, a sophisticated relationship was retrieved between green-vegetation LAI_{2200} and the DVI derived from RapidEye reflectances. The red-edge channel of the RapidEye sensor did not improve modeling results in the dry season with predominantly senescent vegetation. However, with the high resolution it is possible to record the spatial heterogeneity of savanna ecosystems. Sensors with a resolution of RapidEye and bands in the MWIR are expected to yield in higher accuracy of dry-season LAI estimations. Further improvements are possible for the field measurements [44] on which the high-resolution models are based.

A comparison with MODIS LAI (MOD15A2) revealed several inconsistencies. These included a mean negative offset of MOD15A2 and its insensitivity to vegetation anomalies, induced by disturbance like fire. In general, the results of our study are in accordance with other studies carried out under similar conditions and comparable phenological stages. The given differences, mainly overestimations, to the MOD15A2 product are tolerable, especially because the general spatial patterns are consistent in the three methods, field measurement, high-resolution model and MOD15A2.

Our study is a contribution to the validation of standard LAI products in an ecological setup, which is underrepresented in similar studies, especially during the dry season. Despite the discussed variation of the measured and modeled LAI in such reason the overall results prove to be consistent and the standard MODIS LAI product (MOD15A2) is robust.

Acknowledgments

This study was supported by the CuveWaters Integrated Water Resource Management (IWRM) project, funded by the Federal Ministry of Education and Research (BMBF), Germany. The publication was funded by the University of Bayreuth in the funding programme Open Access Publishing. The

authors are grateful to the German Aerospace Center (DLR) and their RapidEye Science Archive (RESA), funded by the Federal Ministry of Economics and Technology (BMWi), Germany, for the provision of the high-resolution satellite imagery. Our particular thanks shall be expressed to Windhoek's Herbarium for their help with the identification of plant samples, and Daniela Kretz for her critical remarks on spelling and use of English grammar.

Author Contributions

Both authors contributed significantly to this manuscript. Cyrus Samimi conceived and designed the research. Both authors designed the sampling campaign. Manuel J. Mayr collected the *in situ* data. Manuel J. Mayr processed and analyzed *in situ* and remote sensing data. Both authors lively discussed the results and their implications. Manuel J. Mayr wrote the paper.

Conflicts of Interest

The authors declare no conflict of interest.

References

1. Seghieri, J.; Floret, C.; Pontanier, R. Plant phenology in relation to water availability: Herbaceous and woody species in the savannas of northern Cameroon. *J. Trop. Ecol.* **1995**, *11*, 237–254.
2. Scholes, R.J.; Archer, S.R. Tree-grass interactions in Savannas. *Ann. Rev. Ecol. Syst.* **1997**, *28*, 517–544.
3. Wagenseil, H.; Samimi, C. Woody vegetation cover in Namibian savannahs: A modelling approach based on remote sensing. *Erdkunde* **2007**, *61*, 325–334.
4. Barclay, H.J. Conversion of total leaf area to projected leaf area in lodgepole pine and Douglas-fir. *Tree Physiol.* **1998**, *18*, 185–193.
5. Weiss, M.; Baret, F.; Smith, G.J.; Jonckheere, I.; Coppin, P. Review of methods for *in situ* leaf area index (LAI) determination Part II. Estimation of LAI, errors and sampling. *Agric. For. Meteorol.* **2004**, *121*, 37–53.
6. Garrigues, S.; Shabanov, N.V.; Swanson, K.; Morisette, J.T.; Baret, F.; Myneni, R.B. Intercomparison and sensitivity analysis of Leaf Area Index retrievals from LAI-2000, AccuPAR, and digital hemispherical photography over croplands. *Agric. For. Meteorol.* **2008**, *148*, 1193–1209.
7. Liu, J.; Chen, J.M.; Cihlar, J.; Park, W.M. A process-based boreal ecosystem productivity simulator using remote sensing inputs. *Remote Sens. Environ.* **1997**, *62*, 158–175.
8. Novick, K.A.; Stoy, P.C.; Katul, G.G.; Ellsworth, D.S.; Siqueira, M.B.S.; Juang, J.; Oren, R. Carbon dioxide and water vapor exchange in a warm temperate grassland. *Oecologia* **2004**, *138*, 259–274.
9. Chen, J.M.; Chen, X.; Ju, W.; Geng, X. Distributed hydrological model for mapping evapotranspiration using remote sensing inputs. *J. Hydrol.* **2005**, *305*, 15–39.
10. Boulain, N.; Cappelaere, B.; Ramier, D.; Issoufou, H.B.A.; Halilou, O.; Seghieri, J.; Guillemin, F.; Oï, M.; Gignoux, J.; Timouk, F. Towards an understanding of coupled physical and biological processes in the cultivated Sahel-2. Vegetation and carbon dynamics. *J. Hydrol.* **2009**, *375*, 190–203.

11. Kraus, T. Ground-based Validation of the MODIS Leaf Area Index Product for East African Rain Forest Ecosystems. Ph.D. Thesis, Friedrich-Alexander University, Erlangen-Nuremberg, Germany, 10 October 2008.
12. Bréda, N.J.J. Ground-based measurements of leaf area index: A review of methods, instruments and current controversies. *Journal Exp. Bot.* **2003**, *54*, 2403–2417.
13. Jonckheere, I.; Fleck, S.; Nackaerts, K.; Muys, B.; Coppin, P.; Weiss, M.; Baret, F. Review of methods for *in situ* leaf area index determination Part I. Theories, sensors and hemispherical photography. *Agric. For. Meteorol.* **2004**, *121*, 19–35.
14. Welles, J.M.; Cohen, S. Canopy structure measurement by gap fraction analysis using commercial instrumentation. *J. Exp. Bot.* **1996**, *47*, 1335–1342.
15. Gower, S.T.; Kucharik, C.J.; Norman, J.M. Direct and indirect estimation of leaf area index, f(APAR), and net primary production of terrestrial ecosystems. *Remote Sens. Environ.* **1999**, *70*, 29–51.
16. Van Gardingen, P.R.; Jackson, G.E.; Hernandez-Daumas, S.; Russell, G.; Sharp, L. Leaf area index estimates obtained for clumped canopies using hemispherical photography. *Agric. For. Meteorol.* **1999**, *94*, 243–257.
17. Chen, J.M.; Black, T.A. Defining leaf area index for non-flat leaves. *Plant. Cell. Environ.* **1992**, *15*, 421–429.
18. Asner, G.P.; Scurlock, J.M.O.; Hicke, J.A. Global synthesis of leaf area index observations: Implications for ecological and remote sensing studies. *Glob. Ecol. Biogeogr.* **2003**, *12*, 191–205.
19. Dorigo, W.A.; Zurita-Milla, R.; de Wit, A.J.W.; Brazile, J.; Singh, R.; Schaepman, M.E. A review on reflective remote sensing and data assimilation techniques for enhanced agroecosystem modeling. *Int. J. Appl. Earth Obs. Geoinf.* **2007**, *9*, 165–193.
20. Qi, J.; Kerr, Y.H.; Moran, M.S.; Weltz, M.; Huete, A.R.; Sorooshian, S.; Bryant, R. Leaf area index estimates using remotely sensed data and BRDF models in a semiarid region. *Remote Sens. Environ.* **2000**, *73*, 18–30.
21. Privette, J.L.; Myneni, R.B.; Knyazikhin, Y.; Mukelabai, M.; Roberts, G.; Tian, Y.; Wang, Y.; Leblanc, S.G. Early spatial and temporal validation of MODIS LAI product in the Southern Africa Kalahari. *Remote Sens. Environ.* **2002**, *83*, 232–243.
22. Tian, Y.; Woodcock, C.E.; Wang, Y.; Privette, J.L.; Shabanov, N.V.; Zhou, L.; Zhang, Y.; Buermann, W.; Dong, J.; Veikkanen, B.; *et al.* Multiscale analysis and validation of the MODIS LAI product I. Uncertainty assessment. *Remote Sens. Environ.* **2002**, *83*, 414–430.
23. Fensholt, R.; Sandholt, I.; Rasmussen, M.S. Evaluation of MODIS LAI, fAPAR and the relation between fAPAR and NDVI in a semi-arid environment using *in situ* measurements. *Remote Sens. Environ.* **2004**, *91*, 490–507.
24. Hill, M.J.; Senarath, U.; Lee, A.; Zeppel, M.; Nightingale, J.M.; Williams, R.J.; McVicar, T.R. Assessment of the MODIS LAI product for Australian ecosystems. *Remote Sens. Environ.* **2006**, *101*, 495–518.
25. Kraus, T.; Schmidt, M.; Dech, S.W.; Samimi, C. The potential of optical high resolution data for the assessment of leaf area index in East African rainforest ecosystems. *Int. J. Remote Sens.* **2009**, *30*, 5039–5059.

26. Serbin, S.P.; Ahl, D.E.; Gower, S.T. Spatial and temporal validation of the MODIS LAI and FPAR products across a boreal forest wildfire chronosequence. *Remote Sens. Environ.* **2013**, *133*, 71–84.
27. Ryu, Y.; Sonnentag, O.; Nilson, T.; Vargas, R.; Kobayashi, H.; Wenk, R.; Baldocchi, D.D. How to quantify tree leaf area index in an open savanna ecosystem: A multi-instrument and multi-model approach. *Agric. For. Meteorol.* **2010**, *150*, 63–76.
28. Okin, G.S. The contribution of brown vegetation to vegetation dynamics. *Ecology* **2010**, *91*, 743–755.
29. Bond, W.J.; van Wilgen, B.W. *Fire and Plants*, 1st ed.; Chapman & Hall: London, UK, 1996.
30. Mendelsohn, J.M.; El Obeid, S.; Roberts, C. *A Profile of North-Central Namibia*; Gamsberg Macmillan Publishers: Windhoek, Namibia, 2000.
31. Kluge, T.; Liehr, S.; Lux, A.; Moser, P.; Niemann, S.; Umlauf, N.; Urban, W. IWRM concept for the Cuvelai Basin in northern Namibia. *Phys. Chem. Earth* **2008**, *33*, 48–55.
32. Mendelsohn, J.M.; Jarvis, A.; Roberts, C.; Robertson, T. *Atlas of Namibia*: *A Portrait of the Land and Its People*; David Philip: Cape Town, South Africa, 2002.
33. RapidEye AG. *RapidEye Satellite Imagery Product Specifications. Version 3.2.*; RapidEye AG: Brandenburg An der Havel, Germany, 2011.
34. Song, C.; Woodcock, C.E.; Seto, K.C.; Lenney, M.P.; Macomber, S.A. Classification and change detection using Landsat TM data: When and how to correct atmospheric effects? *Remote Sens. Environ.* **2001**, *75*, 230–244.
35. Mather, P.M.; Koch, M. *Computer Processing of Remotely-Sensed Images*: *An. Introduction*, 4th ed.; Wiley-Blackwell: Chichester, UK 2011.
36. Yang, W.; Shabanov, N.V.; Huang, D.; Wang, W.; Dickinson, R.E.; Nemani, R.R.; Knyazikhin, Y.; Myneni, R.B. Analysis of leaf area index products from combination of MODIS Terra and Aqua data. *Remote Sens. Environ.* **2006**, *104*, 297–312.
37. Shabanov, N.V.; Huang, D.; Yang, W.; Tan, B.; Knyazikhin, Y.; Myneni, R.B.; Ahl, D.E.; Gower, S.T.; Huete, A.R.; Aragão, L.E.O.C.; *et al.* Analysis and optimization of the MODIS leaf area index algorithm retrievals over broadleaf forests. *IEEE Trans. Geosci. Remote Sens.* **2005**, *43*, 1855–1865.
38. Fang, H.; Jiang, C.; Li, W.; Wei, S.; Baret, F.; Chen, J.M.; Garcia-Haro, J.; Liang, S.; Liu, R.; Myneni, R.B.; *et al.* Characterization and intercomparison of global moderate resolution leaf area index (LAI) products: Analysis of climatologies and theoretical uncertainties. *J. Geophys. Res.: Biogeosci.* **2013**, *118*, 529–548.
39. Mueller-Dombois, D.; Ellenberg, H. *Aims and Methods of Vegetation Ecology*; John Wiley & Sons: New York, NY, USA, 1974.
40. Giladi, I.; Ziv, Y.; May, F.; Jeltsch, F. Scale-dependent determinants of plant species richness in a semi-arid fragmented agro-ecosystem. *J. Veg. Sci.* **2011**, *22*, 983–996.
41. LI-COR Inc. *LAI-2200 Plant. Canopy Analyzer Instruction Manual*; Li-Cor Inc.: Lincoln, NE, USA, 2009.
42. Nilson, T. A theoretical analysis of the frequency of gaps in plant stands. *Agr. Meteorol.* **1971**, *8*, 25–38.
43. Jones, H.G.; Vaughan, R.A. *Remote Sensing of Vegetation*: *Principles, Techniques, and Applications*; Oxford University Press: Oxford, UK and New York, NY, USA, 2010.

44. Kobayashi, H.; Ryu, Y.; Baldocchi, D.D.; Welles, J.M.; Norman, J.M. On the correct estimation of gap fraction: How to remove scattered radiation in gap fraction measurements? *Agric. For. Meteorol.* **2013**, *174–175*, 170–183.
45. White, M.A.; Asner, G.P.; Nemani, R.R.; Privette, J.L.; Running, S.W. Measuring fractional cover and leaf area index in arid ecosystems: Digital camera, radiation transmittance, and laser altimetry methods. *Remote Sens. Environ.* **2000**, *74*, 45–57.
46. Garrigues, S.; Allard, D.; Weiss, M.; Baret, F. Comparing VALERI Sampling Schemes to Better Represent High Spatial Resolution Satellite Pixel from Ground Measurements: How to Characterize an ESU. Available online: http://www.avignon.inra.fr/valeri/methodology/samplingschemes.pdf (accessed on 25 January 2015).
47. Bannari, A.; Morin, D.; Bonn, F.; Huete, A.R. A review of vegetation indices. *Remote Sens. Rev.* **1995**, *13*, 95–120.
48. Baret, F.; Guyot, G. Potentials and limits of vegetation indices for LAI and APAR assessment. *Remote Sens. Environ.* **1991**, *35*, 161–173.
49. Huete, A.R.; Justice, C.; van Leeuwen, W. MODIS Vegetation Index (MOD 13)—Algorithm Theoretical Basis Document (Version 3). Available online: http://modis.gsfc.nasa.gov/data/atbd/atbd_mod13.pdf (accessed on 25 January 2015).
50. Birth, G.S.; McVey, G.R. Measuring the color of growing turf with a reflectance spectrophotometer. *Agron. J.* **1968**, *60*, 640–643.
51. Tucker, C.J. Red and photographic infrared linear combinations for monitoring vegetation. *Remote Sens. Environ.* **1979**, *8*, 127–150.
52. Rouse, J.W., Jr.; Haas, R.H.; Deering, D.W.; Schell, J.A. Monitoring the Vernal Advancement and Retrogradiation (Green Wave Effect) of Natural Vegetation. Available online: http://ntrs.nasa.gov/archive/nasa/casi.ntrs.nasa.gov/19740004927.pdf (accessed on 10 April 2015).
53. Deering, D.W.; Haas, R.H. Using Landsat Digital Data for Estimating Green Biomass. Available online: http://ntrs.nasa.gov/archive/nasa/casi.ntrs.nasa.gov/19800024311.pdf (accessed on 25 January 2015).
54. Ehammer, A.; Fritsch, S.; Conrad, C.; Lamers, J.; Dech, S. Statistical derivation of fPAR and LAI for irrigated cotton and rice in arid Uzbekistan by combining multi-temporal RapidEye data and ground measurements. *Proc. SPIE* **2010**, *782409*, doi:10.1117/12.864796.
55. Morisette, J.T.; Baret, F.; Privette, J.L.; Myneni, R.B.; Nickeson, J.E.; Garrigues, S.; Shabanov, N.V.; Weiss, M.; Fernandes, R.A.; Leblanc, S.G.; *et al.* Validation of global moderate-resolution LAI products: A framework proposed within the CEOS land product validation subgroup. *IEEE Trans. Geosci. Remote Sens.* **2006**, *44*, 1804–1814.
56. Yang, W.; Tan, B.; Huang, D.; Rautiainen, M.; Shabanov, N.V.; Wang, Y.; Privette, J.L.; Huemmrich, K.F.; Fensholt, R.; Sandholt, I.; *et al.* MODIS leaf area index products: From validation to algorithm improvement. *IEEE Trans. Geosci. Remote Sens.* **2006**, *44*, 1885–1896.
57. Kanniah, K.D.; Beringer, J.; Hutley, L.B.; Tapper, N.J.; Zhu, X. Evaluation of Collections 4 and 5 of the MODIS Gross Primary Productivity product and algorithm improvement at a tropical savanna site in northern Australia. *Remote Sens. Environ.* **2009**, *113*, 1808–1822.

58. Willmott, C.J.; Ackleson, S.G.; Davis, R.E.; Feddema, J.J.; Klink, K.M.; Legates, D.R.; O'Donnell, J.; Rowe, C.M. Statistics for the evaluation and comparison of models. *J. Geophys. Res.* **1985**, *90*, 8995–9005.
59. Willmott, C.J.; Robeson, S.M.; Matsuura, K. A refined index of model performance. *Int. J. Climatol.* **2012**, *32*, 2088–2094.
60. Zandler, H.; Brenning, A.; Samimi, C. Quantifying dwarf shrub biomass in an arid environment: Comparing empirical methods in a high dimensional setting. *Remote Sens. Environ.* **2015**, *158*, 140–155.
61. Law, B.E.; Campbell, J.L.; Chen, J.M.; Sun, O.; Schwartz, M.; van Ingen, C.; Verma, S. Terrestrial Carbon Observations: Protocols for Vegetation Sampling and Data Submission, Report of the Global Terrestrial Observing System (GTOS). Available online: http://www.fao.org/gtos/doc/pub55.pdf (accessed on 10 April, 2015).
62. Zhang, J.; Zhang, C. Sampling and sampling strategies for environmental analysis. *Int. J. Environ. Anal. Chem.* **2012**, *92*, 466–478.
63. Roleček, J.; Chytrý, M.; Hájek, M.; Lvončík, S.; Tichý, L. Sampling design in large-scale vegetation studies: Do not sacrifice ecological thinking to statistical purism! *Folia Geobot.* **2007**, *42*, 199–208.
64. Scholes, R.J.; Frost, P.G.H.; Tian, Y. Canopy structure in savannas along a moisture gradient on Kalahari sands. *Glob. Chang. Biol.* **2004**, *10*, 292–302.
65. Ribeiro, N.S.; Saatchi, S.S.; Shugart, H.H.; Washington-Allen, R.A. Aboveground biomass and leaf area index (LAI) mapping for Niassa Reserve, northern Mozambique. *J. Geophys. Res. Biogeosci.* **2008**, *113*, doi:10.1029/2007JG000550.
66. Sea, W.B.; Choler, P.; Beringer, J.; Weinmann, R.A.; Hutley, L.B.; Leuning, R. Documenting improvement in leaf area index estimates from MODIS using hemispherical photos for Australian savannas. *Agric. For. Meteorol.* **2011**, *151*, 1453–1461.
67. Hill, M.J.; Román, M.O.; Schaaf, C.B.; Hutley, L.; Brannstrom, C.; Etter, A.; Hanan, N.P. Characterizing vegetation cover in global savannas with an annual foliage clumping index derived from the MODIS BRDF product. *Remote Sens. Environ.* **2011**, *115*, 2008–2024.
68. Ryu, Y.; Nilson, T.; Kobayashi, H.; Sonnentag, O.; Law, B.E.; Baldocchi, D.D. On the correct estimation of effective leaf area index: Does it reveal information on clumping effects? *Agric. For. Meteorol.* **2010**, *150*, 463–472.
69. Meza-Díaz, B.; Blackburn, G.A. Remote sensing of mangrove biophysical properties: Evidence from a laboratory simulation of the possible effects of background variation on spectral vegetation indices. *Int. J. Remote Sens.* **2003**, *24*, 53–73.
70. Van Leeuwen, W.; Huete, A.R. Effects of standing litter on the biophysical interpretation of plant canopies with spectral indices. *Remote Sens. Environ.* **1996**, *55*, 123–138.
71. Pinty, B.; Lavergne, T.; Widlowski, J.-L.; Gobron, N.; Verstraete, M.M. On the need to observe vegetation canopies in the near-infrared to estimate visible light absorption. *Remote Sens. Environ.* **2009**, *113*, 10–23.
72. Marsett, R.C.; Qi, J.; Heilman, P.; Biedenbender, S.H.; Watson, M.C.; Amer, S.; Weltz, M.; Goodrich, D.; Marsett, R. Remote sensing for grassland management in the arid Southwest. *Rangeland Ecol. Manage.* **2006**, *59*, 530–540.

73. Guerschman, J.P.; Hill, M.J.; Renzullo, L.J.; Barrett, D.J.; Marks, A.S.; Botha, E.J. Estimating fractional cover of photosynthetic vegetation, non-photosynthetic vegetation and bare soil in the Australian tropical savanna region upscaling the EO-1 Hyperion and MODIS sensors. *Remote Sens. Environ.* **2009**, *113*, 928–945.
74. Fang, H.; Li, W.; Myneni, R.B. The impact of potential land cover misclassification on MODIS Leaf Area Index (LAI) estimation: A statistical perspective. *Remote Sens.* **2013**, *5*, 830–844.
75. Myneni, R.B. Personal communication, Boston University, Boston, MA, USA, 2013.
76. Boschetti, L.; Roy, D.; Hoffmann, A.A.; Humber, M. MODIS Collection 5.1 Burned Area Product—MCD45, User's Guide Version 3.0.1. Available online: https://earthdata.nasa.gov/sites/default/files/field/document/MODIS_Burned_Area_Collection51_User_Guide_3.0.pdf (accessed on 26 October 2013).

6. MANUSCRIPT 3: DISTURBANCE FEEDBACKS ON THE HEIGHT OF WOODY VEGETATION IN A SAVANNAH: A MULTI-PLOT ASSESSMENT USING AN UNMANNED AERIAL VEHICLE (UAV)

Manuel J. Mayr, Sophia Malß, Elisabeth Ofner, Cyrus Samimi

International Journal of Remote Sensing (2017), 39 (14), 4761–4785.
DOI: 10.1080/01431161.2017.1362132

INTERNATIONAL JOURNAL OF REMOTE SENSING, 2017
https://doi.org/10.1080/01431161.2017.1362132

Taylor & Francis
Taylor & Francis Group

Disturbance feedbacks on the height of woody vegetation in a savannah: a multi-plot assessment using an unmanned aerial vehicle (UAV)

Manuel J. Mayr[a], Sophia Malß[b], Elisabeth Ofner[a] and Cyrus Samimi [a,c,d]

[a]Institute of Geography (GIB), University of Bayreuth, Bayreuth, Germany; [b]Department of Geosciences, University of Bayreuth, Bayreuth, Germany; [c]Bayreuth Center of Ecology and Environmental Research (BayCEER), University of Bayreuth, Bayreuth, Germany; [d]Institute of African Studies (IAS), University of Bayreuth, Bayreuth, Germany

ABSTRACT

Disturbances affect the woody, i.e. trees and shrubs, and herbaceous vegetation in savannah ecosystems worldwide. In Northern Namibia, livestock grazing and fires depict two prominent agents of disturbance. These affect the structural parameters of vegetation such as the height of woody species. Remote sensing is a tool to quantify such structural parameters. In particular, Image-Based Point Clouds (IBPCs) obtained from unmanned aerial vehicles (UAVs) are nowadays increasingly used for three-dimensional (3D) remote-sensing applications. Here we aim at deriving the height of woody stands through a multi-plot UAV campaign (n = 19) carried out at the end of the dry season. We use direct georeferencing from the navigation-grade instruments on board the UAV in a Structure-from-Motion (SfM) approach. Watershed segmentation is applied to derive plot-scale height metrics (maximum, mean, and median) based on delineated individuals. Fire and grazing – both individually and synergistically – are then investigated for their impacts on UAV-derived height metrics. The results indicate good agreement between the UAV-derived and *in situ*-measured height metrics on the plot scale (coefficient of determination (R^2) approximately 0.7, root mean square error (RMSE) <1.9 m). Underestimations of height are apparent with large, leafless trees. Clumping of equally sized individuals complicated their correct delineation. Grazing was found to be significant for all height metrics as well as in combination with fire for the plots' maxima. We conclude that the approach applied here is able to reproduce the plot-scale heights of woody vegetation with acceptable accuracy. We attribute the observed height reductions with the simultaneous presence of disturbances to legacy effects.

ARTICLE HISTORY
Received 5 January 2017
Accepted 14 July 2017

1. Introduction

Unmanned aerial vehicle (UAV) remote sensing is an emerging field of research and so is its applications. These range from archaeology (Verhoeven 2011; Roosevelt 2014), geomorphology and terrain mapping (Westoby et al. 2012; Harwin and Lucieer 2012; Jaud et al. 2016),

CONTACT Manuel J. Mayr manuel.mayr@uni-bayreuth.de Institute of Geography (GIB), Universitätsstr 30, 95447 Bayreuth, Germany

forestry (Heinzel and Koch 2012; Näsi et al. 2015), and atmospheric monitoring (Rogers and Finn 2013), to more proactive applications such as precision agriculture (Mathews and Jensen 2013; Torres-Sánchez et al. 2013; Candiago et al. 2015) and even landmine detection (Colorado et al. 2015) or active prescribed-fire ignition (Twidwell et al. 2016). Owing to their flexibility in terms of timing of data acquisition and the sensors used, UAVs provide new opportunities also for spatial ecology (Anderson and Gaston 2013). The spatially explicit sampling with resolutions in the range of m to cm is of relevance in the process of upscaling as UAVs potentially enable filling the scale gap between tedious point-based field measurements and the usually coarser-scaled satellite remote-sensing products. In addition, the ability to monitor dynamic processes from repeated acquisitions makes UAVs a suitable tool to address process–function relationships on the local scale. In this context, UAVs have been applied to model animal abundances (Mulero-Pázmány et al. 2015), detect invasive species (Hung, Xu, and Sukkarieh 2014), or to monitor fire impacts on vegetation cover (Breckenridge et al. 2012).

1.1. *UAV photogrammetry and vegetation*

With image-based UAV remote sensing, a set of overlapping imagery is usually acquired and processed using methods of digital photogrammetry (DP) in order to yield mapping products such as digital surface models (DSMs) and (mosaicked) orthoimagery (Colomina and Molina 2014). Whereas traditional DP relies on ground control points (GCPs) for triangulation and georeferencing (Chiang, Tsai, and Chu 2012), which is not always feasible, an automated DP is enabled by solving the orientations of and registration among the imagery using the Structure-from-Motion (SfM) approach (Snavely, Seitz, and Szeliski 2008).

Typically, SfM involves an initial detection of the shared features among the individual imageries based on segmentation procedures, which is followed by a Bundle Block Adjustment (BBA), where image orientations are calculated and tie points are aligned. The resulting three-dimensional (3D) sparse point cloud of the scene is then reconstructed using Multi-View Stereopsis (MVS) techniques in order to yield a dense Image-Based Point Cloud (IBPC) (Harwin and Lucieer 2012; Nex and Remondino 2014). Although the SfM-MVS procedure is solvable without any additional information on image position and orientation (Dandois and Ellis 2010; Xu et al. 2016), direct and indirect (e.g. GCPs or reference imagery) georeferencing of the imagery is commonly applied. For mono-temporal acquisitions, direct georeferencing obviously enhances the automation of the processing workflow. However, UAVs are often intended for low-cost applications, and consequently only provide positional and orientation accuracies in the range of several metres and degrees, respectively. Although trade-offs in absolute spatial accuracy are given, direct georeferencing is successfully applied with such systems (e.g. Chiang, Tsai, and Chu 2012; Zarco-Tejada et al. 2014; Colorado et al. 2015; Díaz-Varela et al. 2015; Gatziolis et al. 2015; Näsi et al. 2015).

IPBC can also facilitate 3D applications. With regard to vegetation, height derivation is probably the most commonly applied 3D measurement (Dandois and Ellis 2013). Vegetation heights at different scales, which are often remotely assessed with expensive Light Detection And Ranging (LiDAR) systems, are highly relevant inputs for allometric models, carbon sequestration studies, and inventories (Salamí, Barrado, and Pastor 2014). In this context, IBPC could allow for rapid and cost-efficient acquisitions that result in high-density

point clouds given suitable surface textures and image resolution. Different results regarding the accuracy of height retrievals from IBPC have been obtained: IBPC was found to be less accurate compared with terrestrial (Fritz, Kattenborn, and Koch 2013) and UAV-LiDAR (Dandois and Ellis 2010), but also similar accuracies (Jensen and Mathews 2016) and strong agreement with LiDAR (Lisein et al. 2013) could be obtained. With both technologies, LiDAR and IBPC, individual tree delineation is critical to deriving reliable heights and stand structures. The methods to discriminate individuals include maxima detection (e.g. local maxima, thresholding) and crown delineation algorithms (e.g. region-growing, watershed segmentation) (Ke and Quackenbush 2011). However, these have been rarely examined with IBPC; e.g. Zarco-Tejada et al. (2014) used a moving-window local maxima detection, whereas Näsi et al. (2015) applied watershed segmentation.

1.2. *Fire, grazing, and vegetation structure in dry savannahs*

In the dry savannahs that cover vast areas of Namibia, the distribution of woody species is limited by precipitation (Scholes and Archer 1997; Sankaran et al. 2005). Disturbances of natural and anthropogenic origin (e.g. fire, herbivory, or droughts) are identified as additional determinants of vegetation structure as they modify the competitive balance between woody and herbaceous species, and affect the growth and survival rates of woody individuals (Bond and Keeley 2005; Holdo 2007; Bond 2008). Fires, which are mainly lit by humans in Southern Africa (Archibald et al. 2010), primarily cause demographic bottlenecks by suppressing seedling recruitment and sapling maturation (Bond and Keeley 2005; Joubert, Smit, and Hoffman 2012; Levick, Baldeck, and Asner 2015). Rather than direct mortality of mature individuals, fires in semi-arid regions often only impose reduced growth rates from canopy scorching and hydraulic damage (Midgley, Lawes, and Chamaillé-Jammes 2010).

Natural herbivory is nowadays largely replaced by livestock grazing due to large parts of Namibia being used as rangelands (Mendelsohn et al. 2002; de Klerk 2004). Prolonged and extensive grazing activities in African savannahs are often accompanied by the expansion of certain woody species that, once established, tend to form thickets and consequently result in pasture degradation (Roques, O'Connor, and Watkinson 2001; Moleele et al. 2002; de Klerk 2004). This phenomenon, termed woody or bush encroachment, was first recognized in Namibia in the 1950s, but could not be controlled effectively since then (de Klerk 2004). Woody encroachment has been identified to be the result of the combined effects of overgrazing and fire exclusion, but more recent studies also emphasize the role of increasing atmospheric carbon dioxide (CO_2) concentrations in this process (e.g. Wigley, Bond, and Hoffman 2010; Bond and Midgley 2012; Stevens et al. 2016).

1.3. *Aims and scope of the study*

In this study, we aim at assessing the plot-scale (i.e. 0.5–2 ha) height metrics of woody vegetation in a Namibian savannah using IPBC acquired with a UAV. Thus, we test whether a low-cost approach that solely relies on the data acquired by the UAV can reliably reproduce the heights of plots consisting of trees and shrubs in an experimental setup. Mostly fragmented and isolated canopies as well as moderate covers should make these savannah ecosystems suitable for height delineations based on IBPC (Dandois and

Ellis 2010), although this has never been explicitly examined to our knowledge. The rare examples aiming at remotely sensed woody vegetation heights (Wessels et al. 2011; Khalefa et al. 2013) and single tree delineation (Chen et al. 2006) in savannahs were all conducted using air- and space-borne LiDAR systems.

If successful, the UAV-derived height metrics could be used to investigate the possible links of prominent disturbance agents, such as fire and livestock grazing, with stand structure. We hypothesize that disturbances generally have a reducing effect on vertical stand structure, i.e. lower average heights with the presence of disturbances. Due to the small-scale heterogeneity of disturbances, e.g. selective grazing or patchy burning, we consider the plot rather than the woody individual as the appropriate spatial scale of investigation here. Remote-sensing approaches addressing such disturbance feedbacks often rely on changes in woody cover, and are thus largely restricted to the growing season in deciduous environments. For partly undeveloped canopies at the end of the dry season – an environmental setting regarded as challenging with the remote sensing of vegetation (e.g. Harwin and Lucieer 2012; Mayr and Samimi 2015) – height retrievals from IBPC could be an alternative parameter to study the disturbance impacts on woody vegetation, but may also assist in the quantification of available biomass.

2. Materials and methods

2.1. *Study area*

The area of interest (Figure 1) is located in the northern Otjozondjupa Region, Namibia, and covers a rectangular bounding box of approximately 3,408 km^2. Located at the western fringe of the Kalahari Basin, the landscape is generally flat with fossil longitudinal dunes, especially in the eastern parts, and occasionally incising ephemeral valleys constituting the main relief features (Mendelsohn et al. 2002; Strohbach 2014). The soils of the Kalahari formation originate from unconsolidated aeolian materials and are characterized by poor nutrient availability (Wang et al. 2007). According to the SoilGrids database (www.soilgrids.org; Hengl et al. 2014), the predominant soil types are Ferralic Arenosols with sand fractions of approximately 80% and Petric Calcisols in the west. The climate is classified as semi-arid, with rainfalls occurring from October to April (Mendelsohn et al. 2002). Mean annual precipitation for the period 1990–2013 is 538 mm at the city of Grootfontein, which lies to the west of the study area, and 496 mm at Farm Gaikos, which is the only official rain gauge available in the study area (NMS 2015). The variability of annual rainfall sums is high, as outlined by the coefficients of variation >30% for both stations. Hence, although years of drought are common, winter frosts too may harm the vegetation locally. The predominant vegetation type is tree-and-shrub savannah, with a noticeable transition from feather-leaved (mainly *Acacia spp.*) to broad-leaved deciduous woody species towards the east (Giess 1971; Mendelsohn et al. 2002). Broad-leaved species (e.g. *Pterocarpus angolensis, Burkea africana*) tend to develop even-sized, mono-specific stands at this location (Graz 2006). Woody encroachment is a serious issue in these parts of Namibia (Mendelsohn et al. 2002; de Klerk 2004; Wagenseil and Samimi 2007). The spread of encroaching species, such as *Acacia mellifera, Dichrostachys cinerea,* and *Terminalia sericea,* is increasingly encountered on rangelands in the region (de Klerk 2004). Since colonial times, Namibia's fire management policy has been focussing on fire prevention and suppression (Beatty 2011; MAWF

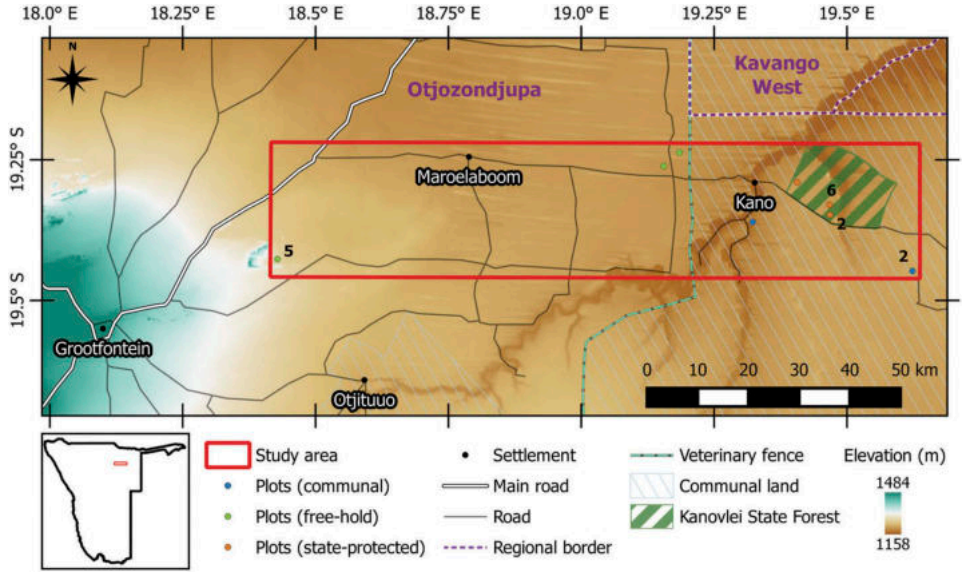

Figure 1. The study area and the plots used for aerial and *in situ* experiments in the northern Otjozondjupa region, Namibia. Black numbers indicate the number of plots if >1 at the given position due to reasons of presentation. Settlements and roads (based on OpenStreetMap (© OpenStreetMap contributors; www.openstreetmap.org)) are also shown in addition to regional administrative boundaries and land tenure (adapted from Mendelsohn et al. (2002)) as well as the Digital Elevation Model (DEM) from NASA's Shuttle Radar Topography Mission (SRTM) at 1 arc-second (i.e. 30 m horizontal resolution) (Farr et al. 2007; SRTM data are available from lpdaac.usgs.gov).

2012). Yet, the fire regime is heterogeneous, with communal rangelands exhibiting frequent burning as fires are used as a traditional tool in land management. In contrast, fires in freehold rangelands are less common, because of the existence of infrastructure and capabilities to extinguish uncontrolled wildfires (Le Roux 2011).

2.2. *Data acquisition*

Aerial and *in situ* samplings were conducted on 19 plots located in three subregions of the study area that covered different tenures and land uses: (i) at three farms in the freehold area, (ii) on the communal rangelands around the village of Kano, and (iii) in the protected areas of Kanovlei State Forest (Figure 1). The maximum distance between the sites was approximately 110 km.

2.2.1. *Flight campaign*

A campaign consisting of 19 flights (i.e. one per plot) was carried out in late September 2015 using a Soleon Coanda x12 UAV (Soleon s.r.l., Varna, Italy) (Figure 2). The UAV is powered by 12 brushless electric engines with rotary wings in a coaxial setup and a payload of 3.4 kg. For flight control and navigation, the UAV operates on a Micro Electro Mechanical Systems (MEMS)-based Inertial Navigation System (INS)/single-frequency global positioning system (L1-GPS) integrated system that is based on assemblies (FlightCtrl v2.5, NaviCtrl v2.0) and software by MikroKopter (HiSystems GmbH, Moormerland, Germany). The imaging system

Figure 2. The Soleon Coanda x12 during data collection in Namibia. As can be seen from the background, canopy development varied between woody species at the time of sampling (late September 2015).

is a consumer-grade Nikon 1 V3 camera with a Nikkor VR 10–30 mm lens (Nikon Corp., Tokyo, Japan), which is mounted on a two-axis gimbal-stabilized platform. This camera comes with a 13.2 × 8.8 mm Complementary Metal–Oxide–Semiconductor (CMOS) sensor and 18.4 megapixels resolution (5232 × 3488 pixels). As our initial intention was to additionally study early green-up species (see the two-camera setup in Figure 2), the first eight flights were conducted with wavelengths <550 nm obstructed by an optical filter mounted on the lens (Optic Makario GmbH, Mönchengladbach, Germany). The remaining 11 flights were completed in Red-Green-Blue (RGB) configuration.

We fixed the focal length to 10 mm and set the manual focus to infinity. All other optical parameters (e.g. shutter speed, aperture, and light sensitivity) were set to automatic for reasons of simplicity. Image acquisition was generally performed around midday in order to minimize shadows, as well as under sunny conditions in order to facilitate optimal radiometric differentiation. All flights were carried out in automatic waypoint mode at a stable forward velocity of 3 m s^{-1} and with a 50% sideward and forward overlap. As the UAV is fairly stable in air and the two-axis gimbal ensures near-nadir angles of the imagery, these overlaps are considered a trade-off between data quality of 3D reconstruction and processing performance. In practice, the overlaps were often higher, as two consecutive images were acquired at many waypoints via infrared triggering, although we admit the pattern behind the double triggering remained unresolved. The altitude above ground (AAG) was approximately 70 m, except for one flight carried out at 60 m. This yielded a ground sampling distance (GSD) <2 cm in all cases (Table 1). From 30 images on average, a mean areal coverage, i.e. the mosaicked footprint, of 3.11 ha could be produced.

2.2.2. *Ground data collection*

The field plots were all contained within the plots of the flight campaign, and their size ranged from 0.65 to 1.86 ha. Homogeneity within the stand was the criterion considered

Table 1. Descriptive statistics (mean, minimum, maximum, median, and standard deviation (SD)) of the flight campaign (n = 19). Columns list the number of images, the areal coverage of the flights, altitude above ground (AAG) from barometric measurement, and ground sampling distance (GSD).

	Images (n)	Coverage (ha)	AAG (m)	GSD (cm)
Mean	30[a]	3.11	74.3	1.67
Min.	14	1.86	60.3	1.11
Max.	40	4.42	82.9	1.82
Median	30.5	3.32	73.8	1.68
SD	5.97	0.82	4.85	0.15

[a] rounded mean.

for plot selection, where it was understood to target flat and even terrain conditions, and a large range of disturbance regimes between the plots.

A total of 322 trees and shrubs >1.5 m were measured on the 19 field plots (Table 2) using a Leica DISTO D510 laser-distance meter (Leica Geosystems AG, Heerbrugg, Switzerland) that was mounted on a tripod. The sampling was conducted along a 30 m regular grid. At each grid point, all woody individuals that were contained in an upward full-frame fisheye photograph (taken at 1 m height) were sampled.

2.2.3. *Disturbance regime*

We estimated the prevailing fire and grazing regime for each plot based on expert interviews with landowners (freehold rangelands), residents (communal rangelands) as well as forestry staff (state-protected forest), in-field recognition (e.g. burning scars), and the National Aeronautics and Space Administration's (NASA) Fire Information for Resource Management System (FIRMS) database (firms.modaps.eosdis.nasa.gov).

To investigate the disturbance impacts on plot heights, plots were grouped according to fire occurrence within the last 15 years, whereas grazing effects were separated

Table 2. Descriptive statistics (number of samples, mean, minimum, maximum, median, and standard deviation (SD)) of the field campaign per plot (n = 19) and in total.

Plot	Samples (n)	Mean	Min.	Max.	Median	SD
gk001	20	7.91	4.1	16.4	7.10	3.26
gk002	10	4.16	2.2	6.8	4.25	1.30
gk003	13	3.25	2.0	4.0	3.30	0.64
gk004	11	5.19	2.3	8.1	4.80	1.75
gk006	16	4.51	2.2	10.1	3.95	2.53
kc002	22	3.35	1.7	6.0	2.90	1.51
kc004	21	4.46	1.6	8.2	4.80	2.16
kc005	4	4.13	1.6	7.5	3.70	2.86
kr001	24	4.39	1.9	7.5	4.35	1.51
kr002	7	1.97	1.5	2.3	2.10	0.30
ks001	25	4.52	1.6	12.0	3.10	3.23
ks002	8	7.44	3.8	12.1	7.35	2.81
ks003	13	6.65	2.4	11.3	6.40	3.02
ks004	31	8.26	4.5	11.2	8.40	1.64
ks005	13	6.20	2.1	11.4	6.10	2.89
ks006	18	7.47	2.5	10.0	8.00	2.45
ks008	29	5.58	2.0	13.0	4.30	3.54
ks009	19	7.17	2.3	11.0	8.00	2.85
ks010	18	6.21	1.6	11.3	6.75	2.95
total	322	5.41	1.5	16.4	5.24	2.27

according to regular (i.e. annual to biennial) and irregular grazing on the plots. Furthermore, a combined disturbance regime was derived based on considerations of intensity as follows:

- low (no fire within 15 years *and* irregular grazing);
- moderate (single fire within 15 years *or* regular grazing); and
- high (several fires within 15 years, *or* single fire within 15 years *and* regular grazing).

2.3. *Processing workflow*

2.3.1. *Photogrammetric processing*

Each of the 19 flights was processed separately and in a highly automated approach using the commercial software Agisoft PhotoScan Professional (v1.2.4; Agisoft LLC, St. Petersburg, Russia) in order to derive orthomosaics, DSMs, and digital elevation models (DEMs) for each plot. PhotoScan uses an SfM approach that is based on matching features (tie points) between the overlapping individual images in order to obtain the 3D models of the entire scene (Westoby et al. 2012). The tie points are retrieved from a modified version of the Scale Invariant Feature Transform (SIFT) algorithm described by Lowe (2004). A detailed description of the SIFT algorithm and its performance is given in Lingua, Marenchino, and Nex (2009).

Preprocessing included manual checks for blurring of the imagery and the conversion of the selected raw imagery to Tagged Image File Format (TIFF). From the flight logs recorded by the UAV, camera trigger points were extracted to yield the approximate spatial reference of the imagery. For the internal orientation of the imagery, we calibrated the lens with Agisoft Lens (v0.4.2; Agisoft LLC, St. Petersburg, Russia). This implementation accounted for focal length, sensor dimensions, and the nonlinear distortion coefficients from Brown's model (Brown 1966).

A BBA was performed in order to align the imagery and to correct the camera positions. Aiming at the performance of the BBA and to facilitate direct georeferencing of the scene, we used the parameters of the calibrated lens as well as the spatial reference (Latitude/Longitude in World Geodetic System 1984 (WGS84) datum) and AAG (in metres) for each image from the on-board instruments, i.e. a 'photolog'. GCPs were not feasible in this study regarding the number of plots sampled. Hence, the external orientation of the imagery relied solely on the on-board navigation instruments: the L1-GPS (u-blox LEA-6S; u-blox AG, Thalwil, Switzerland), which has a circular error probability of 2.5 m for horizontal positioning (u-blox AG 2015), and a barometric sensor, as it is more accurate than the GPS-retrieved heights (Turner, Lucieer, and Watson 2012; Dandois, Olano, and Ellis 2015). The attitude parameters (yaw, pitch, and roll) were not included due to the presence of a gimbal and the accuracy characteristics of the low-cost MEMS-based INS (Turner, Lucieer, and Watson 2012). Based on the BBA, a dense IBPC was created by applying the 'high' quality setting and a 'moderate' depth filter in PhotoScan. At this stage, obviously erroneous points from visual inspection were manually removed from the IBPC. Object surfaces were then reconstructed by creating a 3D triangular irregular network ('mesh'). We used the 'height field' as the surface type, which creates a 2.5D model of the planar surfaces, i.e. the canopy horizontal maxima are

extended to the ground. A posterior hole filling was applied to the mesh using the default settings in PhotoScan. Finally, with the mesh serving as the DSM, orthomosaics of the overlapping imagery could be derived.

2.3.2. *DEM from ground points*

As no high-resolution, survey-grade DEM was available for the study region, an approximate DEM was conducted by classifying bare ground points in the IBPC. As has been shown by Mathews and Jensen (2013) and Jensen and Mathews (2016), UAV-derived ground point classification can reliably reproduce the ground surface for low-terrain environments with moderate covers of vegetation – as was the case here. Ground points were automatically extracted in PhotoScan using the following parameters (Agisoft LLC 2016):

- preparatory DEM points were selected from a regular grid as the lowest values within cells of 10 × 10 m,
- a maximum vertical angle between a potential ground point and the preparatory DEM of 10°, and
- a maximum elevation difference between a potential ground point and the preparatory DEM of 1 m.

Points meeting the angular and elevational conditions were added to the preparatory DEM. Similar to the procedure described earlier, surfaces were subsequently reconstructed ('mesh') from the ground point cloud in order to yield a DEM for each plot.

Finally, orthomosaics, DSMs, and DEMs were resampled to a 10 cm resolution and exported as GeoTIFFs. All products were also clipped to the footprint of the *in situ* plots for further processing.

2.3.3. *Canopy Height Model (CHM)*

By subtracting the DEM from the corresponding DSM, a CHM or a normalized DSM could be derived (Chen et al. 2006). As *in situ* sampling only included woody individuals with a minimum height of 1.5 m (Table 2), this threshold was applied for the CHM as well.

2.3.4. *Woody individuals' delineation*

Although the CHM alone might be sufficient for the height derivation of isolated individuals, connected and overlapping canopies will be treated as a single canopy in this way. To largely overcome this limitation and derive more realistic plot-scale height structures, (inverse) watershed segmentation was frequently applied as a tool with LiDAR-derived CHMs (e.g. Pyysalo and Hyyppä 2002; Chen et al. 2006; Reitberger et al. 2009; Heinzel and Koch 2012; Wallace, Lucieer, and Watson 2014). However, this has rarely been performed with image-based CHMs (e.g. Näsi et al. 2015). Heterogeneous canopies potentially complicate the segmentation process – especially in times of leaf loss, and even some savannah woody species develop flattened to umbrella-shaped canopies. Hence, in order to balance between over- and under-segmentation, the CHM was initially smoothed using a 3 × 3-mean (low-pass) filter. In addition, segments <1 m^2 were merged to their neighbouring segment where applicable and the minimum seed-to-saddle difference was set to 2 m based on on-screen verification. For each of the segments, i.e. the individual canopies, the local maximum and its position were

subsequently extracted from the unfiltered CHM. The performance of the watershed segmentation was assessed for 50 randomly generated points per randomly chosen subplot (30 × 30 m) and by comparing the segmentation results with the manual delineation of crowns from on-screen interpretation.

We used an implementation of the watershed segmentation algorithm provided by System for Automated Geoscientific Analyses - Geographic Information System(SAGA-GIS; Conrad et al. 2015) and calculated the per-plot maximum, mean, and median in order to enable further statistical analysis.

2.3.5. *Statistical analyses*

To evaluate the accuracy of the per-plot UAV-derived heights against the corresponding *in situ* metrics, we computed linear models and root mean square errors (RMSEs). Initial Shapiro–Wilk normality tests suggested normality for all UAV-derived height metrics, but additional normal Quantile-Quantile (QQ-normal) plots confirmed deviations of the data from normal distribution (both not shown). Hence, with regard to test robustness, non-parametric tests were performed to investigate the potential impacts of disturbances on the UAV-derived woody height metrics. All analyses were conducted in R (R Core Team 2014).

3. Results

3.1. *Photogrammetric processing and spatial accuracy*

The photogrammetric processing was successful for each of the 19 data sets. The mean effective overlap of the imagery was 3.98 (Table 3), whereby a value of four would indicate a forward and sideward overlap of 50%. Effective overlap may reflect the number of flight lines as the outer image acquisition lines will always have lower sideward overlaps, which is essentially an issue of areal coverage. The same is true for the number of tie points used for image alignment, which varied largely (min.: 11,123 tie points; max.: 123,621) as a function of the area covered by the image mosaics. Point densities of the dense cloud were generally high as a function of the GSD: the mean was 990.32 and the maximum was 2,182.34 points/m^2, respectively. The maximum was obtained by one flight carried out at an AAG of 60 m.

Regarding the reconstruction accuracy of the IBPC, the RMSE values of re-projection were, in most cases, below one pixel (mean: 0.71 m; max.: 1.17 m; standard deviation (SD): 0.18 m) (Table 3). Image reference positions showed high variation. The RMSE ranged from 0.63 to 10.71 m for the *x*-coordinate, and from 0.72 to 15.94 m for the *y*-coordinate, whereas the respective means were >3 m for both coordinates. RMSE of the *z*-coordinate (i.e. height) yielded better reconstruction accuracies that remained mostly below 1 m (mean: 0.75 m, median: 0.7 m, SD: 0.35 m). The mean of the total positional RMSE was 5.17 m for all flights. A visual inspection of the processed orthomosaics and a comparison with GoogleEarth imagery also revealed good orientations and fairly positional accuracies (Figure 3).

3.2. *Woody individuals' delineation*

The delineation of woody individuals is a critical step for the retrieval of representative plot-scale woody height structures. A comparison carried out on a subsample and with manually delineated crowns revealed promising delineations by the watershed

Table 3. Descriptive statistics (mean, minimum, maximum, median, and standard deviation (SD)) of the photogrammetric image processing for all flights (n = 19). Columns list the effective overlap of imagery, number of tie points for image alignment, the root mean square error (RMSE) of re-projection in pixels (i.e. the offsets between the position of tie points from the estimated camera poses versus their position in the imagery), RMSE of position (x and y from L1-GPS, z from barometric measurement, and total error of xyz), and point density of the dense Image-Based Point Cloud (IBPC).

	Effective overlap	Tie points (n)	RMSE re-projection (pixels)	RMSE position (m) (x, y, z, total)				Point density (number/m^2)
Mean	3.98	73,157.72	0.71	3.46	3.15	0.75	5.17	990.32
Min.	2.47	11,123	0.5	0.63	0.72	0.35	1.08	818.03
Max.	7.7	123,621	1.17	10.71	15.94	1.77	16.1	2,182.34
Median	3.55	70,742	0.66	3.56	2.52	0.7	4.75	940.25
SD	1.22	29,604.61	0.18	2.33	3.36	0.35	3.5	302.15

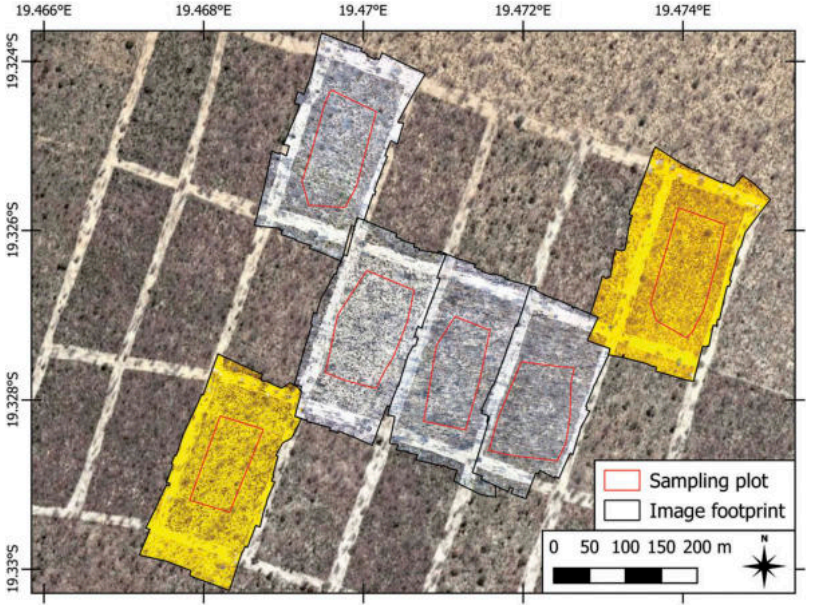

Figure 3. Exemplary orthomosaics from UAV acquisition at Kanovlei State Forest Fire Trial plots, their footprints (black), and the respective *in situ* sampling plots (red). For the yellow mosaics, imagery was acquired with yellow filter that obstructs wavelengths <550 nm mounted on the camera lens. Background image credit: GoogleEarth (© DigitalGlobe).

segmentation: correct assignments to canopy/non-canopy points were generally > 80% (average: 92.63%; Table 4), which may also reflect the moderate covers of woody vegetation. Instead incorrect assignment was accordingly low (> 10% for five plots) and almost exclusively contained omitted canopy points (false negatives; Table 4).

A visual interpretation of the watershed segmentation retrievals generally showed reasonable delineations of individuals with homogeneous canopies, i.e. green canopies and dry bushes with a dense branch structure (Figure 4(a)). Owing to the canopy morphology of many savannah species, the maxima of individuals were not always centred within the crown. For large individual trees with leaf loss, the success of watershed delineation using a CHM appeared to be limited. The sparse branch structure

Table 4. Performance assessment of the automated crown delineation using watershed segmentation based on the smoothed Canopy Height Model (CHM) at 10 cm resolution on randomly chosen 30 × 30 m subplots for each plot (n = 19) and in total. Fifty randomly generated points per subplot were applied to evaluate the correct/incorrect assignment of the automated crown delineation using on-screen, manually delineated crowns from the ortho-mosaics at native resolution as a reference. Shown are points correctly assigned as Canopy (True Positives (TP)) and Non-canopy (True Negatives (TN)), points incorrectly assigned as Canopy (False Positives (FP)) and Non-canopy (False Negatives (FN)) as well as the overall percentages of correct/incorrect assignment. Note that points assigned as TN make up large numbers due to moderate vegetation covers.

	Correctly assigned			Incorrectly assigned		
ID	Canopy (TP)	Non-canopy (TN)	(%)	Canopy (FP)	Non-canopy (FN)	(%)
gk001	6	39	90	3	2	10
gk002	8	36	88	1	5	12
gk003	1	46	94	0	3	6
gk004	3	45	96	0	2	4
gk006	7	39	92	0	4	8
kc002	6	40	92	0	4	8
kc004	5	42	94	0	3	6
kc005	1	48	98	0	1	2
kr001	4	43	94	1	2	6
kr002	0	50	100	0	0	0
ks001	1	48	98	0	1	2
ks002	2	42	88	0	6	12
ks003	5	42	94	0	3	6
ks004	2	43	90	0	5	10
ks005	2	40	84	0	8	16
ks006	1	49	100	0	0	0
ks008	5	38	86	1	6	14
ks009	2	40	84	1	7	16
ks010	4	45	98	0	1	2
total	65	815	92.63	7	63	7.37

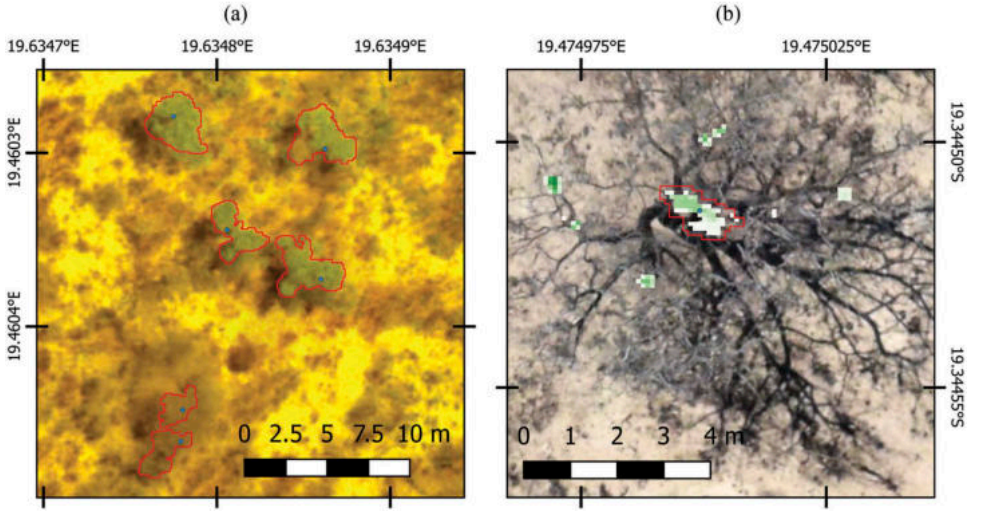

Figure 4. Examples of the delineation of woody individuals (red polygons) and canopy maxima positions (blue points) from watershed segmentation: (a) shrub canopies with and without leaves. Background image: 10 cm-resolution UAV orthomosaic with yellow filter mounted; (b) tree canopy with leaf loss and overlay of the Canopy Height Model (CHM; white to green as a function of increasing height). Background image: UAV orthomosaic at the native resolution of 1.77 cm.

resulted in a dense IBPC of limited density, and hence a strongly fragmented CHM. Consequently, individual crown areas were underestimated and the derived heights potentially do not reflect the actual canopy maxima of these individuals (Figure 4(b)).

3.3. *Plot-scale height retrievals*

The UAV-derived height metrics (maximum, mean, and median) yielded a satisfactory agreement with the corresponding measured heights on a plot scale (Figure 5(a–c)). Generally, a tendency towards a slight overestimation on plots with lower heights, and vice versa, is observed for all UAV-derived height metrics under investigation. Where the coefficients of determination (R^2 and adjusted R^2) consistently range around 0.7 for all height metrics, the RMSE is remarkably higher for UAV-derived maxima (1.86 m) than for mean and median heights (0.91 m and 1.02 m, respectively). This increase in RMSE may reflect the larger range covered by the maximum heights between the individual plots.

In accordance with the linear models, Wilcoxon signed rank tests reveal no significant differences of the group median between the measured and UAV-derived height metrics (Table 5). Again, the 95%-confidence intervals (CI (95%)) result in a broader range around the group median for maximum height compared with the mean and median heights. Mean differences between the groups (i.e. measured vs. UAV-derived) reveal the

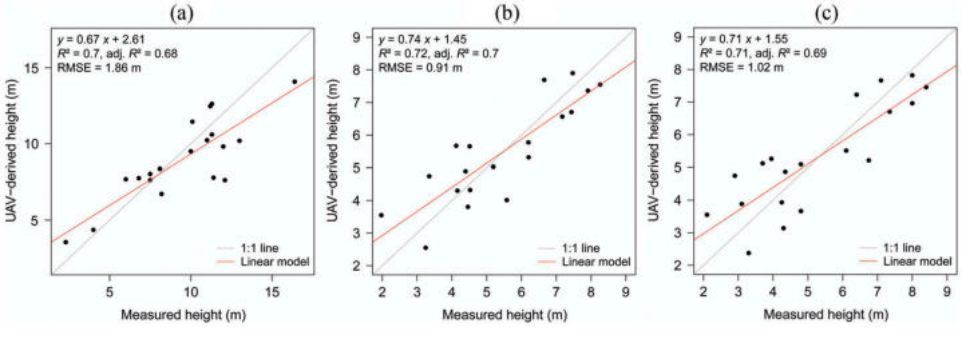

Figure 5. Linear models of UAV-derived and *in situ*-measured height metrics: (a) maximum height (m) per plot; (b) mean height (m) per plot; and (c) median height (m) per plot. Each panel shows data pairs for the individual plots (n = 19; black points), 1:1 line (grey), linear model (red), as well as the linear model equation, coefficients of determination (R^2 and adjusted R^2), and root mean square error (RMSE; in m).

Table 5. Results of the Wilcoxon signed rank tests. The differences of the median between the measured and UAV-derived height metrics (maximum, mean, and median) are compared on a plot scale (n = 19). Summed ranks of positively signed group differences (V) are given, whereas p-values (p) >0.05 indicating no significant differences between the median of the groups were obtained. Columns also show the range of the 95%-confidence interval around the median in m (CI (95%)) and the mean of the differences between the groups in m (mean Δ).

Measured vs. UAV-derived	V	p	CI (95%)	mean Δ
Maximum height	115	0.441	[−0.53; 1.44]	0.51
Mean height	97	0.953	[−0.47; 0.54]	−0.03
Median height	95	1	[−0.56; 0.59]	−0.03

maximum heights from measurement to be 0.51 m higher than those from UAV derivation. For mean and median heights, the UAV-derived heights are negligibly higher (<0.05 m) than those from the measurement.

3.4. *Disturbance impacts on plot heights*

The good agreement between each UAV-derived and measured height metrics (see Section 3.3) allows the former to be used as a surrogate for the latter in assessing potential feedbacks of disturbances on plot height metrics. Fires, i.e. the last fire within 15 years, had no significant effect on these metrics (Table 6). Nevertheless, maximum heights were strongly reduced by the presence of fire as depicted by a median difference of more than 2 m between plots with and without fire occurrence in the last 15 years (Figure 6(a)). Mean and median plot heights did not respond to the presence of fire (Table 6), but were even slightly higher on plots that were affected by fire within the last 15 years (Figure 6(b,c)).

Grazing had a significant effect on all plot height metrics under investigation (Table 6). Regular grazing generally resulted in a reduction of plot-scale heights (Figure 6(d–f)). Only minor reductions of the mean and median plot heights were found with increasing intensities of the combined disturbance regime (Figure 6(h,i)). In contrast, the combined disturbance regime had marginally significant effects on the plots' maxima (Table 6). Figure 6(g) further illustrates that plots with moderate and high intensities of the combined disturbance regime are characterized by lower maximum heights compared with plots with a low disturbance regime. Hence, fire and grazing together contribute to the reduction of plot-scale height maxima.

4. Discussion

4.1. *Image acquisition and photogrammetric processing*

With a nominal forward and sideward overlap of 50%, the overlaps in this study were lower than those recommended by Dandois, Olano, and Ellis (2015) for forested ecosystems. However, the savannah ecosystem under investigation was of lower heights

Table 6. Results of the non-parametric tests on disturbance effects. The impacts of individual disturbances and the combined disturbance regime from fire and grazing on UAV-derived height metrics (maximum, mean, and median) on the plot scale (n = 19) are compared. The impact of fire (last fire) was assessed for the groups with last fire occurrence '<15 years' (n = 12) versus '>15 years' (n = 7). Grazing impacts were assessed for the groups 'regular' (n = 7) versus 'irregular' grazing (n = 12). The combined disturbance regime was grouped into 'low' (n = 4), 'moderate' (n = 8), and 'high' (n = 7); see Section 2.2.3 for further explanation. For the Mann–Whitney tests, columns list the Wilcoxon rank sum statistic (W) and the p-value (p) for each of the height metrics. For the Kruskal–Wallis tests, columns are the chi-squared value (χ^2), the degrees of freedom (df), and the p-value (p) for each of the height metrics.

	Maximum			Mean			Median		
Mann–Whitney test	W		p	W		p	W		p
Last fire	24		0.142	45		0.837	44		0.902
Grazing	66		0.045*	15		0.022*	18		0.045*
Kruskal–Wallis test	χ^2	df	p	χ^2	df	p	χ^2	df	p
Combined disturbance regime	4.849	2	0.089**	0.139	2	0.933	0.04	2	0.98

* significant at the 0.05 level (two-sided); ** significant at the 0.1 level (two-sided).

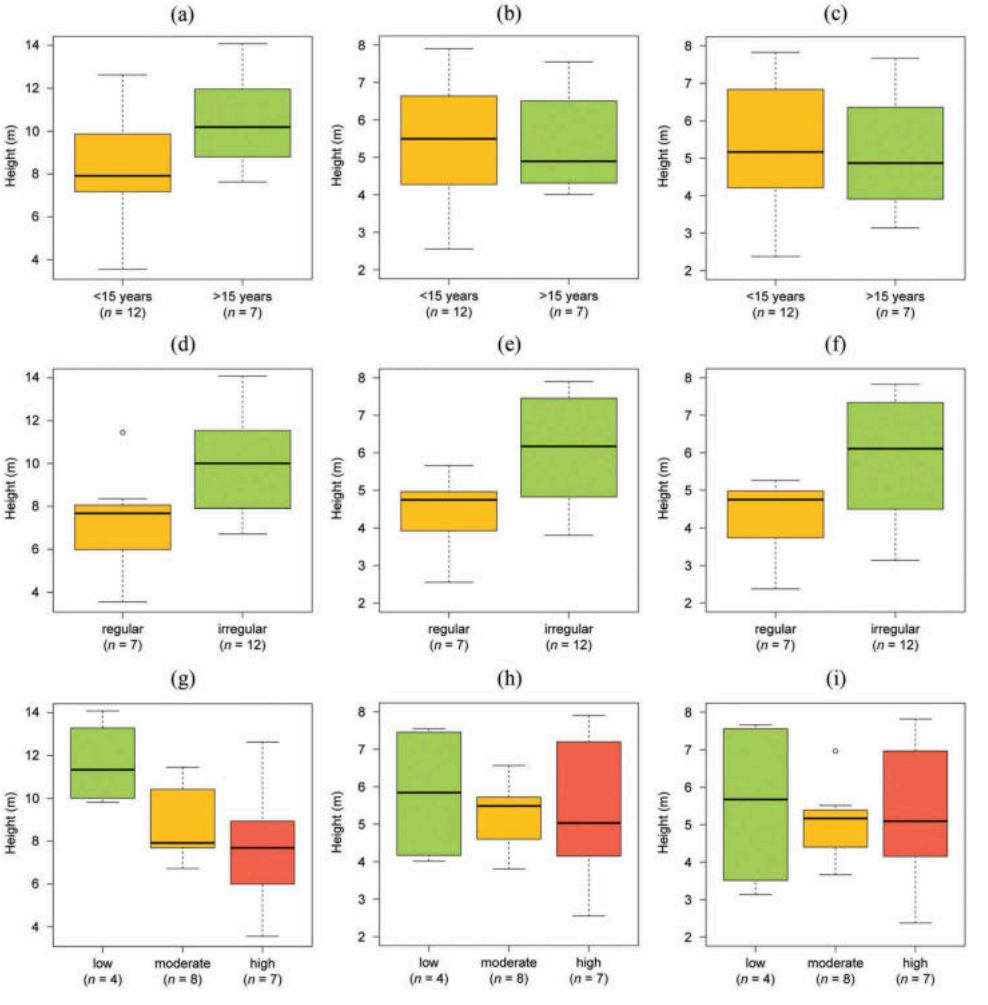

Figure 6. UAV-derived height metrics of woody vegetation and disturbance impacts at the plot scale (n = 19). The box plots show: (a) maximum, (b) mean, and (c) median height (m) versus the last fire occurrence; (d) (*) maximum, (e) (*) mean, and (f) (*) median height (m) versus grazing; (g) (**) maximum, (h) mean, and (i) median height (m) versus the combined disturbance regime from fire and grazing.

Note: * significant at the 0.05 level (two-sided); ** significant at the 0.1 level (two-sided); see also Table 6.

compared with a forest, the terrain was even, and the GSD of <2 cm was fairly high. Woody height delineation was also restricted to the central parts of the mosaicked footprint (i.e. clipping to the *in situ* plots; Figure 3). Consequently, the imagery of the outer flight paths, which usually have the lowest overlaps, was often completely excluded. Still, it has to be noted that increasing overlaps are likely to improve IBPC accuracies, but an examination with varying flight parameters was beyond the scope of this study.

It can be speculated whether the radiometric camera settings (e.g. sensor sensitivity (ISO), exposure, and aperture) should be fixed to yield an increased radiometric homogeneity of the individual imagery. For instance, low values of automatic aperture may

result in (soil) background blurring. As imagery was acquired from a stable forward flight, we emphasized on the optimal ratios of aperture and exposures. Hence, the mean exposure of the 561 images used for processing was 1/834 s (not shown). With a mean of 4.98 (not shown), the aperture was fairly high at the same time and given the lens' range of aperture (i.e. 3.5–5.6). For quantitative spectral analyses instead, radiometric homogeneity between the images and sensor calibration in general would of course be mandatory (Honkavaara et al. 2012; Zarco-Tejada et al. 2014). With feature matching and point cloud reconstruction, radiometric variation may be an issue (Hirschmüller and Scharstein 2009; Mukherjee, Wu, and Wang 2015), but is ubiquitous, and even viable, as a result of the different viewing angles between the imagery. In addition, the numbers of tie points relative to areal coverage and the point densities as a function of GSD were generally high (Table 3). Furthermore, we did not recognize any shortcomings during photogrammetric processing (e.g. lower numbers of tie points for image alignment) with the flights carried out with the yellow filter mounted on the lens. Some degree of blurring in the orthomosaics at native resolution was found here (Figure 4(b)). This remains an unresolved issue, which has also been noticed by other studies (e.g. Mathews and Jensen 2013; Näsi et al. 2015; Torres-Sánchez et al. 2015).

4.2. *Spatial accuracy*

We used a direct georeferencing approach based on the on-board L1-GPS and barometric instrument. These instruments were not of survey-grade accuracy. Hence, the discrepancy in position between the barometric instrument and the imaging sensor on the UAV could be neglected. Furthermore, we did not account for the delay of the camera shutter as the exposures were generally short (Section 4.1) and the UAV was programmed to fly at 3 m s^{-1}. The RMSEs of position were on average <3.5 m and <1 m for horizontal and vertical accuracies, respectively (Table 3), which generally met the expectations with the instruments used. Sub-metric spatial accuracies were unachievable due to the lack of a differential or a Real-Time-Kinematic GPS and the absence of high-resolution, survey-grade maps or imagery for this remote region. In addition, indirect georeferencing (e.g. by means of GCPs) would have required tremendous additional human efforts and thus appeared unfeasible with regard to the multi-plot design of the study. The best freely available reference source by means of resolution and spatial accuracy would have been the Landsat Operational Land Imager (OLI) instrument, which offers a 15 m resolution with the panchromatic band, and a circular error of 12 m (Roy et al. 2014). Instead, we found acceptable consistency of the derived orthomosaics with GoogleEarth, which offers high-resolution imagery, but is potentially affected by large spatial offsets itself (Potere 2008).

The advantage of the approach applied here is the efficient processing of multiple data sets and a largely automated workflow from raw data to orthomosaics. It is certainly not suited for all applications. For an evaluation of UAV-derived heights versus the measured heights at the individual scale, the spatial accuracy of the presented approach would exacerbate the correct allocation of woody individuals. However, for the evaluation of plot-scale woody heights with their *in situ*-measured correspondents, we are convinced that the internal or relative spatial accuracy achieved with the reconstructed model, i.e. the correctness of distances, is of primary importance. The RMSE of re-projection, a measure of relative accuracy,

was on average 0.71 ± 0.18 pixels (Table 3). Studies that used comparable georeferencing and similar software reported slightly higher relative accuracies (Näsi et al. 2015), but also lower relative accuracies (Zarco-Tejada et al. 2014). In these regards, lens calibration, high GSD, and distinct textures in the imagery constituted a framework for accurate feature matching and reconstruction. The IBPCs obtained using the SfM-MVS reconstruction algorithm in Agisoft PhotoScan were previously found to be fairly convenient (e.g. Neitzel and Klonowski 2011; Verhoeven 2011; Roosevelt 2014; Jaud et al. 2016; – among others).

4.3. *Woody vegetation heights derivation*

Terrain properties, i.e. flat and even ground, and a certain openness of the stands, were important prerequisites for successful plot-scale derivation of woody vegetation heights through the CHM in this study. The base heights for the CHM depended on a DEM. As no high-resolution, survey-grade DEM was available for the study region, a DEM was derived from a classification of the dense IBPC. The parameters used in this step are explicitly site-specific as they were identified on-screen and verified through visual inspection. Subsequently, they were uniformly applied to all plots. Ota et al. (2015) compared CHMs from LiDAR, IBPC, and combined sources in a seasonal tropical forest ecosystem, concluding that CHMs relying only on IBPCs obtained the lowest accuracies. These were attributed to ground obscuration as a result of stand density. The CHMs had a 1 m resolution in that study, which is substantially coarser than the 10 cm resolution used here. In another study from two Mediterranean orchards, tree height delineation accuracy was largely reduced with spatial resolutions >35 cm (Zarco-Tejada et al. 2014). Indeed, high spatial resolutions of the input imagery (i.e. <2 cm) and the CHM as applied here were probably among the factors responsible for the promising agreement between the UAV-derived and *in situ* heights (R^2 approximately 0.7, and RMSE <1.9 m; Figure 5). Compared with two studies evaluating plot height metrics from a fully IBPC-based CHM, the agreements found here are lower (Jensen and Mathews 2016) or partly lower (Dandois and Ellis 2013). However, it should be noted that georeferencing was assisted by GCPs and the canopies were generally green in these two studies. Instead, the RMSEs achieved here are similar to those conducted with a comparable set of plot heights (Jensen and Mathews 2016), and lower than those carried out in an ecosystem of taller heights (Dandois and Ellis 2013). In a South African savannah, Khalefa et al. (2013) used space-borne LiDAR, which resulted in moderate agreements with *in situ* heights – probably due to the coarser spatial resolution. In the same region, Wessels et al. (2011) compared airborne LiDAR estimates of woody individuals, reporting overall explained variances of 93%, but acknowledging the underestimation of individuals <2 m. Here, it can only be speculated whether enhanced height agreements are achievable on an individual scale. Our *in situ* sampling design (i.e. height measurements of all individuals >1.5 m that were contained in an upward-facing hemispheric photograph) unfortunately inhibited such an additional investigation. Only heights of the individuals and their distances from the sampling grid were recorded, whereas geo-locational uncertainties of the sampling grid were imposed using a navigation-grade GPS in the field campaign. Instead, we used watershed segmentation to delineate woody individuals in order to derive a representative plot height structure for the mean and median metrics. For plot maxima, the initial CHM would have been sufficient.

A performance assessment of the watershed segmentation by means of a manually delineated subsample revealed correct assignments of canopy/non-canopy points of >80% (Table 4). Dry dense (i.e. bushes) and green canopies were probably the most suited for automated delineation. Canopy green-up prior to the first rains is a phenological feature of certain savannah trees and shrubs, yet poorly understood (Whitecross, Witkowski, and Archibald 2016). Because of their dense branch structure, also dry shrubs could be successfully delineated (Figure 4(a)). Conversely, canopy fragmentation, i.e. over-segmentation, was observed with large-sized trees that had undeveloped canopies at the time of sampling (e.g. *Pterocarpus angolensis, Burkea africana,* or *Schinziophyton rautanenii*). Hence, their heights were potentially underestimated (Figure 4(b)). This is in accordance with other studies (e.g. Dandois and Ellis 2010; Lisein et al. 2013; Torres-Sánchez et al. 2015) that reported IBPC-based 3D reconstruction of heterogeneous and low-density canopies to be challenging. In these regards, it should be mentioned that *in situ* height measurements too are prone to errors (Hunter et al. 2013; Larjavaara, Muller-Landau, and Metcalf 2013).

With highly clumped canopies of similar height, watershed segmentation is likely inaccurate as the algorithm fails to separate these reliably. However, this issue is also apparent with traditional local maxima extraction (e.g. Díaz-Varela et al. 2015). An interesting approach to partly overcome under-segmentation was presented by Chen et al. (2006), who parameterized the moving window used for local maxima determination by means of an empirical relationship between height and crown size in a Californian savannah. Such allometric relationships are problematic for Southern African savannahs, where even intraspecific growth forms vary largely – also as a response to fire and grazing (cf. Archibald and Bond 2003; Holdo 2006).

4.4. *Disturbance impacts* versus *environmental heterogeneity*

Compared with extensive ground-based studies (e.g. Higgins et al. 2007; Poorter et al. 2008), the sample size (n = 19) was small. Still, the sample generated from UAV derivation was sufficient to indicate certain fire and grazing impacts on these plots. The presence of disturbances often caused a reduction in the plot-scale heights of woody vegetation. For regularly grazed plots, this effect was significant for all height metrics under investigation (Table 6). Plot maximum heights were higher on plots that had no fire within the last 15 years (Figure 6(a)), although not significant, and plots classified with a low combined disturbance regime (Figure 6(g)). However, the observed disturbance impacts on plot heights should be regarded in the context of the uncertainties presented with UAV-derived heights (Figure 5).

While the disturbance relations generally appear reasonable, the processes behind them differ. Woody height reductions may refer to an encroachment of shrub species, which is accompanied by changes in species composition. Although no short-term direct link between grazing and woody heights is perceivable, height reductions on these rangelands are probably the outcome of an intense, prolonged grazing regime. Freehold farms were established during the first half of the twentieth century in the region (U. Gressmann, personal communication, 25 February 2015) and communal lands were probably used for livestock ranching even earlier. Similar legacy effects have also been reported for fire impacts in the South African savannahs (e.g. Kennedy and Potgieter 2003; Levick, Baldeck,

and Asner 2015). Although the long-term fire history has not been documented for this region, it can be speculated that the plots, except for the Kanovlei Fire Trials, which were only established in the 1990s, have experienced quasi-similar fire regimes as during our period of observation. This is reasonable for the observed maxima reduction, as these age classes are the least affected by fire due to their size, but also the species-specific adaptions such as thick bark (Bond and Keeley 2005).

Investigating woody covers, e.g. by using object-based image analysis, would shed further light onto the disturbance-vegetation feedbacks on the plots. This would require another flight campaign during the growing season, which was beyond the scope of this study.

From an ecological perspective, however, our analysis of disturbance impacts is a strong simplification of the real world as it suggests an exclusive and direct feedback of fire and grazing on woody vegetation heights in these savannah ecosystems. Environmental variation was intended to be minimized by our study design, e.g. rainfall, flat terrain, and plots regarded as homogenous in terms of their vegetation structure. The latter is admittedly imprecise, as small-scale heterogeneity is inherent to savannahs (Skarpe 1991; Jeltsch et al. 1998). Furthermore, soil properties (e.g. depth, nutrient availability), species differences, and other disturbances (e.g. local frost events, browsing herbivory, or pests) are important determinants of plot-scale woody height that were not considered here. Future studies of disturbance-vegetation feedbacks need to account for these.

5. Conclusions

The study presented here used IBPC acquired through a multi-plot UAV campaign (n = 19) in an experimental setup to derive plot-scale height metrics in a Namibian savannah. Moderate densities of woody vegetation, alongside flat and even terrain as well as the high relative accuracy of the IBPC achieved by a GSD <2 cm, were identified as a suitable framework for the autonomous generation of a CHM here.

The results for the plot-scale height metrics were promising given the season of observation with green and dry canopies, and despite the lack of high-accuracy spatial reference data. Watershed segmentation was, in most cases, found to reasonably delineate individual canopies, and hence to retrieve representative plot height structures. Resultantly, all plot-scale height metrics derived from UAV (maximum, mean, and median) showed good agreement with the corresponding *in situ* measurements. Explained variances (R^2) were generally around 0.7, whereas RMSEs were approximately 1 m for means and medians, and 1.9 m for the maxima. Still, survey-grade navigational systems would increase absolute spatial accuracy, which is critical for many applications, and allow for height assessments on the scale of individuals, which could not be achieved here. A flight campaign during the growing season could solve inaccuracies by means of individual delineation and height as encountered with fragmented, dry canopies. Alternatively, clumped and equally sized canopy delineation may benefit from the incorporation of spectral information to assist the separation of individuals by species.

The evaluation of plot-scale woody vegetation height metrics and their feedbacks with fire and livestock grazing impacts largely met the proposed hypotheses. Significant plot-scale height reductions of all metrics under observation were found for regularly grazed plots. This could be an indication of woody encroachment and combined pasture degradation. Height maxima were also significantly higher with a low combined disturbance regime from fire and

grazing. We attribute the observed height reductions to legacy effects imposed by a longer-term disturbance regime. Still, this model clearly simplifies the complexity of environmental systems. Future work should also include soil properties, species differences as well as other disturbance impacts (e.g. from meteorology, browsing, or pests).

This study highlighted the potential of UAVs for applications in spatial ecology. To the best of our knowledge, it is also the first study to assess the disturbance impacts on the height of woody vegetation by means of a UAV in a savannah ecosystem. Plot height response to disturbances is essential to modelling and quantifying carbon sequestration as (average) heights are strongly linked to available biomass. In these regards, the good agreement found with field measurements is favourable to upscale these to coarser satellite products via high-resolution UAV imagery. Although further research on height derivation and IBPC in different ecosystems and environmental settings is needed, UAVs may operationally assist in the efficient assessments of vegetation structural parameters and environmental monitoring, e.g. phenology and post-disturbance regeneration, in the near future. With regard to Namibia, UAVs could be used to assess rangeland conditions and monitor stands of woody encroachment, especially those that are difficult to access from the ground.

Acknowledgements

The authors would like to express their particular gratitude to the families of Gressmann, Van der Merwe, and Vermaag for their hospitality, local knowledge, and support during the fieldwork. The same goes for the Kanovlei State Forest staff (Ministry of Agriculture, Water and Forestry) – in particular to Wilson Muyenga. The team of the National Botanical Research Institute, Dr Johan Le Roux, Dr David Joubert, and Dr Lameck Mwewa deserve our sincere thanks for their logistic and academic support during several research trips to Namibia. We also thank Hanna Joß for her help with the preprocessing of the UAV imagery, and Daniela Kretz for her critical remarks on the correct use of the English language.

Disclosure statement

No potential conflict of interest was reported by the authors.

Funding

Manuel J. Mayr and Elisabeth Ofner received travel funding from the German Academic Exchange Service (DAAD) as well as the University of Bayreuth's Graduate School.

Geolocation information

19.35°S, 19.00°E

ORCID

Cyrus Samimi http://orcid.org/0000-0001-7001-7893

References

Agisoft, L. L. C. 2016. "Agisoft PhotoScan User Manual: Professional Edition, Version 1.2." *Tutorial*. Accessed 25 August 2016. http://www.agisoft.com/pdf/photoscan-pro_1_2_en.pdf.

Anderson, K., and K. J. Gaston. 2013. "Lightweight Unmanned Aerial Vehicles Will Revolutionize Spatial Ecology." *Frontiers in Ecology and the Environment* 11 (3): 138–146. doi:10.1890/120150.

Archibald, S., R. J. Scholes, D. P. Roy, G. Roberts, and L. Boschetti. 2010. "Southern African Fire Regimes as Revealed by Remote Sensing." *International Journal of Wildland Fire* 19 (7): 861. doi:10.1071/WF10008.

Archibald, S., and W. J. Bond. 2003. "Growing Tall Vs Growing Wide: Tree Architecture and Allometry of Acacia Karroo in Forest, Savanna, and Arid Environments." *Oikos* 102 (1): 3–14. doi:10.1034/j.1600-0706.2003.12181.x.

Beatty, R. 2011. "Annexes – CBFiM Case Studies: Annex 1: CBFiM in Namibia: The Caprivi Integrated Fire Management Programme." In *Community-Based Fire Management: A Review*, 41–47. FAO forestry paper 166. Rome: FAO (Food and Agriculture Organization of the United Nations). Accessed 5 November 2016. http://www.fao.org/docrep/015/i2495e/i2495e10.pdf.

Bond, W. J. 2008. "What Limits Trees in C4 Grasslands and Savannas?" *Annual Review of Ecology, Evolution, and Systematics* 39 (1): 641–659. doi:10.1146/annurev.ecolsys.39.110707.173411.

Bond, W. J., and G. F. Midgley. 2012. "Carbon Dioxide and the Uneasy Interactions of Trees and Savannah Grasses." *Philosophical Transactions of the Royal Society B: Biological Sciences* 367 (1588): 601–612. doi:10.1098/rstb.2011.0182.

Bond, W. J., and J. E. Keeley. 2005. "Fire as a Global 'Herbivore': The Ecology and Evolution of Flammable Ecosystems." *Trends in Ecology & Evolution* 20 (7): 387–394. doi:10.1016/j.tree.2005.04.025.

Breckenridge, R. P., M. Dakins, S. Bunting, J. L. Harbour, and R. D. Lee. 2012. "Using Unmanned Helicopters to Assess Vegetation Cover in Sagebrush Steppe Ecosystems." *Rangeland Ecology & Management* 65 (4): 362–370. doi:10.2111/REM-D-10-00031.1.

Brown, D. C. 1966. "Decentering Distortion of Lenses." *Photogrammetric Engineering* 32 (3): 444–462.

Candiago, S., F. Remondino, M. de Giglio, M. Dubbini, and M. Gattelli. 2015. "Evaluating Multispectral Images and Vegetation Indices for Precision Farming Applications from UAV Images." *Remote Sensing* 7 (4): 4026–4047. doi:10.3390/rs70404026.

Chen, Q., D. Baldocchi, P. Gong, and M. Kelly. 2006. "Isolating Individual Trees in a Savanna Woodland Using Small Footprint Lidar Data." *Photogrammetric Engineering & Remote Sensing* 72 (8): 923–932. doi:10.14358/PERS.72.8.923.

Chiang, K.-W., M.-L. Tsai, and C.-H. Chu. 2012. "The Development of an UAV Borne Direct Georeferenced Photogrammetric Platform for Ground Control Point Free Applications." *Sensors* 12 (7): 9161–9180. doi:10.3390/s120709161.

Colomina, I., and P. Molina. 2014. "Unmanned Aerial Systems for Photogrammetry and Remote Sensing: A Review." *ISPRS Journal of Photogrammetry and Remote Sensing* 92: 79–97. doi:10.1016/j.isprsjprs.2014.02.013.

Colorado, J., I. Mondragon, J. Rodriguez, and C. Castiblanco. 2015. "Geo-Mapping and Visual Stitching to Support Landmine Detection Using a Low-Cost UAV." *International Journal of Advanced Robotic Systems* 12 (9): 1–12. doi:10.5772/61236.

Conrad, O., B. Bechtel, M. Bock, H. Dietrich, E. Fischer, L. Gerlitz, J. Wehberg, V. Wichmann, and J. Böhner. 2015. "System for Automated Geoscientific Analyses (SAGA) V. 2.1.4." *Geoscientific Model Development* 8 (7): 1991–2007. doi:10.5194/gmd-8-1991-2015.

Dandois, J. P., and E. C. Ellis. 2010. "Remote Sensing of Vegetation Structure Using Computer Vision." *Remote Sensing* 2 (4): 1157–1176. doi:10.3390/rs2041157.

Dandois, J. P., and E. C. Ellis. 2013. "High Spatial Resolution Three-Dimensional Mapping of Vegetation Spectral Dynamics Using Computer Vision." *Remote Sensing of Environment* 136: 259–276. doi:10.1016/j.rse.2013.04.005.

Dandois, J. P., M. Olano, and E. C. Ellis. 2015. "Optimal Altitude, Overlap, and Weather Conditions for Computer Vision UAV Estimates of Forest Structure." *Remote Sensing* 7 (10): 13895–13920. doi:10.3390/rs71013895.

de Klerk, J. N. 2004. "Bush Encroachment in Namibia." Report on Phase 1 of the Bush Encroachment Research, Monitoring and Management Project. Windhoek: Ministry of Environment and Tourism.

Díaz-Varela, R. A., R. D. de la Rosa, L. León, and P. J. Zarco-Tejada. 2015. "High-Resolution Airborne UAV Imagery to Assess Olive Tree Crown Parameters Using 3D Photo Reconstruction: Application in Breeding Trials." *Remote Sensing* 7 (4): 4213–4232. doi:10.3390/rs70404213.

Fritz, A., T. Kattenborn, and B. Koch. 2013. "Uav-Based Photogrammetric Point Clouds – Tree Stem Mapping in Open Stands in Comparison to Terrestrial Laser Scanner Point Clouds." *ISPRS - International Archives of the Photogrammetry, Remote Sensing and Spatial Information Sciences* XL-1/W2: 141–146. doi:10.5194/isprsarchives-XL-1-W2-141-2013.

Farr, T. G., P. A. Rosen, E. Caro, R. Crippen, R. Duren, S. Hensley, M. Cobrick, et al. 2007. "The Shuttle Radar Topography Mission." *Reviews of Geophysics* 45(2): RG2004. doi:10.1029/2005RG000183.

Gatziolis, D., J. F. Lienard, A. Vogs, and N. S. Strigul. 2015. "3D Tree Dimensionality Assessment Using Photogrammetry and Small Unmanned Aerial Vehicles." *PloS One* 10 (9): e0137765. doi:10.1371/journal.pone.0137765.

Giess, W. 1971. "A Preliminary Vegetation Map of South West Africa." *Dinteria* 4: 5–114.

Graz, F. P. 2006. "Spatial Diversity of Dry Savanna Woodlands: Assessing the Spatial Diversity of a Dry Savanna Woodland Stand in Northern Namibia Using Neighbourhood-Based Measures." *Biodiversity & Conservation* 15: 1143–1157. doi:10.1007/s10531-004-3105-6.

Harwin, S., and A. Lucieer. 2012. "Assessing the Accuracy of Georeferenced Point Clouds Produced via Multi-View Stereopsis from Unmanned Aerial Vehicle (UAV) Imagery." *Remote Sensing* 4 (12): 1573–1599. doi:10.3390/rs4061573.

Heinzel, J., and B. Koch. 2012. "Investigating Multiple Data Sources for Tree Species Classification in Temperate Forest and Use for Single Tree Delineation." *International Journal of Applied Earth Observation and Geoinformation* 18: 101–110. doi:10.1016/j.jag.2012.01.025.

Hengl, T., J. M. D. Jesus, R. A. MacMillan, N. H. Batjes, G. B. M. Heuvelink, E. Ribeiro, A. Samuel-Rosa, et al. 2014. "SoilGrids1km-Global Soil Information Based on Automated Mapping." *PloS One* 9 (8): e105992. doi:10.1371/journal.pone.0105992.

Higgins, S. I., W. J. Bond, E. C. February, A. Bronn, D. I. W. Euston-Brown, B. Enslin, N. Govender, et al. 2007. "Effects of Four Decades of Fire Manipulation on Woody Vegetation Structure in Savanna." *Ecology* 88 (5): 1119–1125. doi:10.1890/06-1664.

Hirschmüller, H., and D. Scharstein. 2009. "Evaluation of Stereo Matching Costs on Images with Radiometric Differences." *IEEE Transactions on Pattern Analysis and Machine Intelligence* 31 (9): 1582–1599. doi:10.1109/TPAMI.2008.221.

Holdo, R. M. 2006. "Tree Growth in an African Woodland Savanna Affected by Disturbance." *Journal of Vegetation Science* 17 (3): 369–378. doi:10.1111/j.1654-1103.2006.tb02457.x.

Holdo, R. M. 2007. "Elephants, Fire and Frost Can Determine Community Structure and Composition in Kalahari Woodlands." *Ecological Applications* 17 (2): 558–568. doi:10.1890/05-1990.

Honkavaara, E., T. Hakala, L. Markelin, T. Rosnell, H. Saari, and J. Mäkynen. 2012. "A Process for Radiometric Correction of UAV Image Blocks." *Photogrammetrie - Fernerkundung - Geoinformation* 2012 (2): 115–127. doi:10.1127/1432-8364/2012/0106.

Hung, C., Z. Xu, and S. Sukkarieh. 2014. "Feature Learning Based Approach for Weed Classification Using High Resolution Aerial Images from a Digital Camera Mounted on a UAV." *Remote Sensing* 6 (12): 12037–12054. doi:10.3390/rs61212037.

Hunter, M. O., M. Keller, D. Victoria, and D. C. Morton. 2013. "Tree Height and Tropical Forest Biomass Estimation." *Biogeosciences* 10 (12): 8385–8399. doi:10.5194/bg-10-8385-2013.

Jaud, M., S. Passot, R. Le Bivic, C. Delacourt, P. Grandjean, and N. Le Dantec. 2016. "Assessing the Accuracy of High Resolution Digital Surface Models Computed by PhotoScan® and MicMac® in Sub-Optimal Survey Conditions." *Remote Sensing* 8 (6): 465. doi:10.3390/rs8060465.

Jeltsch, F., S. J. Milton, W. R. J. Dean, N. Rooyen, and K. A. Moloney. 1998. "Modelling the Impact of Small-Scale Heterogeneities on Tree-Grass Coexistence in Semi-Arid Savannas." *Journal of Ecology* 86 (5): 780–793. doi:10.1046/j.1365-2745.1998.8650780.x.

Jensen, J. L. R., and A. J. Mathews. 2016. "Assessment of Image-Based Point Cloud Products to Generate a Bare Earth Surface and Estimate Canopy Heights in a Woodland Ecosystem." *Remote Sensing* 8 (1): 50. doi:10.3390/rs8010050.

Joubert, D. F., G. N. Smit, and M. T. Hoffman. 2012. "The Role of Fire in Preventing Transitions from a Grass Dominated State to a Bush Thickened State in Arid Savannas." *Journal of Arid Environments* 87: 1–7. doi:10.1016/j.jaridenv.2012.06.012.

Ke, Y., and L. J. Quackenbush. 2011. "A Review of Methods for Automatic Individual Tree-Crown Detection and Delineation from Passive Remote Sensing." *International Journal of Remote Sensing* 32 (17): 4725–4747. doi:10.1080/01431161.2010.494184.

Kennedy, A. D., and A. L. F. Potgieter. 2003. "Fire Season Affects Size and Architecture of *Colophospermum Mopane* in Southern African Savannas." *Plant Ecology* 167 (2): 179–192. doi:10.1023/A:1023964815201.

Khalefa, E., I. P. J. Smit, A. Nickless, S. Archibald, A. Comber, and H. Balzter. 2013. "Retrieval of Savanna Vegetation Canopy Height from ICESat-GLAS Spaceborne LiDAR with Terrain Correction." *IEEE Geoscience and Remote Sensing Letters* 10 (6): 1439–1443. doi:10.1109/LGRS.2013.2259793.

Larjavaara, M., H. C. Muller-Landau, and J. Metcalf. 2013. "Measuring Tree Height: A Quantitative Comparison of Two Common Field Methods in a Moist Tropical Forest." *Methods in Ecology and Evolution* 4 (9): 793–801. doi:10.1111/2041-210X.12071.

Le Roux, J. 2011. "The effect of land use practices on the spatial and temporal characteristics of savanna fires in Namibia." PhD diss., Friedrich-Alexander-University. Accessed 9 November 2016. www.the-eis.com/data/literature/Johan_le_Roux_Dissertation.pdf.

Levick, S. R., C. A. Baldeck, and G. P. Asner. 2015. "Demographic Legacies of Fire History in an African Savanna." *Functional Ecology* 29 (1): 131–139. doi:10.1111/1365-2435.12306.

Lingua, A., D. Marenchino, and F. Nex. 2009. "Performance Analysis of the SIFT Operator for Automatic Feature Extraction and Matching in Photogrammetric Applications." *Sensors* 9 (5): 3745–3766. doi:10.3390/s90503745.

Lisein, J., M. Pierrot-Deseilligny, S. Bonnet, and P. Lejeune. 2013. "A Photogrammetric Workflow for the Creation of a Forest Canopy Height Model from Small Unmanned Aerial System Imagery." *Forests* 4 (4): 922–944. doi:10.3390/f4040922.

Lowe, D. G. 2004. "Distinctive Image Features from Scale-Invariant Keypoints." *International Journal of Computer Vision* 60 (2): 91–110. doi:10.1023/B:VISI.0000029664.99615.94.

Mathews, A. J., and J. L. R. Jensen. 2013. "Visualizing and Quantifying Vineyard Canopy LAI Using an Unmanned Aerial Vehicle (UAV) Collected High Density Structure from Motion Point Cloud." *Remote Sensing* 5 (5): 2164–2183. doi:10.3390/rs5052164.

MAWF (Ministry of Agriculture, Water and Forestry). 2012. "National Rangeland Management: Policy (Part I) & Strategy (Part II)." *Restoring Namibia's Rangelands*. Accessed 4 November 2016. www.agrinamibia.com.na/index.php?module=Downloads&func=prep_hand_out&lid=255.

Mayr, M. J., and C. Samimi. 2015. "Comparing the Dry Season In-Situ Leaf Area Index (LAI) Derived from High-Resolution RapidEye Imagery with MODIS LAI in a Namibian Savanna." *Remote Sensing* 7 (4): 4834–4857. doi:10.3390/rs70404834.

Mendelsohn, J. M., A. Jarvis, C. Roberts, and T. Robertson. 2002. *Atlas of Namibia - A Portrait of the Land and Its People*. Cape Town: David Philip Publishers.

Midgley, J. J., M. J. Lawes, and S. Chamaillé-Jammes. 2010. "Savanna Woody Plant Dynamics: The Role of Fire and Herbivory, Separately and Synergistically." *Australian Journal of Botany* 58 (1): 1–11. doi:10.1071/BT09034.

Moleele, N. M., S. Ringrose, W. Matheson, and C. Vanderpost. 2002. "More Woody Plants? the Status of Bush Encroachment in Botswana's Grazing Areas." *Journal of Environmental Management* 64 (1): 3–11. doi:10.1006/jema.2001.0486.

Mukherjee, D., J. Q. M. Wu, and G. Wang. 2015. "A Comparative Experimental Study of Image Feature Detectors and Descriptors." *Machine Vision and Applications* 26 (4): 443–466. doi:10.1007/s00138-015-0679-9.

Mulero-Pázmány, M., J. Á. Barasona, P. Acevedo, J. Vicente, and J. J. Negro. 2015. "Unmanned Aircraft Systems Complement Biologging in Spatial Ecology Studies." *Ecology and Evolution* 5 (21): 4808–4818. doi:10.1002/ece3.1744.

Namibia Meteorological Service (NMS). 2015. "Precipitation stations dataset (1990-2015) of the Otjozondjupa and Kavango regions." Unpublished dataset.

Näsi, R., E. Honkavaara, P. Lyytikäinen-Saarenmaa, M. Blomqvist, P. Litkey, T. Hakala, N. Viljanen, T. Kantola, T. Tanhuanpää, and M. Holopainen. 2015. "Using UAV-Based Photogrammetry and Hyperspectral Imaging for Mapping Bark Beetle Damage at Tree-Level." *Remote Sensing* 7 (12): 15467–15493. doi:10.3390/rs71115467.

Neitzel, F., and J. Klonowski. 2011. "Mobile 3D Mapping with a Low-Cost UAV System." *International Archives of the Photogrammetry, Remote Sensing and Spatial Information Sciences* XXXVIII-1/C22: 39–44. doi:10.5194/isprsarchives-XXXVIII-1-C22-39-2011.

Nex, F., and F. Remondino. 2014. "UAV for 3D Mapping Applications: A Review." *Applied Geomatics* 6 (1): 1–15. doi:10.1007/s12518-013-0120-x.

Ota, T., M. Ogawa, K. Shimizu, T. Kajisa, N. Mizoue, S. Yoshida, G. Takao, et al. 2015. "Aboveground Biomass Estimation Using Structure from Motion Approach with Aerial Photographs in a Seasonal Tropical Forest." *Forests* 6 (11): 3882–3898. doi:10.3390/f6113882.

Poorter, L., W. Hawthorne, F. Bongers, and D. Sheil. 2008. "Maximum Size Distributions in Tropical Forest Communities: Relationships with Rainfall and Disturbance." *Journal of Ecology* 96: 495–504. doi:10.1111/j.1365-2745.2008.01366.x.

Potere, D. 2008. "Horizontal Positional Accuracy of Google Earth's High-Resolution Imagery Archive." *Sensors* 8 (12): 7973–7981. doi:10.3390/s8127973.

Pyysalo, U., and H. Hyyppä. 2002. "Reconstructing Tree Crowns from Laser Scanner Data for Feature Extraction." *International Archives of the Photogrammetry, Remote Sensing and Spatial Information Sciences* 34 (3B): 218–221.

R Core Team. 2014. *R: A Language and Environment for Statistical Computing*. Vienna, Austria: R Foundation for Statistical Computing. www.R-project.org.

Reitberger, J., C. Schnörr, P. Krzystek, and U. Stilla. 2009. "3D Segmentation of Single Trees Exploiting Full Waveform LIDAR Data." *ISPRS Journal of Photogrammetry and Remote Sensing* 64 (6): 561–574. doi:10.1016/j.isprsjprs.2009.04.002.

Rogers, K., and A. Finn. 2013. "Three-Dimensional UAV-Based Atmospheric Tomography." *Journal of Atmospheric and Oceanic Technology* 30 (2): 336–344. doi:10.1175/JTECH-D-12-00036.1.

Roosevelt, C. H. 2014. "Mapping Site-Level Microtopography with Real- Time Kinematic Global Navigation Satellite Systems (RTK GNSS) and Unmanned Aerial Vehicle Photogrammetry (UAVP)." *Open Archaeology* 1: 1. doi:10.2478/opar-2014-0003.

Roques, K. G., T. G. O'Connor, and A. R. Watkinson. 2001. "Dynamics of Shrub Encroachment in an African Savanna: Relative Influences of Fire, Herbivory, Rainfall and Density Dependence." *Journal of Applied Ecology* 38 (2): 268–280. doi:10.1046/j.1365-2664.2001.00567.x.

Roy, D. P., M. A. Wulder, T. R. Loveland, C. E. Woodcock, R. G. Allen, M. C. Anderson, D. Helder, et al. 2014. "Landsat-8: Science and Product Vision for Terrestrial Global Change Research." *Remote Sensing of Environment* 145: 154–172. doi:10.1016/j.rse.2014.02.001.

Salamí, E., C. Barrado, and E. Pastor. 2014. "UAV Flight Experiments Applied to the Remote Sensing of Vegetated Areas." *Remote Sensing* 6 (11): 11051–11081. doi:10.3390/rs61111051.

Sankaran, M., N. P. Hanan, R. J. Scholes, J. Ratnam, D. J. Augustine, B. S. Cade, J. Gignoux, et al. 2005. "Determinants of Woody Cover in African Savannas." *Nature* 438 (7069): 846–849. doi:10.1038/nature04070.

Scholes, R. J., and S. R. Archer. 1997. "Tree-Grass Interactions in Savannas." *Annual Review of Ecology and Systematics* 28: 517–544. doi:10.1146/annurev.ecolsys.28.1.517.

Skarpe, C. 1991. "Spatial Patterns and Dynamics of Woody Vegetation in an Arid Savanna." *Journal of Vegetation Science* 2 (4): 565–572. doi:10.2307/3236039.

Snavely, N., S. M. Seitz, and R. Szeliski. 2008. "Modeling the World from Internet Photo Collections." *International Journal of Computer Vision* 80 (2): 189–210. doi:10.1007/s11263-007-0107-3.

Stevens, N., B. F. N. Erasmus, S. Archibald, and W. J. Bond. 2016. "Woody Encroachment over 70 Years in South African Savannahs: Overgrazing, Global Change or Extinction Aftershock?" *Philosophical Transactions of the Royal Society B: Biological Sciences* 371: 1703. doi:10.1098/rstb.2015.0437.

Strohbach, B. J. 2014. "Vegetation of the Eastern Communal Conservancies in Namibia: I. Phytosociological Descriptions." *Koedoe* 56 (1): 18. doi:10.4102/koedoe.v56i1.1116.

Torres-Sánchez, J., F. López-Granados, A. I. D. Castro, and J. M. Peña-Barragán. 2013. "Configuration and Specifications of an Unmanned Aerial Vehicle (UAV) for Early Site Specific Weed Management." *PloS One* 8 (3): e58210. doi:10.1371/journal.pone.0058210.

Torres-Sánchez, J., F. López-Granados, N. Serrano, O. Arquero, and J. M. Peña. 2015. "High-Throughput 3-D Monitoring of Agricultural-Tree Plantations with Unmanned Aerial Vehicle (UAV) Technology." *PloS One* 10 (6): e0130479. doi:10.1371/journal.pone.0130479.

Turner, D., A. Lucieer, and C. Watson. 2012. "An Automated Technique for Generating Georectified Mosaics from Ultra-High Resolution Unmanned Aerial Vehicle (UAV) Imagery, Based on Structure from Motion (Sfm) Point Clouds." *Remote Sensing* 4 (12): 1392–1410. doi:10.3390/rs4051392.

Twidwell, D., C. R. Allen, C. Detweiler, J. Higgins, C. Laney, and S. Elbaum. 2016. "Smokey Comes of Age: Unmanned Aerial Systems for Fire Management." *Frontiers in Ecology and the Environment* 14 (6): 333–339. doi:10.1002/fee.1299.

u-blox AG. 2015. "LEA-6: U-Blox 6 GPS Modules." *Data Sheet*. Accessed 10 October 2016. https://www.u-blox.com/sites/default/files/products/documents/LEA-6_DataSheet_%28UBX-14044797%29.pdf.

Verhoeven, G. 2011. "Taking Computer Vision Aloft - Archaeological Three-Dimensional Reconstructions from Aerial Photographs with Photoscan." *Archaeological Prospection* 18 (1): 67–73. doi:10.1002/arp.399.

Wagenseil, H., and C. Samimi. 2007. "Woody Vegetation Cover in Namibian Savannahs: A Modelling Approach Based on Remote Sensing." *Erdkunde* 61 (4): 325–334. doi:10.3112/erdkunde.2007.04.03.

Wallace, L., A. Lucieer, and C. S. Watson. 2014. "Evaluating Tree Detection and Segmentation Routines on Very High Resolution UAV LiDAR Data." *IEEE Transactions on Geoscience and Remote Sensing* 52 (12): 7619–7628. doi:10.1109/TGRS.2014.2315649.

Wang, L., P. D'Odorico, S. Ringrose, S. Coetzee, and S. A. Macko. 2007. "Biogeochemistry of Kalahari Sands." *Journal of Arid Environments* 71 (3): 259–279. doi:10.1016/j.jaridenv.2007.03.016.

Wessels, K. J., R. Mathieu, B. F. N. Erasmus, G. P. Asner, I. P. J. Smit, J. A. N. Van Aardt, R. Main, et al. 2011. "Impact of Communal Land Use and Conservation on Woody Vegetation Structure in the Lowveld Savannas of South Africa." *Forest Ecology and Management* 261 (1): 19–29. doi:10.1016/j.foreco.2010.09.012.

Westoby, M. J., J. Brasington, N. F. Glasser, M. J. Hambrey, and J. M. Reynolds. 2012. "'Structure-From-Motion' Photogrammetry: A Low-Cost, Effective Tool for Geoscience Applications." *Geomorphology* 179: 300–314. doi:10.1016/j.geomorph.2012.08.021.

Whitecross, M. A., E. T. F. Witkowski, and S. Archibald. 2016. "Assessing the Frequency and Drivers of Early-Greening in Broad-Leaved Woodlands along a Latitudinal Gradient in Southern Africa." *Austral Ecology*. doi:10.1111/aec.12448.

Wigley, B. J., W. J. Bond, and M. T. Hoffman. 2010. "Thicket Expansion in a South African Savanna under Divergent Land Use: Local vs. Global Drivers?" *Global Change Biology* 16: 964–976. doi:10.1111/gcb.2010.16.issue-3.

Xu, Y., J. Ou, H. He, X. Zhang, and J. Mills. 2016. "Mosaicking of Unmanned Aerial Vehicle Imagery in the Absence of Camera Poses." *Remote Sensing* 8 (3): 204. doi:10.3390/rs8030204.

Zarco-Tejada, P. J., R. Diaz-Varela, V. Angileri, and P. Loudjani. 2014. "Tree Height Quantification Using Very High Resolution Imagery Acquired from an Unmanned Aerial Vehicle (UAV) and Automatic 3D Photo-Reconstruction Methods." *European Journal of Agronomy* 55: 89–99. doi:10.1016/j.eja.2014.01.004.

PART III
SYNTHESIS AND OUTLOOK

7. SYNTHESIS

This thesis aimed at modelling fire activity and vegetation using remote sensing data. Thereby, a number of datasets, from global satellite products to ultra-high-resolution imagery from an Unmanned Aerial Vehicle (UAV), were applied. Common and newer methods of remote sensing, such as time series analysis, the application of Spectral Vegetation Indices (SVI), aggregation techniques, and UAV photogrammetry, as well as common predictive modelling techniques were used in order to investigate the following three main hypotheses:

1. **Namibia's fire activity generally follows a productivity gradient. Human activities have the potential to alter this relationship on smaller spatial scales.**

2. **Regionally-calibrated, spectral estimates of green vegetation during the dry season deviate from those obtained with a global satellite product. Due to a coarser base resolution, the latter yields higher generalization and lower estimates of green vegetation.**

3. **The long-term fire regime is reflected by the vertical stand structure. Thus, the presence of fire leads to stand-scale height reductions of woody vegetation, which can be assessed using optical UAV data.**

While the research activities focused on Namibia, some of the findings conducted here may be of relevance to comparable regions, as well as semi-arid ecosystems in general. The following chapter details concluding remarks that can be drawn from the approach applied and the findings presented.

Fire forms distinct spatio-temporal patterns in Namibia with large areas being burned in the central north of Namibia (southern parts of the regions Omusati, Oshana, and Oshikoto), as well as in the North-East (eastern Otjozondjupa, Kavango, and Zambezi Regions). Both fire regime parameters under consideration, i.e. Burned Area (BA) and Fire Occurrence (FO), were spatially autocorrelated. The extensive assessment of Namibia's fire regimes and its indirect controls from multiple spatial predictive models is a considerable achievement of this thesis. As such, the consideration of spatial structures in model evaluation and an inter-comparison of different models enhance the robustness of statements derived therefrom. Seven out of ten models ranked Mean Annual Precipitation (MAP) as the most important control of fire activity in Namibia. Above 400 mm MAP, both BA and FO generally increased. This confirms that productivity is the major control of fire in dry savannas and that fire activity in these ecosystems is essentially limited by fuels.

Productivity was assumed stationary across time, which obscures its inter-annual fluctuations and the resultant variability in fire activity. Apart from MAP, human activities, as measured by the densities of people and livestock, were of higher importance in many models applied here. While it was expected that human activities limit BA, a similar relationship with the number of fires (FO) was found by the best-performing Random Forest (RF) models. The reduction of FO with increasing human activities is somehow contradictory as humans are known to be the main source of ignitions in the region. However this reduction may reflect the fuel consumption and the landscape fragmentation that accompany human activities. As fuels are generally scarce at the arid fringe of

fire-prone ecosystems, human activities and land use seem to be of a critical level for fire across Namibia – even at low population densities there. Contrasting patterns of fire activity were found in the adjacent Otjozondjupa and southern Kavango Regions, where the veterinary fence separates commercial, privately-held farmlands from communal farmlands. These contrasts essentially reflect people's attitude towards fire in the sense that they actively use fire as a tool or aim at its suppression and exclusion. It is surprising that land tenure was not among the most important predictors and contradicts earlier findings from Namibia (see Le Roux (2011)). The reasons thereof could be the known minor treatment of categorical predictors in some of the models applied and the scale of observation used here. It likely that the role of humans on the fire patterns as perceived by the MODIS Burned Area product (MCD45A1) is underestimated. For land management purposes, people aim at controlled burnings, which are often low in spatial extent and intensity. The coarse scale of observation by MCD45A1, i.e. a spatial resolution of 500 m, prevents the reliable detection of such fires. Taking these uncertainties into account, the approach and the findings presented at the national scale provide a framework for future research on (semi-)arid fire regimes and could support policy decisions in Namibia, but would require further investigations on smaller scales.

The spatial scale of observation is a determining factor inherent to any remote sensing application. As was shown with the regional assessment of the Leaf Area Index (LAI) in the study area located in Owamboland, North-Central Namibia, the two models under comparison differ markedly. The empirically-derived model of LAI at 1 km-resolution which was based on the upscaling of field measurements revealed a considerably higher spatial heterogeneity as compared to the estimates from MODIS LAI (MOD15A2). In addition, offsets in absolute terms were present between the two models of LAI. An accurate treatment of non-photosynthetic canopy components in the field measurements and spectral data remain unresolved at this stage. The same is true for background contaminations, which affect both models and are highest during the dry season. A quantification of deteriorating contributions and their spectral response would necessitate a systematic consideration of different background surfaces and canopy covers, but such was beyond the scope of this thesis. Nevertheless, it was hypothesized that the contaminating effects increase as the base resolution of the observation decreases. The finding that the MOD15A2 product, which relies on moderate-resolution MODIS imagery, yields mostly lower values, can be regarded as an indication thereof. However, the issue needs further examination. For instance, the direction of offset between the two models inverted with a recently burned area. This patch was successfully detected as burned by MCD45A1, but MOD15A2 outlined no change in LAI relative to the surrounding unburned areas. The finding is counterintuitive, as both, MCD45A1 and MOD15A2, rely on spectral data of similar resolution, but essentially reflects the different foci of the retrieval algorithms underlying these datasets. Furthermore, the temporal scope of the land cover mask behind MOD15A2, which uses an annual aggregation of the preceding year, appeared to be unsuitable for this particular environment, but is updated in the follow-up release (version 6) of MOD15A2. Although the general patterns of LAI in the study area were captured by MOD15A2, the above findings highlight the need for a critical examination of global remote sensing products. Their evaluation and validation for steady improvement and refining of the underlying algorithms is vital. An increased consideration of dry-season settings in remote sensing studies is desirable, as such essentially helps to enhance our integrated understanding of the ecological processes that take place throughout the year.

The derivation of vertical stand structure by means of UAV data as applied in this thesis was experimental. It was demonstrated that UAVs have the potential to serve as autonomous remote sensing systems and that newer photogrammetric techniques such as SfM-MVS provide maturing means for the modelling of 3D structures. As stand heights are a primary parameter for forest inventories and biomass assessments, UAV data are a useful complement to field surveys. A

considerable advantage of the usage of imaging sensors over LiDAR sensors is the potentially higher density of the Image-Based Point Cloud (IBPC) with top-of-the-canopy elements. It is important to note that the density of the IBPC, and thus the quality of the 3D reconstruction, is the product of the features recognized in the input imagery. Canopies are complex surfaces and their elements are constantly in motion, which complicates their 3D reconstruction. Dry-season phenology reduces the effects of motion, but likewise decreases the abundance of canopy elements of deciduous broad-leaved species. Higher overlaps between the images, i.e. more images per object and lower angular variations, could have partly resolved the height underestimations apparent with sparse branch structures. Nevertheless, the stands' height structures were roughly captured with the UAV approach presented. The absolute number of woody individuals is certainly underestimated as smaller and clumped individuals have a considerable chance to be missed or at least to not to be correctly delineated as canopy vegetation. As a consequence, a feature-based remote sensing of vegetation as facilitated with UAV data prevents some of the uncertainties associated with lower canopy covers and dry-season phenology in traditional pixel-based approaches. The accuracy of the average stand height parameters (mean and median) derived from the IBPC and canopy segmentation was <1 m as compared to field measurements, where higher accuracies can be achieved from the inclusion of survey-grade reference and positional data. The latter would enable multi-temporal assessments of vegetation with growth rates, phenological development, or post-fire regeneration depicting potential targets of investigation.

From the single-date UAV surveys conducted here, there is little evidence that fire will significantly affect the stand structure of woody communities on the long-term. While ecological complexity was obviously neglected, this approach assumed mono-causal stand height reductions due to the long-term presence of fire. This relationship was not supported by the dataset, which suggests two possible causes: firstly, fires are either too infrequent or too low in intensity to seriously affect woody vegetation, and/or secondly, the species community is just well adapted and, thus, largely resilient to the prevailing fire regime. From personal observations in the field, both explanations are feasible. Recently burned plots showed distinct heterogeneity in burning, ranging from only patchy burning that was largely restricted to the herbaceous understorey, to fire scars reaching >5 m and fallen adult trunks as a result of fire. The dominant woody species on certain plots in northern Otjozondjupa, such as *Pterocarpus angolensis*, are known to resist fire due to their thick barks, and resprouting is common with many savannas species. While the assessment focused on heights and generally neglected individuals <1.5 m for methodological reasons, woody densities and cover are additional parameters to consider with assessments of the long-term impact of fire. Their consideration would be valuable to support the finding that stand heights are significantly reduced under regular grazing conditions. This finding was interpreted to be indicative of bush encroachment, but, as height maxima were also reduced within grazed stands, it could point to soil-imposed limitations in productivity as well. It cannot be excluded that the height reductions ultimately result from mechanical rangeland clearings in the past, which illustrates the general uncertainties associated with disturbance histories over a range of several decades.

8. OUTLOOK

A number of unresolved questions arise from the research objectives elaborated and the knowledge generated, and from the shortcomings of the applied approach within this thesis. A personal, yet incomplete, appraisal of remaining questions to be addressed in the future, and ways forward are found in the following chapter.

- *What is needed to improve the quantification of the human role in fire regimes?*

From a remote sensing perspective, fire estimates that also detect small fires from land management purposes are critical for the understanding of human-induced fire regimes. The synergistic use of burned area and active fire approaches, as is done with the release of the newest version of MODIS BA in 2017, is a step in this direction. However, early evaluations suggest only minimal improvements with the smaller fraction of fires (e.g. Zhu et al., 2017). Higher-resolution Landsat data would facilitate a long-term record, but automated (regional) BA detection approaches from Landsat time series are just emerging (e.g. Hawbaker et al., 2017). Moreover, analyses that focus on regions with contrasting fire patterns but quasi-homogenous environmental conditions, such as those outlined for the northern Otjozondjupa and Kavango Regions, could provide valuable insights and generate new hypotheses on the human determination of fire regimes. Interdisciplinary approaches that involve social sciences could be particularly useful in this regard.

- *Are remote sensing and geospatial analysis suitable techniques in order to seasonally forecast fire?*

The study conducted here outlined the patterns of fire in Namibia and inferred the general drivers thereof. This knowledge could serve as a framework for seasonal predictions of fire occurrence. As fuels are a primary factor in Namibia, the preceding seasonal precipitation sums, which can be spatially inferred from remote sensing, are anticipated as a first indicator of the general strength of the upcoming fire season. Fuel availability and condition can, to some degree, be mapped from remote sensing (see below) in order to determine fire hazard. Field measurements of fine fuel biomass and the temporal relation of fuel moisture with microclimatic conditions are considered as useful inputs for the calibration of remotely-sensed fuel estimates. These parameters are available from the field data collection period, however have not yet been analysed. Fuel estimates are essential for the determination of ignition probabilities and the potential damages to human livelihoods and natural resources – together known as fire risk (see Hardy, 2005). In a recent review, Costafreda-Aumedes et al. (2017) conclude that our current capabilities to predict fires in space and time from remote sensing and geospatial analysis remain generally limited. This is attributed to the lack of universal relationships underlying ignitions and the stochastic nature of fire occurrence in general. As has been shown here, also the availability and quality of the predictors that are available to causally infer fire limits our predictive capabilities – especially in developing countries.

- *Which possibilities are available through remote sensing in order to "go beyond green vegetation"?*

As was shown here, feature-based approaches could be essentially useful for the assessment of woody vegetation in a dry-season environment. Admittedly, satellite sensors that provide the required spatial resolutions at no cost are scarce at the moment. Likewise, UAVs are limited in spatial coverage, but are potentially suitable for repeated measurements at the local scale. A recent

study used space-borne, passive microwave observations in order to infer non-photosynthetic woody vegetation (Tian et al., 2017). Also, active sensors, such as SAR, are continuously evolving, and their capabilities for analysing and monitoring vegetation are not yet fully explored (Li and Guo, 2016). The upcoming ICESat-2 mission, which was launched in late 2018, will provide global LiDAR estimates in the near future.

Apart from the woody canopy, the biomass and condition of the surface stratum are important parameters for rangeland assessments and fuel modelling. One major obstacle thereby is canopy obscuration in denser stands, which could, in part, be circumvented by multi-temporal approaches. (Hyper-) spectral approaches that incorporate the SWIR spectrum are promising, as certain SWIR regions are sensitive to plant water content and two dominant compounds of senescent leaves, namely lignin and cellulose. Nevertheless, the soil background may again be a deteriorating influence for lower surface covers.

- *Are fire impacts moderated at the scale of species?*

The study of fire impacts in this thesis did not consider the community involved. In addition, the prevailing disturbance regime was assumed to be representative of the long-term situation. Fire-sensitive species may have been replaced earlier on the burned stands. However, if similar communities are present under different disturbance regimes, there is a reasonable chance that these possess the ability to adapt some of their characteristics, known as functional traits, accordingly. For instance, species exposed to recurring fire could relatively increase their investment in height growth in smaller individuals or bark thickness in adult individuals. An upcoming thesis by Elisabeth Ofner, which is linked to this thesis, is dedicated to shed light into such intra-specific plasticity and the species composition of the stands that were under investigation here.

- *How will climate change affect future fire regimes?*

Future fire activity is often suggested to increase as climate warms on a global scale (see Flannigan et al., 2009). Where current empirical investigations find a global decrease in fire activity since the 2000s, Southern Africa countered this trend (e.g. Andela et al., 2017). The North-East of Namibia experienced an increase in fire activity during this period (not shown). Although future precipitation changes are less certain than temperature, Southern Africa is expected to dry within the 21st century (Niang et al., 2014). Little is also known on the intra-seasonal alteration of precipitation which essentially determines the “temporal window” of fire occurrence. For Namibia, a future aridification will probably continue to constrain fire to regions of higher productivity, but community shifts towards grass could enhance fire activity there. Finally, as humans largely determine ignitions and control fuels, future fire regimes in Namibia and elsewhere will depend on how humans use land and fire for their specific purposes.

BIBLIOGRAPHY

This section lists the literature cited throughout PART I and PART III of this thesis.

Albrecht, R.I., 2016. LIS 0.1 Degree Very High Resolution Gridded Lightning Climatology Data Collection. Data User Guide. https://ghrc.nsstc.nasa.gov/pub/lis/climatology/LIS/doc/LIS_VHRES_Guide.pdf (accessed 18 February 2018).

Albrecht, R.I., Goodman, S.J., Buechler, D.E., Blakeslee, R.J., Christian, H.J., 2016. LIS 0.1 Degree Very High Resolution Gridded Lightning Monthly Climatology (VHRMC). Dataset available online from the NASA Global Hydrology Center DAAC, Huntsville, Alabama, U.S.A. https://ghrc.nsstc.nasa.gov/hydro/details/lisvhrmc (accessed 6 March 2017). DOI: 10.5067/LIS/LIS/DATA302.

Alleaume, S., Hély, C., Le Roux, J., Korontzi, S., Swap, R.J., Shugart, H.H., Justice, C.O., 2005. Using MODIS to evaluate heterogeneity of biomass burning in southern African savannahs: a case study in Etosha. International Journal of Remote Sensing 26 (19), 4219–4237. DOI: 10.1080/01431160500113492.

Allen, H.D., 2008. Fire. Plant functional types and patch mosaic burning in fire-prone ecosystems. Progress in Physical Geography 32 (4), 421–437. DOI: 10.1177/0309133308096754.

Altmann, A., Tolosi, L., Sander, O., Lengauer, T., 2010. Permutation importance. A corrected feature importance measure. Bioinformatics 26 (10), 1340–1347. DOI: 10.1093/bioinformatics/btq134.

Andela, N., Morton, D.C., Giglio, L., Chen, Y., van der Werf, G.R., Kasibhatla, P.S., DeFries, R.S., Collatz, G.J., Hantson, S., Kloster, S., Bachelet, D., Forrest, M., Lasslop, G., Li, F., Mangeon, S., Melton, J.R., Yue, C., Randerson, J.T., 2017. A human-driven decline in global burned area. Science 356 (6345), 1356–1362. DOI: 10.1126/science.aal4108.

Anderson, R.C., Shanks, P.C., Kritis, L.A., Trani, M.G., 2014. Supporting Remote Sensing Research with Small Unmanned Aerial Systems. ISPRS - International Archives of the Photogrammetry, Remote Sensing and Spatial Information Sciences XL-1, 51–56. DOI: 10.5194/isprsarchives-XL-1-51-2014.

Archibald, S., 2016. Managing the human component of fire regimes. Lessons from Africa. Philosophical Transactions of the Royal Society B: Biological Sciences 371 (1696). DOI: 10.1098/rstb.2015.0346.

Archibald, S., Nickless, A., Govender, N., Scholes, R.J., Lehsten, V., 2010a. Climate and the inter-annual variability of fire in southern Africa: a meta-analysis using long-term field data and satellite-derived burnt area data. Global Ecology and Biogeography 19 (6), 794–809. DOI: 10.1111/j.1466-8238.2010.00568.x.

Archibald, S., Roy, D.P., van Wilgen, B.W., Scholes, R.J., 2009. What limits fire? An examination of drivers of burnt area in Southern Africa. Global Change Biology 15 (3), 613–630. DOI: 10.1111/j.1365-2486.2008.01754.x.

Archibald, S., Scholes, R.J., Roy, D.P., Roberts, G., Boschetti, L., 2010b. Southern African fire regimes as revealed by remote sensing. International Journal of Wildland Fire 19 (7), 861–878. DOI: 10.1071/WF10008.

Asner, G.P., 1998. Biophysical and Biochemical Sources of Variability in Canopy Reflectance. Remote Sensing of Environment 64 (3), 234–253. DOI: 10.1016/S0034-4257(98)00014-5.

Asner, G.P., Heidebrecht, K.B., 2002. Spectral unmixing of vegetation, soil and dry carbon cover in arid regions. Comparing multispectral and hyperspectral observations. International Journal of Remote Sensing 23 (19), 3939–3958. DOI: 10.1080/01431160110115960.

Asner, G.P., Levick, S.R., Kennedy-Bowdoin, T., Knapp, D.E., Emerson, R., Jacobson, J., Colgan, M.S., Martin, R.E., 2009. Large-scale impacts of herbivores on the structural diversity of African savannas. Proceedings of the National Academy of Sciences of the United States of America 106 (12), 4947–4952. DOI: 10.1073/pnas.0810637106.

Atkinson, P.M., Jeganathan, C., Dash, J., Atzberger, C., 2012. Inter-comparison of four models for smoothing satellite sensor time-series data to estimate vegetation phenology. Remote Sensing of Environment 123, 400–417. DOI: 10.1016/j.rse.2012.04.001.

Bannari, A., Morin, D., Bonn, F., Huete, A.R., 1995. A review of vegetation indices. Remote Sensing Reviews 13 (1-2), 95–120. DOI: 10.1080/02757259509532298.

Bar Massada, A., Syphard, A.D., Stewart, S.I., Radeloff, V.C., 2012. Wildfire ignition-distribution modelling. A comparative study in the Huron-Manistee National Forest, Michigan, USA. International Journal of Wildland Fire 22, 174–183. DOI: 10.1071/WF11178.

Baret, F., Guyot, G., 1991. Potentials and limits of vegetation indices for LAI and APAR assessment. Remote Sensing of Environment 35 (2-3), 161–173. DOI: 10.1016/0034-4257(91)90009-U.

Beatty, R., 2011. Annexes – CBFiM case studies. Annex 1: CBFiM in Namibia: the Caprivi Integrated Fire Management programme. In: Food and Agriculture Organization of the United Nations (FAO) (Ed.), Community-based fire management. A review. FAO, Rome, pp. 41–47.

Beck, P.S.A., Atzberger, C., Høgda, K.A., Johansen, B., Skidmore, A.K., 2006. Improved monitoring of vegetation dynamics at very high latitudes. A new method using MODIS NDVI. Remote Sensing of Environment 100 (3), 321–334. DOI: 10.1016/j.rse.2005.10.021.

Bergen, K.M., Goetz, S.J., Dubayah, R.O., Henebry, G.M., Hunsaker, C.T., Imhoff, M.L., Nelson, R.F., Parker, G.G., Radeloff, V.C., 2009. Remote sensing of vegetation 3-D structure for biodiversity and habitat. Review and implications for lidar and radar spaceborne missions. Journal of Geophysical Research 114, G00E06. DOI: 10.1029/2008JG000883.

Bond, W.J., 2008. What Limits Trees in C4 Grasslands and Savannas? Annual Review of Ecology, Evolution, and Systematics 39 (1), 641–659. DOI: 10.1146/annurev.ecolsys.39.110707.173411.

Bond, W.J., Keeley, J.E., 2005. Fire as a global 'herbivore': the ecology and evolution of flammable ecosystems. Trends in Ecology & Evolution 20 (7), 387–394. DOI: 10.1016/j.tree.2005.04.025.

Bond, W.J., Midgley, G.F., 2012. Carbon dioxide and the uneasy interactions of trees and savannah grasses. Philosophical Transactions of the Royal Society B: Biological Sciences 367 (1588), 601–612. DOI: 10.1098/rstb.2011.0182.

Boschetti, L., Roy, D., Hoffmann, A.A., Humber, M., 2013. MODIS Collection 5.1 Burned Area Product - MCD45. User's Guide Version 3.0.1, 35 pp. http://modis-fire.umd.edu/files/MODIS_Burned_Area_Collection51_User_Guide_3.0.pdf (accessed 10 December 2016).

Bowman, D.M.J.S., Balch, J., Artaxo, P., Bond, W.J., Cochrane, M.A., D'Antonio, C.M., Defries, R., Johnston, F.H., Keeley, J.E., Krawchuk, M.A., Kull, C.A., Mack, M., Moritz, M.A., Pyne, S., Roos, C.I., Scott, A.C., Sodhi, N.S., Swetnam, T.W., Whittaker, R., 2011. The human dimension of fire regimes on Earth. Journal of Biogeography 38 (12), 2223–2236. DOI: 10.1111/j.1365-2699.2011.02595.x.

Brandt, M., Hiernaux, P., Rasmussen, K., Mbow, C., Kergoat, L., Tagesson, T., Ibrahim, Y.Z., Wélé, A., Tucker, C.J., Fensholt, R., 2016. Assessing woody vegetation trends in Sahelian drylands using MODIS based seasonal metrics. Remote Sensing of Environment 183, 215–225. DOI: 10.1016/j.rse.2016.05.027.

Bréda, N.J.J., 2003. Ground-based measurements of leaf area index. A review of methods, instruments and current controversies. Journal of Experimental Botany 54 (392), 2403–2417. DOI: 10.1093/jxb/erg263.

Breiman, L., 2001. Random Forests. Machine Learning 45 (1), 5–32. DOI: 10.1023/A:1010933404324.

Breiman, L., Friedman, J.H., Stone, C.J., Olshen, R.A., 1984. Classification and Regression Trees. Wadsworth, Belmont, CA.

Butt, B., Turner, M.D., Singh, A., Brottem, L., 2011. Use of MODIS NDVI to evaluate changing latitudinal gradients of rangeland phenology in Sudano-Sahelian West Africa. Remote Sensing of Environment 115 (12), 3367–3376. DOI: 10.1016/j.rse.2011.08.001.

Candiago, S., Remondino, F., de Giglio, M., Dubbini, M., Gattelli, M., 2015. Evaluating Multispectral Images and Vegetation Indices for Precision Farming Applications from UAV Images. Remote Sensing 7 (4), 4026–4047. DOI: 10.3390/rs70404026.

Carrivick, J., Smith, M., Quincey, D., 2016. Structure from motion in the geosciences. John Wiley & Sons, Chichester, UK.

Cerling, T.E., Harris, J.M., MacFadden, B.J., Leakey, M.G., Quade, J., Eisenmann, V., Ehleringer, J.R., 1997. Global vegetation change through the Miocene/Pliocene boundary. Nature 389, 153–158. DOI: 10.1038/38229.

Chen, Q., Baldocchi, D., Gong, P., Kelly, M., 2006. Isolating Individual Trees in a Savanna Woodland Using Small Footprint Lidar Data. Photogrammetric Engineering & Remote Sensing 72 (8), 923–932. DOI: 10.14358/PERS.72.8.923.

Chen, S., McDermid, G.J., Castilla, G., Linke, J., 2017. Measuring Vegetation Height in Linear Disturbances in the Boreal Forest with UAV Photogrammetry. Remote Sensing 9 (12), 1257. DOI: 10.3390/rs9121257.

Colomina, I., Molina, P., 2014. Unmanned aerial systems for photogrammetry and remote sensing. A review. ISPRS Journal of Photogrammetry and Remote Sensing 92, 79–97. DOI: 10.1016/j.isprsjprs.2014.02.013.

Combal, B., Baret, F., Weiss, M., Trubuil, A., Macé, D., Pragnère, A., Myneni, R., Knyazikhin, Y., Wang, L., 2003. Retrieval of canopy biophysical variables from bidirectional reflectance. Remote Sensing of Environment 84 (1), 1–15. DOI: 10.1016/S0034-4257(02)00035-4.

Costafreda-Aumedes, S., Comas, C., Vega-Garcia, C., 2017. Human-caused fire occurrence modelling in perspective. A review. International Journal of Wildland Fire 26 (12), 983–998. DOI: 10.1071/WF17026.

Crawley, M.J., 2007. The R book. John Wiley & Sons, Chichester, UK, Hoboken, NJ.

Curran, P.J., Williamson, H.D., 1985. The accuracy of ground data used in remote-sensing investigations. International Journal of Remote Sensing 6 (10), 1637–1651. DOI: 10.1080/01431168508948311.

Dandois, J., Olano, M., Ellis, E., 2015. Optimal Altitude, Overlap, and Weather Conditions for Computer Vision UAV Estimates of Forest Structure. Remote Sensing 7 (10), 13895–13920. DOI: 10.3390/rs71013895.

Dandois, J.P., Ellis, E.C., 2010. Remote Sensing of Vegetation Structure Using Computer Vision. Remote Sensing 2 (4), 1157–1176. DOI: 10.3390/rs2041157.

Dark, S.J., Bram, D., 2007. The modifiable areal unit problem (MAUP) in physical geography. Progress in Physical Geography 31 (5), 471–479. DOI: 10.1177/0309133307083294.

de Klerk, J.N., 2004. Bush encroachment in Namibia. Report on Phase 1 of the Bush Encroachment Research, Monitoring and Management Project. Ministry of Environment and Tourism, Directorate of Environmental Affairs, Windhoek.

Devine, A.P., Stott, I., McDonald, R.A., Maclean, I.M.D., Wilson, S., 2015. Woody cover in wet and dry African savannas after six decades of experimental fires. Journal of Ecology 103 (2), 473–478. DOI: 10.1111/1365-2745.12367.

Didan, K., Munoz, A.B., Solano, R., Huete, A., 2015. MODIS Vegetation Index User's Guide (MOD13 Series). Version 3.00. https://vip.arizona.edu/documents/MODIS/MODIS_VI_UsersGuide_June_2015_C6.pdf (accessed 7 March 2017).

D'Odorico, P., Okin, G.S., Bestelmeyer, B.T., 2012. A synthetic review of feedbacks and drivers of shrub encroachment in arid grasslands. Ecohydrology 5 (5), 520–530. DOI: 10.1002/eco.259.

Dormann, C.F., McPherson, J.M., Araújo, M.B., Bivand, R., Bolliger, J., Carl, G., Davies, R.G., Hirzel, A., Jetz, W., Kissling, W.D., Kühn, I., Ohlemüller, R., Peres-Neto, P.R., Reineking, B., Schröder, B., Schurr, F.M., Wilson, R., 2007. Methods to account for spatial autocorrelation in the analysis of species distributional data. A review. Ecography 30 (5), 609–628. DOI: 10.1111/j.2007.0906-7590.05171.x.

Dorner, B., Lertzman, K., Fall, J., 2002. Landscape pattern in topographically complex landscapes: issues and techniques for analysis. Landscape Ecology 17 (8), 729–743. DOI: 10.1023/A:1022944019665.

Doxsey-Whitfield, E., MacManus, K., Adamo, S.B., Pistolesi, L., Squires, J., Borkovska, O., Baptista, S.R., 2015. Taking Advantage of the Improved Availability of Census Data. A First Look at the Gridded Population of the World, Version 4. Papers in Applied Geography 1 (3), 226–234. DOI: 10.1080/23754931.2015.1014272.

Ehammer, A., Fritsch, S., Conrad, C., Lamers, J., Dech, S., 2010. Statistical derivation of fPAR and LAI for irrigated cotton and rice in arid Uzbekistan by combining multi-temporal RapidEye data and ground measurements. Proceedings of SPIE 7824, 782409. DOI: 10.1117/12.864796.

Ehleringer, J.R., Monson, R.K., 1993. Evolutionary and Ecological Aspects of Photosynthetic Pathway Variation. Annual Review of Ecology and Systematics 24 (1), 411–439. DOI: 10.1146/annurev.es.24.110193.002211.

Eisfelder, C., Kuenzer, C., Dech, S., 2012. Derivation of biomass information for semi-arid areas using remote-sensing data. International Journal of Remote Sensing 33 (9), 2937–2984. DOI: 10.1080/01431161.2011.620034.

Eklundh, L., Jönsson, P., 2017. TIMESAT 3.3 with seasonal trend decomposition and parallel processing. Software Manual. http://web.nateko.lu.se/timesat/docs/TIMESAT33_SoftwareManual.pdf (accessed 10 December 2017).

Eva, H., Lambin, E.F., 1998. Remote Sensing of Biomass Burning in Tropical Regions. Remote Sensing of Environment 64 (3), 292–315. DOI: 10.1016/S0034-4257(98)00006-6.

Fang, H., Jiang, C., Li, W., Wei, S., Baret, F., Chen, J.M., Garcia-Haro, J., Liang, S., Liu, R., Myneni, R.B., Pinty, B., Xiao, Z., Zhu, Z., 2013a. Characterization and intercomparison of global moderate resolution leaf area index (LAI) products. Analysis of climatologies and theoretical uncertainties. Journal of Geophysical Research: Biogeosciences 118, 1–20. DOI: 10.1002/jgrg.20051.

Fang, H., Li, W., Myneni, R., 2013b. The Impact of Potential Land Cover Misclassification on MODIS Leaf Area Index (LAI) Estimation. A Statistical Perspective. Remote Sensing 5 (2), 830–844. DOI: 10.3390/rs5020830.

Fensholt, R., Rasmussen, K., Nielsen, T.T., Mbow, C., 2009. Evaluation of earth observation based long term vegetation trends. Intercomparing NDVI time series trend analysis consistency of Sahel from AVHRR GIMMS, Terra MODIS and SPOT VGT data. Remote Sensing of Environment 113 (9), 1886–1898. DOI: 10.1016/j.rse.2009.04.004.

Fensholt, R., Sandholt, I., Rasmussen, M.S., 2004. Evaluation of MODIS LAI, fAPAR and the relation between fAPAR and NDVI in a semi-arid environment using in situ measurements. Remote Sensing of Environment 91, 490–507. DOI: 10.1016/j.rse.2004.04.009.

Fernández-Guisuraga, J.M., Sanz-Ablanedo, E., Suárez-Seoane, S., Calvo, L., 2018. Using Unmanned Aerial Vehicles in Postfire Vegetation Survey Campaigns through Large and Heterogeneous Areas. Opportunities and Challenges. Sensors 18 (2), 586. DOI: 10.3390/s18020586.

Fischer, A., 1994. A simple model for the temporal variations of NDVI at regional scale over agricultural countries. Validation with ground radiometric measurements. International Journal of Remote Sensing 15 (7), 1421–1446. DOI: 10.1080/01431169408954175.

Flannigan, M.D., Krawchuk, M.A., de Groot, W.J., Wotton, B.M., Gowman, L.M., 2009. Implications of changing climate for global wildland fire. International Journal of Wildland Fire 18 (5), 483–507. DOI: 10.1071/WF08187.

Friedman, J.H., 1991. Multivariate Adaptive Regression Splines. The Annals of Statistics 19 (1), 1–67. DOI: 10.1214/aos/1176347963.

Furley, P.A., Rees, R.M., Ryan, C.M., Saiz, G., 2008. Savanna burning and the assessment of long-term fire experiments with particular reference to Zimbabwe. Progress in Physical Geography 32 (6), 611–634.

Garrigues, S., Allard, D., Baret, F., Weiss, M., 2006. Influence of landscape spatial heterogeneity on the non-linear estimation of leaf area index from moderate spatial resolution remote sensing data. Remote Sensing of Environment 105 (4), 286–298. DOI: 10.1016/j.rse.2006.07.013.

Garrigues, S., Allard, D., Weiss, M., Baret, F., 2002. Comparing VALERI Sampling Schemes to Better Represent High Spatial Resolution Satellite Pixel from Ground Measurements: How to Characterize an ESU. http://www.avignon.inra.fr/valeri/methodology/samplingschemes.pdf (accessed 2 March 2018).

Garrigues, S., Lacaze, R., Baret, F., Morisette, J.T., Weiss, M., Nickeson, J.E., Fernandes, R., Plummer, S., Shabanov, N.V., Myneni, R.B., Knyazikhin, Y., Yang, W., 2008. Validation and intercomparison of global Leaf Area Index products derived from remote sensing data. Journal of Geophysical Research 113, G02028. DOI: 10.1029/2007JG000635.

Geldenhuys, C.J., 1977. The Effect of Different Regimes of Annual Burning on Two Woodland Communities in Kavango. South African Forestry Journal 103, 32–42.

Geofabrik, OpenStreetMap contributors, 2016. OpenStreetMap data of Namibia. http://download.geofabrik.de/africa/namibia.html (accessed 12 December 2016).

Giglio, L., Boschetti, L., Roy, D., Hoffmann, A.A., Humber, M., 2016. Collection 6 MODIS Burned Area Product User's Guide. Version 1.0. http://modis-fire.umd.edu/files/MODIS_C6_BA_User_Guide_1.0.pdf (accessed 24 June 2017).

Giglio, L., Descloitres, J., Justice, C.O., Kaufman, Y.J., 2003. An Enhanced Contextual Fire Detection Algorithm for MODIS. Remote Sensing of Environment 87 (2-3), 273–282. DOI: 10.1016/S0034-4257(03)00184-6.

Glenn, E.P., Huete, A.R., Nagler, P.L., Nelson, S.G., 2008. Relationship Between Remotely-sensed Vegetation Indices, Canopy Attributes and Plant Physiological Processes. What Vegetation Indices Can and Cannot Tell Us About the Landscape. Sensors 8 (4), 2136–2160. DOI: 10.3390/s8042136.

Govender, N., Trollope, S.W., van Wilgen, B.W., 2006. The effect of fire season, fire frequency, rainfall and management on fire intensity in savanna vegetation in South Africa. Journal of Applied Ecology 43 (4), 748–758. DOI: 10.1111/j.1365-2664.2006.01184.x.

Goward, S.N., Markham, B., Dye, D.G., Dulaney, W., Yang, J., 1991. Normalized difference vegetation index measurements from the advanced very high resolution radiometer. Remote Sensing of Environment 35 (2-3), 257–277. DOI: 10.1016/0034-4257(91)90017-Z.

Guerschman, J.P., Hill, M.J., Renzullo, L.J., Barrett, D.J., Marks, A.S., Botha, E.J., 2009. Estimating fractional cover of photosynthetic vegetation, non-photosynthetic vegetation and bare soil in the Australian tropical savanna region upscaling the EO-1 Hyperion and MODIS sensors. Remote Sensing of Environment 113 (5), 928–945. DOI: 10.1016/j.rse.2009.01.006.

Hantson, S., Arneth, A., Harrison, S.P., Kelley, D.I., Prentice, I.C., Rabin, S.S., Archibald, S., Mouillot, F., Arnold, S.R., Artaxo, P., Bachelet, D., Ciais, P., Forrest, M., Friedlingstein, P., Hickler, T., Kaplan, J.O., Kloster, S., Knorr, W., Lasslop, G., Li, F., Mangeon, S., Melton, J.R., Meyn, A., Sitch, S., Spessa, A., van der Werf, G.R., Voulgarakis, A., Yue, C., 2016. The status and challenge of global fire modelling. Biogeosciences 13 (11), 3359–3375. DOI: 10.5194/bg-13-3359-2016.

Hardin, P.J., Jensen, R.R., 2011. Small-Scale Unmanned Aerial Vehicles in Environmental Remote Sensing. Challenges and Opportunities. GIScience & Remote Sensing 48 (1), 99–111. DOI: 10.2747/1548-1603.48.1.99.

Hardy, C.C., 2005. Wildland fire hazard and risk. Problems, definitions, and context. Forest Ecology and Management 211, 73–82. DOI: 10.1016/j.foreco.2005.01.029.

Hawbaker, T.J., Vanderhoof, M.K., Beal, Y.-J., Takacs, J.D., Schmidt, G.L., Falgout, J.T., Williams, B., Fairaux, N.M., Caldwell, M.K., Picotte, J.J., Howard, S.M., Stitt, S., Dwyer, J.L., 2017. Mapping burned areas using dense time-series of Landsat data. Remote Sensing of Environment 198 (1), 504–522. DOI: 10.1016/j.rse.2017.06.027.

Hay, G.J., Niemann, K.O., Goodenough, D.G., 1997. Spatial thresholds, image-objects, and upscaling. A multiscale evaluation. Remote Sensing of Environment 62 (1), 1–19. DOI: 10.1016/S0034-4257(97)81622-7.

Heinl, M., Frost, P., Vanderpost, C., Sliva, J., 2007. Fire activity on drylands and floodplains in the southern Okavango Delta, Botswana. Journal of Arid Environments 68 (1), 77–87. DOI: 10.1016/j.jaridenv.2005.10.023.

Higgins, S.I., Bond, W.J., February, E.C., Bronn, A., Euston-Brown, D.I.W., Enslin, B., Govender, N., Rademan, L., O'Regan, S., Potgieter, A.L.F., Scheiter, S., Sowry, R., Trollope, L., Trollope, W.S.W., 2007. Effects of four decades of fire manipulation on woody vegetation structure in Savanna. Ecology 88 (5), 1119–1125. DOI: 10.1890/06-1664.

Higgins, S.I., Bond, W.J., Trollope, W.S.W., 2000. Fire, Resprouting and Variability: A Recipe for Grass-Tree Coexistence in Savanna. Journal of Ecology 88 (2), 213–229.

Higgins, S.I., Scheiter, S., Sankaran, M., 2010. The stability of African savannas. Insights from the indirect estimation of the parameters of a dynamic model. Ecology 91 (6), 1682–1692. DOI: 10.1890/08-1368.1.

Hird, J.N., McDermid, G.J., 2009. Noise reduction of NDVI time series. An empirical comparison of selected techniques. Remote Sensing of Environment 113 (1), 248–258. DOI: 10.1016/j.rse.2008.09.003.

Hird, J.N., Montaghi, A., McDermid, G.J., Kariyeva, J., Moorman, B.J., Nielsen, S.E., McIntosh, A.C.S., 2017. Use of Unmanned Aerial Vehicles for Monitoring Recovery of Forest Vegetation on Petroleum Well Sites. Remote Sensing 9 (5), 413. DOI: 10.3390/rs9050413.

Hoffman, M.T., 2003. Human impacts on vegetation. In: Cowling, R.M., Richardson, D.M., Pierce, S.M. (Eds.), Vegetation of Southern Africa. University Press, Cambridge, pp. 507–534.

Hoscilo, A., Balzter, H., Bartholomé, E., Boschetti, M., Brivio, P.A., Brink, A., Clerici, M., Pekel, J.F., 2015. A conceptual model for assessing rainfall and vegetation trends in sub-Saharan Africa from satellite data. International Journal of Climatology 35 (12), 3582–3592. DOI: 10.1002/joc.4231.

Hudak, A.T., Fairbanks, D.H.K., Brockett, B.H., 2004. Trends in fire patterns in a southern African savanna under alternative land use practices. Agriculture, Ecosystems & Environment 101 (2-3), 307–325. DOI: 10.1016/j.agee.2003.09.010.

Huete, A., 2014. Vegetation Indices. In: Njoku, E.G. (Ed.), Encyclopedia of Remote Sensing. Springer, New York, pp. 883–886.

Huete, A., Didan, K., Miura, T., Rodriguez, E., Gao, X., Ferreira, L., 2002. Overview of the radiometric and biophysical performance of the MODIS vegetation indices. Remote Sensing of Environment 83 (1-2), 195–213. DOI: 10.1016/S0034-4257(02)00096-2.

Huffman, G.J., Bolvin, D.T., Nelkin, E.J., Wolff, D.B., Adler, R.F., Gu, G., Hong, Y., Bowman, K.P., Stocker, E.F., 2007. The TRMM Multisatellite Precipitation Analysis (TMPA). Quasi-Global, Multiyear, Combined-Sensor Precipitation Estimates at Fine Scales. Journal of Hydrometeorology 8 (1), 38–55. DOI: 10.1175/JHM560.1.

Hughes, D.A., 2006. Comparison of satellite rainfall data with observations from gauging station networks. Journal of Hydrology 327 (3-4), 399–410. DOI: 10.1016/j.jhydrol.2005.11.041.

Jacques, D.C., Kergoat, L., Hiernaux, P., Mougin, E., Defourny, P., 2014. Monitoring dry vegetation masses in semi-arid areas with MODIS SWIR bands. Remote Sensing of Environment 153, 40–49. DOI: 10.1016/j.rse.2014.07.027.

Jarvis, A., Reuter, H.I., Nelson, A., Guevara, E., 2008. Hole-filled SRTM for the globe Version 4. CGIAR-CSI SRTM 90m Database. http://srtm.csi.cgiar.org (accessed 14 June 2017).

Jensen, J.L.R., Mathews, A.J., 2016. Assessment of Image-Based Point Cloud Products to Generate a Bare Earth Surface and Estimate Canopy Heights in a Woodland Ecosystem. Remote Sensing 8 (1), 50. DOI: 10.3390/rs8010050.

Jiang, J., Ji, X., Yao, X., Tian, Y., Zhu, Y., Cao, W., Cheng, T., 2018. Evaluation of Three Techniques for Correcting the Spatial Scaling Bias of Leaf Area Index. Remote Sensing 10 (2), 221. DOI: 10.3390/rs10020221.

Jonckheere, I., Fleck, S., Nackaerts, K., Muys, B., Coppin, P., Weiss, M., Baret, F., 2004. Review of methods for in situ leaf area index determination. Agricultural and Forest Meteorology 121 (1-2), 19–35. DOI: 10.1016/j.agrformet.2003.08.027.

Jones, H.G., Vaughan, R.A., 2010. Remote sensing of vegetation. Principles, techniques, and applications. Oxford University Press, Oxford.

Justice, C., Belward, A., Morisette, J., Lewis, P., Privette, J., Baret, F., 2000. Developments in the 'validation' of satellite sensor products for the study of the land surface. International Journal of Remote Sensing 21 (17), 3383–3390. DOI: 10.1080/014311600750020000.

Justice, C.O., Giglio, L., Korontzi, S., Owens, J., Morisette, J.T., Roy, D., Descloitres, J., Alleaume, S., Petitcolin, F., Kaufman, Y., 2002. The MODIS fire products. Remote Sensing of Environment 83 (1-2), 244–262. DOI: 10.1016/S0034-4257(02)00076-7.

Justice, C.O., Vermote, E., Townshend, J.R.G., Defries, R., Roy, D.P., Hall, D.K., Salomonson, V.V., Privette, J.L., Riggs, G., Strahler, A., Lucht, W., Myneni, R.B., Knyazikhin, Y., Running, S.W., Nemani, R.R., Wan, Z., Huete, A.R., van Leeuwen, W., Wolfe, R.E., Giglio, L., Muller, J., Lewis, P., Barnsley, M.J., 1998. The Moderate Resolution Imaging Spectroradiometer (MODIS). Land remote sensing for global change research. IEEE Transactions on Geoscience and Remote Sensing 36 (4), 1228–1249. DOI: 10.1109/36.701075.

Kahiu, M.N., Hanan, N.P., 2018. Estimation of Woody and Herbaceous Leaf Area Index in Sub-Saharan Africa Using MODIS Data. Journal of Geophysical Research: Biogeosciences 123 (1), 3–17. DOI: 10.1002/2017JG004105.

Kayitakire, F., Hamel, C., Defourny, P., 2006. Retrieving forest structure variables based on image texture analysis and IKONOS-2 imagery. Remote Sensing of Environment 102 (3-4), 390–401. DOI: 10.1016/j.rse.2006.02.022.

Ke, Y., Quackenbush, L.J., 2011. A review of methods for automatic individual tree-crown detection and delineation from passive remote sensing. International Journal of Remote Sensing 32 (17), 4725–4747. DOI: 10.1080/01431161.2010.494184.

Kennedy, A.D., Potgieter, A.L.F., 2003. Fire season affects size and architecture of *Colophospermum mopane* in southern African savannas. Plant Ecology 167 (2), 179–192. DOI: 10.1023/A:1023964815201.

Kidd, C., Huffman, G., 2011. Global precipitation measurement. Meteorological Applications 18 (3), 334–353. DOI: 10.1002/met.284.

Klein Hentz, Â.M., Strager, M.P., 2018. Cicada (*Magicicada*) Tree Damage Detection Based on UAV Spectral and 3D Data. Natural Science 10 (1), 31–44. DOI: 10.4236/ns.2018.101003.

Knorr, W., Kaminski, T., Arneth, A., Weber, U., 2014. Impact of human population density on fire frequency at the global scale. Biogeosciences 11 (4), 1085–1102. DOI: 10.5194/bg-11-1085-2014.

Knyazikhin, Y., Martonchik, J.V., Myneni, R.B., Diner, D.J., Running, S.W., 1998. Synergistic algorithm for estimating vegetation canopy leaf area index and fraction of absorbed photosynthetically

active radiation from MODIS and MISR data. Journal of Geophysical Research: Atmospheres 103 (D24), 32257–32275. DOI: 10.1029/98JD02462.

Krawchuk, M.A., Moritz, M.A., 2011. Constraints on global fire activity vary across a resource gradient. Ecology 92 (1), 121–132.

Krawchuk, M.A., Moritz, M.A., 2014. Burning issues. Statistical analyses of global fire data to inform assessments of environmental change. Environmetrics 25 (6), 472–481. DOI: 10.1002/env.2287.

Krebs, P., Pezzatti, G.B., Mazzoleni, S., Talbot, L.M., Conedera, M., 2010. Fire regime. History and definition of a key concept in disturbance ecology. Theory in Biosciences 129 (1), 53–69. DOI: 10.1007/s12064-010-0082-z.

Kuhn, M., Johnson, K., 2013. Applied Predictive Modeling. Springer, New York.

Kummerow, C., Barnes, W., Kozu, T., Shiue, J., Simpson, J., 1998. The Tropical Rainfall Measuring Mission (TRMM) Sensor Package. Journal of Atmospheric and Oceanic Technology 15 (3), 809–817. DOI: 10.1175/1520-0426(1998)015<0809:TTRMMT>2.0.CO;2.

Laris, P.S., 2005. Spatiotemporal problems with detecting and mapping mosaic fire regimes with coarse-resolution satellite data in savanna environments. Remote Sensing of Environment 99 (4), 412–424. DOI: 10.1016/j.rse.2005.09.012.

Layberry, R., Kniveton, D.R., Todd, M.C., Kidd, C., Bellerby, T.J., 2006. Daily Precipitation over Southern Africa. A New Resource for Climate Studies. Journal of Hydrometeorology 7 (1), 149–159. DOI: 10.1175/JHM477.1.

Le Roux, J., 2011. The effect of land use practices on the spatial and temporal characteristics of savanna fires in Namibia. Doctoral dissertation, University of Erlangen-Nuremberg, Germany.

Leberl, F., Irschara, A., Pock, T., Meixner, P., Gruber, M., Scholz, S., Wiechert, A., 2010. Point Clouds: Lidar versus 3D Vision. Photogrammetric Engineering & Remote Sensing 76 (10), 1123–1134.

Lefsky, M.A., Cohen, W.B., Parker, G.G., Harding, D.J., 2002. Lidar Remote Sensing for Ecosystem Studies. BioScience 52 (1), 19–30. DOI: 10.1641/0006-3568(2002)052[0019:LRSFES]2.0.CO;2.

Legates, D.R., McCabe, G.J., 1999. Evaluating the use of "goodness-of-fit" measures in hydrologic and hydroclimatic model validation. Water Resources Research 35 (1), 233–241. DOI: 10.1029/1998WR900018.

Lehmann, C., Archibald, S.A., Hoffmann, W.A., Bond, W.J., 2011. Deciphering the distribution of the savanna biome. New Phytologist 191 (1), 197–209. DOI: 10.1111/j.1469-8137.2011.03689.x.

Lehmann, C.E.R., Anderson, T.M., Sankaran, M., Higgins, S.I., Archibald, S., Hoffmann, W.A., Hanan, N.P., Williams, R.J., Fensham, R.J., Felfili, J., Hutley, L.B., Ratnam, J., San Jose, J., Montes, R., Franklin, D., Russell-Smith, J., Ryan, C.M., Durigan, G., Hiernaux, P., Haidar, R., Bowman, D.M.J.S., Bond, W.J., 2014. Savanna Vegetation-Fire-Climate Relationships Differ Among Continents. Science 343, 548–552. DOI: 10.1126/science.1243339.

Lehsten, V., Arneth, A., Spessa, A., Thonicke, K., Moustakas, A., 2016. The effect of fire on tree–grass coexistence in savannas. A simulation study. International Journal of Wildland Fire 25 (2), 137–146. DOI: 10.1071/WF14205.

Lehsten, V., Tansey, K., Balzter, H., Thonicke, K., Spessa, A., Weber, U., Smith, B., Arneth, A., 2009. Estimating carbon emissions from African wildfires. Biogeosciences 6, 349–360.

Lentile, L.B., Holden, Z.A., Smith, A.M.S., Falkowski, M.J., Hudak, A.T., Morgan, P., Lewis, S.A., Gessler, P.E., Benson, N.C., 2006. Remote sensing techniques to assess active fire characteristics and post-fire effects. International Journal of Wildland Fire 15 (3), 319–345. DOI: 10.1071/WF05097.

Levick, S.R., Baldeck, C.A., Asner, G.P., Tjoelker, M., 2015. Demographic legacies of fire history in an African savanna. Functional Ecology 29 (1), 131–139. DOI: 10.1111/1365-2435.12306.

Li, X., Gao, Z., Bai, L., Huang, Y., 2012. Potential of high resolution RapidEye data for sparse vegetation fraction mapping in arid regions. In: International Geoscience and Remote Sensing Symposium (IGARSS). IEEE, Piscataway, NJ, pp. 420–423.

Li, Z., Guo, X., 2016. Remote sensing of terrestrial non-photosynthetic vegetation using hyperspectral, multispectral, SAR, and LiDAR data. Progress in Physical Geography 40 (2), 276–304. DOI: 10.1177/0309133315582005.

Liang, S., Fang, H., Chen, M., Shuey, C.J., Walthall, C., Daughtry, C., Morisette, J., Schaaf, C., Strahler, A., 2002. Validating MODIS land surface reflectance and albedo products. Methods and preliminary results. Remote Sensing of Environment 83 (1-2), 149–162. DOI: 10.1016/S0034-4257(02)00092-5.

Lillesand, T.M., Kiefer, R.W., Chipman, J.W., 2008. Remote sensing and image interpretation, 6th Ed. John Wiley & Sons, Hoboken, NJ.

Lisein, J., Pierrot-Deseilligny, M., Bonnet, S., Lejeune, P., 2013. A Photogrammetric Workflow for the Creation of a Forest Canopy Height Model from Small Unmanned Aerial System Imagery. Forests 4 (4), 922–944. DOI: 10.3390/f4040922.

Lowe, D.G., 2004. Distinctive Image Features from Scale-Invariant Keypoints. International Journal of Computer Vision 60 (2), 91–110. DOI: 10.1023/B:VISI.0000029664.99615.94.

Lutz, J.A., Key, C.H., Kolden, C.A., Kane, J.T., van Wagtendonk, J.W., 2011. Fire Frequency, Area Burned, and Severity. A Quantitative Approach to Defining a Normal Fire Year. Fire Ecology 7 (2), 51–65. DOI: 10.4996/fireecology.0702051.

Maestre, F.T., Bowker, M.A., Puche, M.D., Belén Hinojosa, M., Martínez, I., García-Palacios, P., Castillo, A.P., Soliveres, S., Luzuriaga, A.L., Sánchez, A.M., Carreira, J.A., Gallardo, A., Escudero, A., 2009. Shrub encroachment can reverse desertification in semi-arid Mediterranean grasslands. Ecology Letters 12 (9), 930–941. DOI: 10.1111/j.1461-0248.2009.01352.x.

Maidment, R.I., Allan, R.P., Black, E., 2015. Recent observed and simulated changes in precipitation over Africa. Geophysical Research Letters 42 (19), 8155–8164. DOI: 10.1002/2015GL065765.

Malß, S., 2017. Vegetationsanalysen in Savannenökosystemen Namibias mittels bildspektrometrischer Verfahren auf unterschiedlichen Skalen– ein Methodenvergleich. Unpublished M.Sc. thesis, University of Bayreuth, Germany.

Mathieu, R., Naidoo, L., Cho, M.A., Leblon, B., Main, R., Wessels, K., Asner, G.P., Buckley, J., van Aardt, J., Erasmus, B.F.N., Smit, I.P.J., 2013. Toward structural assessment of semi-arid African savannahs and woodlands. The potential of multitemporal polarimetric RADARSAT-2 fine beam images. Remote Sensing of Environment 138, 215–231. DOI: 10.1016/j.rse.2013.07.011.

Mayr, M., 2012. Deduction of vegetation parameters from remote sensing for the integration into a regional SVAT (soil-vegetation-atmosphere transport) model in central Northern Namibia. Unpublished diploma thesis, University of Vienna, Austria.

McCoy, R.M., 2005. Field methods in remote sensing. Guilford Press, New York.

Mendelsohn, J.M., El Obeid, S., Roberts, C., 2000. A profile of north-central Namibia. Gamsberg Macmillan Publishers, Windhoek.

Mendelsohn, J.M., Jarvis, A., Roberts, C., Robertson, T., 2002. Atlas of Namibia - A portrait of the land and its people. David Philip Publishers, Cape Town.

Midgley, J.J., Lawes, M.J., Chamaillé-Jammes, S., 2010. Savanna woody plant dynamics. The role of fire and herbivory, separately and synergistically. Australian Journal of Botany 58 (1), 1–11. DOI: 10.1071/BT09034.

Ministry of Agriculture, Water and Forestry (MAWF), 2012. National Rangeland Management. Policy (Part I) & Strategy (Part II). Restoring Namibia's Rangelands. www.agrinamibia.com.na/index.php?module=Downloads&func=prep_hand_out&lid=255 (accessed 4 November 2016).

Ministry of Environment and Tourism (MET), 2016. Fire Management Strategy for Namibia's Protected Areas. http://www.met.gov.na/files/downloads/66c_Fire%20Management_Strategy%20Final%20Version.pdf (accessed 15 December 2016).

Mishra, N.B., Mainali, K.P., Crews, K.A., 2016. Modelling spatiotemporal variability in fires in semiarid savannas. A satellite-based assessment around Africa's largest protected area. International Journal of Wildland Fire 25 (7), 730–741. DOI: 10.1071/WF15152.

Moreno, M.V., Chuvieco, E., 2016. Fire Regime Characteristics along Environmental Gradients in Spain. Forests 7 (12), 262. DOI: 10.3390/f7110262.

Moriasi, D.N., Arnold, J.G., van Liew, M.W., Bingner, R.L., Harmel, R.D., Veith, T.L., 2007. Model evaluation guidelines for systematic quantification of accuracy in watershed simulations. Transactions of the American Society of Agricultural and Biological Engineers 50 (3), 885–900.

Morisette, J.T., Baret, F., Privette, J.L., Myneni, R.B., Nickeson, J.E., Garrigues, S., Shabanov, N.V., Weiss, M., Fernandes, R.A., Leblanc, S.G., Kalacska, M., Sanchez-Azofeifa, G.A., Chubey, M., Rivard, B., Stenberg, P., Rautiainen, M., Voipio, P., Manninen, T., Pilant, A.N., Lewis, T.E., Iiames, J.S., Colombo, R., Meroni, M., Busetto, L., Cohen, W.B., Turner, D.P., Warner, E.D., Petersen, G.W., Seufert, G., Cook, R., 2006. Validation of global moderate-resolution LAI products. A framework proposed within the CEOS land product validation subgroup. IEEE Transactions on Geoscience and Remote Sensing 44 (7), 1804–1817. DOI: 10.1109/TGRS.2006.872529.

Mouillot, F., Schultz, M.G., Yue, C., Cadule, P., Tansey, K., Ciais, P., Chuvieco, E., 2014. Ten years of global burned area products from spaceborne remote sensing—A review. Analysis of user needs and recommendations for future developments. International Journal of Applied Earth Observation and Geoinformation 26, 64–79. DOI: 10.1016/j.jag.2013.05.014.

Myneni, R.B., Hoffman, S., Knyazikhin, Y., Privette, J.L., Glassy, J., Tian, Y., Wang, Y., Song, X., Zhang, Y., Smith, G.R., Lotsch, A., Friedl, M., Morisette, J.T., Votava, P., Nemani, R.R., Running, S.W., 2002. Global products of vegetation leaf area and fraction absorbed PAR from year one of MODIS data. Remote Sensing of Environment 83 (1-2), 214–231. DOI: 10.1016/S0034-4257(02)00074-3.

Naidoo, L., Mathieu, R., Main, R., Kleynhans, W., Wessels, K., Asner, G., Leblon, B., 2015. Savannah woody structure modelling and mapping using multi-frequency (X-, C- and L-band) Synthetic Aperture Radar data. ISPRS Journal of Photogrammetry and Remote Sensing 105, 234–250. DOI: 10.1016/j.isprsjprs.2015.04.007.

Naidoo, L., Mathieu, R., Main, R., Wessels, K., Asner, G.P., 2016. L-band Synthetic Aperture Radar imagery performs better than optical datasets at retrieving woody fractional cover in deciduous, dry savannahs. International Journal of Applied Earth Observation and Geoinformation 52, 54–64. DOI: 10.1016/j.jag.2016.05.006.

Näsi, R., Honkavaara, E., Lyytikäinen-Saarenmaa, P., Blomqvist, M., Litkey, P., Hakala, T., Viljanen, N., Kantola, T., Tanhuanpää, T., Holopainen, M., 2015. Using UAV-Based Photogrammetry and Hyperspectral Imaging for Mapping Bark Beetle Damage at Tree-Level. Remote Sensing 7 (11), 15467–15493. DOI: 10.3390/rs71115467.

Nelder, J.A., Wedderburn, R.W.M., 1972. Generalized Linear Models. Journal of the Royal Statistical Society A 135 (3), 370–384. DOI: 10.2307/2344614.

Nex, F., Remondino, F., 2014. UAV for 3D mapping applications. A review. Applied Geomatics 6 (1), 1–15. DOI: 10.1007/s12518-013-0120-x.

Niang, I., Ruppel, O.C., Abdrabo, M.A., Essel, A., Lennard, C., Padgham, J., Urquhart, P., 2014. Africa. In: Barros, V.R., Field, C.B., Dokken, D.J., Mastandrea, M.D., Mach, K.J., Bilir, T.E., Chatterjee, M., Ebi, K.L., Estrada, Y.O., Genova, R.C., Girma, B., Kissel, E.S., Levy, A.N., MacCracken, S., Mastandrea, P.R., White, L.L. (Eds.), Climate Change 2014. Impacts, Adaptation, and Vulnerability. Part B: Regional Aspects. Contribution of Working Group. Cambridge University Press, Cambridge, New York, pp. 1199–1265.

O'Connor, T.G., Puttick, J.R., Hoffman, M.T., 2014. Bush encroachment in southern Africa. Changes and causes. African Journal of Range & Forage Science 31 (2), 67–88. DOI: 10.2989/10220119.2014.939996.

Okin, G.S., Roberts, D.A., Murray, B., Okin, W.J., 2001. Practical limits on hyperspectral vegetation discrimination in arid and semiarid environments. Remote Sensing of Environment 77 (2), 212–225. DOI: 10.1016/S0034-4257(01)00207-3.

Ollinger, S.V., 2011. Sources of variability in canopy reflectance and the convergent properties of plants. The New Phytologist 189 (2), 375–394. DOI: 10.1111/j.1469-8137.2010.03536.x.

Ota, T., Ogawa, M., Shimizu, K., Kajisa, T., Mizoue, N., Yoshida, S., Takao, G., Hirata, Y., Furuya, N., Sano, T., Sokh, H., Ma, V., Ito, E., Toriyama, J., Monda, Y., Saito, H., Kiyono, Y., Chann, S., Ket, N., 2015. Aboveground Biomass Estimation Using Structure from Motion Approach with Aerial Photographs in a Seasonal Tropical Forest. Forests 6 (11), 3882–3898. DOI: 10.3390/f6113882.

Page, S.E., Siegert, F., Rieley, J.O., Boehm, H.-D.V., Jaya, A., Limin, S., 2002. The amount of carbon released from peat and forest fires in Indonesia during 1997. Nature 420 (6911), 61–65. DOI: 10.1038/nature01131.

Pausas, J.G., Ribeiro, E., 2013. The global fire-productivity relationship. Global Ecology and Biogeography 22 (6), 728–736. DOI: 10.1111/geb.12043.

Pereira, J.M.C., 2003. Remote sensing of burned areas in tropical savannas. International Journal of Wildland Fire 12 (4), 259–270. DOI: 10.1071/WF03028.

Petrou, Z.I., Manakos, I., Stathaki, T., Mücher, C.A., Adamo, M., 2015. Discrimination of Vegetation Height Categories With Passive Satellite Sensor Imagery Using Texture Analysis. IEEE Journal of Selected Topics in Applied Earth Observations and Remote Sensing 8 (4), 1442–1455. DOI: 10.1109/JSTARS.2015.2409131.

Pricope, N.G., Binford, M.W., 2012. A spatio-temporal analysis of fire recurrence and extent for semi-arid savanna ecosystems in southern Africa using moderate-resolution satellite imagery. Journal of Environmental Management 100, 72–85. DOI: 10.1016/j.jenvman.2012.01.024.

Privette, J., Myneni, R., Knyazikhin, Y., Mukelabai, M., Roberts, G., Tian, Y., Wang, Y., Leblanc, S.G., 2002. Early spatial and temporal validation of MODIS LAI product in the Southern Africa Kalahari. Remote Sensing of Environment 83, 232–243. DOI: 10.1016/S0034-4257(02)00075-5.

Ramoelo, A., Skidmore, A.K., Cho, M.A., Schlerf, M., Mathieu, R., Heitkönig, I.M.A., 2012. Regional estimation of savanna grass nitrogen using the red-edge band of the spaceborne RapidEye sensor. International Journal of Applied Earth Observation and Geoinformation 19, 151–162. DOI: 10.1016/j.jag.2012.05.009.

Randerson, J.T., Chen, Y., van der Werf, G.R., Rogers, B.M., Morton, D.C., 2012. Global burned area and biomass burning emissions from small fires. Journal of Geophysical Research 117 (G4). DOI: 10.1029/2012JG002128.

RapidEye AG, 2011. RapidEye Satellite Imagery Product Specifications. Version 3.2. RapidEye AG, Brandenburg a. d. Havel.

Roebroeks, W., Villa, P., 2011. On the earliest evidence for habitual use of fire in Europe. Proceedings of the National Academy of Sciences of the United States of America 108 (13), 5209–5214. DOI: 10.1073/pnas.1018116108.

Roleček, J., Chytrý, M., Hájek, M., Lvončík, S., Tichý, L., 2007. Sampling design in large-scale vegetation studies. Do not sacrifice ecological thinking to statistical purism! Folia Geobotanica 42 (2), 199–208. DOI: 10.1007/BF02893886.

Roy, D.P., Boschetti, L., 2009. Southern Africa Validation of the MODIS, L3JRC, and GlobCarbon Burned-Area Products. IEEE Transactions on Geoscience and Remote Sensing 47 (4), 1032–1044. DOI: 10.1109/TGRS.2008.2009000.

Roy, D.P., Boschetti, L., Giglio, L., 2011. Remote Sensing of Global Savanna Fire Occurrence, Extent, and Properties. In: Hill, M.J., Hanan, N.P. (Eds.), Ecosystem function in Savannas. Measurement and modeling at landscape to global scales. CRC Press, Boca Raton, pp. 239–254.

Roy, D.P., Boschetti, L., Justice, C.O., Ju, J., 2008. The collection 5 MODIS burned area product — Global evaluation by comparison with the MODIS active fire product. Remote Sensing of Environment 112 (9), 3690–3707. DOI: 10.1016/j.rse.2008.05.013.

Roy, D.P., Jin, Y., Lewis, P.E., Justice, C.O., 2005. Prototyping a global algorithm for systematic fire-affected area mapping using MODIS time series data. Remote Sensing of Environment 97 (2), 137–162. DOI: 10.1016/j.rse.2005.04.007.

Ruß, G., Brenning, A., 2010. Data Mining in Precision Agriculture. Management of Spatial Information. In: Hüllermeier, E., Kruse, R., Hoffmann, F. (Eds.), Computational Intelligence for Knowledge-Based Systems Design. Springer, Heidelberg, Berlin, pp. 350–359.

Ryu, Y., Sonnentag, O., Nilson, T., Vargas, R., Kobayashi, H., Wenk, R., Baldocchi, D.D., 2010. How to quantify tree leaf area index in an open savanna ecosystem. A multi-instrument and multi-model approach. Agricultural and Forest Meteorology 150 (1), 63–76. DOI: 10.1016/j.agrformet.2009.08.007.

Salamí, E., Barrado, C., Pastor, E., 2014. UAV Flight Experiments Applied to the Remote Sensing of Vegetated Areas. Remote Sensing 6 (11), 11051–11081. DOI: 10.3390/rs61111051.

Sankaran, M., Hanan, N.P., Scholes, R.J., Ratnam, J., Augustine, D.J., Cade, B.S., Gignoux, J., Higgins, S.I., Le Roux, X., Ludwig, F., Ardö, J., Banyikwa, F., Bronn, A., Bucini, G., Caylor, K.K., Coughenour, M.B., Diouf, A., Ekaya, W., Feral, C.J., February, E.C., Frost, P.G.H., Hiernaux, P., Hrabar, H., Metzger, K.L., Prins, H.H.T., Ringrose, S., Sea, W., Tews, J., Worden, J., Zambatis, N., 2005. Determinants of woody cover in African savannas. Nature 438 (7069), 846–849. DOI: 10.1038/nature04070.

Sankaran, M., Ratnam, J., Hanan, N.P., 2008. Woody cover in African savannas: the role of resources, fire and herbivory. Global Ecology and Biogeography 17 (2), 236–245. DOI: 10.1111/j.1466-8238.2007.00360.x.

Sankaran, M., Ratnam, J., Hanan, N.P., 2004. Tree-grass coexistence in savannas revisited - insights from an examination of assumptions and mechanisms invoked in existing models. Ecology Letters 7 (6), 480–490. DOI: 10.1111/j.1461-0248.2004.00596.x.

Scheiter, S., Higgins, S.I., Osborne, C.P., Bradshaw, C., Lunt, D., Ripley, B.S., Taylor, L.L., Beerling, D.J., 2012. Fire and fire-adapted vegetation promoted C4 expansion in the late Miocene. The New Phytologist 195 (3), 653–666. DOI: 10.1111/j.1469-8137.2012.04202.x.

Scholes, R.J., 2003. Savanna. In: Cowling, R.M., Richardson, D.M., Pierce, S.M. (Eds.), Vegetation of Southern Africa. University Press, Cambridge, pp. 258–277.

Scholes, R.J., Archer, S.R., 1997. Tree-Grass Interactions in Savannas. Annual Review of Ecology and Systematics 28 (1), 517–544. DOI: 10.1146/annurev.ecolsys.28.1.517.

Scholes, R.J., Archibald, S., von Maltitz, G., 2011. Emissions from Fire in Sub-Saharan Africa: the Magnitude of Sources, Their Variability and Uncertainty. Global Environmental Research 15 (1), 53–63.

Scholes, R.J., Frost, P.G.H., Tian, Y., 2004. Canopy structure in savannas along a moisture gradient on Kalahari sands. Global Change Biology 10 (3), 292–302. DOI: 10.1046/j.1365-2486.2003.00703.x.

Schumacher, P., Mislimshoeva, B., Brenning, A., Zandler, H., Brandt, M., Samimi, C., Koellner, T., 2016. Do Red Edge and Texture Attributes from High-Resolution Satellite Data Improve Wood Volume Estimation in a Semi-Arid Mountainous Region? Remote Sensing 8 (12), 540. DOI: 10.3390/rs8070540.

Sea, W.B., Choler, P., Beringer, J., Weinmann, R.A., Hutley, L.B., Leuning, R., 2011. Documenting improvement in leaf area index estimates from MODIS using hemispherical photos for Australian savannas. Agricultural and Forest Meteorology 151 (11), 1453–1461. DOI: 10.1016/j.agrformet.2010.12.006.

Sellers, P.J., 1985. Canopy reflectance, photosynthesis and transpiration. International Journal of Remote Sensing 6 (8), 1335–1372. DOI: 10.1080/01431168508948283.

Sellers, P.J., Dickinson, R.E., Randall, D.A., Betts, A.K., Hall, F.G., Berry, J.A., Collatz, G.J., Denning, A.S., Mooney, H.A., Nobre, C.A., Sato, N., Field, C.B., Henderson-Sellers, A., 1997. Modeling the Exchanges of Energy, Water, and Carbon Between Continents and the Atmosphere. Science 275 (5299), 502–509. DOI: 10.1126/science.275.5299.502.

Seymour, C.L., Huyser, O., 2008. Fire and the demography of camelthorn (*Acacia erioloba* Meyer) in the southern Kalahari - evidence for a bonfire effect? African Journal of Ecology 46 (4), 594–601. DOI: 10.1111/j.1365-2028.2007.00909.x.

Siiskonen, H., 1996. Deforestation in the Owambo Region, North Namibia, since the 1850s. Environment and History 2 (3), 291–308. DOI: 10.3197/096734096779522301.

Siljander, M., 2009. Predictive fire occurrence modelling to improve burned area estimation at a regional scale. A case study in East Caprivi, Namibia. International Journal of Applied Earth Observation and Geoinformation 11 (6), 380–393. DOI: 10.1016/j.jag.2009.06.004.

Simard, M., Pinto, N., Fisher, J.B., Baccini, A., 2011. Mapping forest canopy height globally with spaceborne lidar. Journal of Geophysical Research 116, G04021. DOI: 10.1029/2011JG001708.

Simpson, K.J., Ripley, B.S., Christin, P.-A., Belcher, C.M., Lehmann, C.E.R., Thomas, G.H., Osborne, C.P., 2016. Determinants of flammability in savanna grass species. Journal of Ecology 104 (1), 138–148. DOI: 10.1111/1365-2745.12503.

Smit, I., Asner, G.P., Govender, N., Kennedy-Bowdoin, T., Knapp, D.E., Jacobson, J., 2010. Effects of fire on woody vegetation structure in African savanna. Ecological Applications 20 (7), 1865–1875. DOI: 10.1890/09-0929.

Sprintsin, M., Karnieli, A., Berliner, P., Rotenberg, E., Yakir, D., Cohen, S., 2009. Evaluating the performance of the MODIS Leaf Area Index (LAI) product over a Mediterranean dryland planted forest. International Journal of Remote Sensing 30 (19), 5061–5069. DOI: 10.1080/01431160903032885.

Stellmes, M., Frantz, D., Finckh, M., Revermann, R., Röder, A., Hill, J., 2013. Fire frequency, fire seasonality and fire intensity within the Okavango region derived from MODIS fire products. Biodiversity & Ecology 5, 351–362. DOI: 10.7809/b-e.00288.

Stevens, N., Erasmus, B.F.N., Archibald, S., Bond, W.J., 2016. Woody encroachment over 70 years in South African savannahs. Overgrazing, global change or extinction aftershock? Philosophical Transactions of the Royal Society B: Biological Sciences 371 (1703). DOI: 10.1098/rstb.2015.0437.

Strobl, C., Boulesteix, A.-L., Zeileis, A., Hothorn, T., 2007. Bias in random forest variable importance measures: Illustrations, sources and a solution. BMC Bioinformatics 8 (1), 25. DOI: 10.1186/1471-2105-8-25.

Strohbach, B.J., 2013. Vegetation of the Okavango river valley in Kavango West, Namibia. Biodiversity & Ecology 5, 321–329. DOI: 10.7809/b-e.00286.

Stroppiana, D., Brivio, P.A., Grégoire, J.-M., Liousse, C., Guillaume, B., Granier, C., Mieville, A., Chin, M., Pétron, G., 2010. Comparison of global inventories of CO emissions from biomass burning derived from remotely sensed data. Atmospheric Chemistry and Physics 10 (24), 12173–12189. DOI: 10.5194/acp-10-12173-2010.

Swetnam, T.W., Farella, J., Roos, C.I., Liebmann, M.J., Falk, D.A., Allen, C.D., 2016. Multiscale perspectives of fire, climate and humans in western North America and the Jemez Mountains, USA. Philosophical Transactions of the Royal Society B: Biological Sciences 371 (1696). DOI: 10.1098/rstb.2015.0168.

Tarnavsky, E., Grimes, D., Maidment, R., Black, E., Allan, R.P., Stringer, M., Chadwick, R., Kayitakire, F., 2014. Extension of the TAMSAT Satellite-Based Rainfall Monitoring over Africa and from 1983 to Present. Journal of Applied Meteorology and Climatology 53 (12), 2805–2822. DOI: 10.1175/JAMC-D-14-0016.1.

Tian, F., Brandt, M., Liu, Y.Y., Rasmussen, K., Fensholt, R., 2017. Mapping gains and losses in woody vegetation across global tropical drylands. Global Change Biology 23 (4), 1748–1760. DOI: 10.1111/gcb.13464.

Tian, Y., Woodcock, C., Wang, Y., Privette, J., Shabanov, N.V., Zhou, L., Zhang, Y., Buermann, W., Dong, J., Veikkanen, B., Häme, T., Andersson, K., Ozdogan, M., Knyazikhin, Y., Myneni, R.B., 2002. Multiscale analysis and validation of the MODIS LAI product: I. Uncertainty assessment. Remote Sensing of Environment 83 (3), 414–430. DOI: 10.1016/S0034-4257(02)00047-0.

Torres-Sánchez, J., López-Granados, F., Serrano, N., Arquero, O., Peña, J.M., 2015. High-Throughput 3-D Monitoring of Agricultural-Tree Plantations with Unmanned Aerial Vehicle (UAV) Technology. PloS one 10 (6), e0130479. DOI: 10.1371/journal.pone.0130479.

Trigg, S., Flasse, S., 2000. Characterizing the spectral-temporal response of burned savannah using in situ spectroradiometry and infrared thermometry. International Journal of Remote Sensing 21 (16), 3161–3168. DOI: 10.1080/01431160050145045.

Turner, D.P., Ritts, W.D., Cohen, W.B., Gower, S.T., Running, S.W., Zhao, M., Costa, M.H., Kirschbaum, A.A., Ham, J.M., Saleska, S.R., Ahl, D.E., 2006. Evaluation of MODIS NPP and GPP products across multiple biomes. Remote Sensing of Environment 102 (3-4), 282–292. DOI: 10.1016/j.rse.2006.02.017.

Tyc, G., Tulip, J., Schulten, D., Krischke, M., Oxfort, M., 2005. The RapidEye mission design. Acta Astronautica 56 (1-2), 213–219. DOI: 10.1016/j.actaastro.2004.09.029.

van Auken, O.W., 2009. Causes and consequences of woody plant encroachment into western North American grasslands. Journal of Environmental Management 90 (10), 2931–2942. DOI: 10.1016/j.jenvman.2009.04.023.

van Leeuwen, W., Huete, A.R., 1996. Effects of standing litter on the biophysical interpretation of plant canopies with spectral indices. Remote Sensing of Environment 55 (2), 123–138. DOI: 10.1016/0034-4257(95)00198-0.

van Wagtendonk, J.W., Root, R.R., Key, C.H., 2004. Comparison of AVIRIS and Landsat ETM+ detection capabilities for burn severity. Remote Sensing of Environment 92, 397–408. DOI: 10.1016/j.rse.2003.12.015.

van Wilgen, B.W., Govender, N., Biggs, H.C., 2007. The contribution of fire research to fire management. A critical review of a long-term experiment in the Kruger National Park, South Africa. International Journal of Wildland Fire 16 (5), 519–530. DOI: 10.1071/WF06115.

Vapnik, V.N., 1995. The nature of statistical learning theory. Springer, New York.

Verbesselt, J., Somers, B., van Aardt, J., Jonckheere, I., Coppin, P., 2006. Monitoring herbaceous biomass and water content with SPOT VEGETATION time-series to improve fire risk assessment in savanna ecosystems. Remote Sensing of Environment 101 (3), 399–414. DOI: 10.1016/j.rse.2006.01.005.

Verlinden, A., Laamanen, R., 2006. Long Term Fire Scar Monitoring with Remote Sensing in Northern Namibia: Relations Between Fire Frequency, Rainfall, Land Cover, Fire Management and Trees. Environmental Monitoring and Assessment 112 (1-3), 231–253. DOI: 10.1007/s10661-006-1705-1.

Viña, A., Gitelson, A.A., Nguy-Robertson, A.L., Peng, Y., 2011. Comparison of different vegetation indices for the remote assessment of green leaf area index of crops. Remote Sensing of Environment 115 (12), 3468–3478. DOI: 10.1016/j.rse.2011.08.010.

Wagenseil, H., Samimi, C., 2006. Assessing spatio-temporal variations in plant phenology using Fourier analysis on NDVI time series. Results from a dry savannah environment in Namibia. International Journal of Remote Sensing 27 (16), 3455–3471. DOI: 10.1080/01431160600639743.

Wagner, W., Hollaus, M., Briese, C., Ducic, V., 2008. 3D vegetation mapping using small-footprint full-waveform airborne laser scanners. International Journal of Remote Sensing 29 (5), 1433–1452. DOI: 10.1080/01431160701736398.

Ward, D., Wiegand, K., Getzin, S., 2013. Walter's two-layer hypothesis revisited. Back to the roots! Oecologia 172 (3), 617–630. DOI: 10.1007/s00442-012-2538-y.

Wessels, K.J., Mathieu, R., Erasmus, B.F.N., Asner, G.P., Smit, I.P.J., van Aardt, J.A.N., Main, R., Fisher, J., Marais, W., Kennedy-Bowdoin, T., Knapp, D.E., Emerson, R., Jacobson, J., 2011. Impact of communal land use and conservation on woody vegetation structure in the Lowveld savannas of South Africa. Forest Ecology and Management 261 (1), 19–29. DOI: 10.1016/j.foreco.2010.09.012.

West, P.W., 2015. Tree and Forest Measurement, 3rd Ed. Springer International Publishing Switzerland, Cham.

Westoby, M.J., Brasington, J., Glasser, N.F., Hambrey, M.J., Reynolds, J.M., 2012. 'Structure-from-Motion' photogrammetry. A low-cost, effective tool for geoscience applications. Geomorphology 179, 300–314. DOI: 10.1016/j.geomorph.2012.08.021.

Wigley, B.J., Bond, W.J., Hoffman, M.T., 2010. Thicket expansion in a South African savanna under divergent land use. Local vs. global drivers? Global Change Biology 16 (3), 964–976. DOI: 10.1111/j.1365-2486.2009.02030.x.

Wildi, O., 2013. Data analysis in vegetation ecology, 2nd Ed. Wiley-Blackwell, Hoboken, NJ.

Willmott, C.J., Ackleson, S.G., Davis, R.E., Feddema, J.J., Klink, K.M., Legates, D.R., O'Donnell, J., Rowe, C.M., 1985. Statistics for the evaluation and comparison of models. Journal of Geophysical Research: Atmospheres 90 (C5), 8995–9005. DOI: 10.1029/JC090iC05p08995.

Wilson, M.F.J., O'Connell, B., Brown, C., Guinan, J.C., Grehan, A.J., 2007. Multiscale Terrain Analysis of Multibeam Bathymetry Data for Habitat Mapping on the Continental Slope. Marine Geodesy 30, 3–35. DOI: 10.1080/01490410701295962.

Wu, H., Li, Z.-L., 2009. Scale issues in remote sensing. A review on analysis, processing and modeling. Sensors 9 (3), 1768–1793. DOI: 10.3390/s90301768.

Yan, H., Wang, S.Q., Billesbach, D., Oechel, W., Zhang, J.H., Meyers, T., Martin, T.A., Matamala, R., Baldocchi, D., Bohrer, G., Dragoni, D., Scott, R., 2012. Global estimation of evapotranspiration using a leaf area index-based surface energy and water balance model. Remote Sensing of Environment 124, 581–595. DOI: 10.1016/j.rse.2012.06.004.

Yang, W., Shabanov, N.V., Huang, D., Wang, W., Dickinson, R.E., Nemani, R.R., Knyazikhin, Y., Myneni, R.B., 2006. Analysis of leaf area index products from combination of MODIS Terra and Aqua data. Remote Sensing of Environment 104 (3), 297–312. DOI: 10.1016/j.rse.2006.04.016.

Zandler, H., Brenning, A., Samimi, C., 2015. Quantifying dwarf shrub biomass in an arid environment. Comparing empirical methods in a high dimensional setting. Remote Sensing of Environment 158, 140–155. DOI: 10.1016/j.rse.2014.11.007.

Zarco-Tejada, P.J., Diaz-Varela, R., Angileri, V., Loudjani, P., 2014. Tree height quantification using very high resolution imagery acquired from an unmanned aerial vehicle (UAV) and automatic 3D photo-reconstruction methods. European Journal of Agronomy 55, 89–99. DOI: 10.1016/j.eja.2014.01.004.

Zhang, W., Chen, Y., Hu, S., 2007. Retrieving LAI in the Heihe and the Hanjiang river basins using Landsat images for accuracy evaluation on MODIS LAI product. IEEE Transactions on Geoscience and Remote Sensing, 3417–3421. DOI: 10.1109/IGARSS.2007.4423579.

Zhen, Z., Quackenbush, L., Zhang, L., 2016. Trends in Automatic Individual Tree Crown Detection and Delineation—Evolution of LiDAR Data. Remote Sensing 8 (4), 333. DOI: 10.3390/rs8040333.

Zhu, C., Kobayashi, H., Kanaya, Y., Saito, M., 2017. Size-dependent validation of MODIS MCD64A1 burned area over six vegetation types in boreal Eurasia. Large underestimation in croplands. Scientific Reports 7 (1), 4181. DOI: 10.1038/s41598-017-03739-0.

Zook, M., Graham, M., Shelton, T., Gorman, S., 2010. Volunteered Geographic Information and Crowdsourcing Disaster Relief. A Case Study of the Haitian Earthquake. World Medical & Health Policy 2 (2), 7–33. DOI: 10.2202/1948-4682.1069.

PART IV
APPENDIX

A.1 LIST OF THE AUTHOR'S FURTHER CONTRIBUTIONS

Only outputs related to this thesis are listed below.

Publications

Ofner, E., Mayr, M.J., Engelbrecht, B., Samimi, C. (*in preparation*): Functionality vs. taxonomy along ecological gradients: a differentiation of woody communities in the semi-arid savannas of Namibia.

Samimi, C., Mayr, M., Zandler, H. (2015): Die Erde aus der Ferne – Die Erkundung von Klimaparametern und Vegetation mit digitaler Technik. Spektrum – das Wissenschaftsmagazin der Universität Bayreuth 11 (2), 42–45.

Presentations

Mayr, M.J., Malß, S., Joß, H., Ofner, E., Samimi, C.: From toys to tools: assessing vegetation structural parameters and potential disturbance impacts using an Unmanned Aerial Vehicle (UAV). 8th BayCEER Workshop, Bayreuth/Germany, 13 October, 2016.

Mayr, M., Malß, S., Ofner, E., Samimi, C.: Vegetationserfassung mittels Unmanned Aerial Vehicles (UAV): Bestandshöhen und Störungseinflüsse in einer namibischen Savanne. Jahrestagung des Arbeitskreis Biogeographie, Erlangen/Germany, 12–14 May, 2017.

Mayr, M., Vanselow, K., Ofner, E., Samimi, C.: Die räumliche Modellierung ausgewählter Feuerregimeparameter in Namibia. Deutscher Kongress für Geographie, Tübingen/Germany, 30 September–5 October, 2017.

Mayr, M.: Trockenzeitliche Fernerkundung – Feuer und Vegetation der Savannen Namibias. Geographisches Kolloquium der Friedrich-Alexander Universität (FAU), Erlangen/Germany, 24 January, 2018.

Conference posters

Mayr, M., Le Roux, J., Samimi, C.: Identifying the controls of wildfire activity in Namibia using multivariate statistics. EGU General Assembly 2015, Vienna/Austria, 12–17 April, 2015.

Mayr, M.J., Malß, S., Joß, H., Ofner, E., Samimi, C.: UAV-based vegetation mapping in a Namibian savanna: do remotely-sensed structural parameters contain indications of the prevailing disturbance regime? EARSeL 3rd Workshop SIG on Forestry, Krakow/Poland, 15–16 September, 2016.

A.2 EIDESSTATTLICHE ERKLÄRUNG

(§ 8 Satz 2 Nr. 3 PromO Fakultät)

Hiermit versichere ich eidesstattlich, dass ich die Arbeit selbständig verfasst und keine anderen als die von mir angegebenen Quellen und Hilfsmittel benutzt habe (vgl. Art. 64 Abs. 1 Satz 6 BayHSchG).

(§ 8 Satz 2 Nr. 3 PromO Fakultät)

Hiermit erkläre ich, dass ich die Dissertation nicht bereits zur Erlangung eines akademischen Grades eingereicht habe und dass ich nicht bereits diese oder eine gleichartige Doktorprüfung endgültig nicht bestanden habe.

(§ 8 Satz 2 Nr. 4 PromO Fakultät)

Hiermit erkläre ich, dass ich Hilfe von gewerblichen Promotionsberatern bzw. –vermittlern oder ähnlichen Dienstleistern weder bisher in Anspruch genommen habe noch künftig in Anspruch nehmen werde.

(§ 8 Satz 2 Nr. 7 PromO Fakultät)

Hiermit erkläre ich mein Einverständnis, dass die elektronische Fassung der Dissertation unter Wahrung meiner Urheberrechte und des Datenschutzes einer gesonderten Überprüfung unterzogen werden kann.

(§ 8 Satz 2 Nr. 8 PromO Fakultät)

Hiermit erkläre ich mein Einverständnis, dass bei Verdacht wissenschaftlichen Fehlverhaltens Ermittlungen durch universitätsinterne Organe der wissenschaftlichen Selbstkontrolle stattfinden können.

Bayreuth, 23.Januar 2019

Manuel Mayr